INSTITUTO LATINO-AMERICANO DE INFRAESTRUTURA E TERRITÓRIO – ILATIT

PROGRAMA DE PÓS-GRADUAÇÃO INTERDISCIPLINAR EM ENERGIA E SUSTENTABILIDADE

APRENDIZADO DE MÁQUINA APLICADO AO PROGNÓSTICO DE ESTADO DE SAÚDE DE CÉLULAS DE ARMAZENAMENTO DE ENERGIA

GIOVANE RONEI SYLVESTRIN

Foz do Iguaçu - PR
2025

INSTITUTO LATINO-AMERICANO DE INFRAESTRUTURA E TERRITÓRIO – ILATIT

PROGRAMA DE PÓS-GRADUAÇÃO INTERDISCIPLINAR EM ENERGIA E SUSTENTABILIDADE

APRENDIZADO DE MÁQUINA APLICADO AO PROGNÓSTICO DE ESTADO DE SAÚDE DE CÉLULAS DE ARMAZENAMENTO DE ENERGIA

Defesa de Tese de Doutorado apresentada ao Programa de Pós-Graduação Interdisciplinar em Energia e Sustentabilidade da Universidade Federal da Integração Latino-Americana, como requisito parcial à obtenção do título de Doutor em Energia e Sustentabilidade.

Orientador: Dr. Oswaldo Hideo Ando Junior.

Co-orientador: Dr. Joylan Maciel Nunes.

Foz do Iguaçu - PR

2025

Catalogação elaborada pelo Setor de Tratamento da Informação
Catalogação de Publicação na Fonte. UNILA - BIBLIOTECA LATINO-AMERICANA - CENTRAL

S985
Sylvestrin, Giovane Ronei.
Aprendizado de máquina aplicado ao prognóstico de estado de saúde de células de armazenamento de energia / Giovane Ronei Sylvestrin - Foz do Iguaçu-PR, 2025.
[199 f.].: il.

Tese (Doutorado) - Universidade Federal da Integração Latino-Americana. Instituto Latino-Americano de Tecnologia, Infraestrutura e Território. Programa de Pós-Graduação Interdisciplinar em Energia e Sustentabilidade. Foz do Iguaçu-PR.
Orientador: Oswaldo Hideo Ando Junior.
Coorientador: Joylan Maciel Nunes.

1. Baterias. 2. Baterias - estado de saúde. 3. Baterias - segundo uso. 4. Aprendizagem de máquina. 5. Inteligência Artificial - Redes profundas. 6. Engenharia de atributos. I. Ando Junior, Oswaldo Hideo. II. Nunes, Joylan Maciel. III. Título.

CDU 621.352

APROVADA EM 31 DE OUTUBRO DE 2025.

BANCA EXAMINADORA

Documento assinado digitalmente
gov.br
OSWALDO HIDEO ANDO JUNIOR
Data: 20/12/2025 11:25:37-0300
Verifique em https://validar.iti.gov.br

Orientador: Dr. Oswaldo Hideo Ando Junior
UNILA

Documento assinado digitalmente
gov.br
JOYLAN NUNES MACIEL
Data: 20/12/2025 11:13:49-0300
Verifique em https://validar.iti.gov.br

Co-orientador: Dr. Joylan Maciel Nunes
UNILA

Documento assinado digitalmente
gov.br
JUAN MOISES MAURICIO VILLANUEVA
Data: 17/12/2025 19:04:56-0300
Verifique em https://validar.iti.gov.br

Dr. Juan Moises Mauricio Villanueva
UFPB

Documento assinado digitalmente
gov.br
LUCAS VINICIUS HARTMANN
Data: 17/12/2025 16:00:55-0300
Verifique em https://validar.iti.gov.br

Dr. Lucas Vinícius Hartmann
UFPB

Assinado eletronicamente por:
Daniel Augusto Cantane
CPF: ***.469.508-**
Data: 18/12/2025 11:23:28 -03:00

itaipu parquetec

Dr. Daniel Augusto Cantane
Itaipu Parquetec

Documento assinado digitalmente
gov.br
HELTON FERNANDO SCHERER
Data: 19/12/2025 12:13:22-0300
Verifique em https://validar.iti.gov.br

Dr. Helton Fernando Scherer
UNILA

TERMO DE SUBMISSÃO DE TRABALHOS ACADÊMICOS

Nome completo do autor: Giovane Ronei Sylvestrin

Programa: Energia e Sustentabilidade - PPGIES

Tipo de Documento:

( ) graduação	( ) artigo
( ) especialização	( ) trabalho de conclusão de curso
( ) mestrado	( ) monografia
(**X**) doutorado	( ) exame de qualificação
	( ) dissertação
	(X) tese
	( ) CD/DVD – obras audiovisuais

Título do trabalho acadêmico: Aprendizado de Máquina Aplicado ao Prognóstico de Estado de Saúde de Células de Armazenamento de Energia.

Nome do orientador: Dr. Oswaldo Hideo Ando Junior.

Nome do Co-orientador: Dr. Joylan Maciel Nunes.

Data da Defesa: 31/10/2025

Licença não-exclusiva de Distribuição

O referido autor(a):

a) Declara que o documento entregue é seu trabalho original, e que o detém o direito de conceder os direitos contidos nesta licença. Declara também que a entrega do documento não infringe, tanto quanto lhe é possível saber, os direitos de qualquer outra pessoa ou entidade.

b) Se o documento entregue contém material do qual não detém os direitos de autor, declara que obteve autorização do detentor dos direitos de autor para conceder à UNILA – Universidade Federal da Integração Latino-Americana os direitos requeridos por esta licença, e que esse material cujos direitos são de terceiros está claramente identificado e reconhecido no texto ou conteúdo do documento entregue.

Se o documento entregue é baseado em trabalho financiado ou apoiado por outra instituição que não a Universidade Federal da Integração Latino-Americana, declara que

cumpriu quaisquer obrigações exigidas pelo respectivo contrato ou acordo.

Na qualidade de titular dos direitos do conteúdo supracitado, o autor autoriza a Biblioteca Latino-Americana – BIUNILA a disponibilizar a obra, gratuitamente e de acordo com a licença pública *Creative Commons* **Licença 3.0 Unported.**

Foz do Iguaçu, 31 de Outubro de 2025.

gov.br
Documento assinado digitalmente
GIOVANE RONEI SYLVESTRIN
Data: 22/12/2025 12:03:28-0300
Verifique em https://validar.iti.gov.br

_____

Assinatura do Responsável

RESUMO

O rápido crescimento dos veículos elétricos (EVs) intensifica a demanda por armazenamento e torna estratégica a reutilização de baterias em "segundo uso" para aplicações estacionárias. A viabilidade depende de estimativas confiáveis do estado de saúde (*State of Health*, SOH) e da vida útil remanescente (*Remaining Useful Life*, RUL) a partir de sinais de sensores em sistemas de gerenciamento. Esta pesquisa investiga abordagens baseadas em dados para diagnóstico e prognóstico de baterias e propõe um *pipeline* completo de modelagem para estimação de indicadores de saúde. A pesquisa avança em três eixos: (i) revisão sistemática com a metodologia *Proknow*-C, mapeando tendências recentes em *machine learning* (ML) e *deep learning* (DL) para SOH, consolidando um panorama de bases públicas; (ii) *framework* escalável e reprodutível de engenharia e seleção de atributos, com mais de 40 mil variáveis em sete grupos (carga/descarga gerais, corrente constante (CC), tensão constante (CV) e análises derivadas de capacidade incremental e tensão diferencial), combinando seleção univariada e multivariada para formar subconjuntos interpretáveis e de valor preditivo; e (iii) predição de RUL com histórico curto (6 ciclos) no *MIT Battery Dataset* ($LiFePO_4$/grafite), avaliando 12 arquiteturas DL *multibranch*/multicanal (CNN-LSTM/GRU) diretamente nas curvas de dados e em modelo tabular baseado em *boosting* de árvores de decisão, além de fusão por *stacking*. As principais contribuições incluem: (a) síntese crítica e replicável do campo de pesquisa com *Proknow*-C e levantamento de bases públicas; (b) *pipeline* de grande escala para extração e seleção com ênfase em janelas deslizantes e interpretabilidade; (c) demonstração de que a combinação *boosting* e DL permite estimar RUL de forma robusta com histórico curto de ciclos. Como resultados obteve-se: *framework* capaz de extrair um conjunto robusto de 773 atributos finalistas ao longo de 40 modelos, com predominância de janelas deslizantes (~88%); modelos de previsão de capacidade em múltiplos horizontes com MAPE (*Mean Absolute Percentage Error)* < 1%; e, com histórico curto, o *ensemble* por *stacking* alcançou MAPE ~6,0% e RMSE ~40,6 ciclos, superando modelos isolados e posicionando a abordagem no patamar superior da literatura recente. Esses resultados reforçam a aplicabilidade prática do método para acelerar triagem de segundo uso e apoiar decisões de manutenção com menor tempo de ensaio.

Palavras-chave: bateria, predição do estado de saúde, segundo uso, aprendizagem de máquina, redes profundas, engenharia de atributos.

RESUMEN

El rápido crecimiento de los vehículos eléctricos (EVs) intensifica la demanda de almacenamiento de energía y vuelve estratégica la reutilización de baterías en "segundo uso" para aplicaciones estacionarias. La viabilidad depende de estimaciones confiables del estado de salud (State of Health, SOH) y de la vida útil remanente (Remaining Useful Life, RUL) a partir de señales de sensores en sistemas de gestión de baterías. Esta investigación analiza enfoques basados en datos para el diagnóstico y el pronóstico de baterías y propone un pipeline completo de modelado para estimar indicadores de salud. El estudio avanza en tres ejes: (i) una revisión sistemática con Proknow-C, que mapea tendencias recientes en aprendizaje de máquina (ML) y aprendizaje profundo (DL) para SOH y sintetiza bases públicas; (ii) un marco escalable y reproducible de ingeniería y selección de atributos, con más de 40.000 variables en siete grupos (carga/descarga, corriente constante (CC), voltaje constante (CV), y análisis derivados de capacidad incremental y voltaje diferencial), combinando selección univariada y multivariada para formar subconjuntos interpretables; y (iii) predicción de RUL con historial corto (6 ciclos) en el MIT Battery Dataset ($LiFePO_4$/grafito), evaluando 12 arquitecturas DL multirrama/multicanal (CNN-LSTM/GRU) sobre curvas de datos y un modelo tabular con boosting de árboles, además de fusión por stacking. Las contribuciones incluyen una síntesis replicable del campo y un pipeline a gran escala con énfasis en ventanas deslizantes e interpretabilidad, mostrando que la combinación de boosting y DL permite estimar RUL con historial corto. Los resultados incluyen 773 atributos finalistas (predominio de ventanas deslizantes, ~88%), predicción de capacidad en múltiples horizontes con MAPE < 1% y, con historial corto, un ensemble por stacking con MAPE ~6,0% y RMSE ~40,6 ciclos, superando modelos individuales y situando el enfoque entre los mejores de la literatura reciente. Estos hallazgos refuerzan la aplicabilidad del método para acelerar la clasificación de segundo uso y apoyar decisiones de mantenimiento con menor tiempo de ensayo.

Palabras clave: batería; predicción del estado de salud; segundo uso; aprendizaje de máquina; redes profundas; ingeniería de atributos.

ABSTRACT

The rapid growth of electric vehicles (EVs) intensifies the demand for energy storage and makes the reuse of batteries in "second-life" applications for stationary systems a strategic option. Feasibility depends on reliable estimates of State of Health (SOH) and Remaining Useful Life (RUL) derived from sensor signals collected by battery management systems. This research investigates data-driven approaches for battery diagnosis and prognostics and proposes a complete modeling pipeline for estimating health indicators. The study advances along three axes: (i) a systematic review using the Proknow-C methodology, mapping recent trends in machine learning (ML) and deep learning (DL) for SOH and consolidating an overview of public datasets; (ii) a scalable and reproducible framework for feature engineering and selection, with more than 40,000 variables across seven groups (general charge/discharge, constant current (CC), constant voltage (CV), and analyses derived from incremental capacity and differential voltage), combining univariate and multivariate selection to form interpretable, predictive feature subsets; and (iii) short-history (6 cycles) RUL prediction on the MIT Battery Dataset ($LiFePO_4$/graphite), evaluating 12 multibranch/multichannel DL architectures (CNN-LSTM/GRU) directly on the data curves and a tabular model based on decision-tree boosting, as well as fusion via stacking. The main contributions include: (a) a critical and reproducible synthesis of the research field using Proknow-C and a survey of public datasets; (b) a large-scale extraction and selection pipeline emphasizing sliding windows and interpretability; and (c) evidence that combining boosting and DL enables robust RUL estimation with short cycle histories. Results include: a framework capable of extracting a robust set of 773 finalist features across 40 models, with a predominance of sliding-window features (~88%); multi-horizon capacity forecasting models with Mean Absolute Percentage Error (MAPE) < 1%; and, under short-history conditions, a stacking ensemble achieving MAPE ~6.0% and RMSE ~40.6 cycles, outperforming standalone models and placing the approach among the top tier of recent literature. These results reinforce the practical applicability of the method to accelerate second-life screening and support maintenance decisions with reduced testing time.

Keywords: battery; state-of-health prediction; second life; machine learning; deep learning; feature engineering.

LISTA DE FIGURAS

LISTA DE TABELAS

LISTA DE SIGLAS E ABREVIATURAS

AD	Base de Dados de Autores
AI	Artificial Intelligence (Inteligência Artificial)
ANN	Artificial Neural Network (Rede Neural Artificial)
API	Aplication Program Interfaces (Interface de Programação de Aplicativos)
ARIMA	Autoregressive Integrated Moving Average (Média Móvel Integrada Autorregressiva)
ATBLS	Adaptive Time-shifting Broad Learning System
AUTOML	Auto Machine Learning
BESS	Battery Energy Storage Systems (Sistemas de Armazenamento de Energia em Baterias)
BLS	Broad Learning System
BMA	Bayesian Model Averaging
BMLR	Bootstrap Multiple Linear Regression (Regressão Linear Múltipla por Bootstrap)
BNN	Bayesian Neural Network
BP	Bibliography Portfolio (Portfólio Bibliográfico)
BPNN	Back Propagation Neural Network (Rede Neural de Retropropagação)
CAPSNET	Capsule Neural Network
CC	Constant Current (Corrente Constante)
CDTSGANN	Conditional Time Series Generative Adversarial Network
CNN	Convolutional Neural Network (Rede Neural Convolucional)
CRNN	Convolutional Recurrent Neural Network
CV	Constant Voltage (Tensão Constante)
Dataset	Base de dados
DBN	Deep Belief Network
DBNN	Deep Bayesian Neural Network
DCN	Deep Cross Net
DCNN	Deep Convolutional Neural Network
DELM	Deep Elman Neural Network
DGNN	Deep Gaussian Neural Network
DL	Deep Learning
DNN	Deep Neural Network
DRN	Dilated Residual Network
DSMTNET	Dual Self-Attention Multivariate Time Series Estimation Network
DT	Decision Tree (Árvore de Decisão)
ELM	Extreme Learning Machine
ENN	Elman Neural Network
EoL	Endo of Life
EV	Eletrical Vehicle (Veículo Elétrico)
FCNN	Fully Connected Neural Network

Feature	Variável
FFNN	Feedforward Neural Network
GAM	Generalized Additive Model (Modelo Aditivo Generalizado)
GBT	Gradient Boosting Tree
GNN	Graph Neural Network
GRU	Gated Recurrent Unit
GPR	Gaussian Process Regression (Regressão por Processo Gaussiano)
IOWA	Induced Ordered Weighted Averaging
KNN	K-Nearest Neighbors (K-Vizinhos Mais Próximos)
LR	Linear Regression (Regressão Linear)
LSTM	Long Short-Term Memory
MAE	Median Absolute Error (Erro Absoluto Mediano)
MAPE	Mean Absolute Percentage Error (Erro Percentual Absoluto Médio)
MLP	Multi-Layer Perceptron (Perceptron de Múltiplas Camadas)
ML	Machine Learning (Aprendizado de Máquina)
NAR	Nonlinear Autoregressive (Autorregressivo Não Linear)
NARXNN	Nonlinear Autoregressive with Exogenous Input Neural Network
PKNN	Prior Knowledge-Based Neural Network
QRF	Quantile Regression Forest
RBFNN	Radial Basis Function Neural Network
RESNET	Residual Network
RF	Random Forest (Floresta Aleatória)
RMN	Regressive Matching Network
RNN	Recurrent Neural Network (Rede Neural Recorrente)
RPD	Raw Papers Database (Banco de Dados de Artigos Brutos)
RVM	Relevance Vector Machine
SOC	State of Charge (Estado de Carga)
SOH	State of Health (Estado de Saúde)
SVM/SVR	Support Vector Machine / Regressor (Máquina de Vetores de Suporte / Regressor)
SSEL	Secondary Structural Ensemble Learning
TCN	Temporal Convolution Network
TNN	Transformer Neural Network
TL	Transfer Learning (Aprendizado por Transferência)
UNN	Unsupervised Neural Networks (Redes Neurais Não Supervisionadas)
VTN	Vision Transformer Network

SUMÁRIO

1. INTRODUÇÃO

O rápido avanço na utilização de baterias elétricas vem sendo impulsionado principalmente pelo aumento do setor de veículos elétricos (EVs) (H. Li et al., 2017). Segundo relatório da Agência Internacional de Energia (IEA), a frota de EVs em 2023 foi de cerca 45 milhões, com prospecção de que esse número aumente para cerca de 250 milhões em 2030 e 525 milhões em 2035, com 1 a cada 4 veículos sendo elétrico, um crescimento anual de 23% entre 2023 e 2035 (International Energy Agency, 2024). A demanda por baterias de EVs alcançou mais de 750 GWh em 2023, um aumento de 40% em relação a 2022. Estima-se que essa demanda deva crescer quatro vezes e meia até 2030 e quase sete vezes até 2035 em comparação com 2023 (International Energy Agency, 2024). O armazenamento estacionário também aumentará a demanda por baterias, representando cerca de 500 GWh em 2030, o que corresponde a cerca de 12% da demanda total de baterias de EVs (International Energy Agency, 2024). No Brasil, a frota de veículos leves eletrificados superou 300 mil unidades em 2024, mais que dobrando em relação a 2022, com projeções para 3,7 milhões em 2035, representado cerca de 23% da frota de veículos (ABVE, 2025; Fapesp, 2023). A demanda nacional por baterias deve saltar de cerca de 7,1 GWh em 2025 para 20 GWh em 2035 (EPE, 2024).

No contexto automotivo, considera-se fim de vida (*End of Life*, EoL) quando a capacidade de armazenamento decai a cerca de 80% da capacidade nominal (L. Zhang et al., 2020). Embora inadequadas para o uso veicular, essas baterias permanecem utilizáveis em aplicações estacionárias, fomentando aplicações de segundo uso em sistemas de energia (Reinhardt et al., 2019). A chave para operação, manutenção, e para reutilizar essas baterias de forma eficaz reside no prognóstico da saúde da bateria, indicado principalmente por medidas como estado de saúde (*State of Health*, SOH) e vida útil remanescente (*Remaining Useful Life*, RUL) (Lai et al., 2021; Reinhardt et al., 2019). A montagem de baterias de segundo uso depende da combinação de células com estágios de vida semelhantes para garantir o funcionamento adequado e a segurança da tecnologia (Lai et al., 2021; Reinhardt et al., 2019).

Para prognóstico de saúde, as metodologias dividem-se, principalmente, em eletroquímicas, modelos físicos e circuitos elétricos equivalentes (*Equivalent Circuit Model*, ECM), e baseadas em dados (*data-driven*) (Ge et al., 2021; Y. Li et al., 2019a; Shahjalal et al., 2022; Vidal et al., 2020). Abordagens eletroquímicas incluem análises de tensão-capacidade e espectroscopia de impedância eletroquímica (*Electrochemical*

Impedance Spectroscopy, EIS), que costumam ser precisas em ambiente laboratorial controlado, porém menos viáveis em aplicações reais por caráter invasivo e custo (Barré et al., 2013; Bloom et al., 2005a; L. Zhang et al., 2024). Uso de ECMs e filtros adaptativos como o de Kalman e derivados geram estimativas interpretáveis, mas exigem parametrização cuidadosa e são onerosas computacionalmente (Daigle & Kulkarni, 2013; Plett, 2004). Por fim, o uso da abordagem de dados, utilizando aprendizado de máquina (*machine learning*, ML) e redes profundas (*deep learning*, DL), surge com a capacidade de capturar relações não-lineares de sinais padrão (tensão, corrente, temperatura), mas dependem de dados rotulados, amostras consistentes, e enfrentam desafios de generalização e interpretabilidade (Ge et al., 2021; Y. Li et al., 2019a; Shahjalal et al., 2022; Vidal et al., 2020).

Os incrementais avanços em computação e capacidade de processamento, sensoriamento inteligentes e a era do *Big Data* abriram caminho para a exploração do uso da inteligência artificial na abordagem baseada em dados (Severson et al., 2019a; Wang et al., 2021). O volume de pesquisas relacionadas à estimativa do SOH usando ML está em ascensão. Baseado no levantamento do estado da arte realizado (Sylvestrin et al., 2025a), observou-se um aumento de vinte vezes no número de publicações relevantes entre 2018 e 2023.

Uma das primeiras pesquisas de impacto na predição RUL de baterias usando ML, (Severson et al., 2019a) utilizou algoritmo de regressão linear para estimar os ciclos restantes de uma bateria após os 100 ciclos inicias, considerando pouco mais de uma dezena de variáveis, obtendo erros médios percentuais de cerca de 10¨%. Algoritmos mais complexos, que conseguem melhores interpretações em grandes volumes de dados, baseados em DL, como LSTM (*Long Short-Term Memory*) e CNN (*Convolutional Neural Network),* podem melhorar a precisão do prognóstico de saúde, podendo reduzir os erros a valores inferiores a 5%, como demonstrado em (Y. Yang, 2021). As pesquisas apresentadas em (Hossain Lipu et al., 2022; Luo et al., 2022; Zhao, Han, et al., 2023) exploram técnicas de DL para previsão RUL, enquanto em (Liu et al., 2023), utiliza técnicas baseadas em *Transfer Learning*.

Outro aspecto relevante para melhor performance do diagnóstico de saúde é a engenharia de variáveis. A capacidade informativa dos atributos é determinante para performance e generalização (Y. Li et al., 2019b; Zhao, Ling, et al., 2023). Contudo, grande parte dos estudos com *data-driven* utilizam conjuntos restritos de variáveis

baseados no domínio do conhecimento prévio, geralmente poucas dezenas, focados em trechos específicos dos regimes de carga e/ou descarga (Gong et al., 2022b; C. Hu et al., 2014; G. Li et al., 2023; Roman et al., 2021a; Yao et al., 2023; Y. Zhang et al., 2022). Uma linha influente explora a relação entre a capacidade e tensão, Q(V), e seus diferenciais correspondentes a capacidade incremental (IC, dQ/dV) e tensão diferencial (DV, dV/dQ) como indicadores de mecanismo de diagnóstico e predição da saúde (Bloom et al., 2005b; Dubarry et al., 2012; Gong et al., 2022a; Severson et al., 2019b; Xu et al., 2023).

A literatura indica avanços rápidos em abordagens baseadas em dados (ML/DL), porém persistem lacunas: (i) escopo restrito e pouco reprodutível de atributos, com em geral algumas dezenas de variáveis implementadas; (ii) integração limitada de múltiplos domínios de atributos sob uma mesma estrutura; (iii) escassez de *pipelines* escaláveis que combinem seleção multivariada robusta e interpretabilidade; e (iv) viabilidade prática com histórico curto de ciclos, reduzindo custo e tempo de ensaio (Gong et al., 2022b; C. Hu et al., 2014; G. Li et al., 2023; Roman et al., 2021a; Yao et al., 2023; Y. Zhang et al., 2022).

Dada as capacidades preditivas que modelos de ML/DL podem apresentar, e as necessidades de reuso de baterias, esta pesquisa busca responder às lacunas da literatura propondo e avaliando um *pipeline* reprodutível que integra extração massiva de atributos multi-domínio, seleção multietapas orientada por modelo e interpretabilidade, além de arquiteturas DL *multibranch* e *ensembles* por *stacking*, com foco no prognóstico RUL e capacidade futura (SOH indireto) usando dados públicos e histórico reduzido.

1.1. OBJETIVO GERAL E OBJETIVOS ESPECÍFICOS

Esta pesquisa tem como objetivo propor e validar um *pipeline* reprodutível para prognóstico de SOH e RUL de baterias, a partir de sinais padrão de BMS, combinando extração de atributos e modelos de aprendizado de máquina em cenários de histórico curto e amplo.

Para isso os seguintes objetivos específicos são definidos:

1) Conduzir revisão sistemática e quantitativa do estado da arte em SOH/RUL com ML/DL para caracterizar o atual cenário na literatura científica;
2) Projetar e implementar *pipeline* de engenharia de atributos multi-domínio e seleção multietapas, integrando processos uni e multivariados. Tal *pipeline* pode ser utilizado no desenvolvimento de banco de variáveis para utilização em modelos de ML relacionados a saúde de baterias;

3) Desenvolver modelos de predição da capacidade N ciclos a frente (SOH indireto em termos de capacidade) em diferentes janelas de tempo;
4) Desenvolver e avaliar modelos para predição de RUL com histórico curto de 6 ciclos utilizando (i) modelo de *boosting* e, (ii) arquiteturas DL *multibranch* com CNN1D/2D+LSTM/GRU, com variantes bi-direcionais e uso de atenção/concatenação;
5) Analisar ganhos de desempenho através de *stacking* de modelos de DL com *boosting* de árvore de decisão, reportando métricas centrais e estratificadas por faixas de RUL e SOH para entender o perfil das predições;
6) Validar a performance das abordagens de modelagem implementadas com relação as produções da literatura específica.

1.2. JUSTIFICATIVAS E RELEVÂNCIA

A escala de adoção de baterias pressiona requisitos de segurança, confiabilidade e custo, enquanto a economia circular demanda triagem eficiente para segundo uso (Elliott et al., 2020). Estimar SOH e RUL com sinais comuns de sensores presentes em BMS reduz a necessidade de ensaios invasivos e viabiliza caracterização das baterias.

Entretanto, a falta de *pipelines* reprodutíveis que integrem múltiplos domínios de informação e operem com janelas históricas curtas limita a transferência para a prática. Esta pesquisa aborda esses pontos ao unificar engenharia de atributos em larga escala, seleção multivariada com interpretabilidade e integração DL/*boosting*, visando implantação em BMS e ensaios laboratoriais com menor duração.

O impacto esperado inclui: (i) redução de tempo/custo de caracterização; (ii) triagem acelerada para segundo uso; (iii) manutenção preditiva mais precisa; e (iv) base comparável e reutilizável para estudos subsequentes.

1.3. CONTRIBUIÇÃO DA TESE

Esta pesquisa contribui com um conjunto integrado de resultados científicos, metodológicos e práticos para a estimação de SOH e RUL em baterias de íons de lítio de base de dados pública, com foco em reprodutibilidade, interpretabilidade e aplicabilidade sob histórico curto de dados, de forma que destaca-se:

- Revisão sistemática replicável (*Proknow*-C) de SOH/RUL com ML/DL, mapeando tendências de implementações de modelos, lacunas e bases

públicas disponíveis, atualizando o estado da arte no tema de pesquisa.

- *Pipeline* reprodutível de extração de atributos multi-domínio (sinais brutos e derivadas) com alta volumetria.
- Seleção de variáveis multietapas orientada por modelo com interpretabilidade, extraindo subconjuntos compactos e informativos, aptos para composição de banco de variáveis e uso em modelos.
- Aplicação do *pipeline* em base de dados pública, com a implementação de mais de 40 modelos para predição de capacidade futura (SOH) e RUL
- Implementação sob histórico curto para RUL considerando modelos de *boosting* de árvores de decisão e 12 arquiteturas híbridas de DL *multibranch*/multicanais (CNN1D/2D + LSTM/GRU), com estrutura ainda não explorada na literatura.
- Implementação de *ensemble* baseado em *stacking* para predição RUL considerando fusão de modelos DL com *boosting*, superando modelos isolados e frente a abordagens da literatura com significativa redução de ciclos de histórico.
- Avaliação abrangente com análises por segmentação de RUL/SOH e comparação com referências da literatura.

1.4. ORIGINALIDADE DA TESE

Os aspectos de originalidade desta pesquisa baseiam-se nos seguintes pontos elencados a seguir:

Revisão sistemática replicável (*Proknow*-C) aplicada a SOH/RUL: até onde alcança nossa revisão, é a primeira aplicação estruturada do *Proknow*-C ou método sistemático análogo de obtenção de portfólio bibliográfico especificamente para estimação de SOH/RUL com ML/DL.

***Pipeline* unificado de engenharia de variáveis em larga escala**: geração padronizada de mais 40 mil atributos a partir de sinais brutos, integrando domínios e construções temporais. A volumetria inicial de variáveis considera o uso de 100 ciclos de histórico, valor comum encontrado na literatura principalmente para estimação de ciclos de vida antecipada, entretanto, mesmo para histórico curto, o *pipeline* proposto é capaz de extrair variáveis em uma volumetria em escala muito acima da praticada nas pesquisas recentes consultadas (Gong et al., 2022a; X. Hu et al., 2021a; Roman et al., 2021a; Xu et

al., 2023; F. Yang et al., 2020; Y. Zhang et al., 2022), aumentando um campo de atributos de cerca de dezenas para dezenas de milhares.

Estratégia multietapas de seleção de atributos: combinação integrada de correlação, escore de predição, modelos univariados, interpretabilidade SHAP, seleção *forward*, *frameworks BorutaShap* e MRMR, conciliando relevância individual e complementaridade multivariada para reduzir o espaço massivo a conjuntos compactos e interpretáveis de variáveis.

Predição de RUL com histórico curto em *multibranch* DL: implementação e comparação de arquiteturas CNN1D/2D+LSTM/GRU que exploram múltiplas sequências em paralelo, mostrando viabilidade e competitividade sem exigir longos históricos, cenário aderente ao uso real em BMS e testes de caracterização/manutenção.

Fusão modelo *boosting* com DL por *stacking*: integração de predições DL com *boosting* (LightGBM), demonstrando ganhos consistentes sobre modelos isolados e estabelecendo um caminho prático para *ensembles* em dados de baterias.

Evidência empírica do valor de janelas deslizantes: demonstração sistemática de que descritores temporais curtos dominam os conjuntos finalistas de variáveis em modelos baseados em dados tabulares, oferecendo um novo entendimento sobre quais sinais agregam capacidade preditiva.

1.5. CONSIDERAÇÕES FINAIS

Nesta seção apresentou-se uma introdução à temática da pesquisa, apresentando uma contextualização da importância da predição do SOH/RUL dentro do cenário atual de expansão do uso de baterias elétricas. Em seguida descreveu-se o objetivo, as justificativas e a relevância, conjuntamente com as contribuições e os aspectos de originalidade deste estudo. A próxima seção apresenta o delineamento metodológico e descrição do sistema proposto.

2. DELINEAMENTO METODOLÓGICO

Esta seção apresenta o delineamento metodológico desta pesquisa considerando a metodologia planejada, o método da proposta, as ferramentas e tecnologias empregadas no projeto, e o descritivo do sistema proposto.

Por meio da configuração metodológica, do método e atividades apresentadas a seguir, pretende-se atender ao objetivo geral da pesquisa que consiste em desenvolver, analisar e validar um *pipeline* para implementação de modelos de ML/DL, de forma reprodutível e escalável para prognóstico da saúde de baterias em SOH e RUL.

2.1. METODOLOGIA DE PESQUISA

O crescimento do uso de baterias e a necessidade de reaproveitamento em segunda vida exigem estimativas confiáveis de SOH e RUL (Lai et al., 2021; Shahjalal et al., 2022). A literatura recente indica desempenho superior de abordagens *data-driven* (ML/DL) (Y. Li et al., 2019a; Z. Ren & Du, 2023; Shu et al., 2021), porém carece de *pipelines* reprodutíveis e escaláveis que integrem extração massiva de atributos a partir de sinais padrão medidos em baterias, seleção sistemática e multivariada de variáveis. Além disso, permanece em aberto se é possível reduzir o histórico de ciclos recentes exigido para predição sem perda de desempenho, o que é crítico para aplicações práticas.

Sendo assim, define-se nesta pesquisa as seguintes hipóteses: (i) um pipeline estruturado, sistemático e reprodutível de engenharia e seleção multietapas de atributos melhora a precisão, reprodutibilidade e a escalabilidade na estimação de SOH/RUL; (ii) a integração de diferentes domínios de informação (sinais brutos e analises derivadas) supera o uso isolado/limitado de atributos; (iii) é possível reduzir a janela histórica utilizada em prognóstico de saúde sem perda significativa de desempenho.

Com o intuito de verificar tais hipóteses, a metodologia científica adotada neste estudo se enquadra na seguinte classificação de (Gil, 2002):

Natureza: trata-se de uma pesquisa aplicada, uma vez que visa gerar conhecimentos para aplicação prática no desenvolvimento de um *pipeline* reprodutível e escalável aplicada a algoritmos de ML e DL para prognóstico de saúde de baterias. Essa ferramenta é direcionada à solução de problemas de monitoramento e manutenção de sistemas de baterias em operação e na triagem de baterias de segundo uso.

Forma de abordagem do problema: a pesquisa adota uma abordagem quali-quantitativa. Do ponto de vista quantitativo, será realizada a análise estatística do

desempenho dos modelos de ML/DL obtidos considerando o desempenho de publicações na literatura em dados abertos, bem como as variações de modelos implementadas. No aspecto qualitativo, serão avaliados aspectos como a aplicabilidade, adaptabilidade e escalabilidade para desenvolvimento de modelos.

Objetivo: avaliativo-explicativo com componente exploratório. Avalia ganhos de desempenho e explica contribuições de grupos de variáveis/arquiteturas, oferecendo passos sistemáticos para acelerar estudos de diagnóstico e prognóstico de saúde em baterias.

Procedimentos técnicos: utiliza-se de pesquisa bibliográfica para fundamentar o desenvolvimento do processo de estruturação e implementação do *pipeline* de modelagem, e quais algoritmos tendem a oferecer melhor desempenho. Além disso, são realizadas análises estatísticas e de interpretabilidade nos modelos desenvolvidos, através de estudos de aplicação do *pipeline* proposto considerando base de dados pública com considerável uso em outras pesquisas.

2.2. MATERIAIS E TECNOLOGIAS

A solução proposta desenvolve e aplica um *pipeline* reprodutível de extração e seleção em larga escala de atributos, integrando diferentes domínios para modelos *data-driven* de prognóstico, com predição de RUL e SOH indiretamente via capacidade futura utilizando algoritmos de ML e DL.

Para o desenvolvimento da pesquisa escolheu-se a linguagem de programação *Python* que apresenta alto nível de abstração e disponibilidade de bibliotecas e Interfaces de Programação Aplicada (APIs) úteis para projetos que envolvem temática de ciência de dados. Diversos outros recursos são utilizados no projeto e a Tabela 1 exibe os principais equipamentos e tecnologias.

Versão das bibliotecas utilizadas, considerando ambiente *Python* 3.10: *pandas 2.3.2, scikit-learn 1.7.1, pytorch 2.5.1, CUDA 11.8, lightgbm 3.3.2, scipy 1.15.3, pyarrow 21.0.0, h5py 3.14.0, zarr 2.18.3, optuna 4.5.0.*

Tabela 1: Tecnologias, equipamentos e dados empregadas nesta pesquisa.

#	Categoria	Ferramenta	Descrição
1	Linguagem de Programação	*Python*	Linguagem principal dos scripts (pipeline, modelagem e análise).
2	Bibliotecas *Python*	*pandas, numpy, scipy, scikit-learn, lightgbm, PyTorch, pyarrow, zarr, h5py, optuna*	Bibliotecas para a implementação de modelos de ML/DL, pré-processamento, treinamento/otimização de modelos e análise de dados.
3	Ambiente de Desenvolvimento	*Jupyter Notebook* e *scripts Python*	Ambiente interativo de desenvolvimento e execução de códigos.
4	Controle de versões e experimentos	*Git e MLflow*	Versionamento de código/artefatos; rastreamento de métricas, parâmetros e modelos.
5	Armazenamento de dados/variáveis	*Parquet/Arrow, Zarr; SQLite*	Bancos de dados relacionais para armazenamento de variáveis e gerenciamento de dados estruturados (logs de otimização).
6	Ambientes Virtuais	*Conda*	Ferramentas para criar ambientes de desenvolvimento isolado.
7	Equipamentos	*Workstation*	CPU Intel® Core™ i7-13650HX (13ª geração, 2,60 GHz), 16 GB de RAM e GPU NVIDIA GeForce RTX 3050 6 GB de memória dedicada, driver 32.0.15.7261.
8	Fontes de Dados	*MIT Battery Dataset (Severson et al., 2019b)*	Conjuntos de dados de baterias disponíveis publicamente, utilizados para treinar e validar os modelos de prognóstico.

2.3. DESCRITIVO DO SISTEMA PROPOSTO

O desenvolvimento desta pesquisa organiza-se em três etapas interligadas, apresentadas na Figura 1, cada uma correspondendo a um artigo do portfólio da pesquisa.

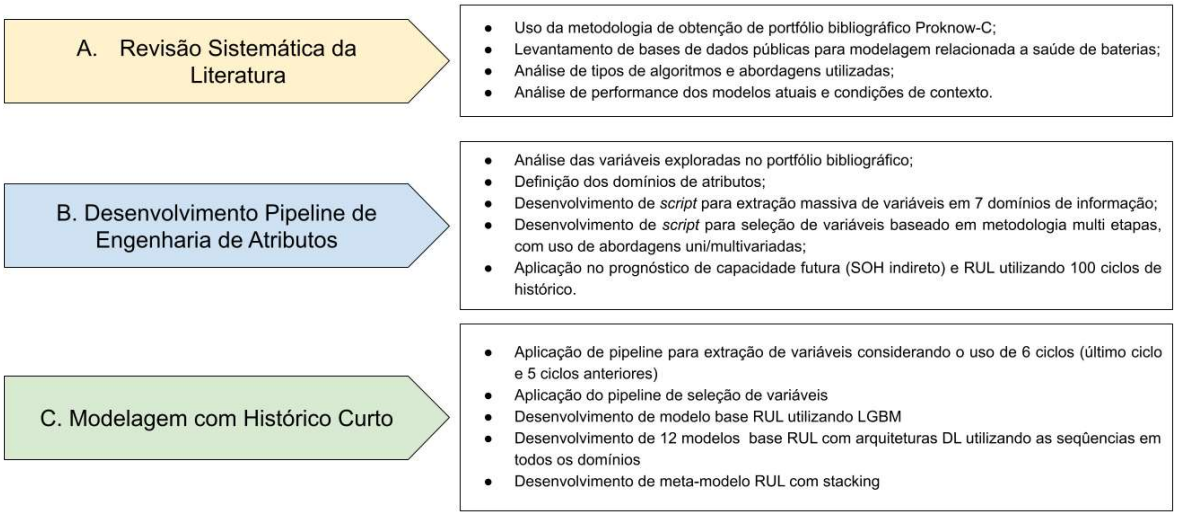

Figura 1: Fluxo geral de desenvolvimento aplicado na pesquisa. Fonte: O Autor, (2025).

Etapa A – Revisão sistemática (*ProKnow*-C).

Corresponde ao levantamento e filtragem de um portfólio bibliográfico sobre abordagens *data-driven* para SOH empregando Proknow-C. A Figura 2 apresenta a

primeira parte do fluxo utilizado nesta pesquisa, com as volumetrias de descarte e seleção dos artigos na etapa de alinhamento de título e reconhecimento científico. Um banco de artigos brutos (BAB) de 6.032 artigos obtido por 192 combinações entre palavras-chave de distintos eixos na base *Scopus*, tem seus artigos analisados quanto a duplicações, removendo 4.682 amostras. A etapa de alinhamento de título faz a remoção de 722 amostras, as quais são divididas em dois repositórios intermediários: alta citação (K) e baixa citação (P).

A segunda parte do fluxo, Figura 3, inicia com a análise dos repositórios intermediários. Os resumos dos artigos presentes no repositório K são analisados, onde nas amostras selecionadas, são extraídos os autores para criação do banco de autores (PB) e compõem o repositório finalista A. No repositório P, para os artigos mais recentes, os resumos são analisados, enquanto publicações mais antigas e com baixa relevância em citações passam pela etapa de verificação se um ou mais autores da amostra está presente em BA, caso esteja presente, o resumo é analisado. A junção dos artigos selecionados forma o repositório finalista B. O portfólio final é a junção dos repositórios A e B, compostos por 534 artigos (~9% da BAB).

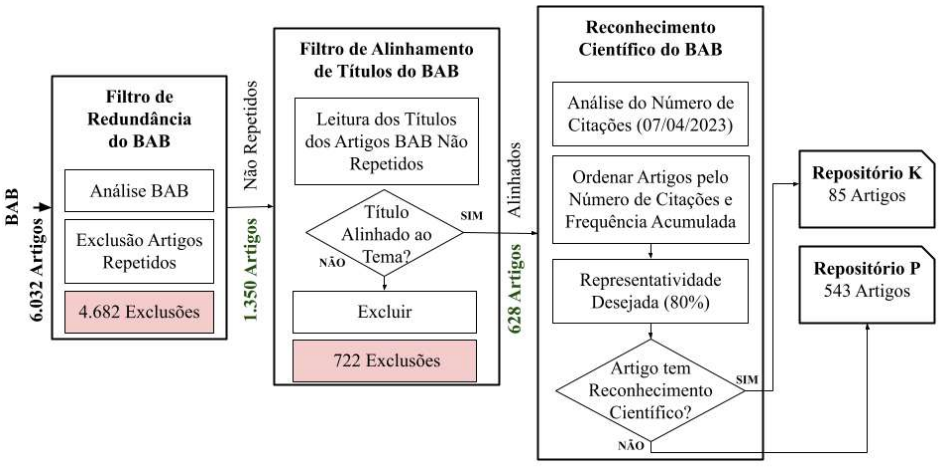

Figura 2: Obtenção de portfólio bibliográfico com Proknow-C: parte 1. Fonte: O Autor, (2025).

Baseado nesse portfólio, a análise bibliométrica e sistêmica identifica tendências como prevalência de DL (LSTM/CNN), uso crescente de bases públicas, e, sobretudo, a lacuna de *pipelines* reprodutíveis e escaláveis que integrem múltiplos domínios de informação e conectem extração/seleção de atributos à modelagem. Os detalhes da metodologia, análises e resultados são detalhados no Artigo I presente no Apêndice A.1.

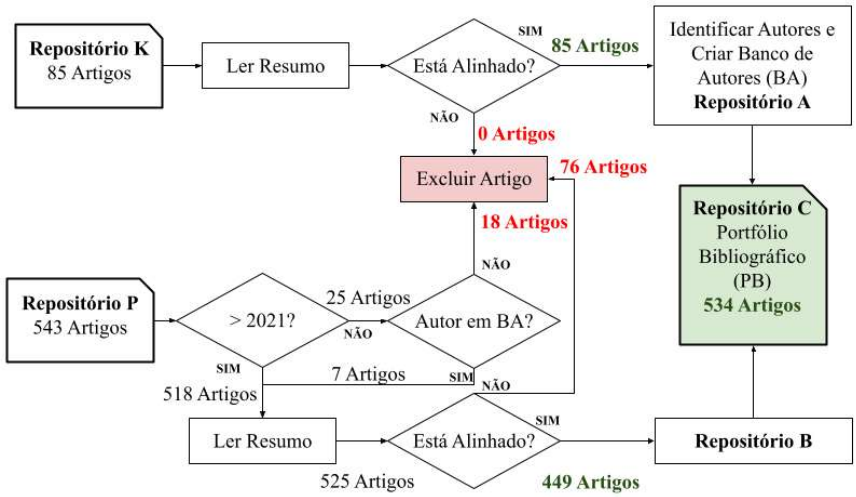

Figura 3: Obtenção de portfólio bibliográfico com Proknow-C: parte 2. Fonte: O Autor, (2025).

Etapa B – *Pipeline* tabular de engenharia/seleção de atributos e modelagem.

A partir das lacunas mapeadas, propõe-se, desenvolve-se e valida-se um *pipeline* reprodutível de extração massiva e seleção multietapas de atributos, integrado à modelagem para prognóstico de capacidade futura e RUL. Considera-se o uso da base de dados *MIT Battery Dataset*, composta por 124 células de $LiFePO_4$/grafite.

São explorados ao todo 7 grupos de atributos presentes na análise do estado da arte de forma isolada: carga geral, descarga geral, segmentos de carga CC e CV, análises derivadas de capacidade incremental e tensão incremental. São empregados processos de agregação estatística sobre os ciclos e conjuntos de ciclos, análise de diferenças entre medidas entre ciclos, atrasos e janelas deslizantes. Considerando um histórico de 100 ciclos, o *pipeline* pode extrair mais de 40 mil variáveis para modelagem.

O *pipeline* para seleção de variáveis e modelagem tabular é apresentado na Figura 4. Cada grupo de atributos passa pela etapa de pré-seleção. Na análise univariada são obtidas informações a respeito de: correlação de Spearman, PPS (*power predective score)*, performance em modelos uni-variável. Na parte multivariada, cada grupo é utilizado na implementação de um modelo de *boosting*, com o objetivo de obter as variáveis mais importantes, processo que permite a avaliação considerando possíveis iterações entre atributos. As melhores variáveis presentes nas análises iniciais uni e multivariada formam o grupo de pré-seleção.

Na etapa seguinte o conjunto de variáveis pré-selecionado é entrada na implementação de um modelo geral, onde após treinamento, as variáveis que estão presentes em 90% do impacto SHAP acumulado são selecionadas. Um modelo reduzido

agora é treinado, e aplica-se uma seleção de variáveis do tipo *forward*. As variáveis selecionadas no *forward* são entradas para o modelo prévio final. Para as variáveis rejeitadas, avalia-se o poder preditivo considerando dois métodos implementados nos *frameworks BorutaShap* e MRMR, onde os atributos comprovados como relevantes são encaminhados para um processo de repescagem considerando as variáveis finalistas no modelo prévio. Uma a uma as variáveis de repescagem são analisadas na adição ao conjunto de variáveis, e em caso de uma variável agregar em termos de performance, é selecionada. Ao final da tentativa de repescagem, se uma ou mais variáveis é adicionada, um novo processo de treinamento é realizado, obtendo assim um modelo finalista.

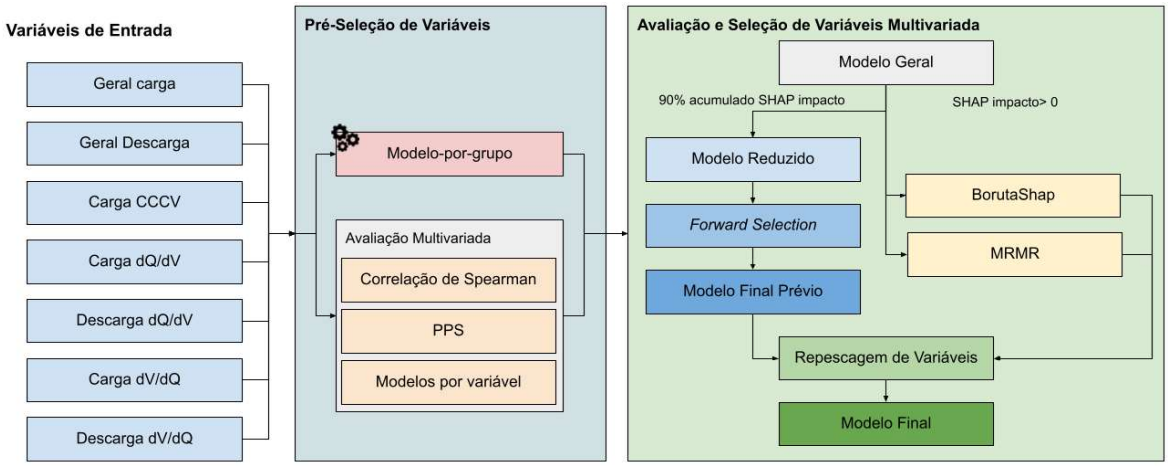

Figura 4: *Pipeline* de extração e seleção de variáveis proposto. Fonte: O Autor, (2025).

Esse processo é detalhado no Artigo II presente no Apêndice A.2. Apresenta-se com detalhe o processo de extração e análise das variáveis, com aplicação do *pipeline* completo em mais de 40 modelos para predição do RUL e capacidade futura em 10, 50, 100 e 250 ciclos a frente.

Etapa C – Modelagem considerando histórico curto, DL *multibranch* e *ensemble* por *stacking*

Etapa que visa desenvolver e analisar o prognóstico RUL com histórico curto considerando: (i) aplicação do *pipeline* de engenharia de atributos da Etapa B para um histórico de 6 ciclos (ciclo atual + 5 *lags*) e modelo de *boosting* LGBM; (ii) 12 variações de arquitetura DL *multibranch*/multicanais (CNN1D/2D + LSTM/GRU), integrando todas as sequências/curvas dos domínios de variáveis explorados pela extração de atributos tabular; (iii) desenvolvimento de *ensembles* por *stacking*.

Na Figura 5 apresenta-se o fluxo geral para os desenvolvimentos dos modelos base e meta considerados. Inicia-se com a extração das sequências e variáveis (bloco A). A

base de dados do MIT é devidamente segmentada para treinamento dos modelos base, meta e avaliação de performance final, teste. Para os modelos base (bloco B), o modelo base LGBM segue o *pipeline* desenvolvido na etapa B anterior, enquanto que os modelos base de DL consideram a estrutura apresentada na Figura 6.

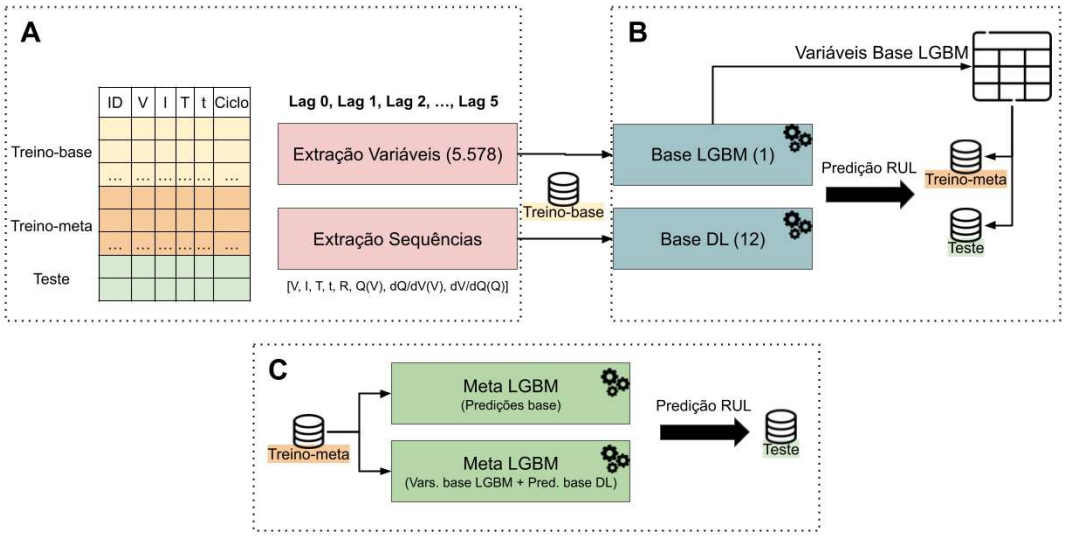

Figura 5: Esquema geral de desenvolvimento da modelagem. Fonte: O Autor, (2025).

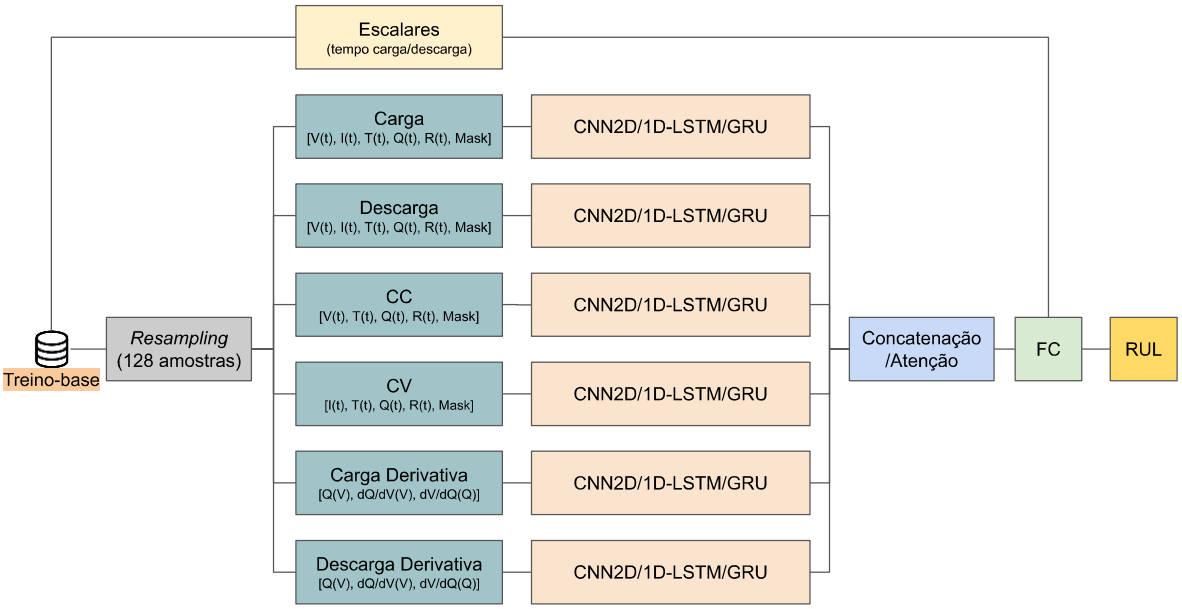

Figura 6: Implementação modelos base de DL. Fonte: O Autor, (2025).

Nas arquiteturas *multibranch*, diferentes grupos de sequências (por exemplo, carga, descarga e curvas derivativas) são processados em ramos paralelos, cada um com uma sub-arquitetura dedicada. As saídas dos ramos são então fundidas (por concatenação ou mecanismos de atenção) e encaminhadas para camadas densas *fully-connected* responsáveis pela predição do RUL. Sobre essas predições, modelos meta do tipo LGBM são treinados em regime de *stacking*, considerando tanto combinações de predições dos

modelos base quanto, em uma segunda abordagem, a integração entre variáveis tabulares finalistas e predições de redes DL selecionadas.

Os detalhes específicos de implementação, como número de variações de arquitetura, configuração dos ramos e canais, tamanho das sequências e parametrizações dos modelos – são apresentados no Artigo III, no Apêndice A.3.

2.4. CONSIDERAÇÕES FINAIS

Esta seção descreveu o *pipeline* completo para implementação de modelos ML/DL de forma reprodutível e escalável visando prognóstico RUL e SOH (via capacidade futura). As Etapas A-C correspondem aos três artigos científicos que, em conjunto, preenchem lacunas de reprodutibilidade, integração de domínios e histórico curto, contribuindo para aplicações práticas em BMS, manutenção preditiva e triagem para segunda vida. A seção seguinte apresenta o desenvolvimento deste projeto, considerando a contextualização de cada artigo desenvolvido, sua relevância, conexão e lacunas compreendidas.

3. DESENVOLVIMENTO

Esta seção apresenta as produções científicas desenvolvidas durante a pesquisa, contextualizando sua relevância, as conexões entre si e as lacunas que buscam preencher. A trajetória que conduziu ao objeto da pesquisa atual é apresentada nas produções correlatas na Tabela 2. Iniciou-se pela compreensão dos sistemas de armazenamento de energia (SAE), suas tecnologias, aplicações e métricas de desempenho, e avançou para a estimação do estado de carga (*State of Charge*, SOC), cobrindo da instrumentação e coleta de sinais ao desenvolvimento de BMS e ao uso de estimadores de estado. Dessa forma, a estimação de SOH tornou-se o passo natural para caracterizar a saúde das baterias e, por consequência, quantificar vida útil remanescente, elemento decisivo para manutenção e reaproveitamento em segundo uso.

Tabela 2: Produções correlatas à pesquisa.

Ano	Tipo	Título	Eixo temático	Contribuição/resultado	Ref.
2020	Capítulo livro	Fundamentos sobre Sistema de Armazenamento de Energia	Fundamentos de SAE, tecnologias e operação	Síntese técnica das tecnologias e arquiteturas de armazenamento; citado em documentação técnica "Armazenamento de Energia Elétrica" da ANEEL (ANEEL, 2022).	(Cantane et al., 2020)
2020	Capítulo livro	Avaliação do Desempenho dos Sistemas de Armazenamento de Energia	Métricas e critérios de desempenho	Caracterização do cenário de desempenho de diferentes tecnologias aplicadas ao armazenamento em sistemas estacionários. citado em documentação técnica "Armazenamento de Energia Elétrica" da ANEEL (ANEEL, 2022).	(Cantane et al., 2020)
2021	Capítulo livro	*Roadmap* tecnológico de sistemas de armazenamento de energia	Tendências e maturidade tecnológica	Mapa de rotas tecnológicas dos sistemas de armazenamento com análise SWOT (forças, fraquezas, oportunidades e ameaças).	(Souza, 2020)
2021	Artigo	*Hardware and Software Development of an Open Source Battery Management System*	Instrumentação e aquisição de dados de operação de bateria elétrica	Desenvolvimento de BMS *open-source*, adaptativo e de baixo custo (até 10 células em série) com hardware/software próprios para monitorar V/I/T e SOC, operando com múltiplas químicas (Li-ion 18650 e Na-$NiCl_2$). Integra telemetria/IoT (Node-RED + IBM Watson), com versatilidade para aplicações em pesquisa e cenários laboratoriais onde BMS comerciais são restritivos.	(Sylvestrin et al., 2021)
2022	Artigo	*Experimental Validation of State of Charge Estimation by Extended Kalman Filter and Modified Coulomb Counting*	Estimação do estado de carga	Implementação e validação de EKF embarcado em BMS de baixo custo para estimação de SOC, atingindo erro máximo ~4%. Proposta de Contagem de Carga Modificada, que usa parâmetros do EKF para lidar com SOC inicial desconhecido e reduzir flutuações, levando o erro máximo a <1% em vários cenários com trade-off precisão-simplicidade.	(Sylvestrin et al., 2022)

Esses aprendizados revelaram que o prognóstico em escala requer modelos que: (i) usem sinais padrão de BMS, (ii) operem com histórico curto para reduzir custo e tempo de ensaio (triagem para segundo uso e manutenção preditiva) e, (iii) conciliem desempenho, interpretabilidade e reprodutibilidade. Disso decorre o objeto central e a hipótese desta tese: é possível estimar SOH e RUL com histórico curto a partir de sinais

padrão, combinando extração extensiva e seleção multietapas de atributos com arquiteturas de DL multirramos e modelos de *boosting*, e fundindo as previsões por *stacking* para elevar desempenho e robustez. Os resultados indicam ser possível reduzir a janela de dados necessária, possibilitando prognóstico mais rápido e prático.

Os três artigos a seguir materializam essa proposta e respondem à hipótese da pesquisa, sendo apresentados na íntegra no Apêndice, na ordem:

- A.1: Artigo 1 intitulado "Uma Revisão do Estado da Arte para Estimação do Estado de Saúde de Baterias Elétricas com Aprendizado de Máquina".
- A.2: Artigo 2 intitulado "Extração Abrangente de Atributos para o Prognóstico da Saúde de Baterias: Identificação de Indicadores Preditivos do Estado de Saúde".
- A.3: Artigo 3 intitulado "Estimativa da Vida Útil Remanescente com Histórico Curto em Baterias Li-Ion: Arquiteturas Multirramos CNN-LSTM/GRU e *Ensemble* por *Stacking*".

3.1. UMA REVISÃO DO ESTADO DA ARTE PARA ESTIMAÇÃO DO ESTADO DE SAÚDE DE BATERIAS ELÉTRICAS COM APRENDIZADO DE MÁQUINA

Artigo desenvolvido com o título original "*State-of-the-Art for Electric Battery State of Health (SoH) Estimation with Machine Learning: A Review*", encontra-se publicado em (Sylvestrin et al., 2025b).

Citação: Sylvestrin, G. R., Maciel, J. N., Amorim, M. L. M., Carmo, J. P., Afonso, J. A., Lopes, S. F., & Ando Junior, O. H. (2025). *State of the Art in Electric Batteries' State-of-Health (SoH) Estimation with Machine Learning: A Review*. Energies, 18(3), 746.

3.1.1. Introdução ao Tema

Este artigo mapeia, de forma sistemática, a pesquisa recente sobre estimação SOH de baterias ML, aplicando o método *ProKnow*-C para construir e analisar um portfólio bibliográfico robusto. O estudo consolida 534 artigos, publicados entre 2018 e 2024; identifica tendências, como a predominância de DL e uso crescente de bases públicas; e descreve fontes de dados amplamente utilizadas, com NASA PCoE respondendo por 51% das origens mapeadas. Algoritmos de DL compõe 57,5% das implementações e LSTM aparece em 22% dos casos, com bases públicas presentes em 60% dos estudos.

3.1.2. Relevância

O artigo estabelece a linha de base conceitual e empírica da pesquisa ao: (i) formalizar um processo reprodutível de seleção e avaliação da literatura com *ProKnow*-C e (ii) dimensionar o campo de pesquisa atual (volumes, fontes de dados, algoritmos e métricas), o que direciona decisões metodológicas dos artigos subsequentes. A construção do portfólio partiu de 6.032 registros, depurados até os 534 estudos finais (~9% do bruto), garantindo abrangência no entendimento da estimativa de SOH utilizando ML.

Em termos de contribuições, este estudo entrega (i) um portfólio robusto e reprodutível de 534 artigos construído via *ProKnow*-C; (ii) uma síntese quantitativa inédita do campo, com evidências do predomínio de DL, crescimento de implementações de *boosting* e *transfer learning*, adesão crescente a bases públicas, mapeando 12 fontes de dados; (iii) um mapeamento de variáveis-alvo relacionadas ao SOH e de performances obtidas no cenário atual; (iv) a primeira aplicação de *ProKnow*-C a SOH com ML.

3.1.3. Conexão entre Artigos

Dentro da pesquisa ele estabelece conexão direta com as outras duas produções sendo:

- Com o Artigo II (*pipeline* de atributos e modelagem com vaiáveis tabulares): os achados sobre tendências de implementações de modelos de *boosting* para variáveis tabulares, bases públicas com alto volume de amostras, a identificação do tipo de atributos implementados e as abordagens de seleção de variáveis, motivaram o desenvolvimento de um *pipeline* reprodutível para extração e seleção uni-multivariada de variáveis, uma lacuna recorrente identificada nas revisões existentes.
- Com o Artigo III (histórico curto, DL e *ensemble*): a predominância de DL (57,5%) e o papel central de LSTM (22%), bem como de redes do tipo CNN e GRU, embasam a exploração de arquiteturas sequenciais e *ensembles*, além de reforçarem a importância de avaliar cenários de dados práticos de BMS, buscando reduzir o tempo para caracterização de uma bateria. Além disso, percebeu-se a necessidade de integrar diferentes fontes de atributos em uma única abordagem de modelo.

3.1.4. Lacunas de Conhecimento

O artigo evidencia que, apesar do crescimento acelerado da área, faltam revisões com metodologia estruturada, sistemática e reprodutível, sendo a primeira produção a aplicar a metodologia *Proknow*-C neste tema de pesquisa. As análises dos artigos do portfólio demostraram que faltam *pipelines* padronizados que integrem múltiplos domínios de variáveis, forneçam uma extração massiva de atributos, e avaliem, de modo sistemático, técnicas de seleção para modelagem, pontos que a pesquisa endereça nos Artigos II e III.

Em síntese, o Artigo I cumpre o papel de fundação analítica da pesquisa: define o panorama, quantifica tendências e explicita lacunas que motivam o *pipeline* desenvolvido e testado nos Artigos II e III.

3.2. EXTRAÇÃO ABRANGENTE DE ATRIBUTOS PARA O PROGNÓSTICO DA SAÚDE DE BATERIAS: IDENTIFICAÇÃO DE INDICADORES PREDITIVOS DO ESTADO DE SAÚDE

Produção em estágio de revisão, submetido em periódico científico da área.

3.2.1. Introdução ao Tema

Este artigo apresenta um *pipeline* sistemático e reprodutível de engenharia e seleção de atributos para prognóstico da saúde de baterias, usando apenas sinais acessíveis padrões medidos em cicladores e BMS (tensão, corrente, temperatura e tempo). O estudo é aplicado na base de dados *MIT Battery Dataset*, composta por 124 células LFP/grafite. São desenvolvidos 40 modelos com o objetivo de estimar: RUL e capacidade de descarga em múltiplos horizontes (10, 50, 100, 250 ciclos à frente). A predição considera qualquer ponto de partida no ciclo de vida de uma bateria, utilizando um histórico de 100 ciclos para extração de variáveis. O desenvolvimento dos modelos considera todas as variáveis disponíveis para modelagem, bem como, modelos restritos a cada grupo de variáveis extraído, aumentando a capacidade de fornecer atributos para serem reutilizados e avaliados em outros estudos.

3.2.2. Relevância

O artigo implementa um procedimento em larga escala (~42 mil variáveis) que unifica atributos de sete grupos, sendo três de sinais brutos (carga, descarga, carga CC/CV) e quatro derivados de curvas Q(V), dQ/dV e dV/dQ, organizados em quatro categorias, primárias, *lags*, janelas deslizantes e diferenças entre ciclos; onde são aplicadas diferentes agregações estatísticas para extração de padrões preditivos. Essa abrangência eleva a

interpretabilidade e captura assinaturas de degradação em diferentes fases/representações operacionais, que na literatura são exploradas isoladamente e com um volume de extração muito reduzido.

Metodologicamente, o *pipeline* integra filtros univariados (Spearman, PPS, modelos 1-variável) e seleção multivariada baseada em SHAP, *forward selection*, *BorutaShap* e MRMR, resultando em subconjuntos compactos e de alto impacto. Com *LightGBM* como algoritmo, o modelo "*All Groups*" atinge MAPE ~10% para RUL e inferior a 1% para capacidade nas diferentes janelas avaliadas, reforçando ganhos de desempenho quando se integram domínios de atributos. Além disso, as variáveis finalistas obtidas revelam um impacto grande no uso de janelas deslizantes, ainda pouco exploradas na literatura.

3.2.3. Conexão entre Artigos

Dentro da pesquisa ele estabelece conexão direta com as outras duas produções sendo:

- Com o Artigo I: este estudo operacionaliza, em forma de *pipeline*, lacunas mapeadas na revisão, a ausência de procedimentos reprodutíveis e escaláveis que combinem múltiplos domínios de variáveis para estimativas de SOH/RUL, e os limites até então de volumetria de extração encontradas.
- Com o Artigo III: é diretamente utilizado com a aplicação do *pipeline* para desenvolvimento de modelo de *boosting* com variáveis tabulares, mostrando-se reprodutível com a redução do número de ciclos de histórico utilizado. As variáveis finalistas obtidas pela aplicação do *pipeline* são aplicadas também em modelo meta de *stacking*, juntamente com predições de modelos com arquitetura de DL.

3.2.4. Lacunas de Conhecimento

A literatura carecia de (i) extração de atributos em larga escala, (ii) padronização de seleção com integração univariada e multivariada e (iii) integração de domínios (sinais e derivados) em um processo reproduzível. O artigo responde a essas lacunas ao propor o primeiro *pipeline* com esse escopo, evidenciando ainda que variáveis de janelas deslizantes são decisivas (~88% dos finalistas) e que a importância de atributos varia por alvo, no caso RUL vs. capacidades multi-horizonte.

Do ponto de vista de resultados comparativos, o *pipeline* demonstra que integrar diversos grupos de atributos reduz erros e melhora a generalização em relação a abordagens que usam conjuntos pequenos e artesanais de atributos, contribuindo com um *benchmark* amplo (mais de 40 modelos) e um repositório de variáveis finalistas para pesquisas futuras e que podem integrar um *feature storage* de referência.

3.3. ESTIMATIVA DA VIDA ÚTIL REMANESCENTE COM HISTÓRICO CURTO EM BATERIAS LI-ION: ARQUITETURAS MULTIRRAMOS CNN-LSTM/GRU E ENSEMBLE POR STACKING

Produção em estágio de revisão, submetido ao periódico científico da área.

3.3.1. Introdução ao Tema

O artigo investiga predição de RUL com histórico curto (6 ciclos: 1 atual e 5 anteriores) em células $LiFePO_4$/grafite do *MIT Battery Dataset*, integrando dois domínios de informação: sinais brutos (segmentação CC/CV) e análises derivadas (IC/DV). As variáveis e sequências (curvas) são utilizadas para alimentar (i) um modelo tabular *LightGBM* baseado em 5.578 variáveis selecionadas por um *pipeline* multietapas (Artigo 2) e (ii) 12 arquiteturas DL *multibranch*/multicanal, com combinações CNN1D/2D + LSTM/GRU, cuja fusão por *stacking* entrega a melhor performance no teste (RMSE ~40,6 ciclos; MAE ~26,1 ciclos; MAPE ~6%).

3.3.2. Relevância

A proposta responde a uma necessidade prática de reduzir o custo/tempo de ensaio e ainda assim obter prognósticos robustos para triagem de segundo uso e manutenção preditiva em campo. Ao provar que 6 ciclos bastam quando combinam-se engenharia de atributos integrada em diferentes domínios, DL *multibranch* e meta-aprendizado por *stacking*, a pesquisa demonstra aplicabilidade imediata sob restrições típicas de BMS e operação real, sendo capaz ainda de fornecer interpretabilidade via seleção SHAP e análise de importância das variáveis. Como contribuições destaca-se:

- Viabilidade com histórico curto: comprova que 6 ciclos são suficientes para erro central baixo (MAE/RMSE/MAPE competitivos), viabilizando uso em campo.
- Integração de domínios: unifica sinais V/I/T/tempo e derivadas IC/DV tanto em modelo tabular (LGBM) quanto em redes DL *multibranch*/multicanal.

- Arquiteturas DL dedicadas: avalia 12 variantes (CNN1D/2D + LSTM/GRU, com/sem bidirecionalidade e atenção), evidenciando quando CNN1D é mais eficiente que CNN2D sob histórico curto.
- *Ensemble* por *stacking*: mostra ganho consistente ao fundir predições (meta-LGBM), superando os melhores modelos base e aumentando robustez.
- Protocolo de avaliação sólido: usa particionamento por célula (treino-base / treino-meta / teste isolado), evitando vazamento e assegurando comparação justa entre modelos.
- Orientação operacional: análise estratificada de erros por faixas de RUL e SOH fornece insumos para decisões de EoL e gestão de risco.
- Aplicabilidade prática: desenho focado em sinais acessíveis a BMS, baixo custo de aquisição e eficiência computacional favorecendo implantação real.

3.3.3. Conexão entre Artigos

O Artigo 3 se apoia diretamente no Artigo 2: reutiliza e valida o *pipeline* sistemático de extração/seleção em um regime mais desafiador (histórico curto), extraindo 5.578 variáveis e chegando a 41 variáveis finalistas distribuídas em 6 dos 7 grupos, com forte presença de estatísticas de janelas deslizantes (~90% das finalistas). Sobre esse alicerce tabular, o Artigo 3 acrescenta as arquiteturas DL *multibranch* e avança com duas estratégias de *stacking*, mostrando ganhos consistentes em relação aos melhores modelos individuais. Assim, o Artigo 2 fornece a infraestrutura de atributos e o Artigo 3 entrega a integração com DL e a fusão por *stacking* em cenário de dados limitados.

3.3.4. Lacunas de Conhecimento

O artigo busca preencher as seguintes lacunas recorrentes na literatura:

- Dependência de históricos longos e/ou dados de início de vida: no desenvolvimento utiliza-se histórico curto (6 ciclos) com desempenho competitivo.
- Subaproveitamento conjunto de sinais brutos, segmentação CC/CV e derivadas IC/DV de forma integrada: o estudo integra todos esses domínios tanto no tabular quanto no DL.

- Ausência de arquiteturas *multibranch*/multicanal alinhadas aos regimes eletroquímicos: são propostas 12 variantes CNN-LSTM/GRU com *branches* específicos (carga, descarga, CC, CV, IC, DV).
- Exploração limitada de *stacking* entre DL e *boosting*: duas estratégias de *stacking* (meta-LGBM) elevam a performance e robustez, superando os melhores modelos base.

Em síntese, o Artigo 3 comprova que a combinação de domínios e abordagens de modelagem (*boosting* e DL), com um *pipeline* de extração e seleção abrangente, viabiliza RUL com histórico curto, condição crítica para implantações reais e triagem de segundo uso.

3.4. CONSIDERAÇÕES FINAIS

Esta seção apresentou o desenvolvimento desta pesquisa na forma de produção científica através da apresentação dos três artigos produzidos que compõem a pesquisa apresentada. Foram discutidas as três frentes dessa pesquisa: (i) revisão sistemática (*ProKnow*-C); (ii) *pipeline* reprodutível de engenharia/seleção massiva de atributos, validado para RUL e capacidade futura; e (iii) predição de RUL com histórico curto por modelos DL *multibranch*, LGBM e *stacking*. Para total entendimento, os artigos produzidos são apresentados na integra no Apêndice (A.1-A.3). Na próxima seção, apresentam-se os resultados principais e discussões.

4. ANÁLISES E DISCUSSÕES DOS RESULTADOS

A revisão sistemática obteve um portfólio com 534 artigos, cujos mais relevantes em termos de citações são apresentados na Tabela 3. A presença de base de dados públicas ocorre em 15 dos 33 artigos que não são de revisão, correspondendo as produções de (Che et al., 2021; Fan et al., 2020; Fermín-Cueto et al., 2020; Gou et al., 2020; Hong et al., 2020a; X. Hu et al., 2021b; Khumprom & Yodo, 2019; P. Li et al., 2020; Qu et al., 2019; L. Ren et al., 2018, 2021; Roman et al., 2021b; Severson et al., 2019a; Tagade et al., 2020; Yu, 2018), Com relação aos artigos mais citados, (Severson et al., 2019b) impulsionou o uso de ML para predição de SOH e, sobretudo, ao disponibilizar uma das primeiras bases para modelagem, o que catalisou reprodutibilidade e comparações, sendo amplamente reutilizado por pesquisas posteriores com muitas citações (Che et al., 2021; Fermín-Cueto et al., 2020; Hong et al., 2020a; X. Hu et al., 2021b; Roman et al., 2021b). Complementarmente, revisões recentes (Ge et al., 2021; Lai et al., 2021; Y. Li et al., 2019a; Shahjalal et al., 2022; Sui et al., 2021; Vidal et al., 2020; Wang et al., 2021) mapeiam desafios, tendências de algoritmos em ML/DL para degradação e SOH, incluindo comparações de desempenho com foco em DL (Vidal et al., 2020; Wang et al., 2021) e sínteses das abordagens e resultados (Ge et al., 2021).

Tabela 3: Principais artigos do PB considerando total de citações.

Título	Citações	Ref.
Data-driven prediction of battery cycle life before capacity degradation	1453	(Severson et al., 2019b)
Long short-term memory recurrent neural network for remaining useful life prediction of lithium-ion batteries	880	(Y. Zhang et al., 2018)
Data-driven health estimation and lifetime prediction of lithium-ion batteries: A review	749	(Y. Li et al., 2019a)
A Data-Driven Approach with Uncertainty Quantification for Predicting Future Capacities and Remaining Useful Life of Lithium-ion Battery	434	(Liu et al., 2021)
Predicting the state of charge and health of batteries using data-driven machine learning	405	(Ng et al., 2020)
Random forest regression for online capacity estimation of lithium-ion batteries	398	(Y. Li et al., 2018)
Remaining useful life prediction for lithium-ion batteries based on a hybrid model combining the long short-term memory and Elman neural networks	316	(X. Li et al., 2019)
Remaining Useful Life Prediction for Lithium-Ion Battery: A Deep Learning Approach	313	(L. Ren et al., 2018)
A Data-Driven Auto-CNN-LSTM Prediction Model for Lithium-Ion Battery Remaining Useful Life	291	(L. Ren et al., 2021)
State-of-health estimation and remaining useful life prediction for the lithium-ion battery based on a variant long short term memory neural network	284	(P. Li et al., 2020)
Machine Learning Applied to Electrified Vehicle Battery State of Charge and State of Health Estimation: State-of-the-Art	267	(Vidal et al., 2020)
Modified Gaussian Process Regression Models for Cyclic Capacity Prediction of Lithium-Ion Batteries	262	(Liu et al., 2019)
A deep learning method for online capacity estimation of lithium-ion batteries	260	(Shen et al., 2019)
Machine learning pipeline for battery state-of-health estimation	246	(Roman et al., 2021b)

A Neural-Network-Based Method for RUL Prediction and SOH Monitoring of Lithium-Ion Battery	245	(Qu et al., 2019)
A novel estimation method for the state of health of lithium-ion battery using prior knowledge-based neural network and markov chain	239	(Dai et al., 2019)
A data-driven predictive prognostic model for lithium-ion batteries based on a deep learning algorithm	237	(Khumprom & Yodo, 2019)
Novel battery state-of-health online estimation method using multiple health indicators and an extreme learning machine	232	(Pan et al., 2018)
Online capacity estimation of lithium-ion batteries with deep long short-term memory networks	230	(W. Li et al., 2021b)
A review on second-life of Li-ion batteries: prospects, challenges, and issues	213	(Shahjalal et al., 2022)
State of health prediction of lithium-ion batteries: Multiscale logic regression and Gaussian process regression ensemble	204	(Yu, 2018)
A novel deep learning framework for state of health estimation of lithium-ion battery	203	(Fan et al., 2020)
A review on state of health estimations and remaining useful life prognostics of lithium-ion batteries	200	(Ge et al., 2021)
Synchronous estimation of state of health and remaining useful lifetime for lithium-ion battery using the incremental capacity and artificial neural networks	195	(S. Zhang et al., 2019)
Deep Reinforcement Learning-Based Energy Storage Arbitrage with Accurate Lithium-Ion Battery Degradation Model	193	(Cao et al., 2020)
State-of-Health Estimation and Remaining-Useful-Life Prediction for Lithium-Ion Battery Using a Hybrid Data-Driven Method	190	(Gou et al., 2020)
Transfer learning with long short-term memory network for state-of-health prediction of lithium-ion batteries	184	(Tan et al., 2020)
Battery Health Prediction Using Fusion-Based Feature Selection and Machine Learning	184	(X. Hu et al., 2021b)
A review of non-probabilistic machine learning-based state of health estimation techniques for Lithium-ion battery	180	(Sui et al., 2021)
A critical review of improved deep learning methods for the remaining useful life prediction of lithium-ion batteries	159	(Wang et al., 2021)
Deep Gaussian process regression for lithium-ion battery health prognosis and degradation mode diagnosis	148	(Tagade et al., 2020)
Model Migration Neural Network for Predicting Battery Aging Trajectories	147	(Tang et al., 2020)
Towards the swift prediction of the remaining useful life of lithium-ion batteries with end-to-end deep learning	144	(Hong et al., 2020a)
Lithium-ion battery capacity estimation — A pruned convolutional neural network approach assisted with transfer learning	142	(Y. Li et al., 2021)
Identification and machine learning prediction of knee-point and knee-onset in capacity degradation curves of lithium-ion cells	142	(Fermín-Cueto et al., 2020)
Deep learning-based prognostic approach for lithium-ion batteries with adaptive time-series prediction and on-line validation	134	(W. Zhang et al., 2020)
Predictive Battery Health Management with Transfer Learning and Online Model Correction	122	(Che et al., 2021)
One-shot battery degradation trajectory prediction with deep learning	121	(W. Li et al., 2021a)
Online health diagnosis of lithium-ion batteries based on nonlinear autoregressive neural network	117	(Khaleghi et al., 2021)
Sorting, regrouping, and echelon utilization of the large-scale retired lithium batteries: A critical review	117	(Lai et al., 2021)

Baseado na revisão da literatura, observou-se uma adoção acelerada de dados públicos: eles aparecem em 60% dos estudos do portfólio e chegam a 76% em 2024. Foram mapeadas 12 fontes abertas, somando 20 bases de dados de diferentes tecnologias de baterias, com predominância das tecnologias de íons de lítio. Houve clara aceleração recente, com 6 novas fontes surgindo entre 2022 e 2023, reforçando reprodutibilidade e comparabilidade no campo.

Com relação aos algoritmos utilizados na literatura, o gráfico da Figura 7 revela uma predominância da implementação de arquiteturas de DL baseadas principalmente em LSTM e CNN. Juntos as abordagens com DL representam cerca de 58% das implementações. Nota-se também a presença de algoritmos baseados em *boosting* de árvores de decisão como o *XGBoost* e o LGBM, onde em especial, apresentam um perfil de crescimento de uso nos últimos dois anos. com LSTM/CNN em destaque.

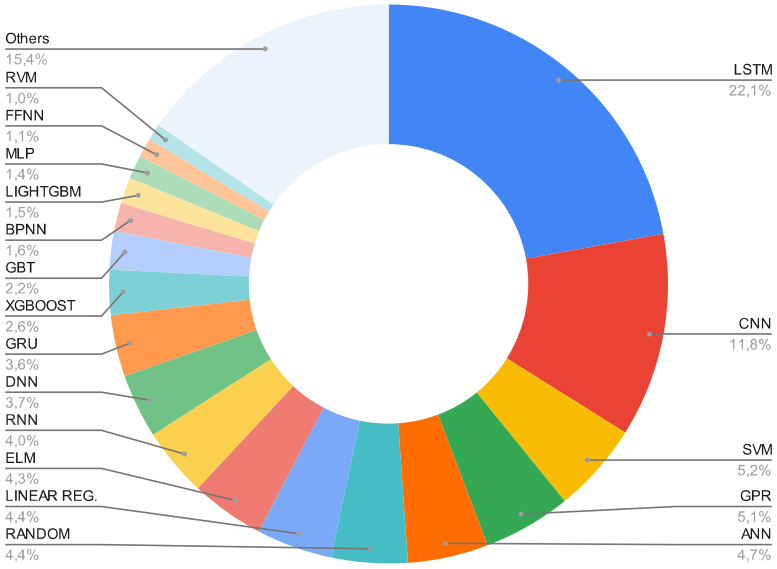

Figura 7: Frequência de algoritmos de ML presentes no portfólio bibliográfico. Fonte: O Autor, (2025).

Na comparação de desempenho, a heterogeneidade de métricas e protocolos (dados e pré-processamentos distintos) limita comparações diretas, mas alguns padrões são consistentes. Em estudos com base comum (MIT), abordagens de ML tipicamente ficam em MAPE ~10%, enquanto métodos de DL, apresentam uma redução de o erro em torno de ~30-50%. Essas evidências ancoram o desenho metodológico dos Artigos 2 e 3.

Considerando a ausência na literatura de *pipeline* massivo de extração de atributos e seleção uni-multivariada com estresse de etapas, o *pipeline* proposto gera mais 40 mil atributos em sete grupos que integram sinais brutos e análises de derivadas. A volumetria extraída em cada grupo é apresentada na Tabela 4, baseado no uso de 100 ciclos de dados históricos. Aplicando a etapa de seleção de variáveis do *pipeline*, os modelos finalistas para o prognóstico RUL e capacidade futura apresentaram a distribuição de variáveis apresentada na Tabela 5. Cabe destacar, que assim como na Tabela 5, as tabelas de análises

a seguir são apresentadas como mapas de calor, em todas elas, as cores variam do vermelho (valores relativamente piores/menores na coluna) ao verde (valores relativamente melhores/maiores), permitindo destacar visualmente os padrões por grupo e por modelo.

Tabela 4: Volumetria de atributos extraídos por grupo.

Grupo	Domínio	Total variáveis
Carga geral	Sinal bruto	7,840
Descarga geral	Sinal bruto	7,840
CCCV carga	Sinal bruto	6,400
dV/dQ carga	Análise diferencial	3,058
dV/dQ descarga	Análise diferencial	3,049
dQ/dV carga	Análise diferencial	7,689
dQ/dV descarga	Análise diferencial	6,738

Considerando o modelo RUL, as variáveis finalistas vêm de forma equilibrada entre grupos, com destaque para o grupo carga/descarga geral, CCCV e dQ/dV descarga. Para a predição da capacidade de curto prazo (10 ciclos à frente), os modelos dependem quase exclusivamente do grupo descarga geral, sugerindo que a degradação de curto prazo é bem capturada diretamente pelas curvas V-I de descarga. Em horizontes maiores (50, 100, 250 ciclos), o conjunto de descarga geral segue dominante, mas cresce a participação de atributos baseados em CCCV e de grupos derivados. No agregado dos 148 atributos finalistas (RUL e capacidade), descarga geral responde por 37,2%, CCCV por 21,6%, carga geral por 12,2%, e dQ/dV descarga por 10,8%. Quando analisado o grupo de variáveis com maiores destaques na avaliação univariada, a sobreposição com as variáveis finalistas foi de apenas 18 atributos, indicando que análises univariadas isolada não garante ganho em conjunto em modelo.

Tabela 5: Total de variáveis finalistas considerando segmentação por grupo.

Grupo	RUL	Capacidade próximos 10 ciclos	Capacidade próximos 50 ciclos	Capacidade próximos 100 ciclos	Capacidade próximos 250 ciclos
Carga geral	8	0	1	4	5
Descarga geral	6	8	11	16	14
CCCV carga	8	0	5	11	8
dQ/dV carga	3	1	0	4	1
dQ/dV descarga	9	0	3	5	7
dV/dQ carga	4	0	0	0	1
dV/dQ descarga	0	0	3	2	0

Com relação ao tipo de variáveis finalistas nos modelos, há predominância de janelas deslizantes (~88%), seguidas por *lags* (~10%), reforçando o valor de dinâmica temporal curta. Avaliando a representação das variáveis nos modelos por grupo (35 modelos), o padrão se repete, dentre as 700 variáveis únicas (724 usadas), atributos de janelas representam ~83%, com larguras de 5 a 100 ciclos, sinal de que é possível reduzir o histórico sem perda relevante.

A Tabela 6 sintetiza o desempenho dos modelos LGBM treinados com diferentes grupos de atributos, tanto para o alvo de RUL quanto para os quatro horizontes de capacidade. Cada linha corresponde a um grupo de atributos, e cada coluna apresenta as métricas de erro (RMSE, MAE, MAPE) em validação e teste; as células em verde representam os melhores resultados (menor erro) dentro de cada coluna, e as em vermelho, os piores. Em geral, os valores de MAPE ficaram próximos de 10% para RUL e abaixo de 1% para previsão de capacidade futura (10, 50, 100 e 250 ciclos à frente). Os modelos que consideram todos os grupos de atributos apresentam o melhor desempenho para todos os alvos de capacidade e também lideram em RMSE para RUL, obtendo ainda ~50% de melhoria em MAE frente a um estudo de referência com *boosting* e poucas variáveis derivadas (F. Yang et al., 2020). Em bases mais restritas, o grupo CCCV apresenta desempenho próximo ao modelo com todos os grupos; para RUL com descarga, dQ/dV descarga supera levemente descarga geral; para capacidade, descarga geral é o grupo mais informativo. Em suma, a Tabela 6 mostra que combinar múltiplas origens de atributos maximiza o desempenho preditivo, ao mesmo tempo em que o modelo permanece robusto mesmo sob limitações de dados.

Tabela 6: Visão geral de performance para modelos LGBM para prognóstico de RUL e capacidade considerando 100 ciclos de histórico.

Modelo	Variável alvo	# variáveis	RMSE		MAE		MAPE	
			Validação	Teste	Validação	Teste	Validação	Teste
Todos os grupos	RUL	38	63,483	94,303	29,956	34,187	9,941	10,772
Carga geral		29	124,425	124,075	27,895	34,794	10,593	13,990
Descarga geral		11	87,595	103,129	28,943	21,974	10,926	8,037
dV/dQ carga		12	117,704	149,335	45,058	54,630	16,100	18,172
dV/dQ descarga		29	69,416	104,087	28,011	28,219	9,901	10,139
dQ/dV carga		33	100,717	136,421	45,098	47,675	15,395	16,421
dQ/dV descarga		46	68,550	102,219	27,319	31,578	9,472	11,010
CCCV carga		24	75,984	110,022	26,434	32,811	9,829	12,232

Modelo	Variável alvo	# variáveis	RMSE		MAE		MAPE	
Todos os grupos	**Capacidade próximos 10 ciclos**	9	1,26E-03	1,48E-03	4,10E-04	4,23E-04	4,39E-02	4,50E-02
Carga geral		40	4,68E-03	4,97E-03	1,24E-03	1,44E-03	1,33E-01	1,53E-01
Descarga geral		12	1,27E-03	1,24E-03	4,18E-04	4,15E-04	4,46E-02	4,40E-02
dV/dQ carga		17	1,28E-02	1,66E-02	4,86E-03	7,69E-03	5,25E-01	8,15E-01
dV/dQ descarga		24	6,87E-03	6,47E-03	3,81E-03	4,13E-03	4,08E-01	4,38E-01
dQ/dV carga		30	9,83E-03	1,28E-02	3,58E-03	6,21E-03	3,83E-01	6,61E-01
dQ/dV descarga		30	5,19E-03	6,95E-03	2,36E-03	3,77E-03	2,54E-01	4,02E-01
CCCV carga		24	4,22E-03	7,55E-03	1,67E-03	1,72E-03	1,78E-01	1,81E-01
Todos os grupos	**Capacidade próximos 50 ciclos**	23	4,28E-03	4,07E-03	1,15E-03	1,03E-03	1,23E-01	1,08E-01
Carga geral		36	5,69E-03	6,34E-03	1,74E-03	1,84E-03	1,85E-01	1,94E-01
Descarga geral		31	4,12E-03	3,89E-03	1,52E-03	1,39E-03	1,61E-01	1,46E-01
dV/dQ carga		27	1,52E-02	1,68E-02	5,26E-03	8,43E-03	5,64E-01	8,95E-01
dV/dQ descarga		31	7,84E-03	7,16E-03	3,90E-03	4,44E-03	4,16E-01	4,76E-01
dQ/dV carga		33	1,21E-02	1,29E-02	4,83E-03	6,02E-03	5,17E-01	6,42E-01
dQ/dV descarga		21	6,59E-03	6,89E-03	3,10E-03	3,58E-03	3,32E-01	3,84E-01
CCCV carga		21	5,54E-03	7,44E-03	2,17E-03	1,93E-03	2,31E-01	2,03E-01
Todos os grupos	**Capacidade próximos 100 ciclos**	42	6,78E-03	7,38E-03	2,12E-03	1,97E-03	2,26E-01	2,08E-01
Carga geral		28	1,04E-02	1,09E-02	2,67E-03	2,26E-03	2,83E-01	2,38E-01
Descarga geral		30	7,65E-03	7,24E-03	2,35E-03	2,23E-03	2,50E-01	2,34E-01
dV/dQ carga		27	1,76E-02	1,77E-02	6,96E-03	8,00E-03	7,42E-01	8,56E-01
dV/dQ descarga		22	1,17E-02	1,04E-02	4,10E-03	4,80E-03	4,39E-01	5,13E-01
dQ/dV carga		30	1,36E-02	1,43E-02	4,73E-03	5,86E-03	5,05E-01	6,26E-01
dQ/dV descarga		32	1,11E-02	1,06E-02	3,97E-03	4,82E-03	4,22E-01	5,15E-01
CCCV carga		28	7,63E-03	9,62E-03	2,99E-03	2,57E-03	3,18E-01	2,71E-01
Todos os grupos	**Capacidade próximos 250 ciclos**	36	1,54E-02	1,34E-02	4,12E-03	3,42E-03	4,39E-01	3,61E-01
Carga geral		32	2,69E-02	1,71E-02	5,53E-03	4,58E-03	5,94E-01	4,83E-01
Descarga geral		23	1,69E-02	1,63E-02	4,78E-03	4,42E-03	5,13E-01	4,68E-01
dV/dQ carga		10	2,60E-02	2,22E-02	9,38E-03	8,98E-03	1,00E+00	9,66E-01
dV/dQ descarga		16	1,85E-02	1,78E-02	7,76E-03	8,48E-03	8,35E-01	9,08E-01
dQ/dV carga		30	2,11E-02	2,08E-02	7,71E-03	8,40E-03	8,41E-01	9,05E-01
dQ/dV descarga		31	1,76E-02	1,53E-02	6,51E-03	6,71E-03	7,00E-01	7,26E-01
CCCV carga		28	1,85E-02	1,48E-02	4,02E-03	4,35E-03	4,32E-01	4,62E-01

Considerando a aplicação do *pipeline* para uma redução para 6 ciclos de dados, a Tabela 7 apresenta a comparação entre os modelos bases e meta. O *ensemble* por *stacking*

(meta-LGBM) usando predições dos modelos base selecionados na otimização de hiperparâmetros, obteve a melhor performance no teste com MAE ~26,1 ciclos, RMSE ~40,6 ciclos, MAPE 6,0%, superando o melhor DL individual (CNN1D-BiLSTM) e o LGBM isolado (~9% MAPE; RMSE ~63,4).

Com relação as variáveis finalistas do modelo base LGBM (41), a tendência do padrão das variáveis se manteve na aplicação do *pipeline* proposto, com ~90% sendo do tipo de janela deslizante. Em termos de performance os resultados se mantiveram no mesmo patamar que quando utilizando 100 ciclos de histórico, demostrando que variáveis tão relevantes quanto ocuparam as variáveis de histórico maior, e que, portanto, o uso de histórico curto é um processo factível na caracterização de baterias.

Analisando a performance das arquiteturas de DL, observa-se que o uso de CNN1D tende a oferecer ganhos em relação às CNN2D no cenário *multibranch* com histórico curto adotado. Uma possível explicação é que as CNN2D tipicamente se beneficiam de janelas temporais mais longas para explorar padrões espaciais nos mapas de medidas×ciclo, com apenas 6 ciclos, essa representação se torna pouco informativa, enquanto a convolução 1D ao longo das sequências já é suficiente para capturar a dinâmica relevante. Como esperado, as redes recorrentes do tipo LSTM apresentaram desempenho ligeiramente superior às GRU, à custa de maior custo computacional. Na etapa de fusão entre os diferentes *branches*, o uso de mecanismos de atenção não trouxe ganhos consistentes em relação à simples concatenação dos vetores de saída das *branches*, dentro do regime de dados e hiperparâmetros considerado.

Tabela 7: Métricas de performance para os modelos no conjunto teste.

Modelo	MAE (ciclos)	RMSE (ciclos)	MAPE (%)	MedAE (ciclos)	RMedSE (ciclos)	MedAPE (%)	sMAPE (%)	WAPE (%)	NMAE	R2
STACKING I	26,081	40,639	6,006	14,912	14,912	4,923	6,076	5,822	0,059	0,980
STACKING II	29,658	53,063	6,388	15,080	15,080	4,731	6,408	6,543	0,069	0,965
CNN1D-BiLSTM	29,520	50,026	6,624	15,929	15,929	5,183	6,794	6,519	0,069	0,970
CNN1D-LSTM	35,527	57,450	7,672	19,672	19,672	6,507	7,822	8,180	0,085	0,957
CNN2D-GRU-ATT	40,277	63,578	8,542	21,358	21,358	7,214	8,427	8,941	0,092	0,952
CNN1D-LSTM-ATT	40,517	64,925	8,610	19,261	19,261	7,158	8,477	9,042	0,094	0,949
LGBM	40,087	63,417	9,419	21,561	21,561	6,897	9,196	8,975	0,094	0,952
CNN1D-BiGRU	43,361	73,582	9,423	21,454	21,454	7,121	9,445	9,886	0,102	0,935
CNN2D-BiGRU	39,219	64,227	10,109	21,962	21,962	7,578	9,696	8,649	0,091	0,950
CNN1D-GRU	41,845	64,019	10,369	25,766	25,766	8,199	10,737	9,437	0,098	0,951
CNN2D-LSTM	43,934	73,309	10,380	24,083	24,083	8,118	10,320	9,833	0,101	0,934
CNN2D-GRU	41,991	64,855	10,704	25,436	25,436	7,824	10,142	9,257	0,098	0,949
CNN2D-LSTM-ATT	43,472	68,086	10,971	26,768	26,768	7,860	10,894	9,706	0,102	0,945
CNN1D-GRU-ATT	53,514	83,730	12,358	26,097	26,097	9,220	12,187	12,028	0,121	0,918
CNN2D-BiLSTM	57,432	87,186	13,057	28,875	28,875	12,066	13,277	12,731	0,133	0,909

Considerando as predições de RUL do modelo *Stacking* I, a análise das métricas por faixas de RUL real, Tabela 8, e por faixas de SOH do ciclo de previsão, Tabela 9, mostra um comportamento em "U", com maiores erros relativos nos extremos. Quando se segmenta pelo RUL verdadeiro, observam-se três regimes: (i) próximo ao fim de vida, o MAE é baixo (~5 ciclos), mas o MAPE é alto (~31%), porque erros pequenos representam uma fração grande do RUL; (ii) na faixa intermediária (~600–970 ciclos), o MAE é moderado (~34-48 ciclos) e os erros relativos são os melhores do conjunto; (iii) em RUL alto (~970-1 700 ciclos), o MAE aumenta (~81 ciclos), enquanto o MAPE fica em torno de 7,5%.

A estratificação por SOH repete o padrão: em SOH mais degradado (0,754-0,85) o MAE é baixo, mas os erros percentuais são altos; em SOH elevado (0,99-1,00) aparecem os melhores erros relativos (sMAPE/WAPE ~3,8%); e as faixas intermediárias (0,94-0,98) concentram MAE maiores (~29-41 ciclos). Em síntese, o modelo é mais estável no "miolo operacional" (RUL médio/alto e SOH elevado), enquanto nos extremos as incertezas relativas aumentam, dessa forma, decisões de manutenção próximas ao EOL devem privilegiar métricas absolutas (MAE), reduzindo a influência das métricas percentuais.

Tabela 8: Performance *Stacking* I por faixa RUL verdadeiro.

Intervalo RUL	MAE (ciclos)	RMSE (ciclos)	MAPE (%)	MedAE (ciclos)	RMedSE (ciclos)	MedAPE (%)	sMAPE (%)	WAPE (%)	NMAE
(-0,001, 81,0]	4,996	6,467	31,259	4,415	4,415	11,497	21,427	12,186	0,125
(81,0, 161,0]	7,070	8,921	5,815	5,795	5,795	5,050	5,976	5,819	0,179
(161,0, 242,0]	13,478	16,272	6,629	12,276	12,276	6,071	6,705	6,672	0,337
(242,0, 322,0]	22,589	33,462	7,852	15,065	15,065	5,359	7,451	7,996	0,572
(322,0, 406,0]	25,654	32,176	7,110	22,542	22,542	6,330	7,008	7,038	0,618
(406,0, 492,0]	25,322	31,719	5,658	21,546	21,546	4,785	5,626	5,638	0,603
(492,0, 614,5]	30,225	38,786	5,508	24,372	24,372	4,475	5,516	5,495	0,472
(614,5, 762,0]	34,026	49,284	4,931	18,207	18,207	2,587	4,955	4,942	0,463
(762,0, 970,5]	48,382	63,045	5,638	36,321	36,321	4,163	5,651	5,686	0,504
(970,5, 1701,0]	81,489	101,282	7,463	71,511	71,511	6,485	7,850	7,488	0,645

Tabela 9: Performance *Stacking* I por faixa SOH verdadeiro.

Intervalo SOH	MAE (ciclos)	RMSE (ciclos)	MAPE (%)	MedAE (ciclos)	RMedSE (ciclos)	MedAPE (%)	sMAPE (%)	WAPE (%)	NMAE
(0,754, 0,85]	5,24116	7,03660	49,28105	4,43774	4,43775	18,25394	30,93180	19,13430	0,19412
(0,85, 0,9]	5,10179	6,39576	10,31707	4,30540	4,30540	6,40553	9,60710	6,82210	0,12004
(0,9, 0,92]	7,54464	9,55671	6,30048	6,19664	6,19672	5,62636	6,52720	6,01670	0,11563
(0,92, 0,94]	14,68884	22,74623	7,07818	10,47362	10,47401	5,49044	7,01080	7,24970	0,12663
(0,94, 0,96]	29,27252	41,83840	7,67356	17,98951	17,98957	6,76468	7,66710	8,43480	0,10568
(0,96, 0,98]	41,00810	60,25015	7,44422	26,05806	26,05806	6,70596	7,53590	7,93270	0,09593
(0,98, 0,99]	34,48851	45,70735	6,18323	26,21656	26,21656	5,01659	6,06010	6,02040	0,12406
(0,99, 1,001]	25,47547	36,80833	3,91699	17,13058	17,13058	2,82186	3,81470	3,82640	0,07520

Em relação a performance considerando a literatura, mesmo com possíveis vieses de particionamento, a Tabela 10 indica que o LGBM base alcançou MAPE ~9%, comparável a estudos que usaram muito mais histórico (100 e 250 ciclos), evidenciando a força das variáveis tabulares do *pipeline*. Já o *Stacking* I mostrou-se superior, reduzindo o erro percentual frente à maioria das publicações com o MIT *Dataset*, exceção para um método CNN3D-CNN2D, que pode ser beneficiado de informações do início de vida, e com janelas históricas maiores.

Tabela 10: Comparação de performance com pesquisas relacionadas a predição de RUL e previsão antecipada com base de dados MIT.

Ref.	Algoritmo	RMSE	MAPE	Observações
(Sanz-Gorrachategui et al., 2021)	MLP	90	-	Uso de 113 das 124 células do conjunto de dados, considerou 10 ciclos de histórico
(Ma et al., 2022)	CNN+RNN	240	9,8	Uso de 30 ciclos de histórico
(Y. Yang, 2021)	CNN3D-CNN2D	-	3,55	Faz uso dos 5 primeiros ciclos e depois de 15 ciclos históricos
(Xu et al., 2023)	CNN-LSTM		11,31	Previsão antecipada com 100 ciclos iniciais
(Hong et al., 2020b)	CNN	76	10,6	Uso de 4 ciclos de histórico
(Gong et al., 2022a)	XGBoost	91,13	7,92	Previsão antecipada com 100 ciclos iniciais
(F. Yang et al., 2020)	GBT	84,9	7,5	Uso de 250 ciclos de histórico
(Hsu et al., 2022)	DNN	65 (1) 40 (2)		Uso do último ciclo (1) ou 100 ciclos (2), considerando casos de RUL abaixo de 750 ciclos.
-	**Proposto (*Stacking* I)**	**40,60**	**6,01**	**Uso de 6 ciclos de histórico-**

Considerando o conjunto de resultados obtidos, os modelos desenvolvidos podem ser integrados a BMS e rotinas de manutenção preditiva utilizando apenas sinais já disponíveis (tensão, corrente, temperatura e tempo). O modelo tabular em LGBM é computacionalmente leve, o que viabiliza sua implementação diretamente em sistemas embarcados do BMS, com baixa latência e reduzido consumo de recursos.

Os modelos de DL, por demandarem mais CPU/GPU, são mais adequados para execução em servidores locais ou em nuvem, quando houver infraestrutura disponível, permitindo inferências mais detalhadas a partir dos mesmos sinais. Para aplicações de triagem de segunda vida, erros em torno de 6% tornam possível um prognóstico rápido, e a análise estratificada por faixas de RUL/SOH oferece subsídios para critérios de aceite e gestão de risco.

Além disso, a previsão multi-horizonte de capacidade, com erros sub-percentuais, abre espaço para estratégias operacionais como balanceamento de carga, carregamento

dinâmico e controle térmico, contribuindo para prolongar a vida útil das baterias e aumentar a segurança do sistema.

4.1. CONSIDERAÇÕES FINAIS

Esta seção apresentou os resultados e discussões principais da pesquisa obtidos no desenvolvimento dos 3 artigos propostos, com foco na apresentação de desempenho utilizando o *pipeline* proposto para prognóstico da capacidade futura e RUL Na próxima seção, apresentam-se as conclusões da pesquisa e continuidades.

5. CONCLUSÕES E CONTINUIDADE DA PESQUISA

Esta pesquisa teve como objetivo desenvolver, analisar e validar um *pipeline* de modelagem com inteligência artificial reprodutível para prognóstico da saúde de baterias (SOH/RUL), usando exclusivamente sinais acessíveis ao sensoriamento padrão em laboratório e BMS (corrente, tensão, temperatura), propondo a implementação de modelos de *boosting* com variáveis tabulares e arquiteturas de aprendizado profundo. A pesquisa foi estruturada em três estudos complementares: (i) uma revisão sistemática utilizando *ProKnow*-C que mapeou o estado da arte, tendências e lacunas; (ii) o desenvolvimento de um *pipeline* massivo e reprodutível de extração e seleção de atributos com modelagem por *boosting*, aplicado a RUL e capacidade futura em múltiplos horizontes; e (iii) o prognóstico com histórico curto, via redes profundas multirramos (CNN/LSTM/GRU) e *stacking* com o modelo tabular.

A análise da literatura apresentou tendência de crescimento no uso de arquiteturas de DL, predominando nos últimos anos, bem como demonstrou haver uma ausência de abordagens integrando diferentes domínios de atributos de forma integrada nos modelos, processos sistemáticos para extração variáveis limitados, e etapas de seleção baseadas em poucas etapas com predominância de uso de métodos univariados. O *pipeline* proposto possibilita a extração massiva de variáveis considerando sete conjuntos de atributos abrangentes, onde considerando 100 ciclos de histórico possibilita a extração de mais de 40 mil variáveis.

Baseando-se em diferentes segmentos de variáveis, e nas múltiplas etapas de seleção, os modelos implementados indicaram subconjuntos compactos de atributos finalistas com poder preditivo, sendo predominante variáveis do tipo janela deslizante (~90%) associadas a agregações estatísticas de medidas de posição, dispersão e forma. Modelos implementados com LGBM alcançaram MAPE inferior a 1% para capacidade futura em todas as janelas avaliadas (10 a 250 ciclos à frente). As variáveis finalistas para os modelos RUL considerando 100 ciclos de histórico revelaram a presença de variáveis relacionadas a janelas curtas, indicando viabilidade de reduzir drasticamente o histórico.

A redução do histórico foi considerada em 5 ciclos recentes e último ciclo, totalizando a necessidade de ciclagem de 6 ciclos para prognostico RUL. Através da implementação de modelo tabular com LGBM explorando o *pipeline* de extração e seleção proposto, e a implementação de arquiteturas de DL que integram os domínios de sinais

brutos e derivadas na forma *multibranch*, observou-se a arquitetura DL CNN1D-BiLSTM como melhor modelo base com MAPE de 6,62%. Considerando a aplicação de *stacking*, integrando DL e LGBM, foi possível reduzir o prognóstico a 6%. A análise do erro segmentado pelo SOH revelou maiores imprecisões no início da vida da bateria e no final da degradação. Os resultados obtidos quando comparados a literatura obtiveram performance que coloca em posição competitiva frente a outras publicações, com considerável redução na necessidade de dados históricos. Portanto, considera-se que o *pipeline* proposto com a integração de diferentes domínios de forma integrada possibilita alcance de melhores resultados na modelagem relacionada ao prognóstico de saúde em baterias.

Em termo de relevância e contribuição científica, a pesquisa desenvolvida avança o estado da arte ao: (i) aplicar uma revisão sistemática estruturada à área, consolidando bases públicas, algoritmos e métricas; (ii) propor um *pipeline* reprodutível de grande escala para engenharia/seleção de atributos que integra análise univariada e multivariada, fornecendo um "catálogo" de preditores robustos para criação de *feature storage*; e (iii) demonstrar, em cenário de histórico limitado, que *ensembles* entre DL *multirramos* e *boosting* elevam a robustez e mantêm desempenho competitivo. Cientificamente, oferece um caminho metodológico transparente, replicável e transferível a diferentes alvos relacionados ao prognóstico de saúde em baterias, fortalecendo a comparabilidade entre estudos e aproximando pesquisa e aplicação.

Operacionalmente, os resultados habilitam três frentes: (i) integração em BMS e processos de manutenção preditiva com implementação em sistema embarcado com modelo tabular (LGBM) e uso de DL em servidor quando disponível; (ii) triagem de segunda vida com janelas curtas, acelerando caracterização e agrupamento de células; e (iii) políticas de operação adaptativa com previsão multi-horizonte de capacidade, apoiando balanceamento de carga, carregamento dinâmico e controle térmico. Em nível sistêmico, a padronização de *pipelines* reprodutíveis e o uso de dados públicos tendem a reduzir barreiras de entrada, acelerar *benchmarks* e favorecer a aplicação em EVs e sistemas estacionário de energia.

Para continuidade da pesquisa sugerem-se as seguintes linhas:

- Generalização e transferência: validar *pipeline* em modelo com múltiplas químicas de bateria (NMC/NCA/LFP), perfis de uso e temperaturas, fazendo uso de *transfer learning* entre bases.

- Prognostico em segundo uso: não existe a disponibilidade de bases com ensaios em células em estágio de degradação de EVs, submetidas a ciclos de carga e descarga simulando sua degradação no segundo uso em sistemas estacionários. A construção desse tipo de base de dados seria de extrema importância para validação do *pipeline* proposto especificamente nessas condições e no desenvolvimento de processos de caracterização de baterias para o segundo uso.
- Sistemas embarcados: implementação de modelo de prognóstico RUL e de capacidade futura compatível em BMS para monitoramento de células e previsão de manutenção em baterias.

REFERÊNCIAS

ABVE. (2025). *Vendas de eletrificados leves de 2024 já ultrapassa, em julho, o total de 2023 - ABVE*. https://abve.org.br/vendas-de-eletrificados-em-2024-ja-ultrapassam-total-de-2023/

ANEEL. (2022). *ARMAZENAMENTO DE ENERGIA ELÉTRICA*. https://biblioteca.aneel.gov.br/Acervo/Detalhe/223173?returnUrl=/Home/Index&guid=1715904005723

Barré, A., Deguilhem, B., Grolleau, S., Gérard, M., Suard, F., & Riu, D. (2013). A review on lithium-ion battery ageing mechanisms and estimations for automotive applications. *Journal of Power Sources*, *241*, 680–689. https://doi.org/10.1016/j.jpowsour.2013.05.040 Review

Bloom, I., Jansen, A. N., Abraham, D. P., Knuth, J., Jones, S. A., Battaglia, V. S., & Henriksen, G. L. (2005a). Differential voltage analyses of high-power, lithium-ion cells: 1. Technique and application. *Journal of Power Sources*, *139*(1), 295–303. https://doi.org/https://doi.org/10.1016/j.jpowsour.2004.07.021

Bloom, I., Jansen, A. N., Abraham, D. P., Knuth, J., Jones, S. A., Battaglia, V. S., & Henriksen, G. L. (2005b). Differential voltage analyses of high-power, lithium-ion cells: 1. Technique and application. *Journal of Power Sources*, *139*(1), 295–303. https://doi.org/https://doi.org/10.1016/j.jpowsour.2004.07.021

Cantane, D. Augusto., Ando Junior, O. Hideo., & Hamerschmidt, M. Biehl. (2020). *Tecnologias de armazenamento de energia aplicadas ao setor elétrico brasileiro*. Editora Scienza.

Cao, J., Harrold, D., Fan, Z., Morstyn, T., Healey, D., & Li, K. (2020). Deep {Reinforcement} {Learning}-{Based} {Energy} {Storage} {Arbitrage} {With} {Accurate} {Lithium}-{Ion} {Battery} {Degradation} {Model}. *IEEE Transactions on Smart Grid*, *11*(5), 4513–4521. https://doi.org/10.1109/TSG.2020.2986333

Che, Y., Deng, Z., Lin, X., Hu, L., & Hu, X. (2021). Predictive Battery Health Management With Transfer Learning and Online Model Correction. *IEEE Transactions on Vehicular Technology*, *70*(2), 1269–1277. https://doi.org/10.1109/TVT.2021.3055811

Dai, H., Zhao, G., Lin, M., Wu, J., & Zheng, G. (2019). A Novel Estimation Method for the State of Health of Lithium-Ion Battery Using Prior Knowledge-Based Neural Network and Markov Chain. *IEEE Transactions on Industrial Electronics*, *66*(10), 7706–7716. https://doi.org/10.1109/TIE.2018.2880703

Daigle, M., & Kulkarni, C. (2013). Electrochemistry-based Battery Modeling for Prognostics. In *PHM 2013 - Proceedings of the Annual Conference of the Prognostics and Health Management Society 2013*.

Dubarry, M., Truchot, C., & Liaw, B. Y. (2012). Synthesize battery degradation modes via a diagnostic and prognostic model. *Journal of Power Sources*, *219*, 204–216. https://doi.org/https://doi.org/10.1016/j.jpowsour.2012.07.016

Elliott, M., Swan, L. G., Dubarry, M., & Baure, G. (2020). Degradation of electric vehicle lithium-ion batteries in electricity grid services. *Journal of Energy Storage*, *32*, 101873. https://doi.org/10.1016/j.est.2020.101873

EPE. (2024). *Plano Decenal de Expansão de Energia 2035*. https://www.epe.gov.br/pt/publicacoes-dados-abertos/publicacoes/plano-decenal-de-expansao-de-energia-2035

Fan, Y., Xiao, F., Li, C., Yang, G., & Tang, X. (2020). A novel deep learning framework for state of health estimation of lithium-ion battery. *Journal of Energy Storage*, *32*.

https://doi.org/10.1016/j.est.2020.101741
Fapesp. (2023). *Obstacles to growth of the electric car market in Brazil : Revista Pesquisa Fapesp*. https://revistapesquisa.fapesp.br/en/obstacles-to-growth-of-the-electric-car-market-in-brazil/
Fermín-Cueto, P., McTurk, E., Allerhand, M., Medina-Lopez, E., Anjos, M. F., Sylvester, J., & dos Reis, G. (2020). Identification and machine learning prediction of knee-point and knee-onset in capacity degradation curves of lithium-ion cells. *Energy and AI*, *1*, 100006. https://doi.org/10.1016/j.egyai.2020.100006
Ge, M.-F., Liu, Y., Jiang, X., & Liu, J. (2021). A review on state of health estimations and remaining useful life prognostics of lithium-ion batteries. *Measurement*, *174*, 109057. https://doi.org/10.1016/j.measurement.2021.109057
Gil, A. C. (2002). *Como elaborar projetos de pesquisa*. Editora Atlas SA.
Gong, D., Gao, Y., Kou, Y., & Wang, Y. (2022a). Early prediction of cycle life for lithium-ion batteries based on evolutionary computation and machine learning. *Journal of Energy Storage*, *51*, 104376. https://doi.org/10.1016/j.est.2022.104376
Gong, D., Gao, Y., Kou, Y., & Wang, Y. (2022b). State of health estimation for lithium-ion battery based on energy features. *Energy*, *257*, 124812. https://doi.org/10.1016/j.energy.2022.124812
Gou, B., Xu, Y., & Feng, X. (2020). State-of-Health Estimation and Remaining-Useful-Life Prediction for Lithium-Ion Battery Using a Hybrid Data-Driven Method. *IEEE Transactions on Vehicular Technology*, *69*(10), 10854–10867. https://doi.org/10.1109/TVT.2020.3014932
Hong, J., Lee, D., Jeong, E.-R., & Yi, Y. (2020a). Towards the swift prediction of the remaining useful life of lithium-ion batteries with end-to-end deep learning. *Applied Energy*, *278*, 115646. https://doi.org/10.1016/j.apenergy.2020.115646
Hong, J., Lee, D., Jeong, E.-R., & Yi, Y. (2020b). Towards the swift prediction of the remaining useful life of lithium-ion batteries with end-to-end deep learning. *Applied Energy*, *278*, 115646. https://doi.org/10.1016/j.apenergy.2020.115646
Hossain Lipu, M. S., Ansari, S., Miah, Md. S., Meraj, S. T., Hasan, K., Shihavuddin, A. S. M., Hannan, M. A., Muttaqi, K. M., & Hussain, A. (2022). Deep learning enabled state of charge, state of health and remaining useful life estimation for smart battery management system: Methods, implementations, issues and prospects. *Journal of Energy Storage*, *55*, 105752. https://doi.org/10.1016/j.est.2022.105752
Hsu, C.-W., Xiong, R., Chen, N.-Y., Li, J., & Tsou, N.-T. (2022). Deep neural network battery life and voltage prediction by using data of one cycle only. *Applied Energy*, *306*, 118134. https://doi.org/10.1016/j.apenergy.2021.118134
Hu, C., Jain, G., Zhang, P., Schmidt, C., Gomadam, P., & Gorka, T. (2014). Data-driven method based on particle swarm optimization and k-nearest neighbor regression for estimating capacity of lithium-ion battery. *Applied Energy*, *129*, 49–55. https://doi.org/https://doi.org/10.1016/j.apenergy.2014.04.077
Hu, X., Che, Y., Lin, X., & Onori, S. (2021a). Battery Health Prediction Using Fusion-Based Feature Selection and Machine Learning. *IEEE Transactions on Transportation Electrification*, *7*(2), 382–398. https://doi.org/10.1109/TTE.2020.3017090
Hu, X., Che, Y., Lin, X., & Onori, S. (2021b). Battery Health Prediction Using Fusion-Based Feature Selection and Machine Learning. *IEEE Transactions on Transportation Electrification*, *7*(2), 382–398. https://doi.org/10.1109/TTE.2020.3017090
International Energy Agency. (2024). *Global EV Outlook 2024 Moving towards increased affordability*.
Khaleghi, S., Karimi, D., Beheshti, S. H., Hosen, Md. S., Behi, H., Berecibar, M., & Van

Mierlo, J. (2021). Online health diagnosis of lithium-ion batteries based on nonlinear autoregressive neural network. *Applied Energy*, *282*, 116159. https://doi.org/10.1016/j.apenergy.2020.116159

Khumprom, P., & Yodo, N. (2019). A data-driven predictive prognostic model for lithium-ion batteries based on a deep learning algorithm. *Energies*, *12*(4). https://doi.org/10.3390/en12040660

Lai, X., Huang, Y., Deng, C., Gu, H., Han, X., Zheng, Y., & Ouyang, M. (2021). Sorting, regrouping, and echelon utilization of the large-scale retired lithium batteries: A critical review. *Renewable and Sustainable Energy Reviews*, *146*, 111162. https://doi.org/10.1016/j.rser.2021.111162

Li, G., Li, B., Li, C., & Wang, S. (2023). State-of-health rapid estimation for lithium-ion battery based on an interpretable stacking ensemble model with short-term voltage profiles. *Energy*, *263*, 126064. https://doi.org/10.1016/j.energy.2022.126064

Li, H., Alsolami, M., Yang, S., Alsmadi, Y. M., & Wang, J. (2017). Lifetime Test Design for Second-Use Electric Vehicle Batteries in Residential Applications. *IEEE Transactions on Sustainable Energy*, *8*(4), 1736–1746. https://doi.org/10.1109/TSTE.2017.2707565

Li, P., Zhang, Z., Xiong, Q., Ding, B., Hou, J., Luo, D., Rong, Y., & Li, S. (2020). State-of-health estimation and remaining useful life prediction for the lithium-ion battery based on a variant long short term memory neural network. *Journal of Power Sources*, *459*. https://doi.org/10.1016/j.jpowsour.2020.228069

Li, W., Sengupta, N., Dechent, P., Howey, D., Annaswamy, A., & Sauer, D. U. (2021a). One-shot battery degradation trajectory prediction with deep learning. *Journal of Power Sources*, *506*, 230024. https://doi.org/10.1016/j.jpowsour.2021.230024

Li, W., Sengupta, N., Dechent, P., Howey, D., Annaswamy, A., & Sauer, D. U. (2021b). Online capacity estimation of lithium-ion batteries with deep long short-term memory networks. *Journal of Power Sources*, *482*, 228863. https://doi.org/10.1016/j.jpowsour.2020.228863

Li, X., Zhang, L., Wang, Z., & Dong, P. (2019). Remaining useful life prediction for lithium-ion batteries based on a hybrid model combining the long short-term memory and {Elman} neural networks. *Journal of Energy Storage*, *21*, 510–518. https://doi.org/10.1016/j.est.2018.12.011

Li, Y., Li, K., Liu, X., Wang, Y., & Zhang, L. (2021). Lithium-ion battery capacity estimation — {A} pruned convolutional neural network approach assisted with transfer learning. *Applied Energy*, *285*, 116410. https://doi.org/10.1016/j.apenergy.2020.116410

Li, Y., Liu, K., Foley, A. M., Zülke, A., Berecibar, M., Nanini-Maury, E., Van Mierlo, J., & Hoster, H. E. (2019a). Data-driven health estimation and lifetime prediction of lithium-ion batteries: A review. *Renewable and Sustainable Energy Reviews*, *113*, 109254. https://doi.org/10.1016/j.rser.2019.109254

Li, Y., Liu, K., Foley, A. M., Zülke, A., Berecibar, M., Nanini-Maury, E., Van Mierlo, J., & Hoster, H. E. (2019b). Data-driven health estimation and lifetime prediction of lithium-ion batteries: A review. *Renewable and Sustainable Energy Reviews*, *113*, 109254. https://doi.org/10.1016/j.rser.2019.109254

Li, Y., Zou, C., Berecibar, M., Nanini-Maury, E., Chan, J. C.-W., van den Bossche, P., Van Mierlo, J., & Omar, N. (2018). Random forest regression for online capacity estimation of lithium-ion batteries. *Applied Energy*, *232*, 197–210. https://doi.org/10.1016/j.apenergy.2018.09.182

Liu, K., Hu, X., Wei, Z., Li, Y., & Jiang, Y. (2019). Modified Gaussian Process Regression

Models for Cyclic Capacity Prediction of Lithium-Ion Batteries. *IEEE Transactions on Transportation Electrification*, *5*(4), 1225–1236. https://doi.org/10.1109/TTE.2019.2944802

Liu, K., Peng, Q., Che, Y., Zheng, Y., Li, K., Teodorescu, R., Widanage, D., & Barai, A. (2023). Transfer learning for battery smarter state estimation and ageing prognostics: Recent progress, challenges, and prospects. *Advances in Applied Energy*, *9*, 100117. https://doi.org/10.1016/j.adapen.2022.100117

Liu, K., Shang, Y., Ouyang, Q., & Widanage, W. D. (2021). A Data-Driven Approach With Uncertainty Quantification for Predicting Future Capacities and Remaining Useful Life of Lithium-ion Battery. *IEEE Transactions on Industrial Electronics*, *68*(4), 3170–3180. https://doi.org/10.1109/TIE.2020.2973876

Luo, K., Chen, X., Zheng, H., & Shi, Z. (2022). A review of deep learning approach to predicting the state of health and state of charge of lithium-ion batteries. *Journal of Energy Chemistry*, *74*, 159–173. https://doi.org/10.1016/j.jechem.2022.06.049

Ma, G., Xu, S., Jiang, B., Cheng, C., Yang, X., Shen, Y., Yang, T., Huang, Y., Ding, H., & Yuan, Y. (2022). Real-time personalized health status prediction of lithium-ion batteries using deep transfer learning. *Energy & Environmental Science*, *15*(10), 4083–4094. https://doi.org/10.1039/D2EE01676A

Ng, M.-F., Zhao, J., Yan, Q., Conduit, G. J., & Seh, Z. W. (2020). Predicting the state of charge and health of batteries using data-driven machine learning. *Nature Machine Intelligence*, *2*(3), 161–170. https://doi.org/10.1038/s42256-020-0156-7

Pan, H., Lü, Z., Wang, H., Wei, H., & Chen, L. (2018). Novel battery state-of-health online estimation method using multiple health indicators and an extreme learning machine. *Energy*, *160*, 466–477. https://doi.org/10.1016/j.energy.2018.06.220

Plett, G. L. (2004). Extended Kalman filtering for battery management systems of LiPB-based HEV battery packs. *Journal of Power Sources*, *134*(2), 262–276. https://doi.org/10.1016/j.jpowsour.2004.02.032

Qu, J., Liu, F., Ma, Y., & Fan, J. (2019). A Neural-Network-Based Method for RUL Prediction and SOH Monitoring of Lithium-Ion Battery. *IEEE Access*, *7*, 87178–87191. https://doi.org/10.1109/ACCESS.2019.2925468

Reinhardt, R., Christodoulou, I., Gassó-Domingo, S., & Amante García, B. (2019). Towards sustainable business models for electric vehicle battery second use: A critical review. *Journal of Environmental Management*, *245*, 432–446. https://doi.org/10.1016/j.jenvman.2019.05.095

Ren, L., Dong, J., Wang, X., Meng, Z., Zhao, L., & Deen, M. J. (2021). A Data-Driven Auto-CNN-LSTM Prediction Model for Lithium-Ion Battery Remaining Useful Life. *IEEE Transactions on Industrial Informatics*, *17*(5), 3478–3487. https://doi.org/10.1109/TII.2020.3008223

Ren, L., Zhao, L., Hong, S., Zhao, S., Wang, H., & Zhang, L. (2018). Remaining Useful Life Prediction for Lithium-Ion Battery: A Deep Learning Approach. *IEEE Access*, *6*, 50587–50598. https://doi.org/10.1109/ACCESS.2018.2858856

Ren, Z., & Du, C. (2023). A review of machine learning state-of-charge and state-of-health estimation algorithms for lithium-ion batteries. *Energy Reports*, *9*, 2993–3021. https://doi.org/10.1016/j.egyr.2023.01.108

Roman, D., Saxena, S., Robu, V., Pecht, M., & Flynn, D. (2021a). Machine learning pipeline for battery state-of-health estimation. *Nature Machine Intelligence*, *3*(5), 447–456. https://doi.org/10.1038/s42256-021-00312-3

Roman, D., Saxena, S., Robu, V., Pecht, M., & Flynn, D. (2021b). Machine learning pipeline for battery state-of-health estimation. *Nature Machine Intelligence*, *3*(5),

447–456. https://doi.org/10.1038/s42256-021-00312-3

Sanz-Gorrachategui, I., Pastor-Flores, P., Pajovic, M., Wang, Y., Orlik, P. V, Bernal-Ruiz, C., Bono-Nuez, A., & Artal-Sevil, J. S. (2021). Remaining Useful Life Estimation for LFP Cells in Second-Life Applications. *IEEE Transactions on Instrumentation and Measurement*, *70*, 1–10. https://doi.org/10.1109/TIM.2021.3055791

Severson, K. A., Attia, P. M., Jin, N., Perkins, N., Jiang, B., Yang, Z., Chen, M. H., Aykol, M., Herring, P. K., Fraggedakis, D., Bazant, M. Z., Harris, S. J., Chueh, W. C., & Braatz, R. D. (2019a). Data-driven prediction of battery cycle life before capacity degradation. *Nature Energy*, *4*(5), 383–391. https://doi.org/10.1038/s41560-019-0356-8

Severson, K. A., Attia, P. M., Jin, N., Perkins, N., Jiang, B., Yang, Z., Chen, M. H., Aykol, M., Herring, P. K., Fraggedakis, D., Bazant, M. Z., Harris, S. J., Chueh, W. C., & Braatz, R. D. (2019b). Data-driven prediction of battery cycle life before capacity degradation. *Nature Energy*, *4*(5), 383–391. https://doi.org/10.1038/s41560-019-0356-8

Shahjalal, M., Roy, P. K., Shams, T., Fly, A., Chowdhury, J. I., Ahmed, Md. R., & Liu, K. (2022). A review on second-life of Li-ion batteries: prospects, challenges, and issues. *Energy*, *241*, 122881. https://doi.org/10.1016/j.energy.2021.122881

Shen, S., Sadoughi, M., Chen, X., Hong, M., & Hu, C. (2019). A deep learning method for online capacity estimation of lithium-ion batteries. *Journal of Energy Storage*, *25*. https://doi.org/10.1016/j.est.2019.100817

Shu, X., Shen, S., Shen, J., Zhang, Y., Li, G., Chen, Z., & Liu, Y. (2021). State of health prediction of lithium-ion batteries based on machine learning: {Advances} and perspectives. *IScience*, *24*(11), 103265. https://doi.org/10.1016/j.isci.2021.103265

Souza, A. A. C. e. (2020). *Ciência, tecnologia e inovação na América Latina : avanços e experiências em abordagem inter(multi)disciplinar*. 273. https://www.pacolivros.com.br/ciencia-tecnologia-e-inovacao-na-america-latina

Sui, X., He, S., Vilsen, S. B., Meng, J., Teodorescu, R., & Stroe, D.-I. (2021). A review of non-probabilistic machine learning-based state of health estimation techniques for {Lithium}-ion battery. *Applied Energy*, *300*, 117346. https://doi.org/10.1016/j.apenergy.2021.117346

Sylvestrin, G. R., Maciel, J. N., Amorim, M. L. M., Carmo, J. P., Afonso, J. A., Lopes, S. F., & Ando Junior, O. H. (2025a). State of the Art in Electric Batteries' State-of-Health (SoH) Estimation with Machine Learning: A Review. *Energies*, *18*(3). https://doi.org/10.3390/en18030746

Sylvestrin, G. R., Maciel, J. N., Amorim, M. L. M., Carmo, J. P., Afonso, J. A., Lopes, S. F., & Ando Junior, O. H. (2025b). State of the Art in Electric Batteries' State-of-Health (SoH) Estimation with Machine Learning: A Review. *Energies*, *18*(3). https://doi.org/10.3390/en18030746

Sylvestrin, G. R., Scherer, H. F., & Ando Junior, O. H. (2022). Experimental Validation of State of Charge Estimation by Extended Kalman Filter and Modified Coulomb Counting. *IEEE Latin America Transactions*, *20*(11), 2395–2403. https://doi.org/10.1109/TLA.2022.9904765

Sylvestrin, G. R., Scherer, H. F., & Hideo Ando Junior, O. (2021). Hardware and Software Development of an Open Source Battery Management System. *IEEE Latin America Transactions*, *19*(7), 1153–1163. https://doi.org/10.1109/TLA.2021.9461844

Tagade, P., Hariharan, K. S., Ramachandran, S., Khandelwal, A., Naha, A., Kolake, S. M., & Han, S. H. (2020). Deep Gaussian process regression for lithium-ion battery health prognosis and degradation mode diagnosis. *Journal of Power Sources*, *445*.

https://doi.org/10.1016/j.jpowsour.2019.227281
Tan, Y., Tan, Y., Zhao, G., & Zhao, G. (2020). Transfer learning with long short-term memory network for state-of-health prediction of lithium-ion batteries. *IEEE Transactions on Industrial Electronics*, *67*(10), 8723–8731. https://doi.org/10.1109/TIE.2019.2946551
Tang, X., Liu, K., Wang, X., Gao, F., Macro, J., & Widanage, W. D. (2020). Model {Migration} {Neural} {Network} for {Predicting} {Battery} {Aging} {Trajectories}. *IEEE Transactions on Transportation Electrification*, *6*(2), 363–374. https://doi.org/10.1109/TTE.2020.2979547
Vidal, C., Malysz, P., Kollmeyer, P., & Emadi, A. (2020). Machine Learning Applied to Electrified Vehicle Battery State of Charge and State of Health Estimation: State-of-the-Art. *IEEE Access*, *8*, 52796–52814. https://doi.org/10.1109/ACCESS.2020.2980961
Wang, S., Jin, S., Bai, D., Fan, Y., Shi, H., & Fernandez, C. (2021). A critical review of improved deep learning methods for the remaining useful life prediction of lithium-ion batteries. *Energy Reports*, *7*, 5562–5574. https://doi.org/10.1016/j.egyr.2021.08.182
Xu, Q., Wu, M., Khoo, E., Chen, Z., & Li, X. (2023). A Hybrid Ensemble Deep Learning Approach for Early Prediction of Battery Remaining Useful Life. *IEEE/CAA Journal of Automatica Sinica*, *10*(1), 177–187. https://doi.org/10.1109/JAS.2023.123024
Yang, F., Wang, D., Xu, F., Huang, Z., & Tsui, K.-L. (2020). Lifespan prediction of lithium-ion batteries based on various extracted features and gradient boosting regression tree model. *Journal of Power Sources*, *476*, 228654. https://doi.org/10.1016/j.jpowsour.2020.228654
Yang, Y. (2021). A machine-learning prediction method of lithium-ion battery life based on charge process for different applications. *Applied Energy*, *292*, 116897. https://doi.org/10.1016/j.apenergy.2021.116897
Yao, X.-Y., Chen, G., Pecht, M., & Chen, B. (2023). A novel graph-based framework for state of health prediction of lithium-ion battery. *Journal of Energy Storage*, *58*, 106437. https://doi.org/10.1016/j.est.2022.106437
Yu, J. (2018). State of health prediction of lithium-ion batteries: Multiscale logic regression and Gaussian process regression ensemble. *Reliability Engineering and System Safety*, *174*, 82–95. https://doi.org/10.1016/j.ress.2018.02.022
Zhang, L., Dai, Y., Li, C., Dang, Y., Zheng, R., Wang, Z., Wang, Y., Cui, Y., Arandiyan, H., Shao, Z., Sun, H., Zhuang, Q., & Liu, Y. (2024). Recent advances in electrochemical impedance spectroscopy for solid-state batteries. *Energy Storage Materials*, *69*, 103378. https://doi.org/https://doi.org/10.1016/j.ensm.2024.103378
Zhang, L., Liu, Y., Pang, B., Sun, B., & Kokko, A. (2020). Second Use Value of China's New Energy Vehicle Battery: A View Based on Multi-Scenario Simulation. *Sustainability*, *12*(1), 341. https://doi.org/10.3390/su12010341
Zhang, S., Zhai, B., Guo, X., Wang, K., Peng, N., & Zhang, X. (2019). Synchronous estimation of state of health and remaining useful lifetime for lithium-ion battery using the incremental capacity and artificial neural networks. *Journal of Energy Storage*, *26*. https://doi.org/10.1016/j.est.2019.100951
Zhang, W., Li, X., & Li, X. (2020). Deep learning-based prognostic approach for lithium-ion batteries with adaptive time-series prediction and on-line validation. *Measurement: Journal of the International Measurement Confederation*, *164*. https://doi.org/10.1016/j.measurement.2020.108052
Zhang, Y., Wik, T., Bergström, J., Pecht, M., & Zou, C. (2022). A machine learning-based

framework for online prediction of battery ageing trajectory and lifetime using histogram data. *Journal of Power Sources*, *526*, 231110. https://doi.org/10.1016/j.jpowsour.2022.231110

Zhang, Y., Xiong, R., He, H., & Pecht, M. G. (2018). Long Short-Term Memory Recurrent Neural Network for Remaining Useful Life Prediction of Lithium-Ion Batteries. *IEEE Transactions on Vehicular Technology*, *67*(7), 5695–5705. https://doi.org/10.1109/TVT.2018.2805189

Zhao, J., Han, X., Ouyang, M., & Burke, A. F. (2023). Specialized deep neural networks for battery health prognostics: Opportunities and challenges. *Journal of Energy Chemistry*, *87*, 416–438. https://doi.org/10.1016/j.jechem.2023.08.047

Zhao, J., Ling, H., Liu, J., Wang, J., Burke, A. F., & Lian, Y. (2023). Machine learning for predicting battery capacity for electric vehicles. *ETransportation*, *15*, 100214. https://doi.org/10.1016/j.etran.2022.100214

APÊNDICES

A.1: Publicação 1

Citação: Sylvestrin, G. R., Maciel, J. N., Amorim, M. L. M., Carmo, J. P., Afonso, J. A., Lopes, S. F., & Ando Junior, O. H. (2025). *State of the Art in Electric Batteries' State-of-Health (SoH) Estimation with Machine Learning: A Review*. Energies, 18(3), 746.

energies

MDPI

Review

State of the Art in Electric Batteries' State-of-Health (SoH) Estimation with Machine Learning: A Review

Giovane Ronei Sylvestrin [1,2], Joylan Nunes Maciel [1,2], Marcio Luís Munhoz Amorim [3], João Paulo Carmo [3], José A. Afonso [4,*], Sérgio F. Lopes [5] and Oswaldo Hideo Ando Junior [1,2,6,*]

1 Interdisciplinary Postgraduate Program in Energy & Sustainability (PPGIES), Federal University of Latin American Integration—UNILA, Paraná City 85867-000, PR, Brazil; giovane.sylvestrin@aluno.unila.edu.br (G.R.S.); joylan.maciel@unila.edu.br (J.N.M.)
2 Research Group on Energy & Energy Sustainability (GPEnSE), Academic Unit of Cabo de Santo Agostinho (UACSA), Federal Rural University of Pernambuco (UFRPE), Cabo de Santo Agostinho 54518-430, PE, Brazil
3 Group of Metamaterials Microwaves and Optics (GMeta), Department of Electrical Engineering (SEL), University of São Paulo (USP), Avenida Trabalhador São-Carlense, Nr. 400, Parque Industrial Arnold Schmidt, São Carlos 13566-590, SP, Brazil; marciolma@usp.br (M.L.M.A.); jcarmo@sc.usp.br (J.P.C.)
4 Center for Microelectromechanical Systems (CMEMS), University of Minho, 4800-058 Guimarães, Portugal
5 Centro Algoritmi/LASI, University of Minho, 4704-553 Guimarães, Portugal; sergio.lopes@dei.uminho.pt
6 Smart Grid Laboratory (LabREI), Center for Alternative and Renewable Research (CEAR), Federal University of Paraiba (UFPB), João Pessoa 58051-900, PB, Brazil
* Correspondence: jose.afonso@dei.uminho.pt (J.A.A.); oswaldo.ando@ufrpe.br (O.H.A.J.)

Abstract: The sustainable reuse of batteries after their first life in electric vehicles requires accurate state-of-health (SoH) estimation to ensure safe and efficient repurposing. This study applies the systematic ProKnow-C methodology to analyze the state of the art in SoH estimation using machine learning (ML). A bibliographic portfolio of 534 papers (from 2018 onward) was constructed, revealing key research trends. Public datasets are increasingly favored, appearing in 60% of the studies and reaching 76% in 2023. Among 12 identified sources covering 20 datasets from different lithium battery technologies, NASA's Prognostics Center of Excellence contributes 51% of them. Deep learning (DL) dominates the field, comprising 57.5% of the implementations, with LSTM networks used in 22% of the cases. This study also explores hybrid models and the emerging role of transfer learning (TL) in improving SoH prediction accuracy. This study also highlights the potential applications of SoH predictions in energy informatics and smart systems, such as smart grids and Internet-of-Things (IoT) devices. By integrating accurate SoH estimates into real-time monitoring systems and wireless sensor networks, it is possible to enhance energy efficiency, optimize battery management, and promote sustainable energy practices. These applications reinforce the relevance of machine-learning-based SoH predictions in improving the resilience and sustainability of energy systems. Finally, an assessment of implemented algorithms and their performances provides a structured overview of the field, identifying opportunities for future advancements.

Keywords: state of health; battery; machine learning; ProKnow-C; public datasets; energy informatics; smart grids; internet of things; deep learning

Academic Editor: Jose Luis Calvo-Rolle

Received: 13 January 2025
Revised: 31 January 2025
Accepted: 4 February 2025
Published: 6 February 2025

Citation: Sylvestrin, G.R.; Maciel, J.N.; Amorim, M.L.M.; Carmo, J.P.; Afonso, J.A.; Lopes, S.F.; Ando Junior, O.H. State of the Art in Electric Batteries' State-of-Health (SoH) Estimation with Machine Learning: A Review. *Energies* **2025**, *18*, 746. https://doi.org/10.3390/en18030746

1. Introduction

The worldwide increase in battery usage is evident in various fields, especially in electric vehicles. Research efforts aim to improve battery efficiency, extend lifespan, and reduce charging time, driven by the demands of a growing global market. Alongside

advancements in technology, vehicle battery reuse has emerged as a key area of focus. Batteries can serve automotive purposes until their capacity drops to about 80% of the nominal value. Beyond this point, replacement is necessary to meet the power requirements of vehicles [1]. However, the cells from these batteries can still be repurposed for other applications, such as stationary energy storage systems connected to photovoltaic generation devices. This process, known as second use, offers a sustainable way to extend battery life.

The repurposing of a second-use battery is still a process that requires improvement because of construction and safety difficulties. Accurate estimation of batteries' SoH is pivotal in advancing sustainable energy solutions. By integrating SoH predictions into smart grids and IoT systems, it is possible to optimize energy management, enhance system resilience, and reduce waste, aligning with broader energy informatics and sustainability goals. With increasing computational advances, the presence of smart sensors, and the era of big data, there has been growing research interest in applying machine-learning (ML) algorithms of artificial intelligence [2–4]. Accurate SoH characterization is essential for assessing cells suitable for reuse. As new datasets become available, the volume of research connecting ML to SoH estimation continues to grow, as demonstrated by numerous recent studies [5–9].

The estimation of the SoH of batteries is a critical step for enhancing their lifecycle management, especially in applications where reliability and performance are paramount [1]. Commonly employed methods for SoH estimation can be broadly classified into electrochemical approaches and model-based, data-driven, and hybrid methods [10–13]. Electrochemical approaches, although less common in operational environments because of their invasive nature, offer unparalleled precision for understanding battery degradation mechanisms. For instance, differential voltage analysis and differential capacity analysis [14,15] are used to track specific aging signatures by analyzing voltage–capacity profiles during charge/discharge cycles. These methods, combined with techniques like cyclic voltammetry [16] or advanced electrochemical impedance spectroscopy [17], provide detailed insights into phenomena such as lithium plating and active material loss. Although such methods are typically applied in laboratory settings, recent advances in sensor technology and signal processing aim to make them more feasible for real-time SoH estimation [15].

Model-based methods rely on electrochemical or equivalent-circuit models to predict the SoH by capturing the physical and chemical behaviors of the battery [18]. Techniques such as electrochemical impedance spectroscopy [19], Kalman filtering [18], and particle filtering [20] are widely used in this category. These methods offer precise insights into battery performance but often require complex parameter tuning and are computationally intensive [18,20].

Data-driven methods, on the other hand, utilize ML and DL algorithms to analyze large datasets and uncover patterns indicative of battery degradation [10]. These methods excel in modeling nonlinear relationships and adapting to diverse battery chemistries and usage patterns [10,11]. However, their reliance on large amounts of labeled data and challenges in interpretability limit their direct application in some scenarios [10,11,13]. Hybrid methods combine the strengths of model-based and data-driven approaches, leveraging physical models to enhance the interpretability and robustness of ML-based predictions. In [21,22], hybrid approaches integrating equivalent-circuit models with ML techniques are proposed, achieving a balance between accuracy and computational complexity. Despite their promise, hybrid methods often require significant domain-specific expertise and extensive computational resources [23].

Recent advancements in computational power and the availability of large datasets have significantly boosted the prominence of data-driven methods, making them a corner-

stone in SoH estimation for large-scale applications, like electric vehicles and stationary energy storage systems [10,11]. Nonetheless, challenges persist regarding data availability, algorithmic generalization, and system interpretability [13].

The work presented in [10] provides a list of advantages and disadvantages of using ML algorithms, highlighting the need for open platforms for data sharing and modeling techniques as a necessary step for the advancement of the research field. In the context of challenges and prospects, studies [24–26], which focus on exploring DL techniques for estimating the remaining battery life, are also noteworthy, while in [27], this theme is reviewed from the perspective of transfer-learning usage. In [28], challenges and prospects are addressed considering the importance of feature extraction, construction, and selection for health state modeling. The importance of battery health characterization is presented in [12], under the challenges of scaling second-use batteries. In [11], a relevant review of state-of-charge (SoC) and -health estimation is presented, where the authors reveal comparative results mainly considering neural networks, such as feedforward neural networks (FFNNs), recurrent neural networks (RNNs), and long short-term memories (LSTMs). Studies [29–31] also provide a review focused on comparing techniques for studying battery degradation. In all the relevant review papers in recent years that have been analyzed, a common gap can be pointed out: the absence of a structured methodology that underpins the analysis portfolio and leads to the authors' conclusions.

Although significant research has been conducted on data-driven algorithms for SoH estimation, systematic methodologies are lacking to ensure the selection of highly relevant studies for constructing a reliable state-of-the-art overview. The absence of such approaches makes it difficult to identify emerging trends in the field. In this context, and given the relevance of the topic, this work aims to explore the recent state-of-the-art panorama, from the last 5 years, for the estimation of batteries' SoHs. To achieve this, we start with the explanation and demonstration of a structured and systematic methodology, known as ProKnow-C (Knowledge Development Process Constructivist) [32], to obtain a centralized bibliographic portfolio on the topic of predicting the health states of batteries, using ML. ProKnow-C is a structured process designed to assist researchers in systematically identifying, selecting, and analyzing a bibliographic portfolio aligned with their research objectives [32–34]. It stands out as a comprehensive approach for conducting literature reviews because it combines quantitative and qualitative criteria, ensuring the inclusion of highly relevant and impactful studies while minimizing biases often present in manual selection processes [32,35]. By applying this methodology, we aim to construct a robust bibliographic portfolio that provides a reliable foundation for evaluating the state of the art in batteries' SoH estimations. In this way, this paper's contributions are summarized as follows:

Application of the ProKnow-C Methodology: The presentation and demonstration of the ProKnow-C systematic methodology for building a bibliographic portfolio. This systematic approach allows for rigorous and structured literature reviews.

Characterization of the Research Scenario (State of the Art): Characterization of the current scenario of studies in the health-state estimation of batteries, using ML by analyzing 534 relevant articles published between 2018 and 2024. This provides a comprehensive state of the art in the current research field.

Public Dataset Compilation: Presentation, detailing, and summary of 20 public datasets from 12 different sources, primarily from university research centers, for selecting suitable datasets for research in SoH, SoC, and battery energy storage systems.

Machine-Learning and Deep-Learning Algorithms: Research of the main ML algorithms used in studies predicting response variables related to battery degradation, including deep-learning, hybrid, and transfer-learning models.

Performance Analysis of SoH Estimation Models: A comprehensive performance analysis of state-of-health estimation models, focusing on various response variables, including SoH, remaining-useful-life, current-lifecycle, capacity, trajectory, and early-useful-life predictions. The comparison involves 21 studies, allowing for both fair and broader comparisons.

First Study Applying ProKnow-C to Batteries' SoHs: This study is the first to apply the ProKnow-C systematic review method in the context of batteries' state-of-health estimations. This pioneering application sets a new standard for structured literature reviews in this field.

The remainder of this paper is organized as follows: Section 2 details a systematic review using the ProKnow-C methodology, enabling rigorous and structured literature selection, mapping the state of the art in studies and experiments and available open datasets for the applicability of these techniques. Section 3 discusses in detail the content analysis of the bibliographic review, as well as the analyses of the papers composing the bibliographic portfolio on this topic, including the main databases and ML algorithms, along with the key literary studies. Additionally, this section explores the potential practical applications of SoH estimation in energy informatics, smart grids, and IoT systems, highlighting its role in enhancing energy efficiency, sustainability, and operational resilience. Finally, Section 4 offers concluding remarks, summarizes the main results, and provides suggestions for future research, exploring potential developments based on the integration of artificial intelligence in various scenarios while identifying gaps and opportunities for future research.

2. Systematic Review

The adoption of systematic processes for bibliographic surveying allows for optimizing the quality of the material obtained on a particular topic, as it makes the process more analytical and rigorous, thereby improving the reliability of the results found. As this is an initial and fundamental stage for all research development, methods that increase the robustness of a bibliographic portfolio are essential [36].

In this paper, the systematic method ProKnow-C is employed to obtain a recent and scientifically relevant bibliographic portfolio on the use of ML in estimating SoHs of batteries. ProKnow-C was developed at the Laboratory of Multicriteria Methodologies in Decision Support (LabMCDA) at the Federal University of Santa Catarina (UFSC) and patented in 2010 [32]. This method has been applied in research in various areas, and some examples of ProKnow-C applications can be observed in [33,35,36].

Within the field of electric batteries, the ProKnow-C method was applied in [34] to define the state of the art in lithium-ion-battery recycling. Although related, the present study specifically focuses on analyzing the state of the art in SoH estimation using ML methods. To date, no similar study applying ProKnow-C has been observed.

The ProKnow-C method consists of four main stages [36]:

- Selection of a portfolio of papers on the research topic: This involves defining research keywords, searching in databases, and filtering articles based on alignment with the research objective, citation metrics, and relevance;
- Bibliometric analysis of the portfolio: This stage examines scientific indicators, such as the number of articles, citation counts, authors, and journals, to assess the portfolio's comprehensiveness and scientific impact;
- Systemic analysis: The selected articles are deeply analyzed for insights and patterns and the identification of possible research gaps;

- Definition of the research question and objective: The results from the previous stages are synthesized to refine the scope and formulate precise research questions and objectives.

This paper presents the results of the first three stages of the ProKnow-C method, along with the analysis of the selected relevant papers. These stages represent a comprehensive state-of-the-art review of the broader research field, serving as a basis for refining the focus to a more specific and well-defined niche.

Other well-known systematic review methods can be found in the literature and may be used as alternatives to ProKnow-C. The PRISMA (Preferred Reporting Items for Systematic Reviews and Meta-Analyses) [37] emphasizes transparency and replicability through strict adherence to predefined inclusion and exclusion criteria, making it widely regarded as a gold standard in fields such as energy systems, environmental science, artificial intelligence, and other technical domains [38–40]. However, PRISMA does not include a bibliometric evaluation phase or tools for multicriteria decision-making, which are central to ProKnow-C. Similarly, SALSA (Search, Appraisal, Synthesis, and Analysis) [41] focuses more on synthesizing and analyzing evidence but lacks the portfolio alignment capabilities of ProKnow-C, which ensures a targeted and relevant selection of articles. Another method, Scoping Reviews, is designed to map the breadth and depth of the literature on a topic, making it well-suited for exploratory studies or identifying gaps in the literature [42]. Although Scoping Reviews provides a broad overview, it is less structured in terms of bibliometric evaluation and often does not employ multicriteria tools to refine the portfolio, which are key strengths of ProKnow-C [43].

However, as with any method, ProKnow-C has its limitations. The subjective alignment analysis stage, although useful for tailoring the portfolio to specific objectives, may reduce repeatability [35]. Additionally, its reliance on citation metrics might overlook emerging but seldom-cited studies [35].

2.1. Bibliographic Portfolio Selection

This section describes the selection of the bibliographic portfolio, initially, the set of axes and keywords that encompass the theme of this research, i.e., the use of ML in estimating SoH, was defined. As shown in Table 1, axis 1 corresponds to the study object, which is batteries. Axes 2 and 3 encompass terms related to the definition of SoH and its estimation, respectively. Axis 4 includes terms related to artificial intelligence algorithms, machine learning, deep learning, and ensembles.

Table 1. Research axes for the bibliographic portfolio selection.

Axis 1	Axis 2	Axis 3	Axis 4
battery	state of health	estimation	machine learning
	cycle life	prediction	neural network
	lifetime	features	transfer learning
	aging	second use	artificial intelligence
	degradation		boosting
	useful life		quantile regression
			ensemble
			deep learning

The axes were combined using the conditional logic AND, resulting in 192 combinations searched in the Scopus database. Filters were established for documents of the types of papers and reviews, searching for the keywords in titles, keywords, and abstracts, as well as defining a research horizon of publications of up to 5 years old. The Scopus database was selected because of the larger volume of papers returned compared to other databases, such as Web of Science, as well as the presence of journals focused on areas possibly related to the research. An example of a condition resulting from the combination of axes was (TITLE-ABS-KEY(battery) and TITLE-ABS-KEY(state of health) and TITLE-ABS-KEY(prediction) and TITLE-ABS-KEY(neural network) and PUBYEAR > 2017 and (LIMIT-TO (DOCTYPE, "ar") OR LIMIT-TO (DOCTYPE, "re")).

Table 2 presents the adherence metrics for the keywords used in the combinations of axes. The percentages shown quantify the portions of the total number of raw articles in which a particular keyword was included in the performed combinations. Within axis 2 combinations, a higher adherence rate to the term "state of health" is observed, while in axis 3 and 4 combinations, the keywords "prediction" and "neural network" stand out, respectively. These adherence metrics suggest that within the theme of research related to battery's state of health, the term "state of health" tends to be more applied, often in connection with "prediction" studies utilizing "neural networks". It is important to note that although some terms show low adherence rates, they remain relevant for identifying potentially important papers that may explore emerging trends in an area of research still underexplored.

Table 2. Adherence to the research axes.

Axis	Keyword	Keyword Adherence Rate
Axis 2	state of health	29.3%
	degradation	20.6%
	aging	17.7%
	useful life	13.6%
	cycle life	10.9%
	lifetime	7.9%
Axis 3	prediction	36.5%
	estimation	30.9%
	features	24.9%
	second use	7.8%
Axis 4	neural network	36.9%
	machine learning	28.6%
	deep learning	14.6%
	ensemble	6.2%
	transfer learning	5.5%
	artificial intelligence	4.5%
	boosting	3.4%
	quantile regression	0.3%

This search was conducted on 14 January 2024, resulting in a total of 6032 papers (with 275 papers from 2024). Although there were papers from 2024, for the calculation of a publication horizon of up to 5 years, research from 2018 onward was considered, thus having 6 complete years of publications for analysis plus two weeks of publications in 2024. The papers were exported in ".csv" format in each iteration of the 192 combinations of axes.

The initial flow proposed by ProKnow-C is presented in Figure 1. The objective of this first stage is to significantly reduce the volume of papers in the RPD (raw paper database) obtained from the combinations of research axes. To achieve this, filters are applied to perform a preliminary selection of articles related to the research theme. The following filters are applied:

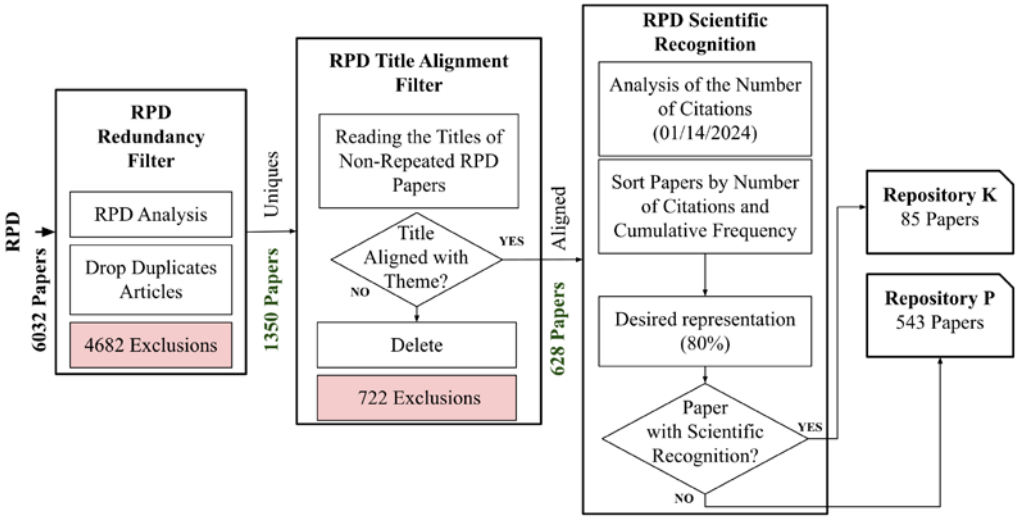

Figure 1. Flow I for obtaining the bibliographic portfolio.

Redundancy Filter: This is the first step of ProKnow-C, where the RPD papers are analyzed for duplication. In this stage, the ".csv" files resulting from the axis combinations were processed through a Python script that performed concatenation and removal of duplicates according to the title and publication year fields. A total of 4682 samples were removed from the RPD.

Title Alignment Filter: This involves reading the papers' titles to assess whether they are aligned with the research theme, as identified by the researchers. Out of the 1350 papers remaining after the previous filter, 722 were deemed to be not aligned with the research. Among the papers not selected were studies focused on SoH analysis in electrochemical contexts and laboratory experimental phases, which are considered as preliminary steps before exploring databases and implementing ML models.

Scientific Recognition Filter: This step involves analyzing the number of citations within the RPD. In this step, the remaining 672 papers are sorted in descending order by citation count. According to the cumulative percentage of citations and a predefined cutoff percentage, the portfolio is divided into two repositories: K and P. The K repository consists of papers considered as scientifically recognized, containing 80% of the citations in the input portfolio for this filter, totaling 85 publications in the case study. The cutoff percentage is determined by the researchers, with [32,36] recommending a range between 70% and 90%. The P repository comprises 543 papers exceeding the defined cutoff threshold.

The second flow of article selection steps for the bibliographic portfolio, using ProKnow-C, is presented in the flowchart in Figure 2. In this second phase of the method, the objective is to verify the alignment of the papers remaining from the first phase with the content presented in their abstracts. The following steps are applied:

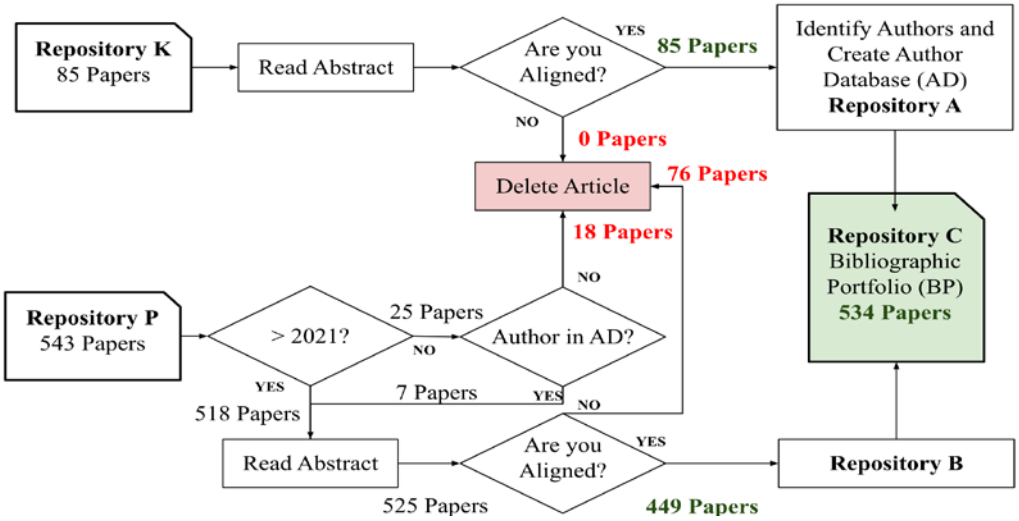

Figure 2. Flow II for obtaining the bibliographic portfolio.

K Repository Alignment: The abstracts of the papers considered as scientifically recognized are analyzed by the researcher(s) to determine whether the research aligns with the intended research objectives. If the article is aligned, it remains in the ProKnow-C flow; otherwise, it is excluded. The 85 articles in repository K were considered as aligned with SoH estimations using ML.

Creation of the Author Database (AD) and Repository A: This step involves identifying the authors of the papers approved in the previous step and creating a database of authors deemed as relevant to the research theme. The selected papers are considered as aligned with the research theme and form repository A, which constitutes the first part of the final portfolio.

P Repository Alignment: This step analyzes the papers that did not reach the level of scientific recognition. These papers are divided into two categories based on their year of publication. Articles published more than two years ago are pre-selected if one of their authors is present in the AD corresponding to repository A. If no match is found in the author database, the papers are excluded. The remaining papers are then evaluated for abstract alignment, and if the expected alignment is confirmed, they are approved in the flow and included in repository B. Recent articles are not evaluated based on the AD; instead, their abstracts are directly analyzed for alignment, and approved papers are added to repository B. In this case study, in the initial analysis of repository P, which contained a total of 543 papers, 518 were recent publications from the past two years. Of the twenty-five articles older than two years, eighteen were excluded because of the absence in the AD, and the remaining seven were added to the group containing the 518 recent papers. Of the 525 papers analyzed in this stage, 449 were found to be aligned and formed repository B.

Creation of Repository C: This step involves combining repositories A and B to form the final bibliographic portfolio resulting from the application of ProKnow-C. The final portfolio comprises papers aligned with the research theme, including scientifically recognized studies in terms of citations, recent articles with potential, and publications by researchers deemed as relevant to the field.

The union of repositories A and B forms the final bibliographic portfolio with 534 papers, representing about 9% of the initial raw paper portfolio. From this group, a high degree of alignment with the research is expected, along with the ability to describe the current state of the art, serving as a basis for the development of the target research. Table 3 presents the 40 most relevant papers in terms of the number of citations in the final portfolio. This number is based on the recommendation from [32] to evaluate an ideal vol-

ume of between 20 and 40 papers. However, each field of research and development phase has its own characteristics that influence the ideal volume of papers. Because this work aims to reveal the current research scenario within SoH estimation using ML, a portfolio approximately ten times larger than the volume recommended by [21] was constructed to enable more robust inferences regarding the algorithms employed, datasets used, and performances achieved.

Table 3. Top 40 papers from the bibliographic portfolio.

Title	Citations	Ref.
Data-driven prediction of battery cycle life before capacity degradation	1453	[1]
Long short-term memory recurrent neural network for remaining-useful-life prediction of lithium-ion batteries	880	[44]
Data-driven health estimation and lifetime prediction of lithium-ion batteries: A review	749	[10]
A data-driven approach with uncertainty quantification for predicting future capacities and remaining useful life of lithium-ion batteries	434	[45]
Predicting the states of charge and health of batteries using data-driven machine learning	405	[46]
Random forest regression for online capacity estimation of lithium-ion batteries	398	[47]
Remaining-useful-life prediction for lithium-ion batteries based on a hybrid model combining the long short-term memory and Elman neural networks	316	[48]
Remaining-useful-life prediction for lithium-ion batteries: A deep-learning approach	313	[49]
A data-driven auto-CNN-LSTM prediction model for lithium-ion-batteries' remaining useful life	291	[50]
State-of-health estimation and remaining-useful-life prediction for the lithium-ion battery based on a variant long short-term memory neural network	284	[51]
Machine learning applied to electrified-vehicle-batteries' state-of-charge and state-of-health estimations: State of the art	267	[11]
Modified Gaussian process regression models for cyclic capacity prediction of lithium-ion batteries	262	[52]
A deep-learning method for online capacity estimation of lithium-ion batteries	260	[53]
Machine-learning pipeline for batteries' state-of-health estimations	246	[54]
A neural-network-based method for RUL prediction and SOH monitoring of lithium-ion batteries	245	[55]
A novel estimation method for the state of health of lithium-ion batteries using a prior-knowledge-based neural network and a Markov chain	239	[56]

Table 3. *Cont.*

Title	Citations	Ref.
A data-driven predictive prognostic model for lithium-ion batteries based on a deep-learning algorithm	237	[57]
Novel battery state-of-health online estimation method using multiple health indicators and an extreme-learning machine	232	[58]
Online capacity estimation of lithium-ion batteries with deep long short-term memory networks	230	[59]
A review of second-life Li-ion batteries: prospects, challenges, and issues	213	[12]
State-of-health prediction of lithium-ion batteries: Multiscale logic regression and Gaussian process regression ensemble	204	[60]
A novel deep-learning framework for the state-of-health estimation of lithium-ion batteries	203	[61]
A review of state-of-health estimations and remaining-useful-life prognostics of lithium-ion batteries	200	[13]
Synchronous estimation of state of health and remaining useful lifetime for lithium-ion batteries using the incremental capacity and artificial neural networks	195	[62]
Deep-reinforcement-learning-based energy storage arbitrage with accurate lithium-ion-battery degradation model	193	[63]
State-of-health estimation and remaining-useful-life prediction for lithium-ion batteries using a hybrid data-driven method	190	[64]
Transfer learning with a long short-term memory network for the state-of-health prediction of lithium-ion batteries	184	[65]
Battery health prediction using fusion-based feature selection and machine learning	184	[66]
A review of non-probabilistic machine-learning-based state-of-health estimation techniques for lithium-ion batteries	180	[67]
A critical review of improved deep-learning methods for the remaining-useful-life prediction of lithium-ion batteries	159	[5]
Deep Gaussian process regression for lithium-ion-batteries' health prognosis and degradation mode diagnosis	148	[68]
Model migration neural network for predicting battery-aging trajectories	147	[69]
Toward the swift prediction of the remaining useful life of lithium-ion batteries with end-to-end deep learning	144	[8]
Lithium-ion-batteries' capacity estimation—A pruned convolutional neural network approach assisted by transfer learning	142	[7]

Table 3. *Cont.*

Title	Citations	Ref.
Identification and machine-learning prediction of the knee point and knee onset in capacity degradation curves of lithium-ion cells	142	[70]
Deep-learning-based prognostic approach for lithium-ion batteries with adaptive time-series prediction and online validation	134	[71]
Predictive battery-health management with transfer learning and online model correction	122	[72]
One-shot battery-degradation-trajectory prediction with deep learning	121	[73]
Online health diagnosis of lithium-ion batteries based on a nonlinear autoregressive neural network	117	[74]
Sorting, regrouping, and echelon utilization of large-scale retired lithium batteries: A critical review	117	[9]

Among the papers listed in Table 3, we consider the work in [1] to be one of the most important in the field, a cornerstone article on the use of ML in predicting batteries' SoHs. Furthermore, it was responsible for constructing one of the first openly available datasets and widely disseminated in subsequent studies. The decision to allow research reproduction by keeping the dataset open certainly contributed to the increase in the number of publications in the field, allowing researchers to overcome limitations in result reproducibility and understanding and compare approaches. For example, several studies, [8,54,66,70,72], make use of this dataset and have a significant number of citations.

The studies conducted by [5,9–13,67] correspond to reviews, whereas [9,10,12] present more qualitative views regarding the use of ML in studying battery degradation, pointing out challenges and trends, types of algorithms that can be employed, and the potential gain that data-driven inferencing techniques can have in the characterization of second-use batteries. In [11], a more focused survey is conducted on the performance of some ML algorithms, with a comparison between different neural network structures, including DL architectures. Similarly, in [5], the authors also perform an analysis of DL algorithms, a topic which is also present in [67], along with other non-probabilistic methods. In [13], approaches are presented, along with comparisons of algorithms and their performances in predicting SoH response variables.

The presence of public datasets is evident in 15 out of the 33 non-review papers from Table 3, namely, studies [1,8,49–51,54,55,57,60,61,64,66,68,70,72], which utilize data from institutions such as the Prognostics Data Repository (NASA), the Center for Advanced Life Cycle Engineering (CALCE, the University of Maryland), the Massachusetts Institute of Technology (MIT, which constructed the dataset in [1]), and the University of Oxford. Further details about the datasets and techniques will be discussed later, considering analyses of the entire portfolio obtained.

2.2. Bibliometric Analysis of the Bibliographic Portfolio

After defining the bibliographic portfolio, the bibliometric analysis stage seeks a quantitative analysis of the information present in the publications and their characteristics [36]. In this paper, five aspects presented in [35] were considered: (i) scientific recognition of the papers; (ii) recognition of the authors; (iii) recognition of the journals; (iv) most used keywords; (v) bibliographic reviews.

2.2.1. Scientific Recognition of the Papers

The first analysis concerns the publication history within the 534 papers of the final bibliographic portfolio, which is shown in the graph in Figure 3, in terms of annual volume and cumulative frequency. It is noted that approximately 45% of the portfolio corresponds to publications from 2023 (and the first two weeks of 2024), indicating the ongoing relevance of the addressed topic and instigation for discoveries in the research field as a trend. This trend highlights the rapid expansion of research in battery SoH estimation, driven by advancements in artificial intelligence (AI) and the growing demand for sustainable energy storage solutions. The alignment of research topics among authors in recent years reflects the global focus on the reuse of lithium-ion batteries and their role in mitigating environmental impacts associated with electric-vehicle-battery waste [12].

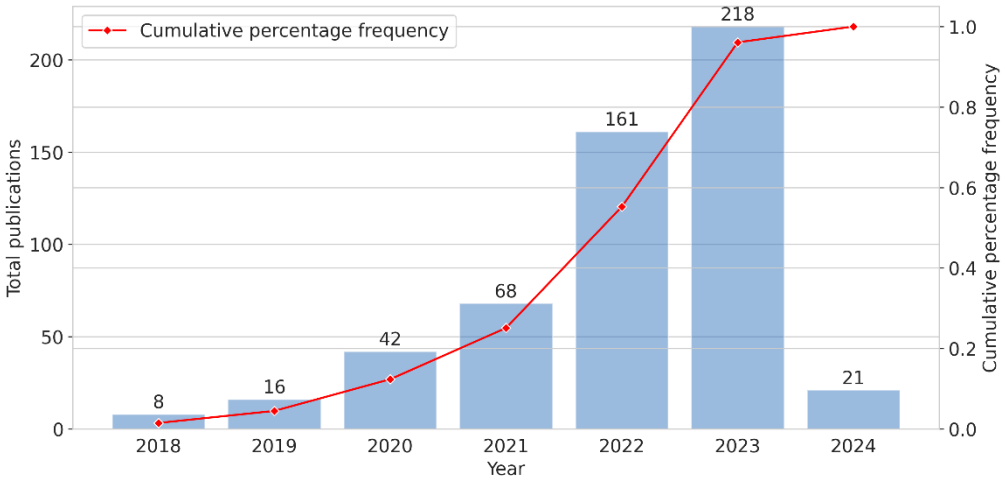

Figure 3. Volumetric analysis of the year of publication in the bibliographic portfolio.

The selected papers from the first week of 2024 already represent a higher volume than the publications from 2018 and 2019, indicating that the alignment of research topics among authors is more recent. Overall, we can observe a trend of research growth in the area when analyzing the growth curve within the obtained portfolio. This is further supported by the intensification of the automobile electrification process, which requires robust methodologies to ensure effective battery health monitoring and reuse [75–77].

Another analysis performed corresponds to the scientific relevance of the papers in the portfolio according to the year of publication, as presented in Figure 4. It is possible to identify the top three most cited papers in the portfolio, published in 2018 and 2019. These cornerstone studies, focused on the use of ML techniques for SoH estimation, have laid the foundation for subsequent studies and have significantly influenced citation patterns. The increasing density of publications over the years, coupled with a reduction in citation intervals, indicates an accelerated dissemination and application of SoH methodologies.

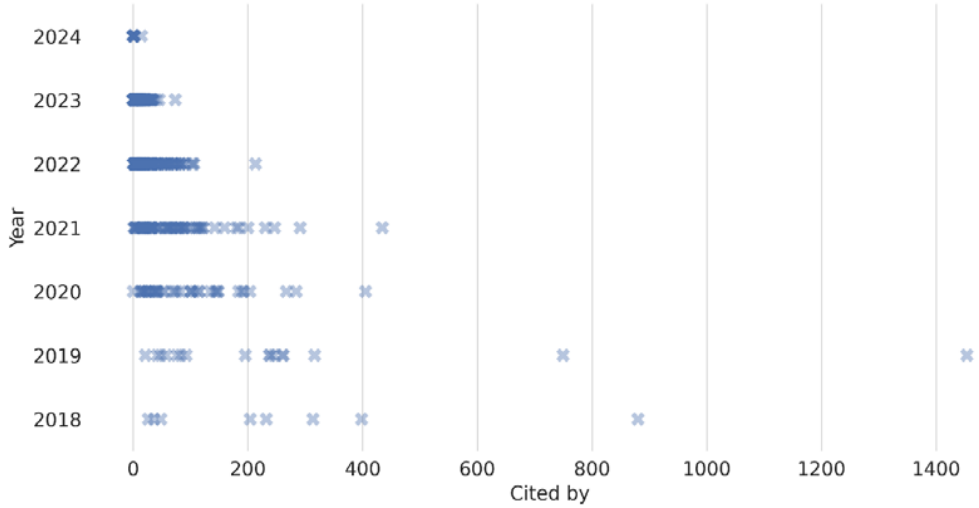

Figure 4. Analysis of the number of citations per year of publication in the bibliographic portfolio.

2.2.2. Author Recognition

The bibliographic portfolio consists of 2593 authors, of which 1967 are unique. The analysis of the distribution of the number of authors per article, presented in Figure 5, indicates that on average and in the median, the articles have five authors, with 30% of the publications having six or more authors, and 98% of the publications having up to ten authors. This median aligns with common collaborative efforts in technical and scientific research, particularly in interdisciplinary fields, such as ML and battery SoH estimation, where diverse expertise is critical.

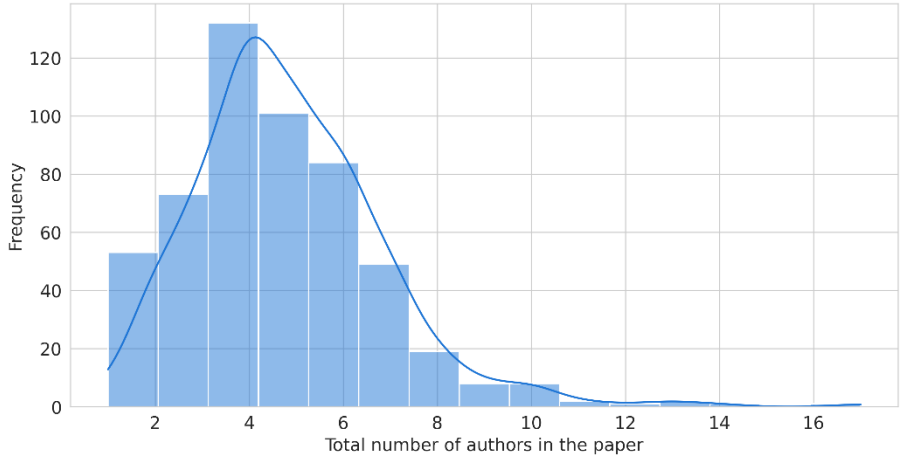

Figure 5. Analysis of the number of authors per publication in the bibliographic portfolio.

The graph in Figure 6 presents the number of papers in which an author is involved. For example, we notice that only one author is present in nine articles in the BP, while 1586 authors are present in only a single article in the BP. Approximately 80% of the authors are present in only one publication, while only 10% of the authors are present in two or more publications. This distribution highlights a high dispersion degree of knowledge within the portfolio, indicative of a field still expanding and attracting a broad range of contributors. Although this diversity enriches the field, it also emphasizes the need for more concentrated and sustained collaborations among leading authors to build upon foundational research.

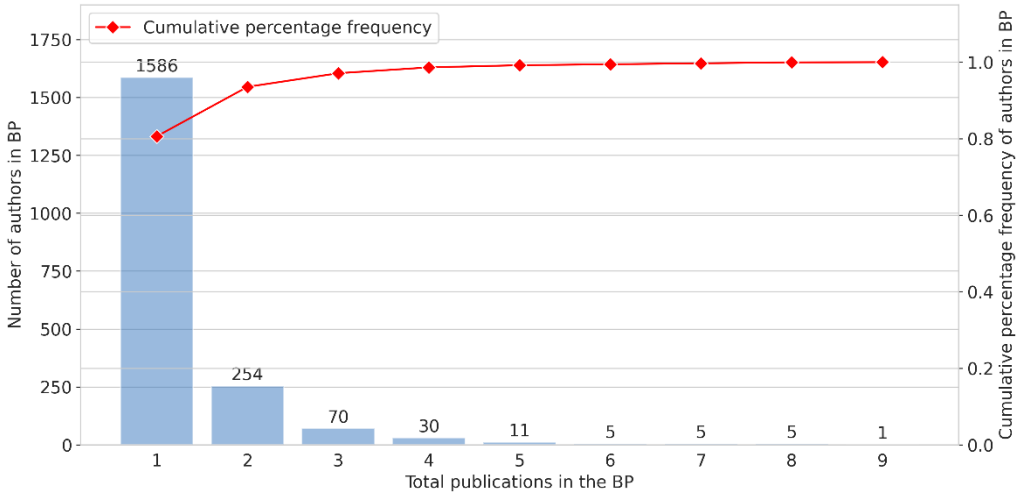

Figure 6. Analysis of the number of publications per author in the bibliographic portfolio.

Figures 7 and 8 provide additional insight. Figure 7 shows the top 30 most prolific authors in the portfolio, offering a reference for identifying influential researchers in the field. Figure 8 illustrates the connections between authors, revealing networks of collaboration. These interconnected clusters suggest that some authors are central to advancing SoH estimation using ML, potentially forming hubs of expertise within this research area.

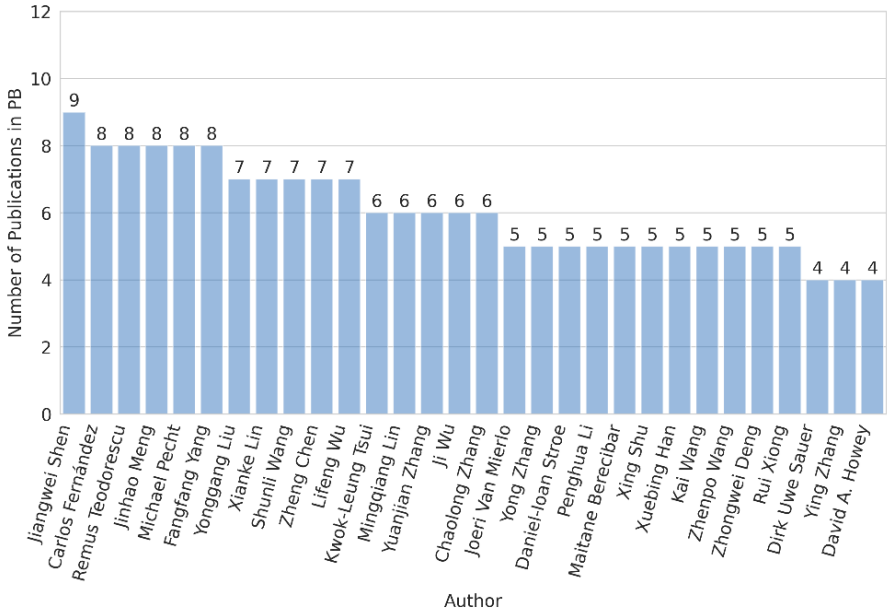

Figure 7. Top 30 authors with the highest participation in the bibliographic portfolio.

Figures 5–8 together underline the importance of collaboration networks and prolific authors in driving innovation. Mapping these connections offers a valuable tool for researchers aiming to identify trends, access seminal studies, or join active research groups in batteries' SoHs and ML.

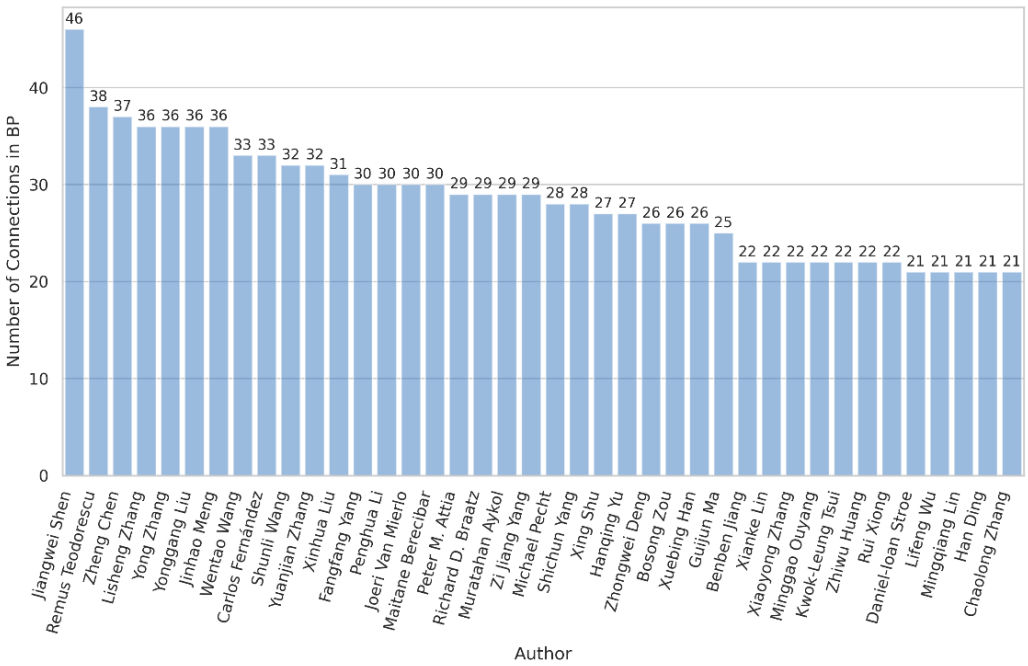

Figure 8. Authors with the most connections within the bibliographic portfolio.

2.2.3. Relevance of Journals

The distribution of journals, as presented in Figure 9, highlights the diversity of publication venues. Journals with one publication in the portfolio were grouped into the "Others" category. About 13% of the portfolio is present in these journals, indicating the variety of journals covering the topic. The category "Others" comprises 72 journals. The *Journal of Energy Storage* is the most represented, accounting for 15% of the total number of publications in the portfolio, emphasizing its central role in disseminating research on batteries' SoHs.

Approximately 55% of the papers in the final portfolio are open access, reflecting the increasing emphasis on making research accessible to a broader audience. Among them is the journal *Energies*. The diversity of journals within this portfolio also reflects a range of main subjects, including sustainable and renewable energies, information technology and computing, system control and automation, computer science and engineering, electrical and electronic engineering, and, primarily, artificial intelligence and ML. This demonstrates how the SoH estimation of batteries is a broad research field and that researchers from different areas are seeking solutions through artificial intelligence.

Figure 9 highlights the growing centralization of SoH research in a few key journals, indicating a maturing field. This concentration not only facilitates a more focused dissemination of cutting-edge research but also provides a reliable reference for scholars and practitioners aiming to access the most impactful findings in the area.

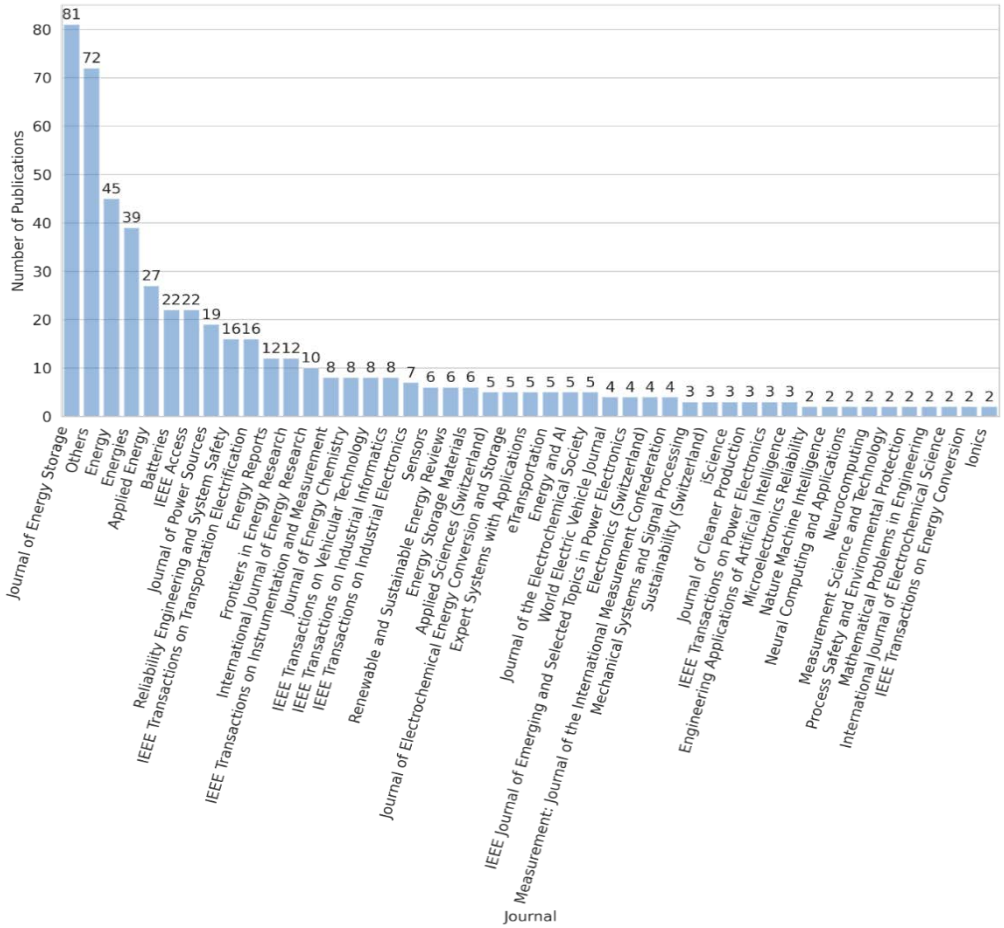

Figure 9. Distribution of the number of publications by journal in the bibliographic portfolio.

2.2.4. Relevance of Keywords

The bibliographic portfolio consists of 2753 keywords, of which 1044 are unique. Figure 10 presents the distribution of the keywords, where a significant concentration is observed for the terms "lithium-ion battery" and "state of health", which are, indeed, the objects and central themes of this research. The prominence of "state of health" reinforces its position as a pivotal concept in this study, guiding much of the research efforts in this field. Additionally, "machine learning" appears as the fifth most frequent term, reflecting the critical role of artificial intelligence in advancing battery SoH estimation.

The term "remaining useful life" is also notable, corresponding to one of the main response variables in the study of the SoH. Regarding techniques, the frequent appearances of "LSTM neural networks" and "deep learning" highlight the increasing adoption of advanced computational models. This reflects the growing sophistication in predictive analytics, as researchers seek more accurate and robust approaches to model battery degradation.

Figure 11 depicts the distribution of keyword connections within the selected papers. The pattern of terms mirrors the previous distribution, showing how central keywords, such as "state of health" and "machine learning", branch out across diverse contexts. This interconnectedness illustrates the multidisciplinary nature of SoH research, bridging fields like energy systems, artificial intelligence, and sustainability.

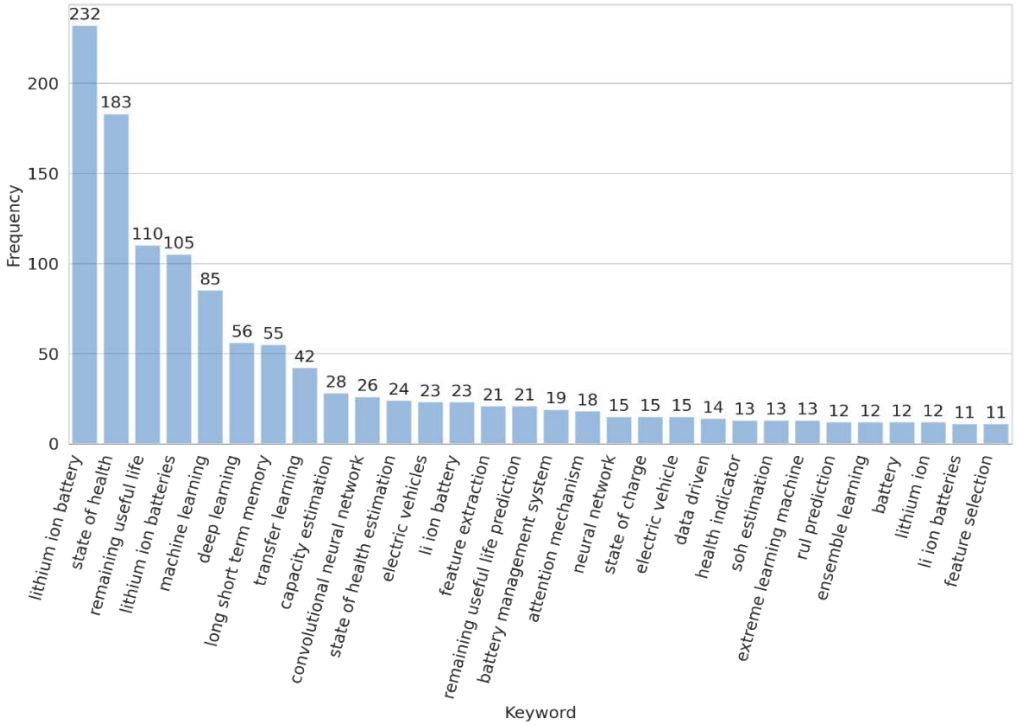

Figure 10. Distribution of keywords in the bibliographic portfolio.

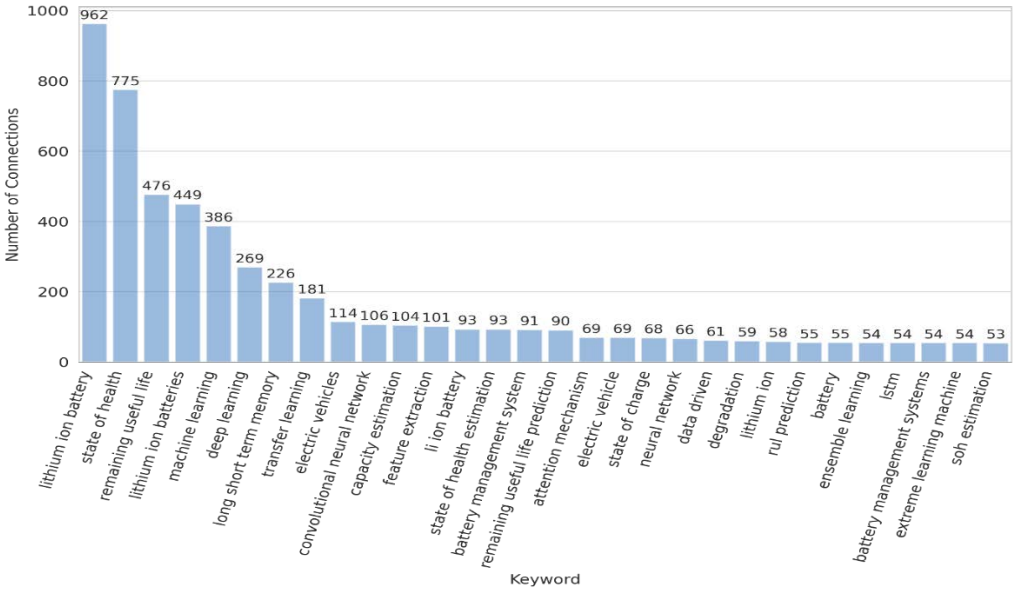

Figure 11. Number of connections of keywords within the bibliographic portfolio.

Figures 10 and 11 together emphasize the importance of keywords in structuring and advancing the field. Although the dominant terms reflect the current research focus, the variety and connections among keywords indicate the evolving boundaries of the field and its responsiveness to emerging challenges and technologies.

3. Content Analysis

The bibliographic portfolio of 534 papers, following the ProKnow-C methodology analyzed in the previous section, was explored to characterize the current scenario in the field of SoH estimation in batteries. First, we outline the survey of public databases found in the bibliographic portfolio, followed by the techniques and algorithms implemented in the papers. The algorithms are further analyzed according to categories of modeling,

including DL, algorithmic hybridization, and transfer learning. A situational overview of the performance is highlighted, and key review studies in the field are analyzed. This section concludes with implications for energy informatics and intelligent systems.

3.1. Portfolio Overview

Except for review papers, the objectives of the studies are directly related to establishing various forms, either algorithmically or through different approaches, to perform SoH estimation. In the presentation of the most cited papers in Table 3, it is noted that there is a significant focus on testing different types of ML algorithms and how their methods can increase the accuracy of SoH estimation. This is the case with the study presented in [44] with long short-term memory (LSTM) neural networks, the combination of LSTM and extreme-learning-machine (ELM) neural networks presented in [48], or the use of ensemble methods, such as bagging in decision trees, through the random forest (RF) algorithm in [47]. In summary, papers with the highest number of citations in the portfolio typically focus on increasing estimation accuracy through experiments related to algorithms.

Compatible studies can also be highlighted, such as the study presented in [78], which compares the LSTM, FNN, and CNN neural network algorithms, where the LSTM algorithm achieved the best performance, with an MAPE (mean absolute percentage error) of around 0.5%, compared to about 1.5% for FNN and 2% for CNN networks. In [79], the authors compare different probabilistic and time-series algorithms (ARIMAX, linear quantile regression, bootstrap multiple linear regression, and Bayesian bootstrap multiple linear regression), with the best results obtained from the Bayesian bootstrap multiple linear regression algorithm's quantile regression, which achieved MAPE values ranging from 0.2% to 1%. Other highlighted comparative studies include [66,80].

The concept of feature engineering, which includes manipulation and selection, is a relevant theme presented in the portfolio, as much of the algorithm's performance lies in the stress of creating features that provide discrimination for predictions. Study [81] introduces an autonomous feature selection method, which is based first on an initial selection considering correlation coefficients, tree algorithms, and a variance factor, followed by an iterative method for feature combination. In [82], an analysis of feature engineering for SoH estimation is presented, evaluating different techniques for feature creation and selection, such as univariate selection by Pearson correlation, feature importance, feature clustering, genetic algorithms, and sequential feature selection. The authors concluded that the use of sequential selection presented a good balance between performance and computational cost. Feature tests were evaluated using SVM and ExtraTree-based algorithms. Other studies focusing on features can be consulted in [81,83–96].

The quest for automating modeling processes was found in the development of an autoML approach in [97]. The framework built is capable of performing the entire modeling cycle using Bayesian optimization, eliminating the need for researchers from other fields to spend time on laborious steps, such as feature extraction, construction, and selection. The results obtained yielded MAEs (median absolute errors) ranging from about 0.02% to 0.05% for SoH estimation.

Interpretability model analyses were found in studies [98,99], based on the use of a technique known as SHAP (Shapley Additive Explanations). SHAP is based on a theoretical game approach that seeks to explain the output of any ML model by quantifying how each feature impacts the model's prediction [100,101]. Other model interpretability approaches were also addressed in [102–105].

Approaches related to hyperparameter tuning were also found in the portfolio. In [106], the authors explore the Bayesian optimization of hyperparameters in a combination of DCNN and LSTM neural networks, achieving an RMSE (root-mean-square error) of 0.0061

for SoH estimation. In study [107], a pipeline optimization based on a tree and genetic algorithm is presented. Study [108] also uses a genetic algorithm as a means of parameter optimization, presenting a framework for SoH estimation, with errors of about 2%.

The use of sensors for capturing battery conditions implies tabular data; however, studies were found in the portfolio, which analyze the implementation of image-based algorithms for SoH prediction. In [109], the authors propose a method capable of using only one charge and discharge cycle for SoH prediction, using image processing of current and voltage curves. Using transfer learning, the authors achieved an MAPE in the range of 10%. Transfer learning is also used in the algorithm based on battery curve image analysis in [110]. The authors analyze images of one cycle, five cycles, and ten cycles, with MAEs of about fifty, fifty-five, and sixty cycles, respectively, using eight pretrained networks, such as ResNet and GoogleNet. Other studies using algorithms from the computer vision area were found in [111–113].

Regarding the cell technologies employed, almost all the publications correspond to lithium-ion technology, among which we can highlight LFP (lithium iron phosphate), LCO (lithium cobalt oxide), NCA (lithium nickel cobalt aluminum oxide), and NMC (lithium nickel manganese cobalt oxide) battery types. Only three studies made use of battery technologies different from lithium. Study [114] analyzes the estimation of the SoHs of removed lead–acid batteries, aiming for reuse. In [115], lead–acid batteries are also analyzed, and the authors develop an SoH prediction model using LSTM networks based on charge curve data. In [116], the authors use a neural network to predict the remaining lifespan of a zinc-ion battery.

3.2. Literature Review

Within the article selection process, 38 papers correspond to review papers, and they are presented in Table 4. The papers are essentially divided into reviews with qualitative analyses (e.g., trends, challenges, and general overviews), as well as papers more focused on a specific set of techniques and surveying performances and the extraction of degradation features and health indicators. In all the analyzed papers, there was no indication of the use of a methodological process for selecting the bibliographic portfolio, highlighting the importance of this work as a point of evolution within the research field.

Table 4. Review papers in the bibliographic portfolio.

Title	Year	Cited	Ref.
Data-driven health estimation and lifetime prediction of lithium-ion batteries: A review	2019	749	[10]
Machine learning applied to electrified-vehicle-batteries' state-of-charge and state-of-health estimation: State of the art	2020	267	[11]
A review of second-life Li-ion batteries: prospects, challenges, and issues	2022	213	[12]
A review of state-of-health estimations and remaining-useful-life prognostics of lithium-ion batteries	2021	200	[13]
A review of non-probabilistic machine-learning-based state-of-health estimation techniques for lithium-ion batteries	2021	180	[67]

Table 4. *Cont.*

Title	Year	Cited	Ref.
A critical review of improved deep-learning methods for the remaining-useful-life prediction of lithium-ion batteries	2021	159	[5]
Sorting, regrouping, and echelon utilization of large-scale retired lithium batteries: A critical review	2021	117	[9]
Big training data for artificial-intelligence-based Li-ion diagnoses and prognoses	2020	100	[117]
Machine learning in state-of-health and remaining-useful-life estimation: Theoretical and technological developments in battery degradation modeling	2022	88	[118]
State-of-health prediction of lithium-ion batteries based on machine learning: Advances and perspectives	2021	81	[119]
A critical review of improved deep convolutional neural networks for multi-timescale state prediction of lithium-ion batteries	2022	75	[30]
A review of deep-learning approaches to predict the states of health and states of charge of lithium-ion batteries	2022	69	[26]
A critical review of online battery-remaining-useful-lifetime prediction methods	2021	62	[120]
Artificial neural networks, gradient boosting, and support vector machines for electric-vehicle-batteries' state estimation: A review	2022	57	[31]
State-of-health estimation and remaining-useful-life assessment of lithium-ion batteries: A comparative study	2022	43	[121]
A review of modern machine-learning techniques in the prediction of the remaining useful life of lithium-ion batteries	2023	34	[122]
Overview of machine-learning methods for lithium-ion-batteries' remaining-useful-lifetime prediction	2021	33	[123]
A review of machine-learning-based state-of-charge and state-of-health estimation algorithms for lithium-ion batteries	2023	33	[124]
Transfer learning for batteries' smarter-state estimation and aging prognostics: Recent progress, challenges, and prospects	2023	32	[27]
Review of "gray box" lifetime modeling for lithium-ion batteries: Combining physics and data-driven methods	2022	31	[125]

Table 4. *Cont.*

Title	Year	Cited	Ref.
Deep-learning-enabled state-of-charge, state-of-health, and remaining-useful-life estimations for smart battery management systems: Methods, implementations, issues, and prospects	2022	26	[24]
Explainability-driven model improvement for SOH estimation of lithium-ion batteries	2023	20	[126]
State estimation models of lithium-ion batteries for battery management systems: Status, challenges, and future trends	2023	20	[127]
State-of-charge, remaining-useful-life, and knee-point estimations based on artificial intelligence and machine learning for lithium-ion EV batteries: A comprehensive review	2022	19	[128]
The development of machine-learning-based remaining-useful-life predictions for lithium-ion batteries	2023	17	[129]
Comprehensive review of battery state estimation strategies using machine learning for battery management systems of aircraft propulsion batteries	2023	16	[130]
A comprehensive review of lithium-ion-batteries' state-of-health prognosis methods combining aging mechanism analysis	2023	11	[131]
Research progress and application of deep learning in remaining-useful-life, state-of-health, and battery thermal management of lithium batteries	2023	11	[132]
A review of the prediction of the health state and serving life of lithium-ion batteries	2022	7	[6]
Specialized deep neural networks for battery health prognostics: Opportunities and challenges	2023	7	[25]
Machine-learning techniques' suitability to estimate the retained capacity in lithium-ion batteries from partial charge/discharge curves	2023	7	[133]
Deep feature extraction in lifetime prognostics of lithium-ion batteries: Advances, challenges, and perspectives	2023	6	[28]
Comparing deep-learning methods to predict the remaining useful life of lithium-ion batteries	2022	4	[134]
Machine-learning-based remaining-useful-life prediction techniques for lithium-ion-battery management systems: A comprehensive review	2023	2	[29]
Feature–target pairing in machine learning for battery health diagnosis and prognosis: A critical review	2023	2	[135]

Table 4. *Cont.*

Title	Year	Cited	Ref.
Research on methods for extracting aging characteristics and the health status of lithium-ion batteries based on small samples	2022	1	[136]
Electric-vehicle-batteries' capacity degradation and health estimation using machine-learning techniques: A review	2023	0	[137]
Open access dataset, code library, and benchmarking deep-learning approaches for state-of-health estimations of lithium-ion batteries	2024	0	[138]

Figure 12 shows that the number of review article publications within the portfolio has been increasing over the years, albeit with a considerably lower coefficient compared to that of the overall volumetric analysis. There appears to be a difference between 2022 and 2023, suggesting a potential trend toward stability in the coming years.

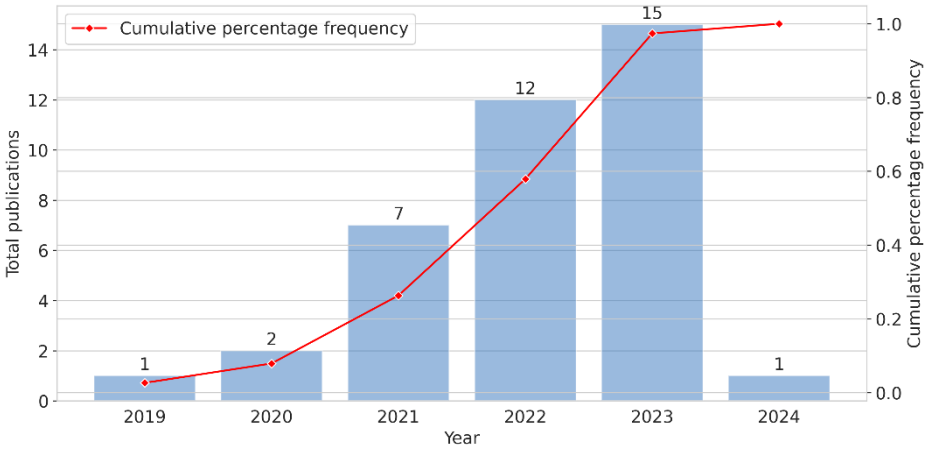

Figure 12. Volumetric analysis of the publication year of review papers in the BP.

The most cited review article in the portfolio is the study presented in [10], which examines big-data techniques regarding their feasibility and cost effectiveness in dealing with battery health in real-world applications. The methods are categorized, and advantages and limitations are identified. The authors begin by presenting methods that do not involve model training, such as the differential analysis of charge and discharge profiles, stress tests, and thermal analyses. Then, they review the use of ML for SoH estimation, highlighting the fundamental step of feature extraction. They categorize these features into three main groups: (i) model-fitted features, which depend on tests like internal resistance and are not easily accessible by sensors in a BMS (battery management system); (ii) processed external features, which are the results of differential analyses; and (iii) direct external features, which are all the variables that a sensor can collect within the battery system and can generate a large number of variables. The authors also briefly review non-probabilistic ML methods, such as artificial neural networks, SVMs, and probabilistic models, like Gaussian regression.

The non-probabilistic methods are the central theme of the study presented in [67], where five types of ML algorithms for batteries' SoH estimation are reviewed: linear regression, SVM, KNN, neural networks, and ensemble methods. The study comparatively outlines the advantages and applicability of the different methods from a theoretical standpoint. Three aspects are considered for comparing the methods: the algorithm's

performance based on five performance metrics (RMSE, MAE, AE, APE, and MaxE), the publication trend obtained by counting the number of publications in the last ten years, and the training modes considering feature extraction and selection. The study used 144 papers considered as relevant and published up to 10 years before (with the reference year being 2021), however, without revealing the criteria used for obtaining the portfolio. The authors conclude that neural-network-based methods and SVMs are still under research and that DL methods have shown great potential in SoH estimation under complex battery-aging conditions, especially when big data are available, and that ensemble methods, like random forest, can be considered as an emerging alternative for balancing data size and accuracy.

Regarding the use of ML techniques in second-life batteries, the study presented in [9] reviewed the status and challenges of large-scale second-life applications. The authors discuss methodologies for classifying and regrouping retired batteries. They propose a rapid, multilevel, and multidimensional classification method for large-scale use. The classification method involves first solving a one-dimensional classification problem to obtain similar batteries in terms of their reaction stage. Then, a multidimensional classification is performed based on capacity and internal resistance, where usage scenarios are evaluated, for example, to determine whether the priority use is for energy or power supply. The second life is also discussed in the review presented in [12], which analyzes economic, technical, and environmental factors related to the use of second-life lithium-ion batteries, including SoH estimation methods.

Regarding the reviews from this year, it is worth highlighting the study in [27], which presents the first systematic review of transfer-learning applications in the field of battery management, focusing on batteries' state estimations and aging prognoses. The authors provide the state of the art in terms of principles, algorithmic structures, advantages, and disadvantages. For SoH estimation, a survey of papers in the field showed that transfer strategies focus on problem domain adaptation and the fine-tuning of the final model. The difficulties pointed out by the authors in using transfer learning lie in the low labeling degree of the data, which depends on the data acquisition capability at shorter intervals in a BMS. This is exacerbated by the low frequency of actual battery capacity testing during usage, especially for SoH estimation purposes.

3.3. Public Databases

Analyzing the non-review papers present in the bibliographic portfolio, it was found that about 41% make use of proprietary and closed datasets, without sharing repositories for use in other studies. On the other hand, a significant and increasingly growing portion of papers conduct investigations using public datasets, comprising 59% of the non-review papers in the portfolio. As emphasized in [11], advancements in the field of ML for estimating batteries' SoHs rely on information sharing so that new research can develop and result comparisons can occur, thereby allowing inferences about techniques that may enhance estimation accuracy. This scenario demonstrates this sharing trend, leading to faster and more voluminous developments in the research field. It is worth noting that fair comparative analyses of models/approaches also require the sharing of data splits used for training and testing/validation; only then can comparisons be made when dealing with the same population.

Figure 13 demonstrates that author-provided datasets have the highest frequency of use. However, the majority of these datasets are complementary to public datasets. Among these, the highlight goes to the use of data provided by the Prognostics Center of Excellence Dataset Repository [139], from NASA, which accounts for 51% of the open datasets used in the surveyed portfolio. The dataset presented in [1], developed at the

Massachusetts Institute of Technology (MIT), also constitutes an important data source in the surveyed papers.

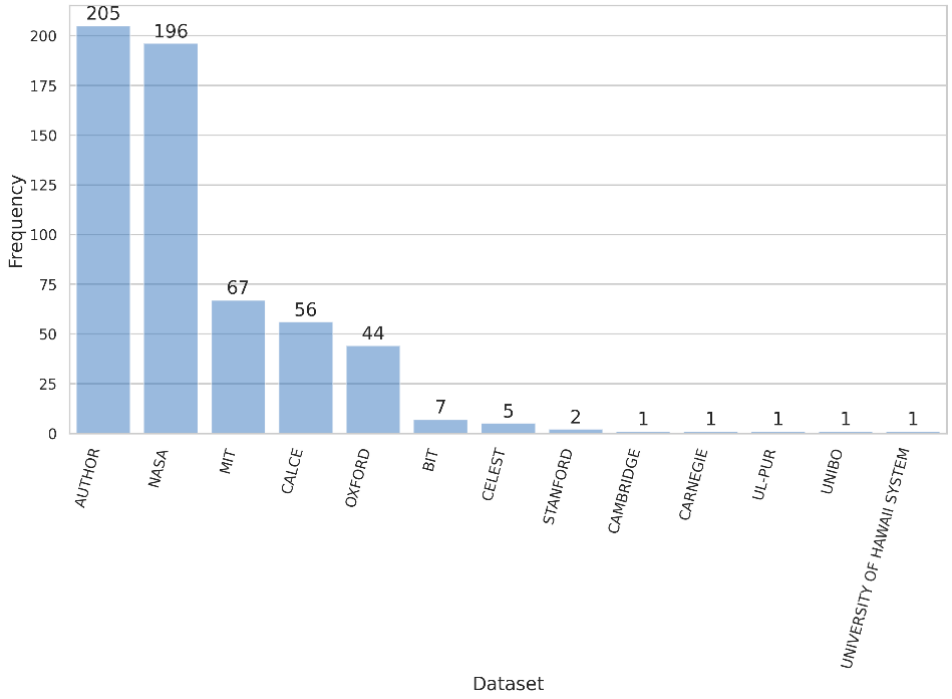

Figure 13. Volumetric analysis of datasets used in the papers of the bibliographic portfolio.

The evolution of the proportion of closed and public datasets is presented in Figure 14. It is noticeable that the volume of applications using public datasets starts to become predominant from 2022, with the use of public datasets being about 3.2 times higher in 2023. This increase could be because of the research trend of using multiple datasets, and because more data sources are available, the application of public datasets would tend to increase. Therefore, to mitigate this effect, Figure 14 considers only the Boolean condition of whether a public dataset was used or not, and the results are similar, with the number of papers using public datasets in 2023 being about 2.3 times higher than those using closed datasets.

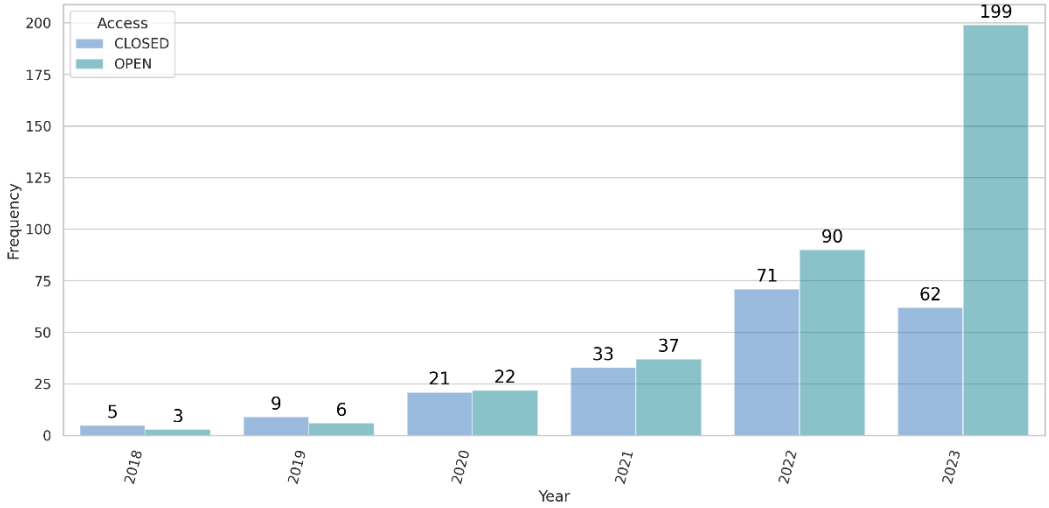

Figure 14. Annual evolution in the BP of papers using public datasets versus closed datasets.

Through an evaluation according to the dataset origin, Figure 15 illustrates the evolution of the dataset usage over the years in the bibliographic portfolio (BP). The increasing use of NASA datasets is noticeable, followed by the usage of the MIT [1], Oxford, and CALCE datasets. Other public datasets with even lower levels of usage are also identified in the portfolio: the Beijing Institute of Technology (BIT), Carnegie Mellon University, Stanford University, Cambridge University, the University of Hawaii, Purdue University (UL-PUR), the University of Bologna (UNIBO), and the Center for Electrochemical Energy Storage Ulm–Karlsruhe (CELEST).

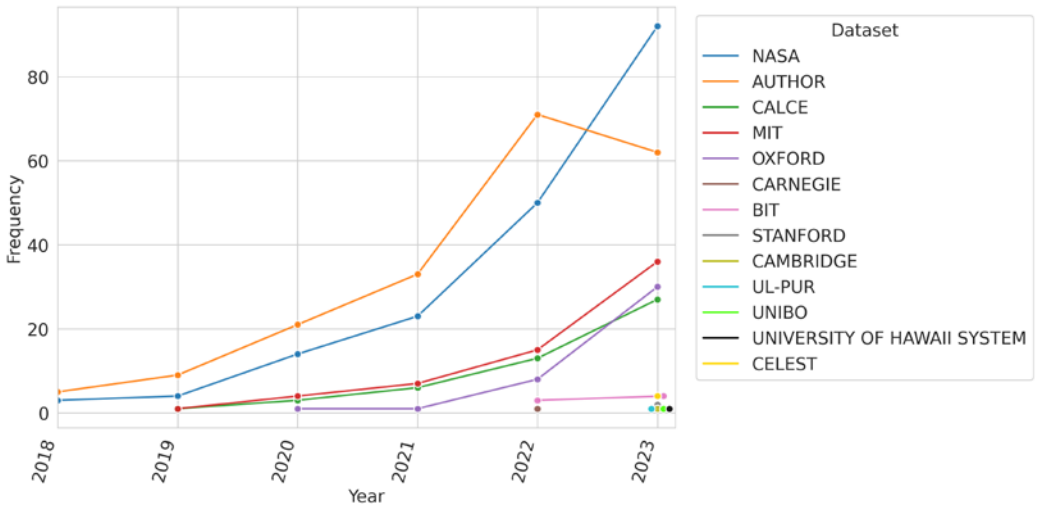

Figure 15. Annual evolution, in the BP, of the origin of public and author datasets.

Table 5 provides a summary of each of the public datasets found in the portfolio, as well as their characteristics and in which papers they were used. In total, 12 sources of public data were revealed, corresponding to 20 different datasets, all using lithium technology as the main source of the analyzed batteries. The synthesis of these databases constitutes important information for future studies, as it facilitates the selection and design of new studies on SoHs.

In the NASA repository, two datasets are available for developing models aimed at estimating SoHs. The first dataset contains 34 lithium-ion 18,650 cells with a capacity of 2 Ah, undergoing processes of charging, discharging, and impedance measurements. Various temperatures are used, including 4 °C, 24 °C, and 44 °C, with the charging process consisting of constant current until 4.2 V, followed by constant voltage until reaching the cutoff current. Different discharge regimes are adopted. The second dataset corresponds to 28 lithium-ion 18,650 cells with a capacity of 2.2 Ah that are continuously cycled with randomly generated current profiles. Reference charge and discharge cycles are also performed after a random fixed interval. In total, the cells are divided into seven equal groups, with the cycles occurring at a temperature of 40 °C. In five groups, the charging cycle follows the traditional constant current–constant voltage (CC-CV) pattern, followed by randomly selected discharges. In two groups, both the charging and discharging processes are selected randomly. The cycling processes of the cells are terminated when their capacity reached either 80% or 50% of the initial capacity, depending on the type of test defined. Both NASA datasets are provided in ".mat" extension files.

Table 5. Datasets included in the bibliographic portfolio.

Dataset	Cell Type	Features	No. of Cells	Refs.	Link
NASA	Li-ion 18650	V, I, T, IR, time	34	[49–51,54,55,57,60,61,64,66,68,78–81,87,91,96,97,106,107,140–314]	https://www.nasa.gov/intelligent-systems-division/discovery-and-systems-health/pcoe/pcoe-data-set-repository/
	Li-ion 18650	V, I, T, time	28		
MIT	$LiFePO_4$/graphite	V, I, T, IR, time	124	[1,8,54,66,70,72,83,92,94,99,102,104,110,111,140,144,199,205,253,269,277,299,315–359]	https://data.matr.io/1/projects/5c48dd2bc625d700019f3204
CALCE	$LiCoO_2$	V, I, T, time	15	[54,64,66,150,157,159,161,162,170,172–175,180,182,187,192–195,200,206,208,209,215,217,220,222,228,229,231,236,240,244,249,263,264,269,270,282,288,312,328,330,344,347,360–369]	https://calce.umd.edu/battery-data
	$LiCoO_2$	V, I, T, IR, time	12		
	$LiCoO_2$	V, I, time	16		
OXFORD	Li-ion 18650	V, I, T, time	8	[54,88,92,99,140,142,152,156,157,179,180,194,201,209,225,235,263,269,277–279,281,293,295,311,313,330,348,354,369–383]	https://ora.ox.ac.uk/objects/uuid:03ba4b01-cfed-46d3-9b1a-7d4a7bdf6fac
	Li-ion 18650	V, I, T, time	6		https://ora.ox.ac.uk/objects/uuid:9aae61af-2949-49f1-8ad5-6aea448979e5
	Li-ion 18650	V, I, T, IR, time	12		https://ora.ox.ac.uk/objects/uuid:de62b5d2-6154-426d-bcbb-30253ddb7d1e
BIT	LFP/graphite	V, I, T, time	77	[325,335,384–388]	https://data.mendeley.com/datasets/kw34hhw7xg/2
STANFORD	NMC (INR21700M50T)	V, I, T, IR, time	10	[165,389]	https://osf.io/qsabn/?view_only=2a03b6c78ef14922a3e244f3d549de78
CELEST	NCA	V, I, T, IR, time	66	[369,389–392]	https://zenodo.org/records/6405084
	NMC	V, I, T, IR, time	55		
	NCA + NMC	V, I, T, IR, time	9		
UL-PUR	NCA	V, I, T, IR, time	35	[194]	https://www.batteryarchive.org/index.html
UNIBO	Li-ion 18650	V, I, T, IR, time	27	[212]	https://data.mendeley.com/datasets/n6xg5fzsbv/1
CAMBRIDGE	LCO/graphite	V, I, T, IR, time	12	[393]	https://zenodo.org/records/3633835
University of Hawaii System	LFP/graphite	V, I, T, time	6	[394]	https://data.mendeley.com/datasets/y8nstxmdrg/1
	NMC	V, I, T, time	6		
CARNEGIE	Li-ion 18650	V, I, T, time	30	[395]	https://kilthub.cmu.edu/articles/dataset/eVTOL_Battery_Dataset/14226830/1

The dataset developed in [1] consists of 124 LiFePO4/graphite cells with a capacity of 1.1 Ah and a nominal voltage of 3.3 V. The cells were cycled at a temperature of 30 °C, being charged with a fast-charging policy of one or two steps, in the C1(Q1)–C2 format. Here, C1 and C2 represent the first and second constant current steps, respectively, and Q1 is the state of the charge (SoC, %) at which the currents change. The second current step terminates at 80% of the SoC, after which the cells charge at 1C CC-CV. The charging step can occur in a range of 72 different protocol profiles, with the discharge maintaining the same pattern across all the cycles. The cycles are terminated when the cell's capacity reaches 80% of its initial capacity. All the data are provided in ".mat" format.

The Center for Advanced Life Cycle Engineering (CALCE) at the University of Maryland provides three datasets of LiCoO2 batteries, including two sets of prismatic cells and one set of pouch cells (16 cells). The first dataset, consisting of 15 cells, features cells with capacities of 0.9 Ah and 1.1 Ah, cycled at a controlled temperature of 23 °C, with standard CC-CV charging cycles. Different depths and rates of discharging/charging are evaluated. The cycles are performed until reaching 80% of the nominal capacity. The data are provided in multiple ".txt" files. The second dataset, comprising 12 cells, follows a similar format to the first one, with cells of 1.35 Ah undergoing tests at different temperatures (25 °C, 35 °C, 45 °C, and 55 °C), and various charge and discharge profiles. The data are also provided in ".txt" format. The third dataset contains 16 pouch cells, each with a capacity of 1.5 Ah, where the data were generated to assess the effects of partial charge and discharge cycles on battery capacity degradation. The temperature in all the tests is controlled at 25 °C. The data are provided in ".mat" format.

The Battery Laboratory Intelligence at the University of Oxford provides three datasets that can be explored in modeling. The first corresponds to long-term battery aging tests, featuring eight cells of 740 mAh, maintained at a controlled temperature of 40 °C. The cells were subjected to a CC-CV charging profile, followed by a discharge profile obtained from the Artemis urban profile. The data are stored in ".mat" format. The second dataset contains data from six cells of 16 Ah, collected from a one-year experiment, following real-world usage profiles of grid-connected battery applications. The data are provided in ".csv" format. The third dataset contains long-term data from 12 cells of 3 Ah, aiming to study the influence of the usage history dependence on the cell degradation. Four groups of three cells each were subjected to combined charging profiles comprising fixed calendar periods and cyclic aging applied in various orders. Cells in groups 1 and 2 were subjected to one day of cycling followed by five days of aging at C/2 and C/4, respectively. Cells in groups 3 and 4 were subjected to two days of cycling followed by ten days of aging at C/2 and C/4, respectively. The tests are conducted at a controlled temperature of 23 °C. The data are available in ".txt" format.

The dataset presented by the Beijing Institute of Technology (BIT), as introduced in study [384], consists of 77 batteries of 2.4 Ah cycled with fixed or arbitrary current profiles. Twenty-two batteries were cycled with fixed current profiles for both charging (1C, 2C, or 3C) and discharging (1C, 2C, or 3C). Fifty-five batteries were cycled with arbitrary usage profiles for charging (following a uniform distribution between 1C, 2C, or 3C and randomly changing every five cycles) and a specified discharge current (3C). The data are provided in ".csv" format.

The dataset from Stanford University, collected at the Stanford Energy Control Laboratory, was created in 2022 and is presented in [396]. It consists of 10 $LiNiMnCoO_2$/graphite cells, model INR21700-M50T, with a capacity of 4.85 Ah. For the tests, the cells were maintained at 23 °C and charged according to the CC-CV protocol, with charging rates of C/4, C/2, 1C, and 3C. The discharge aging experiments were designed to simulate a typical driving pattern of electric vehicles in the form of the Urban Dynamometer Driving

Schedule (UDDS), reducing the battery's SoC from 80% to 20%. The files are provided with ".xlsx" and ".mat" extensions.

Three datasets are provided by the Center for Electrochemical Energy Storage Ulm–Karlsruhe. They originated in 2022, using sixty-six NCA cells (3.5 Ah) in dataset 1, fifty-five NCM cells (3.5 Ah) in dataset 2, and nine NCA-NCM cells (2.5 Ah) in dataset 3. The cells in datasets 1 and 2 were maintained at controlled temperatures of 25 °C, 35 °C, and 45 °C, while the cells in dataset 3 were kept at 25 °C. The charging process of the cells followed the CC-CV protocol, with rates of 0.25 C, 0.5 C, and 1C, and with constant discharges of 1C. The files are provided with a ".csv" extension.

The dataset provided by Underwriters Laboratories, Inc. at Purdue University consists of 35 NCA cells. Of this dataset, 21 cells are cylindrical-type lithium-ion 18650, cycled at 0.5C between 2.7 and 4.2 V (0–100% SoC) at room temperature, to various levels of capacity reduction (10%, 15%, and 20%). The remaining 14 cells are pouch-type, cycled at 1C between 2.7 and 4.2 V (0–100% SoC), also at room temperature, with capacity reductions of 10–20%. The data are provided in ".csv" format.

The data provided in July 2023 by UNIBO Powertools corresponds to cycling experiments of 27 batteries, considering the use of batteries from different manufacturers, cells with various nominal capacities, and cycling conducted until the end of the cell's life, producing data at different stages of the lifespan. Three types of tests were conducted: (i) a standard test, where the battery was discharged at a current of 5 A in the main cycles; (ii) a high-current test, where the battery was discharged at a current of 8 A in the main cycles; (iii) a pre-conditioned test, where the battery cells are stored in environments at 45 °C for 90 days before conducting the test. The charging process is CC-CV at 1.8 A and 4.2 V (a 100 mA cutoff point). The data are provided in ".csv" format.

The dataset provided by Cambridge University corresponds to the work developed in [397], where continuous charge and discharge cycles were conducted on 12 lithium-ion cells Eunicell LR2032 ($LiCoO_2$/graphite), with a capacity of 45 mAh. The cells were cycled at controlled temperatures of 25 °C, 35 °C, and 45 °C. Each cycle consists of a CC-CV charge at a rate of 1C up to 4.2 V and a CC discharge at a rate of 2C up to 3 V. Electrochemical impedance spectroscopy (EIS) is measured at nine different stages of charging/discharging during each even-numbered cycle, in the frequency range from 0.02 Hz to 20 kHz, with an excitation current of 5 mA, following a 15 min open-circuit period at 0% SoC and 100% SoC. The dataset is provided in multiple ".txt" files.

The data from the University of Hawaii System correspond to two datasets, each composed of nine cells, one of type LFP, with a capacity of 1.1 Ah (APR18650M1B), and the other of type NMC, with a capacity of 3.5 Ah (INR18650MJ1). The cells were cycled under different protocols, with temperature controlled between −15 °C and 55 °C. Charging processes were of the CC-CV type, with rates of C/25 and 1C, and continuous discharges of C/25, C/5, and 1C. The details about the dataset construction can be found in [398], with the data being provided with a ".txt" extension.

The dataset provided by Carnegie Mellon University consists of 30 cylindrical cells Sony–Murata 18650 VTC-6 (3 Ah) cycled at a controlled temperature of 25 °C. The charging and discharging configurations varied, with durations ranging from 400 s to 1000 s. The data are available in ".csv" format.

3.4. Techniques and Algorithms

A survey of the techniques addressed in the papers of the bibliographic portfolio, as presented in Table 6, revealed the use of 81 distinct techniques by the authors. With 161 applications, LSTM-type DL neural networks account for approximately 22% of the techniques evaluated in the portfolio, followed by CNN-type DL networks, with 12%, and

with SVM, GPR, and simple artificial neural networks (ANNs) each accounting for about 5%, which together result in almost 50% of the techniques evaluated in the non-review papers of the portfolio. Although a set of only five algorithms represents almost half of the evaluations, forty-one algorithms are evaluated only once in these studies, representing about 6% of the techniques evaluated, with a representation of 11% when techniques implemented up to three times were grouped, corresponding to fifty-six algorithms. Figure 16 presents the distribution of the techniques found in the portfolio.

Table 6. Frequency of machine-learning techniques presented in the bibliographic portfolio.

Algorithm	Frequency	Type	Algorithm	Frequency	Type
LSTM	161	Neural Network	Regressive matching network	1	Neural Network
CNN	86	Neural Network	Bls	1	Time Series
SVM	38	Kernel Method	Semi-Markov model	1	Statistical Method
GPR	37	Statistical Method	Autoregression nested sequence	1	Statistical Method
ANN	34	Neural Network	Automl	1	-
RANDOM FOREST	32	Decision Tree	Quantile regression forest	1	Quantile Regression
LINEAR REGRESSION	32	Linear Model	Sparse Bayesian learning	1	Statistical Method
ELM	31	Neural Network	Ssel	1	Time Series
RNN	29	Neural Network	Survival model	1	Survival Model
DNN	27	Neural Network	Atbls	1	Time Series
GRU	26	Neural Network	Tdnn	1	Neural Network
XGBOOST	19	Decision Tree	Transformer neural network	1	Neural Network
GRADIENT BOOSTING TREE	16	Decision Tree	Unsupervised learning	1	Unsupervised
BPNN	12	Neural Network	Unsupervised neural networks	1	Neural Network

Table 6. *Cont.*

Algorithm	Frequency	Type	Algorithm	Frequency	Type
LIGHTGBM	11	Decision Tree	Vgg11	1	Neural Network
MLP	10	Neural Network	Vision transformer network	1	Neural Network
FFNN	8	Neural Network	Quantum clustering	1	Clustering
RVM	7	Kernel Method	Deep reinforcement learning	1	Neural Network
TCN	6	Neural Network	Pknn	1	Neural Network
NAR	5	Time Series	Narxnn	1	Time Series
RIDGE REGRESSION	5	Linear Model	Densenet	1	Neural Network
ENN	5	Neural Network	Dgnn	1	Neural Network
ADABOOST	5	Decision Tree	Dilated residual network	1	Neural Network
GRAPH NEURAL NETWORK	4	Neural Network	Dsmtnet	1	Neural Network
DECISION TREE	4	Decision Tree	Efficientnet	1	Neural Network
ELASTIC NET REGRESSION	3	Linear Model	Ddan	1	Neural Network
KNN	3	Neighborhood Method	Extreme deep factorization machine	1	Neural Network
RBFNN	3	Neural Network	Fcnn	1	Neural Network
ARIMA	3	Time Series	Dcn	1	Neural Network
DBN	3	Neural Network	Fuzzy clustering	1	Clustering
DCNN	3	Neural Network	Generalized additive model	1	Statistical Method
DELM	3	Neural Network	Alexnet	1	Neural Network
LINEAR QUANTILE REGRESSION	2	Quantile Regression	Googlenet	1	Neural Network

Table 6. *Cont.*

Algorithm	Frequency	Type	Algorithm	Frequency	Type
LOGISTIC REGRESSION	2	Linear Model	Dbnn	1	Neural Network
EXTRATREES	2	Decision Tree	Crnn	1	Neural Network
BOOTSTRAP MULTIPLE LINEAR REGRESSION	2	Linear Model	Induced ordered weighted averaging	1	Statistical Method
BNN	2	Neural Network	Lasso regression	1	Linear Model
K-MEANS	2	Clustering	Cdtsgann	1	Neural Network
RESNET	2	Neural Network	Capsnet	1	Neural Network
CATBOOST	2	Decision Tree	Genetic models	1	Genetic Algorithm
BMA	1	Statistical Method			

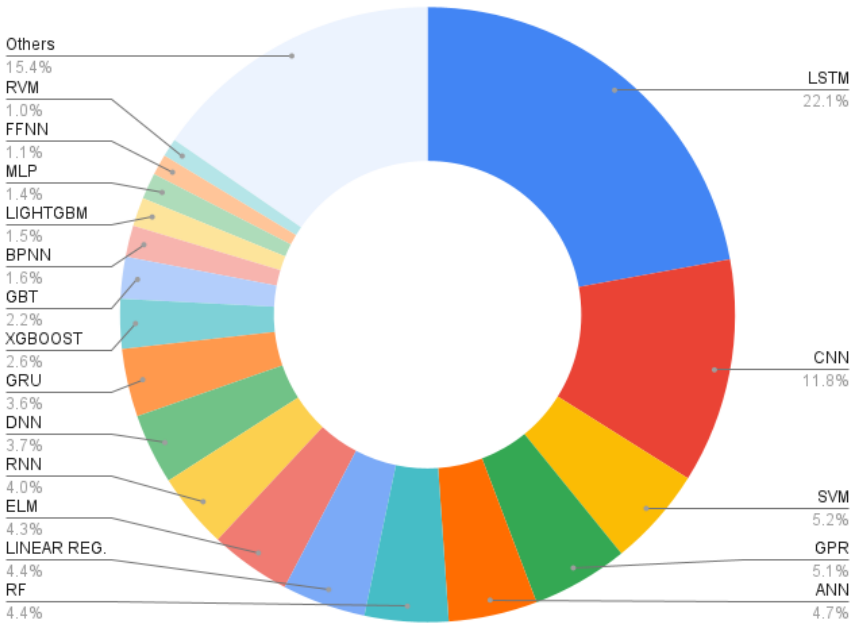

Figure 16. Frequency of ML algorithms presented in the BP.

When analyzing the algorithms implemented in the portfolio, grouped according to their category of origin, the use of techniques based on neural networks reaches the significant mark of 66% of the implementations, followed by decision-tree-based algorithms (including tree ensembles), with about 12%. Kernel methods, probabilistic statistical models, and linear regressions each account for approximately 6% of the implementations found. This analysis is presented in Figure 17.

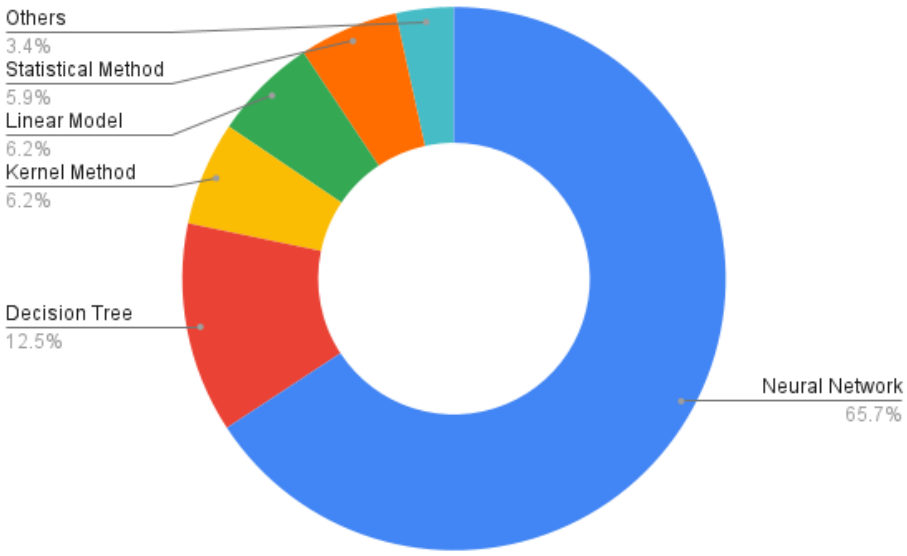

Figure 17. Frequency of groups of ML algorithms presented in the BP.

Excluding the use of neural networks, tree-based methods have gained considerable representation in the portfolio. Notably, ensemble methods, such as boosting, were employed in [83,272,399], along with implementations of popular boosting algorithms, like XGBoost in [262,400,401], LightGBM in [402–404], and CatBoost in [405,406], which have gained prominence in the field of tabular data prediction in recent studies. The use of bagging can be identified in the implementation of decision-tree ensembles, such as random forest, as explored in studies [47,161,407]. Kernel-based methods, such as SVMs, can be classified as algorithms belonging to a classical and dated approach [408], yet they were considerably analyzed in the portfolio in studies [323,409,410]. The use of classical and highly interpretable linear regression was explored in 45 studies, among which, notable studies include those presented in [1,80,146,238,321,411,412].

Another approach of relative importance corresponds to algorithms that are a part of statistical methodologies, where, out of the 43 implementations in the portfolio, 37 corresponded to the use of the GPR algorithm, with examples of implementations and analyses found in [329,369,413–415]. As presented below, the GPR algorithm demonstrated significant usage in hybrid methodologies, ranking sixth in usage within the portfolio when considering hybridized algorithms. Another point worth noting is the interpretation conducted by studies that sought to analyze degradation through classical time-series approaches, as presented in [79], which implements the ARIMAX (AutoRegressive Integrated Moving Average Model with eXogenous input) method, and in study [416] using the ARIMA (AutoRegressive Integrated Moving Average Model) method. The NAR (Nonlinear Autoregressive) model is explored in [64].

The evolution of algorithmic categories throughout the horizon comprising the bibliographic portfolio is presented in Figure 18. It is worth noting that the authors consistently focused on exploring neural network implementations throughout the entire time horizon, with the difference from other categories maintaining a growing profile. It is possible to observe a significant increase in the implementation of decision-tree-based algorithms from 2022 to 2023. The implementation of linear models has also been gaining momentum, mainly because of the comparisons that these simpler models can offer compared to more complex algorithms. Additionally, they present greater interpretability of variables and, therefore, of the modeling [6,104,417]. The use of time-series techniques has remained relatively constant in the portfolio, which, in contrast to the increasing volume of publications per year, indicates that the percentage of implementation compared to that of other

categories has been decreasing. Algorithms related to clustering, quantile regression, the neighborhood method, and unsupervised learning were more recently implemented within the portfolio, between 2022 and 2023.

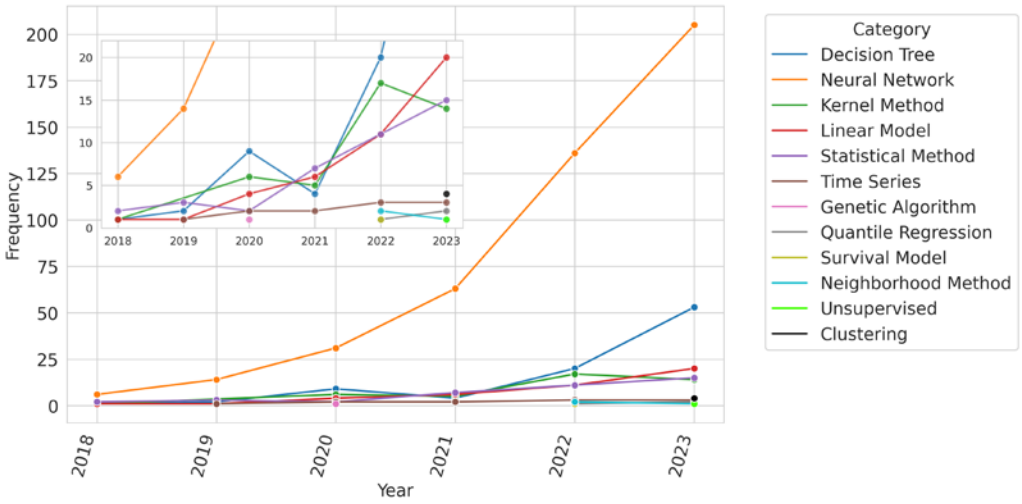

Figure 18. Evolution of algorithmic implementation in the BP by category.

Going deeper into the analysis of the two main categories of algorithms implemented in the portfolio, the graphs in Figure 19 depict the distributions of neural network and decision-tree algorithms. In the neural network category, following the observations from the overall analysis, there is a dominance of LSTM and CNN networks, followed by simple neural networks, algorithms based on well-known networks, such as extreme-learning machines and RNNs. In the decision-tree algorithms, there is a predominance of ensemble bagging using the random forest algorithm, accounting for 35% of the tree implementations in the portfolio, followed by boosting algorithms, such as XGBoost, GBT, LGBM, and Adaboost. A detailed exploration of this type of ensemble can be observed in battery degradation studies, with approximately 60% of the tree implementations in the portfolio.

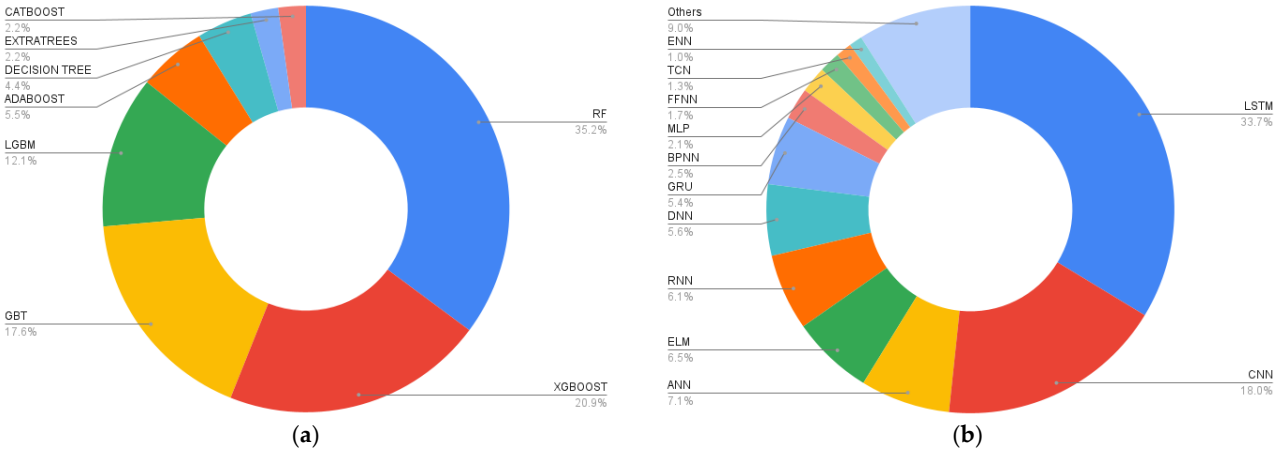

Figure 19. Frequencies of implemented algorithms: (**a**) decision trees; (**b**) neural networks.

When analyzing the evolution of techniques implemented in the portfolio, as depicted in Figure 20, it is noticeable that the use of LSTM networks predominates throughout almost the entire analyzed time horizon. The use of CNN networks began to gain prominence from publications in 2021. The use of the random forest became the third most implemented technique in the portfolio's works in 2023; however, the use of simple ANNs showed a sharp decline in the last year. Implementations of the SVM method seem to be decelerating, with a decrease in usage in 2021 and maintaining the number of implementations in 2023

compared to 2022. The use of GRU networks also appears to be trending, becoming the fourth most implemented algorithm in 2023. As a baseline and comparative algorithm, linear regression also demonstrates an increase in the number of implementations over the horizon. Other algorithms that seem to be experiencing a growing exploration are DNN, GPR, and XGBoost.

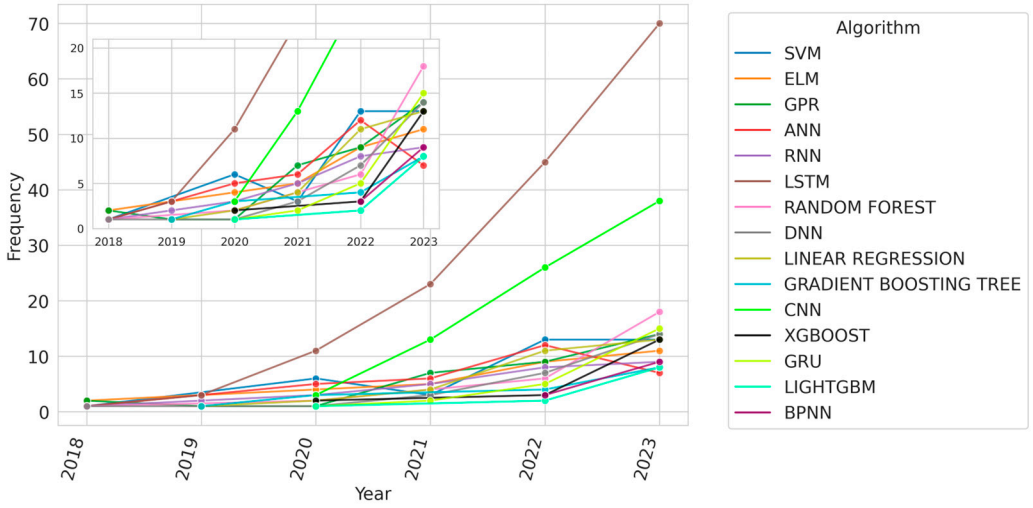

Figure 20. Evolution of algorithmic implementation in the bibliographic portfolio.

The evolution of the portfolio's main neural network implementations is presented in the graph in Figure 21. As previously highlighted, the use of LSTM and CNN networks is at the forefront of authors' research in the field, with LSTM networks being the main technique in this category from 2020 onward, and CNNs gaining prominence from 2021. It is noteworthy to highlight some recent jumps in implementations in the portfolio, from 2022 to 2023, such as the exploration of GRU, DNN, ELM, and BPNN techniques. It is striking to see the resurgence of the exploration of more classical networks, such as BPNNs, by authors in the field.

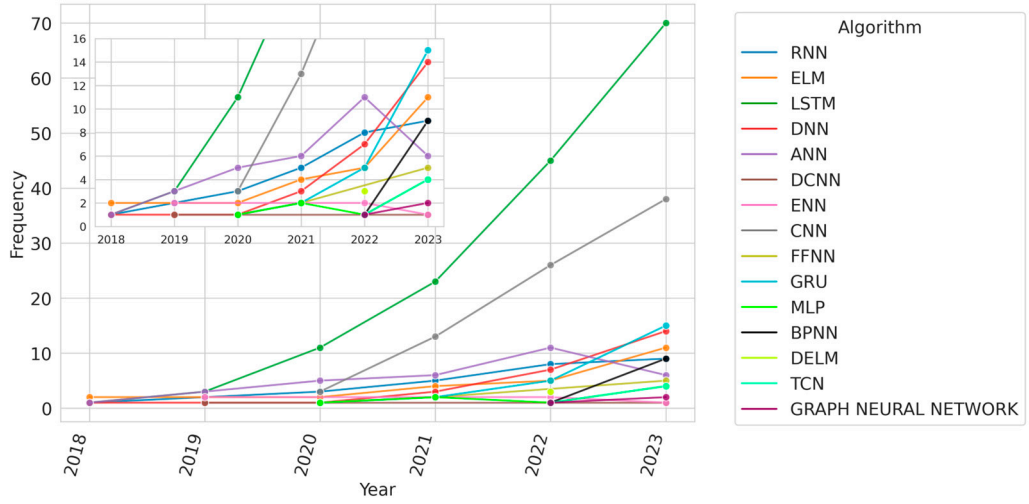

Figure 21. Evolution of neural network algorithmic implementation in the BP.

Because of its secondary prominence in the portfolio, we also present the evolution of decision-tree-based algorithms in Figure 22. The evolution of the random forest algorithm's usage over the years can be observed, with a notable increase in 2023, and the possible replacement of GBT boosting by newer versions, such as XGBoost and LightGBM.

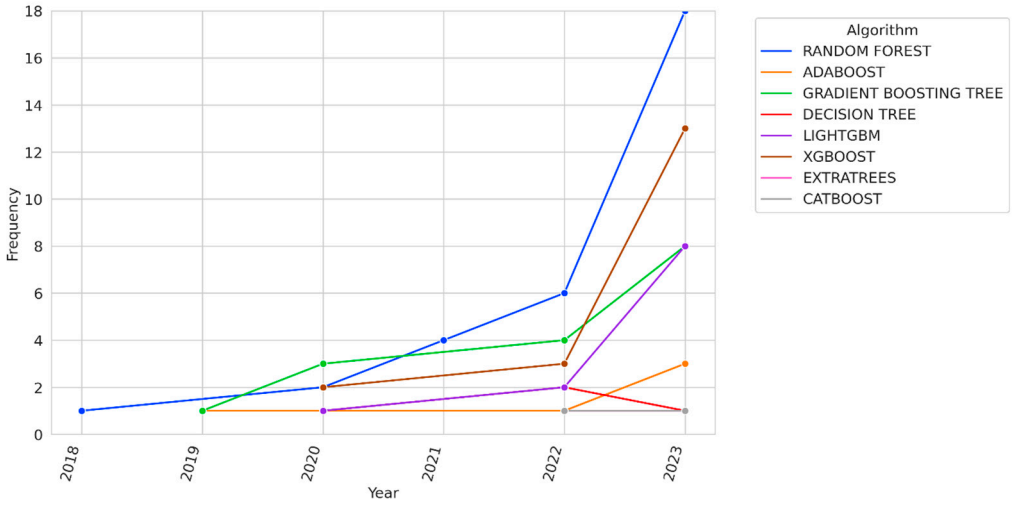

Figure 22. Evolution of decision-tree-based algorithmic implementation in the portfolio.

3.4.1. Deep-Learning Models

ML, as a subfield of artificial intelligence, employs algorithms and statistical techniques to construct predictive models. Neural networks represent a subset of ML algorithms that have seen their structural complexity increase over time, in tandem with computational advancements. This complexity primarily manifests in the augmentation of intermediate layers within networks, enhancing the algorithm's ability to discern patterns and giving rise to a subfield known as DL algorithms [418,419]. Traditional ML algorithms often outperform DL methods in scenarios of limited data availability. However, as datasets expand, traditional ML algorithms tend to reach performance plateaus, while DL algorithms demonstrate significant superiority over other learning strategies [418].

The expected potential of DL techniques can be observed in the bibliographic portfolio. Within the set of techniques belonging to neural-network-based algorithms, 307 papers using DL algorithms were identified, representing a significant 57.5% of the portfolio. This demonstrates a strong trend within this research field. DL algorithms were considered as those with more than three hidden layers. Although there is no consensus among authors and researchers in the field regarding the exact number of layers required to characterize a network as DL, some references consider this number of layers to indicate "light" DL networks, while "heavy" DL networks can have from tens to hundreds of hidden layers [420,421].

A comparative analysis of the evolution of the proportion of DL usage in neural network algorithms is shown in Figure 23. There is noticeable stability in the proportion, discounting the factor of publication volume in the early years, which settles between 80% and 90% in the last 3 years of the portfolio.

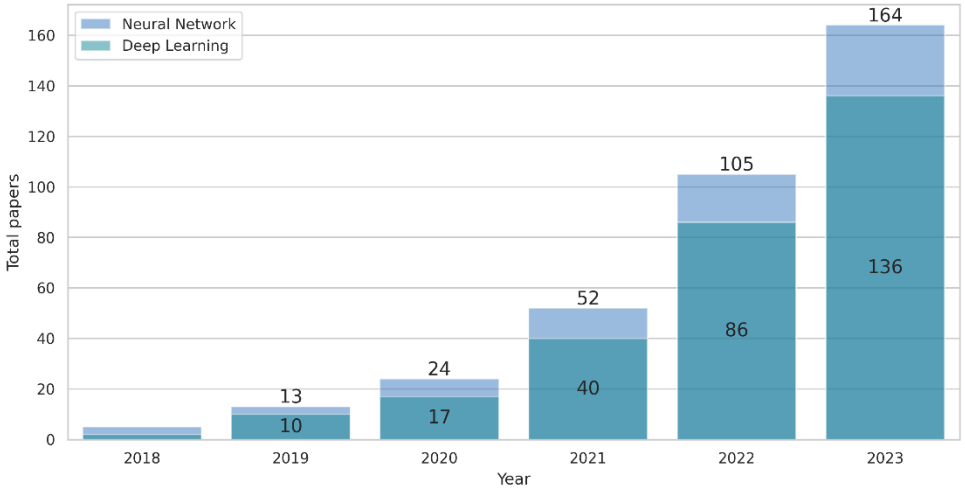

Figure 23. Proportion of DL implementation in neural network techniques in the portfolio.

The volume of DL technique implementations in the portfolio is presented in Table 7, with a visual proportion overview shown in Figure 24. In Table 7, the term "Frequency" refers to the number of implementations recorded for each technique. Papers in the portfolio may present more than one implementation within the same study. Together, LSTM and CNN techniques account for 60% of the implementations, while RNN, DNN, and GRU techniques stand out, with implementations in more than 20 papers each. In total, 23 techniques were implemented only once.

Table 7. Survey of DL techniques implemented by authors in the bibliographic portfolio.

Algorithm	Frequency	Algorithm	Frequency	Algorithm	Frequency
LSTM	161	RESNET	2	PKNN	1
CNN	86	ELM	2	DBNN	1
RNN	29	BPNN	2	DSMTNET	1
DNN	27	EFFICIENTNET	1	DCN	1
GRU	26	CRNN	1	DDAN	1
ANN	10	VISION TRANS-FORMER NETWORK	1	DEEP REIN-FORCE-MENT LEARN-ING	1
MLP	8	VGG11	1	DELM	1
TCN	6	TRANSFORMER NEURAL NETWORK	1	GOOGLENET	1
ENN	5	TDNN	1	DENSENET	1
FFNN	5	BNN	1	ALEXNET	1
GRAPH NN	4	CAPSNET	1	EDFM	1
DBN	3	REGRESSIVE MATCH-ING NETWORK	1	DILATED RESIDUAL NETWORK	1
DCNN	3	CDTSGANN	1	FCNN	1

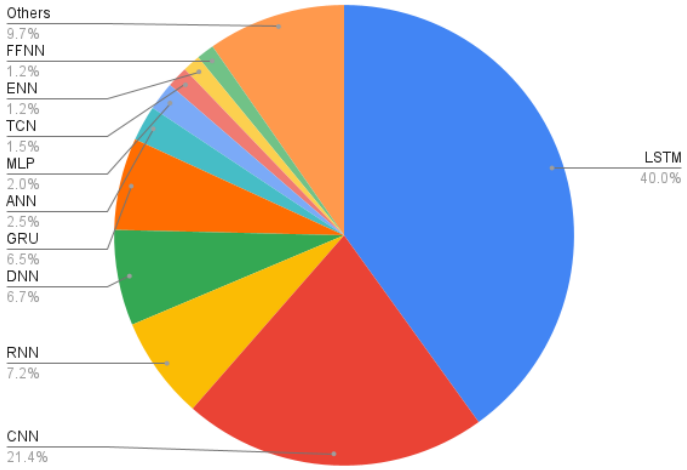

Figure 24. Distribution of techniques in DL implementations in the portfolio.

The evolution of the main DL algorithms implemented in the portfolio is presented in Figure 25, which shows that the most implemented algorithm is the LSTM network. In addition to the rising trends of LSTM and CNN networks, we again highlight the recent implementation trends of DNN and GRU algorithms, as well as the first relevant implementations of the DCNN algorithm, found in 2023, which combines characteristics of DNN and CNN networks.

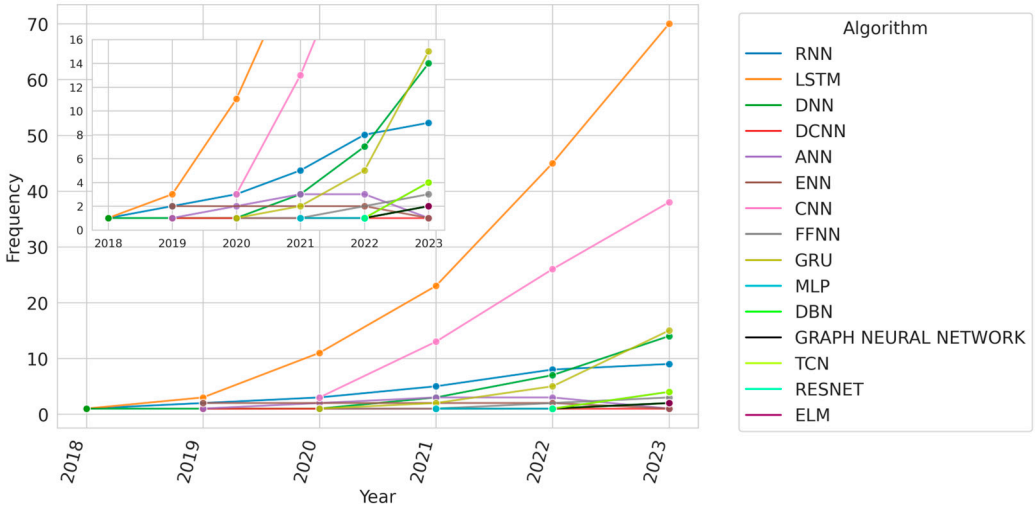

Figure 25. Evolution of DL algorithmic implementation in the BP.

In [44], which is the main DL publication according to the citation count, the authors employ a hybrid LSTM-RNN model to capture long-term information regarding the relationship between a battery's capacity and its degradation, emphasizing that such a dual approach is recommended to avoid overfitting issues. Another work utilizing a hybrid technique based on LSTM is presented in [48], using an Elman neural network (ENN). The concept of transfer learning, which involves the use of neural networks trained and fine-tuned in large datasets and then fine-tuned on their final layers in a specific dataset to transfer knowledge to another problem, is discussed in [65], which implements an LSTM network. Other examples of studies using LSTMs can be found in [51,59,422,423].

Regarding relevance by citation count, the main studies using DL are presented in Table 8, where it is notable that the use of LSTM is present in six out of the ten studies. Another interesting point is the use of a hybrid approach by the publications, using two DL algorithms in this case. The table also highlights the datasets used by the authors, with half the publications utilizing public data Additionally, the table includes a marking to

indicate whether the implementation was hybrid, where more than one algorithm was used to determine the same prediction.

Table 8. Main publications in the portfolio with DL implementation.

Algorithm	Hybrid	Dataset	Title	Year	Cited	Ref.
LSTM, RNN	Yes	Author	Long short-term memory recurrent neural network for remaining-useful-life prediction of lithium-ion batteries	2018	880	[44]
LSTM, GPR	Yes	Author	A data-driven approach with uncertainty quantification for predicting future capacities and remaining useful life of lithium-ion batteries	2021	434	[45]
LSTM, ENN	Yes	Author	Remaining-useful-life prediction for lithium-ion batteries based on a hybrid model combining the long short-term memory and Elman neural networks	2019	316	[48]
DNN	No	NASA	Remaining-useful-life prediction for lithium-ion batteries: A deep-learning approach	2018	313	[49]
CNN, LSTM	Yes	NASA	A data-driven auto-CNN-LSTM prediction model for lithium-ion-batteries' remaining useful life	2021	291	[50]
LSTM	No	NASA	State-of-health estimation and remaining-useful-life prediction for lithium-ion batteries based on a variant long short-term memory neural network	2020	284	[51]
DCNN	No	Author	A deep-learning method for online capacity estimation of lithium-ion batteries	2019	260	[53]
DNN	No	CALCE, NASA, MIT, OXFORD	Machine-learning pipeline for batteries' state-of-health estimations	2021	246	[54]
LSTM	No	NASA	A neural-network-based method for RUL prediction and SOH monitoring of lithium-ion batteries	2019	245	[55]
PKNN	No	Author	A novel estimation method for the states of health of lithium-ion batteries using a prior-knowledge-based neural network and a Markov chain	2019	239	[56]

The five most recent studies with DL implementation in the bibliographic portfolio are presented in Table 9. The publications correspond to the year 2024, which, in total, had 17 publications on the subject in the first two weeks of the year (the total number of portfolio publications in 2024 was 21). The five highlighted papers make use of public datasets (16 out of 17 in total for the year), with two publications implementing a hybrid approach with DL (seven out of seventeen in total for the year), including the use of a decision-tree-based algorithm.

Table 9. Recent publications in the portfolio with DL implementation.

Algorithm	Hybrid	Dataset	Title	Year	Cited	Ref.
GCN	No	NASA, OXFORD	State-of-health and remaining-useful-life predictions of lithium-ion batteries with a conditional graph convolutional network	2024	2	[179]
RNN	No	MIT	Jellyfish-optimized recurrent neural network for state-of-health estimations of lithium-ion batteries	2024	2	[336]
LSTM	No	NASA, CALCE	Remaining-useful-life predictions of lithium Batteries based on a CNN–Mogrifier LSTM-MMD	2024	1	[192]
MLP, GRU	Yes	NASA, CALCE	An MLP–mixer and mixture of expert models for remaining-useful-life predictions of lithium-ion batteries	2024	0	[220]
RF, GRU	Yes	NASA	State-of-health estimations for lithium-ion batteries using a random forest and a gated recurrent unit	2024	0	[221]

3.4.2. Hybrid Models

Hybrid ML models combine different ML techniques and algorithms to enhance prediction performance by leveraging the strengths of each method while compensating for their individual weaknesses [48,424]. Within the bibliographic portfolio, a total of 135 publications have implemented this approach. The evolution of hybrid model usage in the portfolio is depicted in Figure 26. As shown, it can be inferred that the use of hybrid approaches in SoH estimation is a recent field of exploration, with a significant increase in implementations in 2023. Considering the volume of portfolio publications, the use of hybrid approaches represents approximately 30% of the papers surveyed, a jump of nearly 50% compared to 2022, where it was present in about 18% of publications. In the first two weeks of 2024, a total of nine papers with hybrid approaches were published.

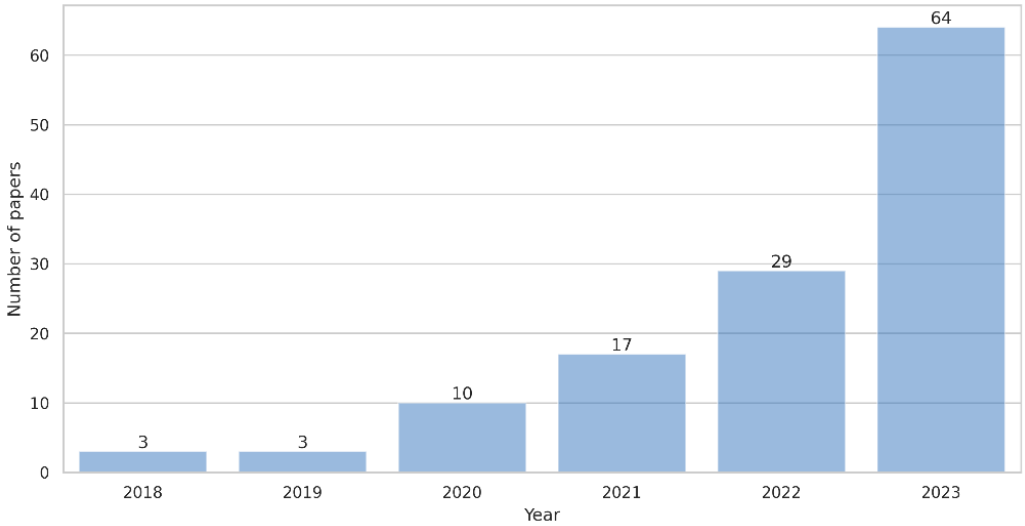

Figure 26. Evolution of hybrid algorithmic implementation in the BP.

The most utilized techniques in the hybrid modeling approach also correspond to the use of DL networks, such as LSTM and CNN, with a considerable advantage, with 74 and 51 implementations, respectively, as indicated in Figure 27. Other DL algorithms, such as GRU and RNN, are also notable, for example, in [232,233,381,425]. Other classical algorithms, such as SVM and GPR, found in [149,426], and decision-tree-based algorithms, like RF, XGBoost, and LightGBM, present in [80,221,427], are also noteworthy.

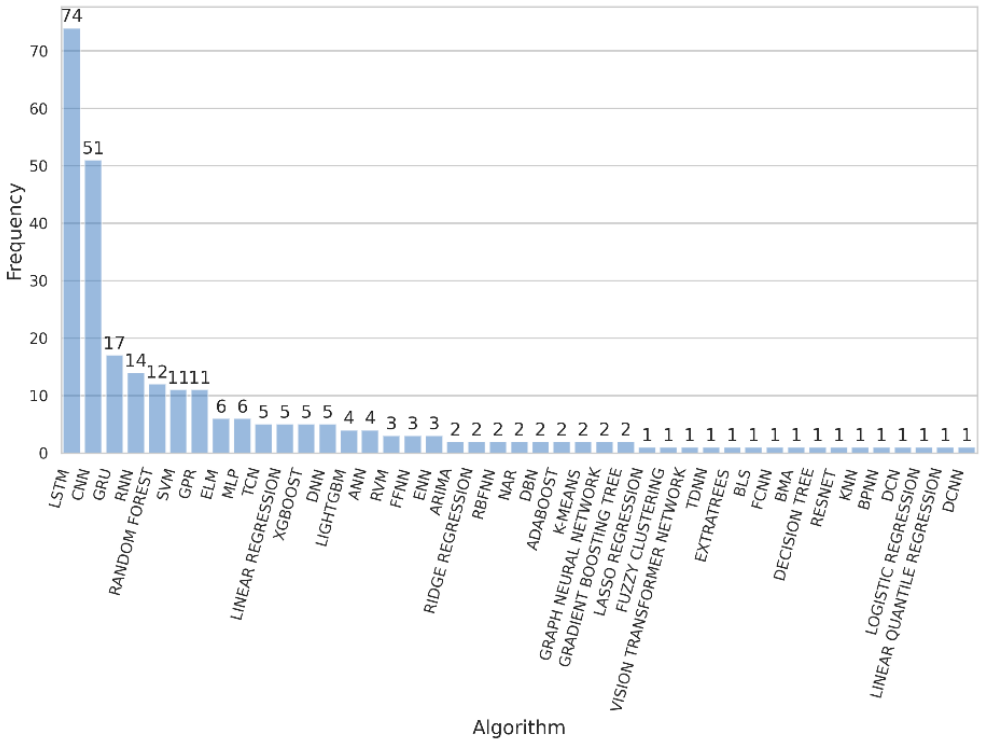

Figure 27. Frequency of techniques addressed in papers with hybrid algorithms in the BP.

The evolution of the implementations of the main algorithms is presented in Figure 28. It is possible to observe the increases in the implementations of LSTM and CNN networks, in line with previous results, and the recent evolution of the use of GRU and RF algorithms, with a peak in usage in 2023.

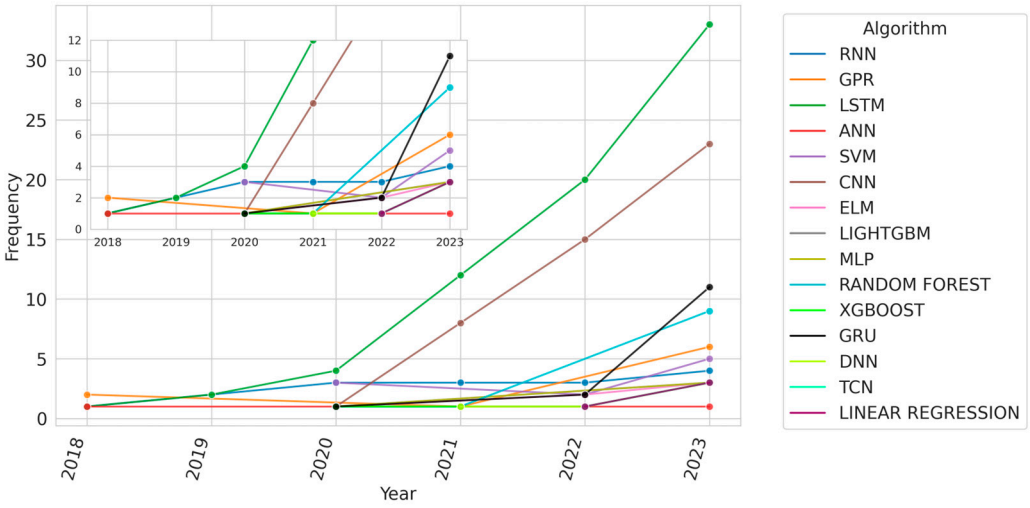

Figure 28. Evolution of hybrid algorithmic implementation in the bibliographic portfolio.

Figure 29 presents the found combinations resulting from the analysis of hybrid algorithms in the portfolio. The primary combination occurs with the LSTM and CNN networks, with 27 implementations in the portfolio. Algorithms that appear individually in the survey reflect either a hybrid approach (e.g., the integration of different configurations of the same algorithm, such as combining a 2-dimensional CNN with a 3-dimensional CNN), or methodologies that incorporate filters (e.g., the Kalman filter) and optimization algorithms as a part of their design. In total, 65 papers presented combinations of algorithms that were implemented only once in the portfolio, indicating that many researchers still evaluate different approaches of hybrid models.

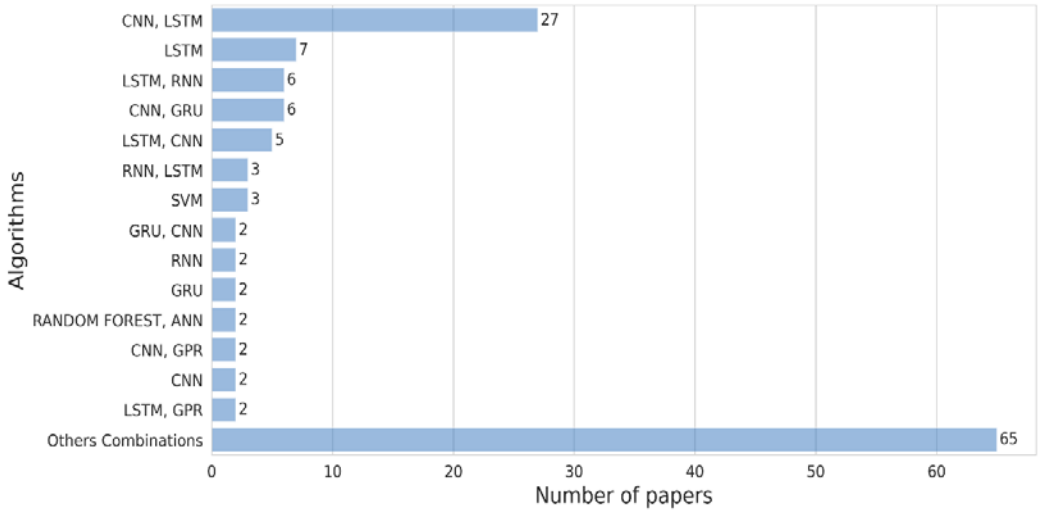

Figure 29. Combinations of algorithms found in papers with a hybrid approach in the BP.

The combinations of each algorithm in the portfolio are presented in Table 10, allowing for the identification of hybrid approaches, evaluated by the authors, within the portfolio, which can serve as a starting point for testing hybrid models in new research. A visualization of these combinations is shown in Figure 30, where centers of algorithmic connections can be observed, revolving around LSTM, CNN, RF, and GPR techniques. As demonstrated in Table 10 and Figure 30, LSTM networks exhibit a considerable range of combinations with other algorithms, including decision-tree, statistical, kernel, neighborhood, and clustering algorithms, as well as other neural network architectures.

Table 10. Connections between algorithms in papers with a hybrid approach in the BP.

Algorithm	Algorithmic Connections
LSTM	DCNN, FFNN, CNN, ANN, ENN, DNN, TCN, RNN, XGBOOST, BMA, GRAPH NEURAL NETWORK, SVM, GPR, DBN, GRU, RANDOM FOREST, FUZZY CLUSTERING, BPNN, LINEAR QUANTILE REGRESSION, MLP, RESNET, ADABOOST
RANDOM FOREST	ANN, NAR, LINEAR REGRESSION, GRADIENT-BOOSTING DECISION TREE, GPR, LIGHTGBM, XGBOOST, LSTM, SVM, RBFNN, RIDGE REGRESSION, KNN, GRU, EXTRATREES, ELM
SVM	ARIMA, DECISION TREE, ELM, LSTM, GPR, RBFNN, RANDOM FOREST, RIDGE REGRESSION, LINEAR REGRESSION, GRU, RNN

Table 10. *Cont.*

Algorithm	Algorithmic Connections
GRU	CNN, DNN, LSTM, RNN, TCN, MLP, RANDOM FOREST, ELM, LINEAR REGRESSION, SVM
CNN	LSTM, DNN, GRU, GRAPH NEURAL NETWORK, FCNN, GPR, FFNN, MLP, TCN, RESNET
GPR	LOGIC REGRESSION, ANN, LSTM, LINEAR REGRESSION, RANDOM FOREST, GRADIENT-BOOSTING DECISION TREE, CNN, SVM, RBFNN, RIDGE REGRESSION
XGBOOST	LSTM, LIGHTGBM, MLP, LASSO REGRESSION, RANDOM FOREST, KNN, RIDGE REGRESSION, GRADIENT-BOOSTING DECISION TREE, EXTRATREES, LINEAR REGRESSION
LINEAR REGRESSION	RANDOM FOREST, GRADIENT-BOOSTING DECISION TREE, GPR, LIGHTGBM, XGBOOST, RIDGE REGRESSION, EXTRATREES, SVM, GRU
RIDGE REGRESSION	GPR, SVM, RBFNN, RANDOM FOREST, LIGHTGBM, XGBOOST, GRADIENT-BOOSTING DECISION TREE, EXTRATREES, LINEAR REGRESSION
LIGHTGBM	MLP, XGBOOST, LASSO REGRESSION, RANDOM FOREST, RIDGE REGRESSION, GRADIENT-BOOSTING DECISION TREE, EXTRATREES, LINEAR REGRESSION
GRADIENT-BOOSTING DECISION TREE	LINEAR REGRESSION, RANDOM FOREST, GPR, LIGHTGBM, XGBOOST, RIDGE REGRESSION, EXTRATREES
MLP	LIGHTGBM, XGBOOST, LASSO REGRESSION, CNN, LSTM, VISION TRANSFORMER NETWORK, GRU
EXTRATREES	LIGHTGBM, XGBOOST, RIDGE REGRESSION, RANDOM FOREST, GRADIENT-BOOSTING DECISION TREE, LINEAR REGRESSION
TCN	LSTM, GRU, DNN, DCN, CNN, RESNET
ELM	RVM, SVM, DBN, GRU, RANDOM FOREST
DNN	CNN, LSTM, GRU, K-MEANS, TCN
RNN	LSTM, NAR, TDNN, GRU, SVM
RBFNN	K-MEANS, GPR, SVM, RANDOM FOREST, RIDGE REGRESSION
ENN	ARIMA, LSTM, ADABOOST
RESNET	CNN, LSTM, TCN
ANN	LSTM, RANDOM FOREST, GPR
NAR	RNN, TDNN, RANDOM FOREST
LASSO REGRESSION	LIGHTGBM, MLP, XGBOOST
ARIMA	SVM, ENN
TDNN	NAR, RNN
RVM	ELM, BLS
DBN	LSTM, ELM

Table 10. *Cont.*

Algorithm	Algorithmic Connections
KNN	RANDOM FOREST, XGBOOST
K-MEANS	RBFNN, DNN
GRAPH NEURAL NETWORK	CNN, LSTM
FFNN	LSTM, CNN
ADABOOST	ENN, LSTM
LINEAR QUANTILE REGRESSION	LSTM
LOGIC REGRESSION	GPR
BMA	LSTM
DCN	TCN
BLS	RVM
BPNN	LSTM
FUZZY CLUSTERING	LSTM
FCNN	CNN
DECISION TREE	SVM
DCNN	LSTM
VISION TRANSFORMER NETWORK	MLP

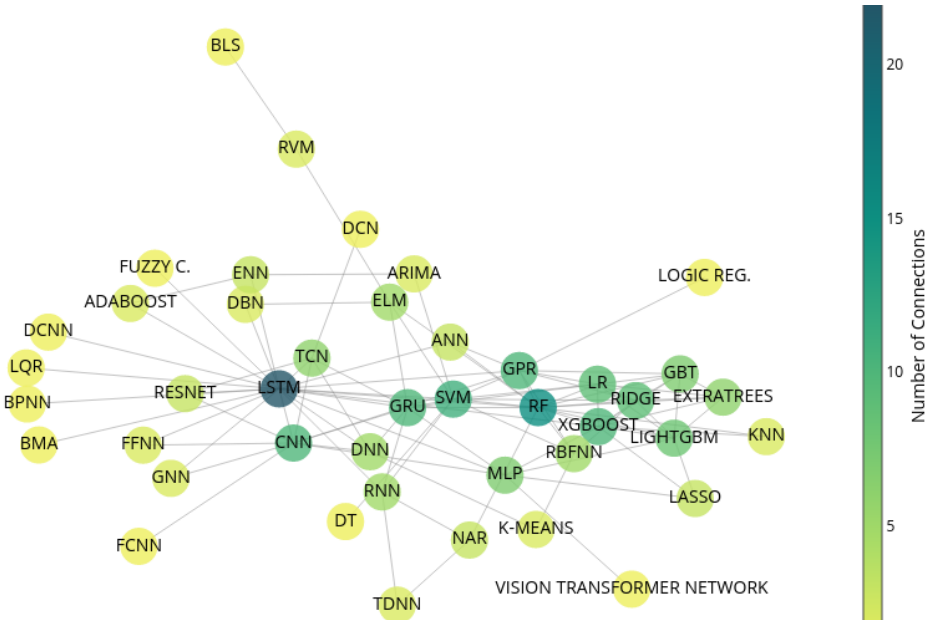

Figure 30. Connections between algorithms in papers with a hybrid approach in the BP.

Tables 11 and 12 present, respectively, the most relevant and most recent studies with hybrid modeling present in the bibliographic portfolio.

Table 11. Key publications in the portfolio with hybrid model implementation.

Algorithm	Dataset	Title	Year	Cited	Ref.
LSTM, RNN	Author	Long short-term memory recurrent neural network for remaining-useful-life predictions of lithium-ion batteries	2018	880	[44]
LSTM, GPR	Author	A data-driven approach with uncertainty quantification for predicting future capacities and the remaining useful life of lithium-ion batteries	2021	434	[45]
LSTM, ENN	Author	Remaining-useful-life prediction for lithium-ion batteries based on a hybrid model combining the long short-term memory and Elman neural networks	2019	316	[48]
CNN, LSTM	NASA	A data-driven auto-CNN-LSTM prediction model for lithium-ion-batteries' remaining useful life	2021	291	[50]
Logic Regression, GPR	NASA	State-of-health prediction of lithium-ion batteries: Multiscale logic regression and Gaussian process regression ensemble	2018	204	[60]
GRU, CNN	NASA	A novel deep-learning framework for state-of-health estimation of lithium-ion batteries	2020	203	[61]
NAR, RF	Author	State-of-health estimation and remaining-useful-life prediction for lithium-ion batteries using a hybrid data-driven method	2020	190	[64]
LSTM, RNN	Author	Deep-learning-based prognostic approach for lithium-ion batteries with adaptive time-series prediction and online validation	2020	134	[71]
3-CNN, 2-CNN	MIT	A machine-learning prediction method of lithium-ion-battery life based on charge processes for different applications	2021	113	[315]
CNN, LSTM, DNN	NASA, CALCE	Remaining-useful-life assessment for lithium-ion batteries using a CNN-LSTM-DNN hybrid method	2021	108	[236]

Table 12. Most recent publications in the portfolio with hybrid model implementation.

Algorithm	Dataset	Title	Year	Cited	Ref.
SVM, RNN	NASA CALCE	Data-driven transfer-stacking-based state-of-health estimation for lithium-ion batteries	2024	14	[270]
RF, GRU	NASA	State-of-health estimation for lithium-ion batteries using a random forest and a gated recurrent unit	2024	0	[221]
CNN, GPR	Author	Probabilistic lithium-ion-batteries' state-of-health predictions using convolutional neural networks and a Gaussian process regression	2024	0	[414]

Table 12. *Cont.*

Algorithm	Dataset	Title	Year	Cited	Ref.
CNN, LSTM, TCN, RESNET	Author	A machine-learning framework for remaining-useful-lifetime prediction of Li-ion batteries using diverse neural networks	2024	0	[428]
CNN, GRU	NASA	Lithium-ion-batteries' state-of-health estimations using a hybrid model based on a convolutional neural network and a bidirectional gated recurrent unit	2024	0	[223]

Among the most relevant studies, the use of LSTM or CNN was present in seven out of the ten papers. This predominance is expected, given the previous findings; however, the presence of these algorithms in the hybrid models for the highly cited papers also demonstrates that their implementation leads to promising results in SoH estimation. A similar perspective occurs in the analysis of the most recent studies, indicating that researchers continue to develop hybrid models around these neural network architectures. As shown further ahead, the performance of studies that employed hybrid approaches sometimes yielded superior results compared to the use of simple models, as was the case in [335], which used GPR with LSTM and managed to reduce MAPE levels by approximately 50% compared to those in [1].

3.4.3. Transfer-Learning Models

Transfer-learning (TL) techniques involve the process where a model trained in a particular primary dataset is reused as a starting point to train a new model in a new dataset [429–431]. In this case, the knowledge from the model obtained from the first dataset can be transferred to the model with the second dataset. This technique is especially useful when the second dataset is limited in volume or when training a model from scratch presents a high computational cost [429–431]. This principle is widely used in tasks in the areas of computer vision and natural language processing [429–431].

Given that data for estimating the health state of a battery require experimental effort (e.g., the programming of generalist tests, cycling processes until their end of life, and data collection), which, in turn, takes time, the use of TL within this research field can be useful for leveraging the volume of available open data, as well as aggregating new data collected in a cycle of studies, and, thus, transferring learning to more customized datasets. This idea was found in 42 publications, as shown by the annual evolution in the graph in Figure 31 (two publications belong to the year 2024). The emergence of this learning method only occurred in 2020 within the portfolio, with the years 2022 and 2023 being the main publication years.

The survey of ML techniques employed in these publications mainly identified the use of LSTM networks, which accounts for approximately 40% of the implementations, as shown in Figure 32. Also noticeable is the use of decision-tree-based techniques, such as in [354] with Adaboost implementation, and well-known DL networks in computer vision tasks, such as GoogleNet and ResNet, present in [110]. The key publications using TL and the most recent publications found in the portfolio are presented in Tables 13 and 14, respectively.

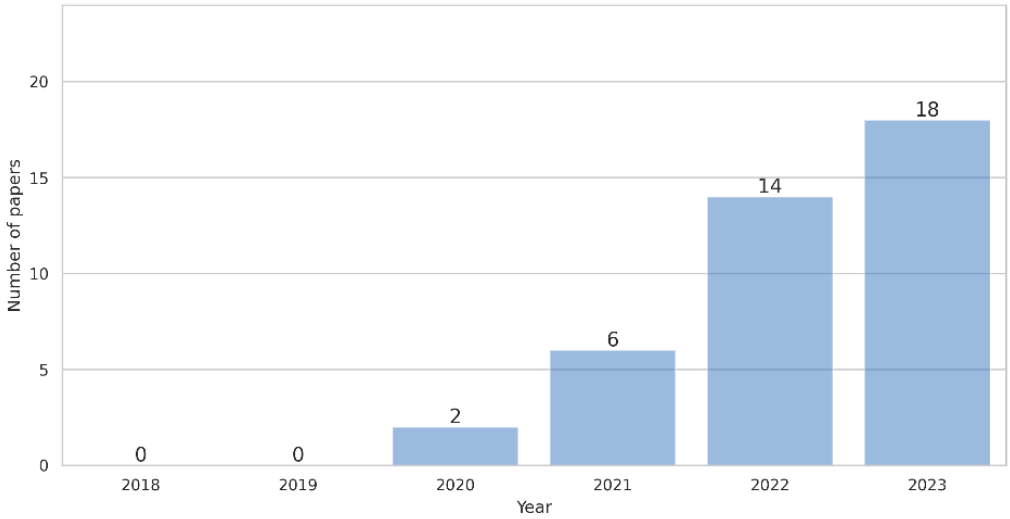

Figure 31. Evolution of TL algorithm implementation in the bibliographic portfolio.

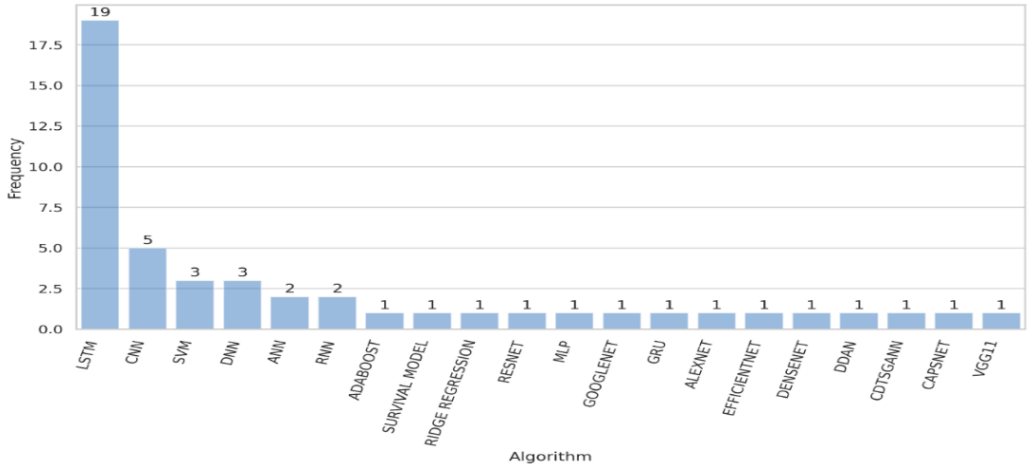

Figure 32. Frequency of techniques addressed in papers with TL algorithms in the BP.

Table 13. Key publications in the portfolio with TL implementation.

Algorithm	Dataset	Title	Year	Cited by	Ref.
LSTM	AUTHOR	Transfer learning with long short-term memory networks for state-of-health prediction of lithium-ion batteries	2020	184	[65]
CNN	AUTHOR	Lithium-ion-batteries' capacity estimation—A pruned convolutional neural network approach assisted by transfer learning	2021	142	[7]
GRU	MIT	Predictive battery health management with transfer learning and online model correction	2021	122	[72]
LSTM	MIT	Battery health estimation with degradation pattern recognition and transfer learning	2022	102	[316]

Table 13. *Cont.*

Algorithm	Dataset	Title	Year	Cited by	Ref.
KERNEL RIDGE REGRESSION	NASA	State-of-health estimation of lithium-ion batteries based on semi-supervised transfer component analysis	2020	100	[238]
LSTM	AUTHOR	A flexible state-of-health prediction scheme for lithium-ion-battery packs with a long short-term memory network and transfer learning	2021	81	[432]
LSTM	NASA, CALCE	Forecasting the state-of-health of lithium-ion batteries using a variational long short-term memory with transfer learning	2021	65	[249]
LSTM	AUTHOR	A hybrid transfer-learning scheme for remaining-useful-life prediction and cycle-life-test optimization of different formulations of Li-ion power batteries	2021	60	[433]
CNN	BIT	Real-time personalized health status prediction of lithium-ion batteries using deep transfer learning	2022	42	[385]
LSTM	CALCE	A long short-term memory neural-network-based Wiener process model for remaining-useful-life prediction	2022	39	[362]

Table 14. Most recent publications in the portfolio with TL implementation.

Algorithm	Dataset	Title	Year	Cited by	Ref.
SVM, RNN	NASA, CALCE	Data-driven transfer-stacking-based state-of-Health estimation for lithium-ion batteries	2024	14	[270]
LSTM	NASA	Transfer-learning-based remaining-useful-life prediction of lithium-ion batteries considering the capacity regeneration phenomenon	2024	0	[296]
-	-	Transfer learning for batteries' smarter state estimation and aging prognostics: Recent progress, challenges, and prospects	2023	32	[27]
CAPSNET	AUTHOR	Novel image-based rapid RUL prediction for Li-ion batteries using a capsule network and transfer learning	2023	9	[109]
CNN	STANFORD, BIT	Voltage-relaxation-based state-of-health estimation of lithium-ion batteries using convolutional neural networks and transfer learning	2023	4	[389]

3.5. Performance Analysis

To evaluate the performance obtained in the bibliographic portfolio, the MIT dataset, which was produced in [1], was selected. This dataset was chosen because the authors recorded the sets of cells used in the training, testing, and validation splits, thus allowing other studies to replicate the sets and conduct a fair comparison of results. However, most of the analyzed publications chose to perform different splits, making a direct comparison

difficult. In these cases, the comparisons are empirical, and there is an associated probability of a particular approach being better than another. Among the arguments used are concerns related to the quality of the data from some cells, as well as supposed bias in the training split based on differences in the distribution of the cycles used in [1]. Another point that drew attention was cases where authors performed splits of training, testing, and validation while keeping data samples from all the cells in each set, which impacts the reliability of the results presented, as per the performances in the articles highlighted below.

Table 15 summarizes the RUL (remaining-useful-life) prediction performances in publications that had the same validation set, totaling five papers. The validation sets are referred to as the 1° Test and 2° Test by the authors in [1]. The 1° Test includes batteries under the same cycling conditions as those of the training set, while the 2° Test corresponds to batteries with a different usage profile. Notably, the performance gain achieved in [335] is highlighted, where the MAPE errors in both test sets are reduced by over 50% compared to that of the baseline study [1]. This improvement was achieved using the same 100 cycles of information for the prediction and implementing a hybrid model using the LSTM DL technique along with the GPR algorithm. However, such significant results were not found in the use of the LSTM-CNN combination in [333], where a range of errors similar to that of the baseline study [1] was observed despite employing more complex techniques. In [317], an increase in performance is evident with a hybrid approach involving neural networks, linear regression, and RF, using a reduced set of 80 cycles. These findings suggest that efforts in algorithmic selection do not necessarily guarantee higher performance, and steps such as feature construction and selection may represent an even more relevant stage in research.

In Table 16, the rest of the performance survey with the MIT dataset, conducted in the bibliographic portfolio, is presented. Here, the authors did not maintain the same modeling and validation splits, and there are variations in the target variables. Therefore, all the comparisons made may exhibit significant bias. The targets described in the table are presented to maintain the nomenclature adopted by the authors. The target's "early battery lifetime", also referred to in studies as the "early cycle life", aims to determine the total number of cycles a battery will present based on data from the first cycles of a battery. The "end of life" in the analyzed studies is related to determining the total number of cycles considering data from the last cycles, without necessarily knowing the entire battery history. Therefore, it is generally accompanied by models that determine the remaining number of cycles (RULs) and/or the current cycle. The "capacity" target was linked to studies that used regression models in predicting time series ("capacity trajectories"), where the evolution of the battery capacity over time is obtained or the prediction on a short horizon, such as the discharge capacity in the next cycle, can be used for SoH updates.

Table 15. Prediction performance of studies using the same samples for validation with MIT dataset.

Algorithm	1° Test		2° Test		Cycles	Title	Year	Cited	Ref.
	RMSE	MAPE	RMSE	MAPE					
Linear regression	118	14.1	214	10.7	100	Data-driven prediction of the battery cycle life before capacity degradation	2019	811	[1]
RF, linear regression, ANN	80	9.8	174	7.5	80	Prognostics of the battery cycle life in the early-cycle stage based on a hybrid model	2021	41	[317]
Ridge Reg Enet Reg RF MLP CNN	125 132 141 140 72	-	188 196 197 218 204	-	100	Statistical learning for accurate and interpretable battery lifetime predictions	2021	30	[102]
CNN, MLP	114	8.54	178	11.31	100	A hybrid ensemble deep-learning approach for the early prediction of batteries' remaining useful life	2023	9	[333]
GPR, LSTM	30	5.52	51	5.35	100	Joint modeling for early predictions of Li-ion-batteries' cycle life and degradation trajectory	2023	3	[335]

Table 16. Prediction performance of studies in the portfolio using different samples for validation with the MIT dataset.

Algorithm	Target	MAPE	RMSE	RMSPE	MAE	MRE	R^2	Observations	Ref.	Year
Bayesian ridge	Capacity (Ah)	0.45		0.76				- Predicting capacity considering only a short portion of partial charge/discharge data - Requires a 15 min sample of operation - Utilizes charging and discharging steps - 63 cells for training, 10 for calibration, 51 for testing (split based on the distribution of cycle numbers in the dataset, maintaining the same distribution across all the sets)	[54]	2021
GPR		1.00		1.91						
RF		0.11		0.14						
DNN		0.23		0.45						
CNN	RUL	10.6	76					- Utilization of four cycles - Incorporation of charging and discharging steps - 86 cells for training, 19 for validation, 19 for testing	[8]	2020

Table 16. *Cont.*

Algorithm	Target	MAPE	RMSE	RMSPE	MAE	MRE	R^2	Observations	Ref.	Year
GBT	RUL	7.5	84.9		58.6	0.94		- Usage of 250 cycles - Incorporation of the discharge stage - Data split into 2/3 for training and 1/3 for testing; no specification if cells from the training set are excluded from the test set; the splitting process is repeated four times, and the performances are analyzed - Performance corresponds to the average of the four cases	[83]	2020
CNN	Early battery lifetime	3.80 (1) 1.30 (2) 1.12 (3) 1.21 (4) 1.12 (5)	42 (1) 19 (2) 13 (3) 13 (4) 11 (5)		33 (1) 13 (2) 11 (3) 10 (4) 9 (5)			- Testing for the use of the first 20 (1), 40 (2), 60 (3), 80 (4), 100 (5) cycles for battery life prediction - Utilization of the first five cycles and the last fifteen cycles for RUL prediction - Incorporation of the charging stage - 94 cells for training, 30 for testing	[315]	2021
	RUL	3.55	11		9					
DNN	End of life	7.78 (1) 3.97 (2)	57 (1) 33 (2)					- Testing for the use of the last 1 (1) to 100 (2) cycles. - Incorporation of the discharging stage - EoL = current cycle + cycles used for data collection + RUL. - 65 cells for training, 16 for testing (discarding 43 cells) - Majority of RMSE for RUL < 50 cycles, larger errors for cells with fewer than 100 cycles - * Errors for predicting the current life cycle increase infinitely for cells with over 750 cycles (author's justification based on the low sample quantity for this scenario)	[318]	2022
	Cycle life		<65 (1) <40 (2) >90 *							
	RUL		<65 (1) <40 (2)							

Table 16. *Cont.*

Algorithm	Target	MAPE	RMSE	RMSPE	MAE	MRE	R^2	Observations	Ref.	Year
SVR	Capacity trajectory (Ah)	1.61		3.22				- Use of the last 20 cycles - Estimates the evolution of capacity trajectory over time until EoL (time series using regression) - Incorporation of both charging and discharging stages. - 84 cells for training, 40 for testing	[253]	2022
RF		0.93		2.12						
GPR		1.35		2.58						
ANN		1.13		1.92						
CNN	RUL	4.15	27.47		16.09			- Use of 10 cycles - Incorporation of the charging stage - 70% of the data for training, 30% for testing (does not specify if cells from the training set were excluded from testing)	[319]	2022
Linear reg, (1)	RUL		90			53.81 *		- Use of 10 cycles - Does not exclude cells from training during testing; 60% of the data for training, 20% for validation, and 20% for testing - Incorporation of the charging stage - Classification model to predict if a battery has less than 150 cycles of RUL or 150 cycles or more of RUL - RUL Approaches: - (1): Does not consider the classification model - (2): Regression model for each predicted RUL class in the classification model - * Considering cases where RUL > 150 cycles: 18.51, 10.51, 9.79, respectively - For capacity, the author evaluated 100 **, 150 ***, and 200 **** cycles ahead	[321]	2021
MLP (1)			52			23.03 *				
Logistic reg. + MLP (2)			49			15.2 *				
MLP	Discharge capacity after "x" cycles.					0.24 ** 0.45 *** 0.64 ****				

Table 16. *Cont.*

Algorithm	Target	MAPE	RMSE	RMSPE	MAE	MRE	R^2	Observations	Ref.	Year
Transfer Learning (CNN + RNN + "fully connected")	Capacity (Ah)	0.176 *	2.57 *				0.999 *	- Use of the last 30 cycles to predict the capacity of the next cycle and RUL - The author does not assess the performance of estimating the capacity trajectory for horizons longer than one cycle - Use of the charging stage - Use of the MIT dataset to train a model and evaluate the performance of the model with transfer learning on a dataset constructed by the author - Author's dataset contains information from 77 LFP/graphite cells of 1.1 Ah. - 22 cells separated for testing - * Performance considering training with the author's dataset. - ** Performance considering transfer learning from a model pretrained with the MIT dataset	[385]	2022
		0.328 **	4.65 **				0.997 **			
	RUL	8.72 *	186 *				0.804 *			
		9.80 **	240 **				0.770 **			
Elastic net	RUL	5.21	43.38				0.98	- Use of 100 cycles - Use of both charging and discharging stages - No exclusion of cells from training in testing; 70% of the data for training, 30% for testing	[329]	2022
GPR		5.26	43.71				0.98			
SVM		5.88	53.04				0.97			
RF		8.17	84.69				0.92			
DT ensemble		7.93	88.74				0.91			
XGBoost		7.92	91.13				0.92			
RVM		10.32	96.21				0.89			
DT		9.59	106.62				0.87			

Table 16. *Cont.*

Algorithm	Target	MAPE	RMSE	RMSPE	MAE	MRE	R^2	Observations	Ref.	Year
CNN, LSTM	Cycle life	2.28 (1)	19 (1)		14 (1)		0.9980 (1)	- Testing of usage from the last 50 (1), 60 (2), 70 (3), 80 (4), 90 (5), 100 (6) cycles - Usage of both charging and discharging stages - 93 cells for training and 31 for testing (split based on the distribution of cycle numbers in the dataset, maintaining the same distribution in all the sets)	[327]	2022
		4.59 (2)	50 (2)		33 (2)		0.9869 (2)			
		3.02 (3)	25 (3)		18 (3)		0.9967 (3)			
		3.43 (4)	25 (4)		19 (4)		0.9967 (4)			
		1.84 (5)	16 (5)		13 (5)		0.9985 (5)			
		1.47 (6)	11 (6)		9 (6)		0.9993 (6)			
	RUL	2.16 (1)	12 (1)		8 (1)		0.9993 (1)			
		3.17 (2)	15 (2)		12 (2)		0.9989 (2)			
		1.93 (3)	11 (3)		8 (3)		0.9994 (3)			
		1.85 (4)	14 (4)		10 (4)		0.9990 (4)			
		1.72 (5)	13 (5)		9 (5)		0.9992 (5)			
		1.25 (6)	8 (6)		6 (6)		0.9997 (6)			
Graph Neural Network	Capacity trajectory (Ah)	0.009 *			0.0377 *		0.9399 *	- Using 350 measurement points as input. - Usage of the charging stage. - 70% of the cells used for training and 30% for testing. - Estimates the evolution of capacity trajectory over time until End of Life (time series using regression). - * Performance based on the worst predicted cell. - ** Performance based on the best predicted cell.	[92]	2023
		0.004 **			0.0025 **		0.9894 **			

Table 16. *Cont.*

Algorithm	Target	MAPE	RMSE	RMSPE	MAE	MRE	R^2	Observations	Ref.	Year
LightGBM	SoH (%)		1.751					- Estimation of SoH based on 300 s measurements - Usage of the discharge stage - Cells 91 and 100 from the MIT dataset are used for training, cell 124 used for testing - * Model considering LightGBM, XGBoost, Random Forest (RF), SVR, GPR as base models, and linear regression as a meta-model	[99]	2023
XGBoost			1.616							
RF			1.721							
SVR			1.926							
GPR			1.539							
Stacking			1.489 *							
LSTM	SoH (%) after "x" cycles	0.016 (1)		1.81 (1)	0.0098 (1)			- Testing prediction horizons of 25 (1), 50 (2), 100 (3), 150 (4), 200 (5), 250 (6), 300 (7), 350 (8), 400 (9) cycles ahead - Usage of charge and discharge stages - 64% of the cells are used for training, 20% for validation, and 16% for testing (cells cannot be in more than one set) - Average of performances per cell	[144]	2023
		0.021 (2)		2.30 (2)	0.0130 (2)					
		0.024 (3)		2.80 (3)	0.0140 (3)					
		0.024 (4)		2.86 (4)	0.0120 (4)					
		0.031 (5)		3.60 (5)	0.0180 (5)					
		0.026 (6)		3.00 (6)	0.0150 (6)					
		0.030 (7)		3.49 (7)	0.0200 (7)					
		0.032 (8)		3.70 (8)	0.0200 (8)					
		0.033 (9)		3.80 (9)	0.0201 (9)					

Table 16. *Cont.*

Algorithm	Target	MAPE	RMSE	RMSPE	MAE	MRE	R^2	Observations	Ref.	Year
RF	Cycle life	0.57			4.65			- Usage of 100 cycles. - Utilization of charge and discharge stages. - 75% of the data used for training, 25% used for testing (cells from the training set were not excluded from testing). - Discrepant results compared to the literature, potential model validation error by the author.	[334]	2022
ResNet50	Early lifetime		119.98				0.8501	- Use of the first 100 cycles for predicting the total lifespan. - Utilization of images obtained from plots with voltage and capacity information as features. - 80 cells for training and 43 cells for testing, process repeated five times.	[111]	2024
CNN			115.85				0.8557			
LeNet			129.77				0.8197			
AlexNet			91.51				0.9121			
VGG16			122.19				0.8466			

Through a comparison analysis, it is possible to observe performance improvements compared to the baseline study in [315], with a MAPE of around 3.5% using a CNN. In [8], the authors achieved significant performance with a CNN and only four cycles of data as input to the algorithm, a reduction that provides new perspectives for the use and conditioning of batteries. Using TL, the authors in [385] achieved results within the error magnitudes of the studies that use only one dataset, demonstrating that TL can be a useful tool for aggregating the volume of information from other types of experimental tests and cell technologies to overcome data limitations. In [327], the best results for RUL prediction were achieved, with MAPE values below 2%. The authors conducted tests considering different data usage intervals, ranging from 50 to 100 cycles, and using a hybrid LSTM-CNN approach. Conversely, in [334], the authors claim errors around half a cycle, well below those presented in various consulted studies. The use of data from all the cells during training ends up bringing a possible leakage when validating the algorithm because the pattern of all the cells was passed to the model, which, consequently, did not develop proper learning but possible "rote memorization", associating levels of variable values with related life cycles. This point highlights the importance of correctly analyzing the results for the dissemination of research in the field.

This analysis reveals significant challenges in comparing RUL prediction models because of inconsistencies in data splitting, target variables, and evaluation metrics across different studies. Although advancements have been observed, particularly with hybrid models, like LSTM-GPR and the application of TL, the lack of standardized methodologies hinders direct comparisons and hinders the identification of truly superior approaches. The use of limited data cycles in training, as demonstrated in [8], and the exploration of feature engineering, as suggested by the results in [317], present promising avenues for future research. However, it is crucial to emphasize the importance of rigorous data splitting procedures, avoiding data leakage, as observed in [334], to ensure the reliability and generalizability of the obtained results. Notably, for most of the analyzed models, MAPE errors of around 10% have become achievable with the development of algorithms and open datasets. Moving forward, establishing standardized datasets and evaluation protocols will be essential to facilitate progress in the field and enable more meaningful comparisons between different RUL prediction models.

3.6. The Importance of SoH in Smart Systems, Energy Informatics, and Smart Grids

Accurate battery SoH estimates, derived from ML algorithms and analyses based on large datasets, have significant implications for energy informatics and intelligent systems, such as smart grids. This study explores some of the key applications connecting SoH prediction to improvements in energy efficiency and sustainability.

Energy Informatics and Energy Management in Smart Grids: Energy informatics, the integration of information systems and energy, plays a fundamental role in the efficient management of smart grids. Accurate SoH estimation enables more effective management of second-life batteries by integrating them into storage and distribution networks. This approach not only reduces waste but also enhances the reliability and resilience of electrical grids, especially in contexts involving renewable energy sources [1,10,12].

IoT Devices and Sustainability: SoH prediction models based on DL techniques, such as LSTM and CNN networks, facilitate the preventive maintenance of IoT devices that rely on batteries. These models support a more sustainable economy by optimizing replacement cycles and extending the lifespans of connected smart devices [48,54,64]. The use of these devices in smart grids also reduces reliance on manual interventions, promoting greater automation and efficiency [9,12].

Real-Time Monitoring and Control: Wireless sensor networks (WSNs) integrated with SoH algorithms offer real-time monitoring capabilities, essential for dynamic system adjustments. In smart grids, this enables load balancing and the optimization of the energy distribution, improving the overall system performance [54].

Environmental Impact and Sustainability: The reuse of batteries, underpinned by reliable SoH estimates, contributes to a circular economy by reducing the environmental impact and the carbon footprint associated with the production of new batteries [9,12]. Hybrid models, such as the combination of LSTM with Elman neural networks (ENNs), have already demonstrated accuracy gains of up to 50% compared to classical approaches, increasing confidence in battery reuse for storage systems and smart grids [48].

Through these applications, SoH prediction not only enhances the management and efficiency of smart grids but also reinforces the connections among energy informatics, sustainability, and technological innovation. This highlights the importance of robust prediction methods for the future of intelligent energy systems.

Additionally, it is essential to emphasize that accurate SoH prediction significantly contributes to the evolution of intelligent systems by reducing operational uncertainties and enabling the seamless integration of emerging technologies. The precise forecasting of SoH enhances system reliability by enabling the optimized allocation of energy resources, such as second-life batteries, across diverse use cases. These advancements also support the adoption of predictive maintenance systems, which reduce operational costs while maximizing energy efficiency and long-term sustainability. By converging machine-learning techniques, such as deep neural networks, with advanced data management platforms, SoH becomes a critical metric for decision-making in smart grids and the IoT, driving resilience and sustainability in energy infrastructure.

4. Conclusions

This study highlights the growing importance of ML techniques in estimating the SoHs of batteries, as evidenced by a systematic bibliographic portfolio analysis. The application of ProKnow-C enabled the objective selection of 534 relevant papers from an initial pool of 6032 publications, providing a structured and replicable methodology for characterizing research within this domain.

The results reveal several key trends. First, there has been a significant increase in scientific production in this area, particularly since 2022, with 40% of the selected papers published in 2023. The increasing relevance of battery reuse, driven by the expansion of the electric vehicle market, is expected to further boost research in SoH estimation. Second, the analysis highlights the importance of open datasets, with 60% of the reviewed studies using publicly available data. The NASA Prognostics Center of Excellence repository remains the most cited source, accounting for over half of the open data usage. Overall, the portfolio analysis revealed the presence of 12 available open data sources, with 6 of these sources published in the years 2022 and 2023.

From a methodological perspective, DL techniques, especially LSTM networks and CNNs, dominate the field, with DL accounting for 58% of the implementations. Hybrid approaches, including those combining LSTM and CNNs, are increasingly prominent, representing approximately 25% of the reviewed studies. The emergence of TL in publications since 2022 also highlights a promising avenue for leveraging diverse datasets to address data scarcity and heterogeneity in SoH modeling.

Performance evaluations based on the MIT dataset indicate that classical approaches achieve mean absolute percentage errors of approximately 10%, whereas DL techniques have reduced errors by 50% in some cases. Some studies report prediction errors as low as 1–4% using CNNs, emphasizing the potential of advanced algorithms in this field.

The results presented underscore the critical role of SoH predictions in advancing energy informatics and intelligent energy systems. Accurate SoH estimates enable the integration of second-life batteries into smart grids, enhancing their reliability, supporting renewable energy utilization, and optimizing energy distribution in interconnected systems. Additionally, the application of SoH prediction models in IoT devices and wireless sensor networks facilitates preventive maintenance, reduces waste, and contributes to a circular economy. These methodologies not only transform energy systems by aligning with the goals of efficiency and sustainability but also enhance operational resilience through real-time decision-making processes. This potential extends to the design of smarter, greener infrastructures that meet the evolving demands of global energy markets.

The findings and insights derived from this study, along with prior research conducted by the authors in the field of SoH estimation and energy systems, have contributed significantly to shaping future research directions. The accumulated knowledge from these studies served as a foundation for defining key research gaps, refining methodological approaches, and aligning investigations with emerging challenges in this domain. By integrating lessons learned from previous studies, this review strengthens the proposition of future research strategies and the advancement of machine-learning applications in battery-health prediction [434–439]. Future research could further explore the integration of these methodologies into real-world applications, strengthening their role in smart energy management.

In summary, this study provides a comprehensive characterization of the current stage of the research in battery SoH estimation using artificial intelligence, made possible through the application of a systematic bibliographic portfolio assessment. Notably, no prior review had applied this methodology in this field. These findings contribute to (i) the presentation and exemplification of the use of a systematic methodology for obtaining a bibliographic portfolio, ProKnow-C; (ii) the characterization of the current landscape in the field of SoH estimation using ML; (iii) the presentation of open data sources and their key characteristics, including datasets recently made available, which contribute to the development of new research and comparisons of approaches in this area of development; and (iv) the assessment of performance levels achieved by different researchers in their work, considering the techniques used and modeling conditions applied.

Despite these contributions, this study has limitations. The selection of articles may be subject to bias because of the researchers' prior knowledge and the constraints of ProKnow-C. The integration of generative AI tools with ProKnow-C presents a promising avenue to reduce selection bias by automating and improving the evaluation of titles and abstracts while significantly accelerating the time required to construct a bibliographic portfolio. Furthermore, this study did not conduct a quantitative evaluation of the quality of individual datasets or the specific impacts of variables provided by these datasets. It also lacks an in-depth analysis of the computational performance and predictive power of the surveyed algorithms.

To address these gaps and advance the research in this field, future research directions include:

- Feature-engineering processes with an emphasis on explainability analysis and behavior evaluation across different datasets;
- Implementation of models using the identified open datasets, focusing on assessing the applicability of transfer learning to address datasets with limited volumes;
- Integration of the ProKnow-C methodology with generative AI, aimed at automating the selection process and reducing bias in bibliographic portfolio construction.

Author Contributions: Conceptualization, G.R.S., J.N.M., M.L.M.A., J.P.C., J.A.A., S.F.L. and O.H.A.J.; methodology, G.R.S., J.N.M. and O.H.A.J.; validation, J G.R.S., J.N.M., M.L.M.A., J.P.C., J.A.A., S.F.L. and O.H.A.J.; investigation and simulation, G.R.S., J.N.M. and O.H.A.J.; writing—original draft preparation, G.R.S., J.N.M., J.A.A., S.F.L. and O.H.A.J.; writing—review and editing, G.R.S., J.N.M., M.L.M.A., J.P.C., J.A.A., S.F.L. and O.H.A.J.; project administration, O.H.A.J.; funding acquisition, J.A.A. and S.F.L. All authors have read and agreed to the published version of the manuscript.

Funding: This research was partially supported by the FACEPE agency (Fundação de Amparo a Pesquisa de Pernambuco) throughout a project with references APQ-0616-9.25/21 and APQ-0642-9.25/22. O.H.A.J. were funded by the Brazilian National Council for Scientific and Technological Development (CNPq), grants number 407531/2018-1, 303293/2020-9, 405385/2022-6, 405350/2022-8, and 40666/2022-3, as well as the Program in Energy Systems Engineering (PPGESE) Academic Unit of Cabo de Santo Agostinho (UACSA), Federal Rural University of Pernambuco (UFRPE). G.R.S. was funded by the Federal University of Latin American Integration (UNILA). J.P.C. was supported by a PQ scholarship with the reference number CNPq 305858/2023-8.

Data Availability Statement: Not applicable.

Conflicts of Interest: The authors declare no conflicts of interest.

Abbreviations

AD	Author Database
AI	Artificial Intelligence
ANN	Artificial Neural Network
ARIMA	Autoregressive Integrated Moving Average
ATBLS	Adaptive Time-shifting Broad-Learning System
AUTOML	Auto-Machine Learning
BESS	Battery Energy Storage Systems
BLS	Broad-Learning System
BMA	Bayesian Model Averaging
BMLR	Bootstrap Multiple Linear Regression
BMS	Battery Management System
BNN	Bayesian Neural Network
BP	Bibliography Portfolio
BPNN	Back Propagation Neural Network
CAPSNET	Capsule Neural Network
CC-CV	Constant Current–Constant Voltage
CDTSGANN	Conditional Time Series Generative Adversarial Network
CNN	Convolutional Neural Network
CRNN	Convolutional Recurrent Neural Network
DBN	Deep Belief Network
DBNN	Deep Bayesian Neural Network
DCN	Deep Cross Net
DCNN	Deep Convolutional Neural Network
DELM	Deep Elman Neural Network
DGNN	Deep Gaussian Neural Network
DL	Deep Learning
DNN	Deep Neural Network
DRN	Dilated Residual Network
DSMTNET	Dual Self-Attention Multivariate Time Series Estimation Network
DT	Decision Tree
ELM	Extreme-Learning Machine
ENN	Elman Neural Network
FCNN	Fully Connected Neural Network

FFNN	Feedforward Neural Network
GAM	Generalized Additive Model
GBT	Gradient-Boosting Tree
GNN	Graph Neural Network
GRU	Gated Recurrent Unit
GPR	Gaussian Process Regression
IOWA	Induced Ordered Weighted Averaging
KNN	K-Nearest Neighbors
LCO	Lithium Cobalt Oxide
LFP	Lithium Iron Phosphate
LR	Linear Regression
LSTM	Long Short-Term Memory
MAE	Median Absolute Error
MAPE	Mean Absolute Percentage Error
MLP	Multilayer Perceptron
ML	Machine Learning
NAR	Nonlinear Autoregressive
NARXNN	Nonlinear Autoregressive with Exogenous Input Neural Network
NCA	Lithium Nickel Cobalt Aluminum Oxide
NMC	Lithium Nickel Manganese Cobalt Oxide
PKNN	Prior Knowledge-Based Neural Network
QRF	Quantile Regression Forest
RBFNN	Radial Basis Function Neural Network
RESNET	Residual Network
RF	Random Forest
RMN	Regressive Matching Network
RMSE	Root Mean Squared Error
RNN	Recurrent Neural Network
RPD	Raw Papers Database
RUL	Remaining Useful Life
RVM	Relevance Vector Machine
SoC	State of Charge
SoH	State of Health
SVM/SVR	Support Vector Machine/Regressor
SSEL	Secondary Structural Ensemble Learning
TCN	Temporal Convolution Network
TNN	Transformer Neural Network
TL	Transfer Learning
UNN	Unsupervised Neural Networks
VTN	Vision Transformer Network
PKNN	Prior Knowledge-Based Neural Network
NARXNN	Nonlinear Autoregressive with Exogenous Input Neural Network
DGNN	Deep Gaussian Neural Network

References

1. Severson, K.A.; Attia, P.M.; Jin, N.; Perkins, N.; Jiang, B.; Yang, Z.; Chen, M.H.; Aykol, M.; Herring, P.K.; Fraggedakis, D.; et al. Data-Driven Prediction of Battery Cycle Life before Capacity Degradation. *Nat. Energy* **2019**, *4*, 383–391. [CrossRef]
2. Akbar, K.; Zou, Y.; Awais, Q.; Baig, M.J.A.; Jamil, M. A Machine Learning-Based Robust State of Health (SOH) Prediction Model for Electric Vehicle Batteries. *Electronics* **2022**, *11*, 1216. [CrossRef]
3. Hu, X.; Che, Y.; Lin, X.; Deng, Z. Health Prognosis for Electric Vehicle Battery Packs: A Data-Driven Approach. *IEEE/ASME Trans. Mechatron.* **2020**, *25*, 2622–2632. [CrossRef]
4. Lee, C.H.; Wu, C.H. A Novel Big Data Modeling Method for Improving Driving Range Estimation of EVs. *IEEE Access* **2015**, *3*, 1980–1993. [CrossRef]

5. Wang, S.; Jin, S.; Bai, D.; Fan, Y.; Shi, H.; Fernandez, C. A Critical Review of Improved Deep Learning Methods for the Remaining Useful Life Prediction of Lithium-Ion Batteries. *Energy Rep.* **2021**, *7*, 5562–5574. [CrossRef]
6. Pang, X.; Zhong, S.; Wang, Y.; Yang, W.; Zheng, W.; Sun, G. A Review on the Prediction of Health State and Serving Life of Lithium-Ion Batteries. *Chem. Rec.* **2022**, *22*, e202200131. [CrossRef]
7. Li, Y.; Li, K.; Liu, X.; Wang, Y.; Zhang, L. Lithium-Ion Battery Capacity Estimation—A Pruned Convolutional Neural Network Approach Assisted with Transfer Learning. *Appl. Energy* **2021**, *285*, 116410. [CrossRef]
8. Hong, J.; Lee, D.; Jeong, E.-R.; Yi, Y. Towards the Swift Prediction of the Remaining Useful Life of Lithium-Ion Batteries with End-to-End Deep Learning. *Appl. Energy* **2020**, *278*, 115646. [CrossRef]
9. Lai, X.; Huang, Y.; Deng, C.; Gu, H.; Han, X.; Zheng, Y.; Ouyang, M. Sorting, Regrouping, and Echelon Utilization of the Large-Scale Retired Lithium Batteries: A Critical Review. *Renew. Sustain. Energy Rev.* **2021**, *146*, 111162. [CrossRef]
10. Li, Y.; Liu, K.; Foley, A.M.; Zülke, A.; Berecibar, M.; Nanini-Maury, E.; Van Mierlo, J.; Hoster, H.E. Data-Driven Health Estimation and Lifetime Prediction of Lithium-Ion Batteries: A Review. *Renew. Sustain. Energy Rev.* **2019**, *113*, 109254. [CrossRef]
11. Vidal, C.; Malysz, P.; Kollmeyer, P.; Emadi, A. Machine Learning Applied to Electrified Vehicle Battery State of Charge and State of Health Estimation: State-of-the-Art. *IEEE Access* **2020**, *8*, 52796–52814. [CrossRef]
12. Shahjalal, M.; Roy, P.K.; Shams, T.; Fly, A.; Chowdhury, J.I.; Ahmed, M.R.; Liu, K. A Review on Second-Life of Li-Ion Batteries: Prospects, Challenges, and Issues. *Energy* **2022**, *241*, 122881. [CrossRef]
13. Ge, M.-F.; Liu, Y.; Jiang, X.; Liu, J. A Review on State of Health Estimations and Remaining Useful Life Prognostics of Lithium-Ion Batteries. *Measurement* **2021**, *174*, 109057. [CrossRef]
14. Bloom, I.; Jansen, A.N.; Abraham, D.P.; Knuth, J.; Jones, S.A.; Battaglia, V.S.; Henriksen, G.L. Differential Voltage Analyses of High-Power, Lithium-Ion Cells: 1. Technique and Application. *J. Power Sources* **2005**, *139*, 295–303. [CrossRef]
15. Barré, A.; Deguilhem, B.; Grolleau, S.; Gérard, M.; Suard, F.; Riu, D. A Review on Lithium-Ion Battery Ageing Mechanisms and Estimations for Automotive Applications. *J. Power Sources* **2013**, *241*, 680–689. [CrossRef]
16. Aurbach, D.; Markovsky, B.; Levi, M.D.; Levi, E.; Schechter, A.; Moshkovich, M.; Cohen, Y. New Insights into the Interactions between Electrode Materials and Electrolyte Solutions for Advanced Nonaqueous Batteries. *J. Power Sources* **1999**, *81–82*, 95–111. [CrossRef]
17. Zhang, L.; Dai, Y.; Li, C.; Dang, Y.; Zheng, R.; Wang, Z.; Wang, Y.; Cui, Y.; Arandiyan, H.; Shao, Z.; et al. Recent Advances in Electrochemical Impedance Spectroscopy for Solid-State Batteries. *Energy Storage Mater.* **2024**, *69*, 103378. [CrossRef]
18. Plett, G.L. Extended Kalman Filtering for Battery Management Systems of LiPB-Based HEV Battery Packs. *J. Power Sources* **2004**, *134*, 262–276. [CrossRef]
19. Hu, X.; Li, S.; Peng, H. A Comparative Study of Equivalent Circuit Models for Li-Ion Batteries. *J. Power Sources* **2012**, *198*, 359–367. [CrossRef]
20. Daigle, M.; Kulkarni, C. Electrochemistry-Based Battery Modeling for Prognostics. In Proceedings of the Annual Conference of the PHM Society 2013, New Orleans, LA, USA, 14–17 October 2013.
21. Singh, S.; Ebongue, Y.E.; Rezaei, S.; Birke, K.P. Hybrid Modeling of Lithium-Ion Battery: Physics-Informed Neural Network for Battery State Estimation. *Batteries* **2023**, *9*, 301. [CrossRef]
22. Su, S.; Li, W.; Mou, J.; Garg, A.; Gao, L.; Liu, J. A Hybrid Battery Equivalent Circuit Model, Deep Learning, and Transfer Learning for Battery State Monitoring. *IEEE Trans. Transp. Electrif.* **2023**, *9*, 1113–1127. [CrossRef]
23. Xing, Y.; Ma, E.W.M.; Tsui, K.-L.; Pecht, M. An Ensemble Model for Predicting the Remaining Useful Performance of Lithium-Ion Batteries. *Microelectron. Reliab.* **2013**, *53*, 811–820. [CrossRef]
24. Hossain Lipu, M.S.; Ansari, S.; Miah, M.S.; Meraj, S.T.; Hasan, K.; Shihavuddin, A.S.M.; Hannan, M.A.; Muttaqi, K.M.; Hussain, A. Deep Learning Enabled State of Charge, State of Health and Remaining Useful Life Estimation for Smart Battery Management System: Methods, Implementations, Issues and Prospects. *J. Energy Storage* **2022**, *55*, 105752. [CrossRef]
25. Zhao, J.; Han, X.; Ouyang, M.; Burke, A.F. Specialized Deep Neural Networks for Battery Health Prognostics: Opportunities and Challenges. *J. Energy Chem.* **2023**, *87*, 416–438. [CrossRef]
26. Luo, K.; Chen, X.; Zheng, H.; Shi, Z. A Review of Deep Learning Approach to Predicting the State of Health and State of Charge of Lithium-Ion Batteries. *J. Energy Chem.* **2022**, *74*, 159–173. [CrossRef]
27. Liu, K.; Peng, Q.; Che, Y.; Zheng, Y.; Li, K.; Teodorescu, R.; Widanage, D.; Barai, A. Transfer Learning for Battery Smarter State Estimation and Ageing Prognostics: Recent Progress, Challenges, and Prospects. *Adv. Appl. Energy* **2023**, *9*, 100117. [CrossRef]
28. Li, C.; Zhang, H.; Ding, P.; Yang, S.; Bai, Y. Deep Feature Extraction in Lifetime Prognostics of Lithium-Ion Batteries: Advances, Challenges and Perspectives. *Renew. Sustain. Energy Rev.* **2023**, *184*, 113576. [CrossRef]
29. Samanta, A.; Williamson, S. Machine Learning-Based Remaining Useful Life Prediction Techniques for Lithium-Ion Battery Management Systems: A Comprehensive Review. *IEEJ J. Ind. Appl.* **2023**, *12*, 22004793. [CrossRef]
30. Wang, S.; Ren, P.; Takyi-Aninakwa, P.; Jin, S.; Fernandez, C. A Critical Review of Improved Deep Convolutional Neural Network for Multi-Timescale State Prediction of Lithium-Ion Batteries. *Energies* **2022**, *15*, 5053. [CrossRef]

31. Manoharan, A.; Begam, K.M.; Aparow, V.R.; Sooriamoorthy, D. Artificial Neural Networks, Gradient Boosting and Support Vector Machines for Electric Vehicle Battery State Estimation: A Review. *J. Energy Storage* **2022**, *55*, 105384. [CrossRef]
32. Ensslin, L.; Ensslin, S.R.; Lacerda, R.T.d.O.; Tasca, J.E. *ProKnow-C, Knowledge Development Process–Constructivist: Processo Técnico Com Patente de Registro Pendente Junto ao INPI*; INPI: Rio de Janeiro, Brazil, 2010.
33. Ensslin, S.R.; Ensslin, L.; Yamakawa, E.K.; Nagaoka, M.P.T.; Aoki, A.R.; Siebert, L.C. Processo Estruturado de Revisão Da Literatura e Análise Bibliométrica Sobre Avaliação de Desempenho de Processos de Implementação de Eficiência Energética. *Rev. Bras. Energ.* **2014**, *20*, 21–50.
34. Regatieri, H.R.; Ando Junior, O.H.; Salgado, J.R. Systematic Review of Lithium-Ion Battery Recycling Literature Using ProKnow-C and Methodi Ordinatio. *Energies* **2022**, *15*, 1485. [CrossRef]
35. Maciel, J.N.; Javier Giménez Ledesma, J.; Hideo Ando Junior, O. Forecasting Solar Power Output Generation: A Systematic Review with the Proknow-C. *IEEE Lat. Am. Trans.* **2021**, *19*, 612–624. [CrossRef]
36. Ensslin, L.; Ensslin, S.R.; Pinto, H. de M. Processo de Investigação e Análise Bibliométrica: Avaliação Da Qualidade Dos Serviços Bancários. *Rev. Adm. Contemp.* **2013**, *17*, 325–349. [CrossRef]
37. Page, M.J.; McKenzie, J.E.; Bossuyt, P.M.; Boutron, I.; Hoffmann, T.C.; Mulrow, C.D.; Shamseer, L.; Tetzlaff, J.M.; Akl, E.A.; Brennan, S.E.; et al. The PRISMA 2020 Statement: An Updated Guideline for Reporting Systematic Reviews. *PLoS Med.* **2021**, *18*, e1003583. [CrossRef]
38. Osorio, M.A.A.; Concepcion, R.; Dadios, E. Multi-Source Energy Harvesting Systems: A PRISMA Approach on Energy Sources and Optimization Strategies. In Proceedings of the 2023 IEEE 15th International Conference on Humanoid, Nanotechnology, Information Technology, Communication and Control, Environment, and Management (HNICEM), Coron, Philippines, 19–23 November 2023; pp. 1–6.
39. Arévalo, P.; Ochoa-Correa, D.; Villa-Ávila, E. Systematic Review of the Effective Integration of Storage Systems and Electric Vehicles in Microgrid Networks: Innovative Approaches for Energy Management. *Vehicles* **2024**, *6*, 2075–2105. [CrossRef]
40. Prior, J.; Drees, T.; Miro, M.; Kuhlenkötter, B. Systematic Literature Review of Heuristic-Optimized Microgrids and Energy-Flexible Factories. *Clean Technol.* **2024**, *6*, 1114–1141. [CrossRef]
41. Grant, M.J.; Booth, A. A Typology of Reviews: An Analysis of 14 Review Types and Associated Methodologies. *Health Inf. Libr. J.* **2009**, *26*, 91–108. [CrossRef]
42. Munn, Z.; Peters, M.D.J.; Stern, C.; Tufanaru, C.; McArthur, A.; Aromataris, E. Systematic Review or Scoping Review? Guidance for Authors When Choosing between a Systematic or Scoping Review Approach. *BMC Med. Res. Methodol.* **2018**, *18*, 143. [CrossRef] [PubMed]
43. Arksey, H.; O'Malley, L. Scoping Studies: Towards a Methodological Framework. *Int. J. Soc. Res. Methodol.* **2005**, *8*, 19–32. [CrossRef]
44. Zhang, Y.; Xiong, R.; He, H.; Pecht, M.G. Long Short-Term Memory Recurrent Neural Network for Remaining Useful Life Prediction of Lithium-Ion Batteries. *IEEE Trans. Veh. Technol.* **2018**, *67*, 5695–5705. [CrossRef]
45. Liu, K.; Shang, Y.; Ouyang, Q.; Widanage, W.D. A Data-Driven Approach with Uncertainty Quantification for Predicting Future Capacities and Remaining Useful Life of Lithium-Ion Battery. *IEEE Trans. Ind. Electron.* **2021**, *68*, 3170–3180. [CrossRef]
46. Ng, M.-F.; Zhao, J.; Yan, Q.; Conduit, G.J.; Seh, Z.W. Predicting the State of Charge and Health of Batteries Using Data-Driven Machine Learning. *Nat. Mach. Intell.* **2020**, *2*, 161–170. [CrossRef]
47. Li, Y.; Zou, C.; Berecibar, M.; Nanini-Maury, E.; Chan, J.C.-W.; van den Bossche, P.; Van Mierlo, J.; Omar, N. Random Forest Regression for Online Capacity Estimation of Lithium-Ion Batteries. *Appl. Energy* **2018**, *232*, 197–210. [CrossRef]
48. Li, X.; Zhang, L.; Wang, Z.; Dong, P. Remaining Useful Life Prediction for Lithium-Ion Batteries Based on a Hybrid Model Combining the Long Short-Term Memory and Elman Neural Networks. *J. Energy Storage* **2019**, *21*, 510–518. [CrossRef]
49. Ren, L.; Zhao, L.; Hong, S.; Zhao, S.; Wang, H.; Zhang, L. Remaining Useful Life Prediction for Lithium-Ion Battery: A Deep Learning Approach. *IEEE Access* **2018**, *6*, 50587–50598. [CrossRef]
50. Ren, L.; Dong, J.; Wang, X.; Meng, Z.; Zhao, L.; Deen, M.J. A Data-Driven Auto-CNN-LSTM Prediction Model for Lithium-Ion Battery Remaining Useful Life. *IEEE Trans. Ind. Inform.* **2021**, *17*, 3478–3487. [CrossRef]
51. Li, P.; Zhang, Z.; Xiong, Q.; Ding, B.; Hou, J.; Luo, D.; Rong, Y.; Li, S. State-of-Health Estimation and Remaining Useful Life Prediction for the Lithium-Ion Battery Based on a Variant Long Short Term Memory Neural Network. *J. Power Sources* **2020**, *459*, 228069. [CrossRef]
52. Liu, K.; Hu, X.; Wei, Z.; Li, Y.; Jiang, Y. Modified Gaussian Process Regression Models for Cyclic Capacity Prediction of Lithium-Ion Batteries. *IEEE Trans. Transp. Electrif.* **2019**, *5*, 1225–1236. [CrossRef]
53. Shen, S.; Sadoughi, M.; Chen, X.; Hong, M.; Hu, C. A Deep Learning Method for Online Capacity Estimation of Lithium-Ion Batteries. *J. Energy Storage* **2019**, *25*, 100817. [CrossRef]
54. Roman, D.; Saxena, S.; Robu, V.; Pecht, M.; Flynn, D. Machine Learning Pipeline for Battery State-of-Health Estimation. *Nat. Mach. Intell.* **2021**, *3*, 447–456. [CrossRef]

55. Qu, J.; Liu, F.; Ma, Y.; Fan, J. A Neural-Network-Based Method for RUL Prediction and SOH Monitoring of Lithium-Ion Battery. *IEEE Access* **2019**, *7*, 87178–87191. [CrossRef]
56. Dai, H.; Zhao, G.; Lin, M.; Wu, J.; Zheng, G. A Novel Estimation Method for the State of Health of Lithium-Ion Battery Using Prior Knowledge-Based Neural Network and Markov Chain. *IEEE Trans. Ind. Electron.* **2019**, *66*, 7706–7716. [CrossRef]
57. Khumprom, P.; Yodo, N. A Data-Driven Predictive Prognostic Model for Lithium-Ion Batteries Based on a Deep Learning Algorithm. *Energies* **2019**, *12*, 660. [CrossRef]
58. Pan, H.; Lü, Z.; Wang, H.; Wei, H.; Chen, L. Novel Battery State-of-Health Online Estimation Method Using Multiple Health Indicators and an Extreme Learning Machine. *Energy* **2018**, *160*, 466–477. [CrossRef]
59. Li, W.; Sengupta, N.; Dechent, P.; Howey, D.; Annaswamy, A.; Sauer, D.U. Online Capacity Estimation of Lithium-Ion Batteries with Deep Long Short-Term Memory Networks. *J. Power Sources* **2021**, *482*, 228863. [CrossRef]
60. Yu, J. State of Health Prediction of Lithium-Ion Batteries: Multiscale Logic Regression and Gaussian Process Regression Ensemble. *Reliab. Eng. Syst. Saf.* **2018**, *174*, 82–95. [CrossRef]
61. Fan, Y.; Xiao, F.; Li, C.; Yang, G.; Tang, X. A Novel Deep Learning Framework for State of Health Estimation of Lithium-Ion Battery. *J. Energy Storage* **2020**, *32*, 101741. [CrossRef]
62. Zhang, S.; Zhai, B.; Guo, X.; Wang, K.; Peng, N.; Zhang, X. Synchronous Estimation of State of Health and Remaining Useful Lifetime for Lithium-Ion Battery Using the Incremental Capacity and Artificial Neural Networks. *J. Energy Storage* **2019**, *26*, 100951. [CrossRef]
63. Cao, J.; Harrold, D.; Fan, Z.; Morstyn, T.; Healey, D.; Li, K. Deep Reinforcement Learning-Based Energy Storage Arbitrage with Accurate Lithium-Ion Battery Degradation Model. *IEEE Trans. Smart Grid* **2020**, *11*, 4513–4521. [CrossRef]
64. Gou, B.; Xu, Y.; Feng, X. State-of-Health Estimation and Remaining-Useful-Life Prediction for Lithium-Ion Battery Using a Hybrid Data-Driven Method. *IEEE Trans. Veh. Technol.* **2020**, *69*, 10854–10867. [CrossRef]
65. Tan, Y.; Tan, Y.; Zhao, G.; Zhao, G. Transfer Learning with Long Short-Term Memory Network for State-of-Health Prediction of Lithium-Ion Batteries. *IEEE Trans. Ind. Electron.* **2020**, *67*, 8723–8731. [CrossRef]
66. Hu, X.; Che, Y.; Lin, X.; Onori, S. Battery Health Prediction Using Fusion-Based Feature Selection and Machine Learning. *IEEE Trans. Transp. Electrif.* **2021**, *7*, 382–398. [CrossRef]
67. Sui, X.; He, S.; Vilsen, S.B.; Meng, J.; Teodorescu, R.; Stroe, D.-I. A Review of Non-Probabilistic Machine Learning-Based State of Health Estimation Techniques for Lithium-Ion Battery. *Appl. Energy* **2021**, *300*, 117346. [CrossRef]
68. Tagade, P.; Hariharan, K.S.; Ramachandran, S.; Khandelwal, A.; Naha, A.; Kolake, S.M.; Han, S.H. Deep Gaussian Process Regression for Lithium-Ion Battery Health Prognosis and Degradation Mode Diagnosis. *J. Power Sources* **2020**, *445*, 227281. [CrossRef]
69. Tang, X.; Liu, K.; Wang, X.; Gao, F.; Macro, J.; Widanage, W.D. Model Migration Neural Network for Predicting Battery Aging Trajectories. *IEEE Trans. Transp. Electrif.* **2020**, *6*, 363–374. [CrossRef]
70. Fermín-Cueto, P.; McTurk, E.; Allerhand, M.; Medina-Lopez, E.; Anjos, M.F.; Sylvester, J.; dos Reis, G. Identification and Machine Learning Prediction of Knee-Point and Knee-Onset in Capacity Degradation Curves of Lithium-Ion Cells. *Energy AI* **2020**, *1*, 100006. [CrossRef]
71. Zhang, W.; Li, X.; Li, X. Deep Learning-Based Prognostic Approach for Lithium-Ion Batteries with Adaptive Time-Series Prediction and on-Line Validation. *Meas. J. Int. Meas. Confed.* **2020**, *164*, 108052. [CrossRef]
72. Che, Y.; Deng, Z.; Lin, X.; Hu, L.; Hu, X. Predictive Battery Health Management with Transfer Learning and Online Model Correction. *IEEE Trans. Veh. Technol.* **2021**, *70*, 1269–1277. [CrossRef]
73. Li, W.; Sengupta, N.; Dechent, P.; Howey, D.; Annaswamy, A.; Sauer, D.U. One-Shot Battery Degradation Trajectory Prediction with Deep Learning. *J. Power Sources* **2021**, *506*, 230024. [CrossRef]
74. Khaleghi, S.; Karimi, D.; Beheshti, S.H.; Hosen, M.S.; Behi, H.; Berecibar, M.; Van Mierlo, J. Online Health Diagnosis of Lithium-Ion Batteries Based on Nonlinear Autoregressive Neural Network. *Appl. Energy* **2021**, *282*, 116159. [CrossRef]
75. Sultan, Y.A.; Eladl, A.A.; Hassan, M.A.; Gamel, S.A. Enhancing Electric Vehicle Battery Lifespan: Integrating Active Balancing and Machine Learning for Precise RUL Estimation. *Sci. Rep.* **2025**, *15*, 777. [CrossRef] [PubMed]
76. Olsson, L.; Fallahi, S.; Schnurr, M.; Diener, D.; Van Loon, P. Circular Business Models for Extended EV Battery Life. *Batteries* **2018**, *4*, 57. [CrossRef]
77. Reinhardt, R.; Christodoulou, I.; Gassó-Domingo, S.; Amante García, B. Towards Sustainable Business Models for Electric Vehicle Battery Second Use: A Critical Review. *J. Environ. Manag.* **2019**, *245*, 432–446. [CrossRef] [PubMed]
78. Sheikh, S.S.; Shah, F.A.; Athar, S.O.; Khalid, H.A. A Data-Driven Comparative Analysis of Lithium-Ion Battery State of Health and Capacity Estimation. *Electr. Power Components Syst.* **2023**, *51*, 1–11. [CrossRef]
79. Bracale, A.; De Falco, P.; Di Noia, L.P.; Rizzo, R. Probabilistic State of Health and Remaining Useful Life Prediction for Li-Ion Batteries. In Proceedings of the 2021 IEEE Texas Power and Energy Conference (TPEC), College Station, TX, USA, 2–5 February 2021; IEEE: Piscataway, NJ, USA, 2021; pp. 1–6.

80. Li, F.; Zhang, L.; Chen, B.; Gao, D.; Cheng, Y.; Zhang, X.; Yang, Y.; Gao, K.; Huang, Z. An Optimal Stacking Ensemble for Remaining Useful Life Estimation of Systems Under Multi-Operating Conditions. *IEEE Access* **2020**, *8*, 31854–31868. [CrossRef]
81. Liu, G.; Zhang, X.; Liu, Z. State of Health Estimation of Power Batteries Based on Multi-Feature Fusion Models Using Stacking Algorithm. *Energy* **2022**, *259*, 124851. [CrossRef]
82. Paulson, N.H.; Kubal, J.; Ward, L.; Saxena, S.; Lu, W.; Babinec, S.J. Feature Engineering for Machine Learning Enabled Early Prediction of Battery Lifetime. *J. Power Sources* **2022**, *527*, 231127. [CrossRef]
83. Yang, F.; Wang, D.; Xu, F.; Huang, Z.; Tsui, K.-L. Lifespan Prediction of Lithium-Ion Batteries Based on Various Extracted Features and Gradient Boosting Regression Tree Model. *J. Power Sources* **2020**, *476*, 228654. [CrossRef]
84. Greenbank, S.; Howey, D.A. Piecewise-Linear Modelling with Automated Feature Selection for Li-Ion Battery End-of-Life Prognosis. *Mech. Syst. Signal Process.* **2023**, *184*, 109612. [CrossRef]
85. Wu, J.; Su, H.; Meng, J.; Lin, M. State of Health Estimation for Lithium-Ion Battery via Recursive Feature Elimination on Partial Charging Curves. *IEEE J. Emerg. Sel. Top. Power Electron.* **2023**, *11*, 131–142. [CrossRef]
86. Greenbank, S.; Howey, D. Automated Feature Extraction and Selection for Data-Driven Models of Rapid Battery Capacity Fade and End of Life. *IEEE Trans. Ind. Inform.* **2022**, *18*, 2965–2973. [CrossRef]
87. Peng, J.; Zheng, Z.; Zhang, X.; Deng, K.; Gao, K.; Li, H.; Chen, B.; Yang, Y.; Huang, Z. A Data-Driven Method with Feature Enhancement and Adaptive Optimization for Lithium-Ion Battery Remaining Useful Life Prediction. *Energies* **2020**, *13*, 752. [CrossRef]
88. Ren, Z.; Du, C.; Ren, W. State of Health Estimation of Lithium-Ion Batteries Using a Multi-Feature-Extraction Strategy and PSO-NARXNN. *Batteries* **2022**, *9*, 7. [CrossRef]
89. Fei, Z.; Zhang, Z.; Yang, F.; Tsui, K.-L.; Li, L. Early-Stage Lifetime Prediction for Lithium-Ion Batteries: A Deep Learning Framework Jointly Considering Machine-Learned and Handcrafted Data Features. *J. Energy Storage* **2022**, *52*, 104936. [CrossRef]
90. Tang, T.; Yuan, H. The Capacity Prediction of Li-Ion Batteries Based on a New Feature Extraction Technique and an Improved Extreme Learning Machine Algorithm. *J. Power Sources* **2021**, *514*, 230572. [CrossRef]
91. Wang, Z.; Liu, N.; Guo, Y. Adaptive Sliding Window LSTM NN Based RUL Prediction for Lithium-Ion Batteries Integrating LTSA Feature Reconstruction. *Neurocomputing* **2021**, *466*, 178–189. [CrossRef]
92. Wang, Z.; Yang, F.; Xu, Q.; Wang, Y.; Yan, H.; Xie, M. Capacity Estimation of Lithium-Ion Batteries Based on Data Aggregation and Feature Fusion via Graph Neural Network. *Appl. Energy* **2023**, *336*, 120808. [CrossRef]
93. Cui, Z.; Gao, X.; Mao, J.; Wang, C. Remaining Capacity Prediction of Lithium-Ion Battery Based on the Feature Transformation Process Neural Network. *Expert Syst. Appl.* **2022**, *190*, 116075. [CrossRef]
94. Yao, X.-Y.; Chen, G.; Hu, L.; Pecht, M. A Multi-Model Feature Fusion Model for Lithium-Ion Battery State of Health Prediction. *J. Energy Storage* **2022**, *56*, 106051. [CrossRef]
95. Fu, P.; Chu, L.; Hou, Z.; Guo, Z.; Lin, Y.; Hu, J. State-of-Health Prediction Using Transfer Learning and a Multi-Feature Fusion Model. *Sensors* **2022**, *22*, 8530. [CrossRef]
96. Himadri Sekhar, B.; Sindhu, S.; Amalendu Bikash, C.; Chandan Kumar, C. State-of-Health Estimation and End of Life Prediction for the Lithium-Ion Battery by Correlatable Feature-Based Machine Learning Approach. *Int. J. Perform. Eng.* **2021**, *17*, 825. [CrossRef]
97. Luo, C.; Zhang, Z.; Qiao, D.; Lai, X.; Li, Y.; Wang, S. Life Prediction under Charging Process of Lithium-Ion Batteries Based on AutoML. *Energies* **2022**, *15*, 4594. [CrossRef]
98. Lee, G.; Kim, J.; Lee, C. State-of-Health Estimation of Li-Ion Batteries in the Early Phases of Qualification Tests: An Interpretable Machine Learning Approach. *Expert Syst. Appl.* **2022**, *197*, 116817. [CrossRef]
99. Li, G.; Li, B.; Li, C.; Wang, S. State-of-Health Rapid Estimation for Lithium-Ion Battery Based on an Interpretable Stacking Ensemble Model with Short-Term Voltage Profiles. *Energy* **2023**, *263*, 126064. [CrossRef]
100. Lundberg, S.M.; Lee, S.-I. A Unified Approach to Interpreting Model Predictions. In Proceedings of the 31st International Conference on Neural Information Processing Systems, Long Beach, CA, USA, 4–9 December 2017; Guyon, I., Von Luxburg, U., Bengio, S., Wallach, H., Fergus, R., Vishwanathan, S., Garnett, R., Eds.; Curran Associates, Inc.: Brooklyn, NY, USA, 2017; Volume 30.
101. Lundberg, S.M.; Erion, G.; Chen, H.; DeGrave, A.; Prutkin, J.M.; Nair, B.; Katz, R.; Himmelfarb, J.; Bansal, N.; Lee, S.-I. From Local Explanations to Global Understanding with Explainable AI for Trees. *Nat. Mach. Intell.* **2020**, *2*, 56–67. [CrossRef]
102. Attia, P.M.; Severson, K.A.; Witmer, J.D. Statistical Learning for Accurate and Interpretable Battery Lifetime Prediction. *J. Electrochem. Soc.* **2021**, *168*, 090547. [CrossRef]
103. Lee, G.; Kwon, D.; Lee, C. A Convolutional Neural Network Model for SOH Estimation of Li-Ion Batteries with Physical Interpretability. *Mech. Syst. Signal Process.* **2023**, *188*, 110004. [CrossRef]
104. Zhang, H.; Su, Y.; Altaf, F.; Wik, T.; Gros, S. Interpretable Battery Cycle Life Range Prediction Using Early Cell Degradation Data. *IEEE Trans. Transp. Electrif.* **2023**, *9*, 2669–2682. [CrossRef]

105. Pang, X.; Yang, W.; Wang, C.; Fan, H.; Wang, L.; Li, J.; Zhong, S.; Zheng, W.; Zou, H.; Chen, S.; et al. A Novel Hybrid Model for Lithium-Ion Batteries Lifespan Prediction with High Accuracy and Interpretability. *J. Energy Storage* **2023**, *61*, 106728. [CrossRef]
106. Kong, D.; Wang, S.; Ping, P. State-of-Health Estimation and Remaining Useful Life for Lithium-Ion Battery Based on Deep Learning with Bayesian Hyperparameter Optimization. *Int. J. Energy Res.* **2022**, *46*, 6081–6098. [CrossRef]
107. Reddy, M.C.; Viswanath, M.N.; Varma, P.S. Remaining Useful Life Prediction of Lithium Ion Battery Using Tree Based Pipe-Line Optimization Tool. *J. Adv. Res. Dyn. Control Syst.* **2020**, *12*, 1955–1960. [CrossRef]
108. Shu, X.; Li, G.; Shen, J.; Lei, Z.; Chen, Z.; Liu, Y. A Uniform Estimation Framework for State of Health of Lithium-Ion Batteries Considering Feature Extraction and Parameters Optimization. *Energy* **2020**, *204*, 117957. [CrossRef]
109. Couture, J.; Lin, X. Novel Image-Based Rapid RUL Prediction for Li-Ion Batteries Using a Capsule Network and Transfer Learning. *IEEE Trans. Transp. Electrif.* **2023**, *9*, 958–967. [CrossRef]
110. Couture, J.; Lin, X. Image- and Health Indicator-Based Transfer Learning Hybridization for Battery RUL Prediction. *Eng. Appl. Artif. Intell.* **2022**, *114*, 105120. [CrossRef]
111. He, N.; Wang, Q.; Lu, Z.; Chai, Y.; Yang, F. Early Prediction of Battery Lifetime Based on Graphical Features and Convolutional Neural Networks. *Appl. Energy* **2024**, *353*, 122048. [CrossRef]
112. Zhao, X.; He, H.; Li, J.; Wei, Z.; Huang, R.; Shi, M. From Grayscale Image to Battery Aging Awareness—A New Battery Capacity Estimation Model with Computer Vision Approach. *IEEE Trans. Ind. Inform.* **2023**, *19*, 8965–8975. [CrossRef]
113. Li, Y.; Li, K.; Liu, X.; Zhang, L. Fast Battery Capacity Estimation Using Convolutional Neural Networks. *Trans. Inst. Meas. Control* **2020**, 0142331220966425. [CrossRef]
114. Teng, J.-H.; Chen, R.-J.; Lee, P.-T.; Hsu, C.-W. Accurate and Efficient SOH Estimation for Retired Batteries. *Energies* **2023**, *16*, 1240. [CrossRef]
115. Huang, C.; Li, N. Fast Health State Estimation of Lead–Acid Batteries Based on Multi-Time Constant Current Charging Curve. *Electronics* **2023**, *12*, 4552. [CrossRef]
116. Lu, S.; Yin, Z.; Liao, S.; Yang, B.; Liu, S.; Liu, M.; Yin, L.; Zheng, W. An Asymmetric Encoder–Decoder Model for Zn-Ion Battery Lifetime Prediction. *Energy Rep.* **2022**, *8*, 33–50. [CrossRef]
117. Dubarry, M.; Beck, D. Big Data Training Data for Artificial Intelligence-Based Li-Ion Diagnosis and Prognosis. *J. Power Sources* **2020**, *479*, 228806. [CrossRef]
118. Rauf, H.; Khalid, M.; Arshad, N. Machine Learning in State of Health and Remaining Useful Life Estimation: Theoretical and Technological Development in Battery Degradation Modelling. *Renew. Sustain. Energy Rev.* **2022**, *156*, 111903. [CrossRef]
119. Shu, X.; Shen, S.; Shen, J.; Zhang, Y.; Li, G.; Chen, Z.; Liu, Y. State of Health Prediction of Lithium-Ion Batteries Based on Machine Learning: Advances and Perspectives. *iScience* **2021**, *24*, 103265. [CrossRef]
120. Wang, S.; Jin, S.; Deng, D.; Fernandez, C. A Critical Review of Online Battery Remaining Useful Lifetime Prediction Methods. *Front. Mech. Eng.* **2021**, *7*, 719718. [CrossRef]
121. Toughzaoui, Y.; Toosi, S.B.; Chaoui, H.; Louahlia, H.; Petrone, R.; Le Masson, S.; Gualous, H. State of Health Estimation and Remaining Useful Life Assessment of Lithium-Ion Batteries: A Comparative Study. *J. Energy Storage* **2022**, *51*, 104520. [CrossRef]
122. Sharma, P.; Bora, B.J. A Review of Modern Machine Learning Techniques in the Prediction of Remaining Useful Life of Lithium-Ion Batteries. *Batteries* **2023**, *9*, 13. [CrossRef]
123. Jin, S.; Sui, X.; Huang, X.; Wang, S.; Teodorescu, R.; Stroe, D.-I. Overview of Machine Learning Methods for Lithium-Ion Battery Remaining Useful Lifetime Prediction. *Electronics* **2021**, *10*, 3126. [CrossRef]
124. Ren, Z.; Du, C. A Review of Machine Learning State-of-Charge and State-of-Health Estimation Algorithms for Lithium-Ion Batteries. *Energy Rep.* **2023**, *9*, 2993–3021. [CrossRef]
125. Guo, W.; Sun, Z.; Vilsen, S.B.; Meng, J.; Stroe, D.I. Review of "Grey Box" Lifetime Modeling for Lithium-Ion Battery: Combining Physics and Data-Driven Methods. *J. Energy Storage* **2022**, *56*, 105992. [CrossRef]
126. Wang, F.; Zhao, Z.; Zhai, Z.; Shang, Z.; Yan, R.; Chen, X. Explainability-Driven Model Improvement for SOH Estimation of Lithium-Ion Battery. *Reliab. Eng. Syst. Saf.* **2023**, *232*, 109046. [CrossRef]
127. Zhou, L.; Lai, X.; Li, B.; Yao, Y.; Yuan, M.; Weng, J.; Zheng, Y. State Estimation Models of Lithium-Ion Batteries for Battery Management System: Status, Challenges, and Future Trends. *Batteries* **2023**, *9*, 131. [CrossRef]
128. Shah, A.; Shah, K.; Shah, C.; Shah, M. State of Charge, Remaining Useful Life and Knee Point Estimation Based on Artificial Intelligence and Machine Learning in Lithium-Ion EV Batteries: A Comprehensive Review. *Renew. Energy Focus* **2022**, *42*, 146–164. [CrossRef]
129. Li, X.; Yu, D.; Søren Byg, V.; Daniel Ioan, S. The Development of Machine Learning-Based Remaining Useful Life Prediction for Lithium-Ion Batteries. *J. Energy Chem.* **2023**, *82*, 103–121. [CrossRef]
130. Raoofi, T.; Yildiz, M. Comprehensive Review of Battery State Estimation Strategies Using Machine Learning for Battery Management Systems of Aircraft Propulsion Batteries. *J. Energy Storage* **2023**, *59*, 106486. [CrossRef]
131. Xiao, Y.; Wen, J.; Yao, L.; Zheng, J.; Fang, Z.; Shen, Y. A Comprehensive Review of the Lithium-Ion Battery State of Health Prognosis Methods Combining Aging Mechanism Analysis. *J. Energy Storage* **2023**, *65*, 107347. [CrossRef]

132. He, W.; Li, Z.; Liu, T.; Liu, Z.; Guo, X.; Du, J.; Li, X.; Sun, P.; Ming, W. Research Progress and Application of Deep Learning in Remaining Useful Life, State of Health and Battery Thermal Management of Lithium Batteries. *J. Energy Storage* **2023**, *70*, 107868. [CrossRef]
133. Beltran, H.; Sansano, E.; Pecht, M. Machine Learning Techniques Suitability to Estimate the Retained Capacity in Lithium-Ion Batteries from Partial Charge/Discharge Curves. *J. Energy Storage* **2023**, *59*, 106346. [CrossRef]
134. Zraibi, B.; Mansouri, M.; Loukili, S.E. Comparing Deep Learning Methods to Predict the Remaining Useful Life of Lithium-Ion Batteries. *Mater. Today Proc.* **2022**, *62*, 6298–6304. [CrossRef]
135. Huang, Z.; Sugiarto, L.; Lu, Y.-C. Feature–Target Pairing in Machine Learning for Battery Health Diagnosis and Prognosis: A Critical Review. *EcoMat* **2023**, *5*, e12345. [CrossRef]
136. Zhou, Y.; Chang, Y.; Wang, Y.; Li, R. Research on Methods for Extracting Aging Characteristics and Health Status of Lithium-Ion Batteries Based on Small Samples. *J. Renew. Sustain. Energy* **2022**, *14*, 24101. [CrossRef]
137. Das, K.; Kumar, R. Electric Vehicle Battery Capacity Degradation and Health Estimation Using Machine-Learning Techniques: A Review. *Clean Energy* **2023**, *7*, 1268–1281. [CrossRef]
138. Wang, F.; Zhai, Z.; Liu, B.; Zheng, S.; Zhao, Z.; Chen, X. Open Access Dataset, Code Library and Benchmarking Deep Learning Approaches for State-of-Health Estimation of Lithium-Ion Batteries. *J. Energy Storage* **2024**, *77*, 109884. [CrossRef]
139. Orzech, G. *Prognostics Center of Excellence Data Set Repository*; NASA: Washington, DC, USA, 2022.
140. Duan, W.; Song, S.; Xiao, F.; Chen, Y.; Peng, S.; Song, C. Battery SOH Estimation and RUL Prediction Framework Based on Variable Forgetting Factor Online Sequential Extreme Learning Machine and Particle Filter. *J. Energy Storage* **2023**, *65*, 107322. [CrossRef]
141. Yao, L.; Wen, J.; Xu, S.; Zheng, J.; Hou, J.; Fang, Z.; Xiao, Y. State of Health Estimation Based on the Long Short-Term Memory Network Using Incremental Capacity and Transfer Learning. *Sensors* **2022**, *22*, 7835. [CrossRef] [PubMed]
142. Yang, X.; Ma, B.; Xie, H.; Wang, W.; Zou, B.; Liang, F.; Hua, X.; Liu, X.; Chen, S. Lithium-Ion Battery State of Health Estimation with Multi-Feature Collaborative Analysis and Deep Learning Method. *Batteries* **2023**, *9*, 120. [CrossRef]
143. Peng, S.; Sun, Y.; Liu, D.; Yu, Q.; Kan, J.; Pecht, M. State of Health Estimation of Lithium-Ion Batteries Based on Multi-Health Features Extraction and Improved Long Short-Term Memory Neural Network. *Energy* **2023**, *282*, 128956. [CrossRef]
144. Jorge, I.; Mesbahi, T.; Samet, A.; Boné, R. Time Series Feature Extraction for Lithium-Ion Batteries State-Of-Health Prediction. *J. Energy Storage* **2023**, *59*, 106436. [CrossRef]
145. Zhang, C.; Wang, S.; Yu, C.; Xie, Y.; Fernandez, C. Improved Particle Swarm Optimization-Extreme Learning Machine Modeling Strategies for the Accurate Lithium-Ion Battery State of Health Estimation and High-Adaptability Remaining Useful Life Prediction. *J. Electrochem. Soc.* **2022**, *169*, 080520. [CrossRef]
146. Maleki, S.; Ray, B.; Hagh, M.T. Hybrid Framework for Predicting and Forecasting State of Health of Lithium-Ion Batteries in Electric Vehicles. *Sustain. Energy Grids Netw.* **2022**, *30*, 100603. [CrossRef]
147. Wu, W.; Lu, S. Remaining Useful Life Prediction of Lithium-Ion Batteries Based on Data Preprocessing and Improved ELM. *IEEE Trans. Instrum. Meas.* **2023**, *72*, 1–14. [CrossRef]
148. Zhang, Y.; Ma, H.; Wang, S.; Li, S.; Guo, R. Indirect Prediction of Remaining Useful Life for Lithium-Ion Batteries Based on Improved Multiple Kernel Extreme Learning Machine. *J. Energy Storage* **2023**, *64*, 107181. [CrossRef]
149. Sun, C.; Qu, A.; Zhang, J.; Shi, Q.; Jia, Z. Remaining Useful Life Prediction for Lithium-Ion Batteries Based on Improved Variational Mode Decomposition and Machine Learning Algorithm. *Energies* **2022**, *16*, 313. [CrossRef]
150. Tang, X.; Wan, H.; Wang, W.; Gu, M.; Wang, L.; Gan, L. Lithium-Ion Battery Remaining Useful Life Prediction Based on Hybrid Model. *Sustainability* **2023**, *15*, 6261. [CrossRef]
151. Xue, K.; Yang, J.; Yang, M.; Wang, D. An Improved Generic Hybrid Prognostic Method for RUL Prediction Based on PF-LSTM Learning. *IEEE Trans. Instrum. Meas.* **2023**, *72*, 1–21. [CrossRef]
152. Tian, A.; Yang, C.; Gao, Y.; Li, T.; Wang, L.; Chang, C.; Jiang, J. A State of Health Estimation Method of Lithium-Ion Batteries Based on DT-IC-V Health Features Extracted from Partial Charging Segment. *Int. J. Green Energy* **2023**, *20*, 997–1011. [CrossRef]
153. Guo, Y.; Yang, D.; Zhao, K.; Wang, K. State of Health Estimation for Lithium-Ion Battery Based on Bi-Directional Long Short-Term Memory Neural Network and Attention Mechanism. *Energy Rep.* **2022**, *8*, 208–215. [CrossRef]
154. Pugalenthi, K.; Park, H.; Hussain, S.; Raghavan, N. Remaining Useful Life Prediction of Lithium-Ion Batteries Using Neural Networks with Adaptive Bayesian Learning. *Sensors* **2022**, *22*, 3803. [CrossRef] [PubMed]
155. Hell, S.M.; Kim, C.D. Development of a Data-Driven Method for Online Battery Remaining-Useful-Life Prediction. *Batteries* **2022**, *8*, 192. [CrossRef]
156. Zhu, C.; Gao, M.; He, Z.; Wu, H.; Sun, C.; Zhang, Z.; Bao, Z. State of Health Prediction for Li-Ion Batteries with End-to-End Deep Learning. *J. Energy Storage* **2023**, *65*, 107218. [CrossRef]
157. Bao, X.; Chen, L.; Lopes, A.M.; Li, X.; Xie, S.; Li, P.; Chen, Y. Hybrid Deep Neural Network with Dimension Attention for State-of-Health Estimation of Lithium-Ion Batteries. *Energy* **2023**, *278*, 127734. [CrossRef]

158. Guo, X.; Wang, K.; Yao, S.; Fu, G.; Ning, Y. RUL Prediction of Lithium Ion Battery Based on CEEMDAN-CNN BiLSTM Model. *Energy Rep.* **2023**, *9*, 1299–1306. [CrossRef]
159. Sheng, H.; Zhou, Y.; Bai, L.; Shi, L. Transfer State of Health Estimation Based on Cross-Manifold Embedding. *J. Energy Storage* **2022**, *47*, 103555. [CrossRef]
160. Liu, R. Remaining Useful Life Prediction of Lithium-Ion Batteries Using Multiple Kernel Extreme Learning Machine. *Recent Adv. Comput. Sci. Commun.* **2022**, *15*, 715–721. [CrossRef]
161. Wu, J.; Cheng, X.; Huang, H.; Fang, C.; Zhang, L.; Zhao, X.; Zhang, L.; Xing, J. Remaining Useful Life Prediction of Lithium-Ion Batteries Based on PSO-RF Algorithm. *Front. Energy Res.* **2023**, *10*, 937035. [CrossRef]
162. Sahoo, S.; Hariharan, K.S.; Agarwal, S.; Swernath, S.B.; Bharti, R.; Han, S.; Lee, S. Transfer Learning Based Generalized Framework for State of Health Estimation of Li-Ion Cells. *Sci. Rep.* **2022**, *12*, 13173. [CrossRef] [PubMed]
163. Li, N.; He, F.; Ma, W.; Wang, R.; Jiang, L.; Zhang, X. An Indirect State-of-Health Estimation Method Based on Improved Genetic and Back Propagation for Online Lithium-Ion Battery Used in Electric Vehicles. *IEEE Trans. Veh. Technol.* **2022**, *71*, 12682–12690. [CrossRef]
164. Jiang, J.; Zhao, S.; Zhang, C. State-of-Health Estimate for the Lithium-Ion Battery Using Chi-Square and ELM-LSTM. *World Electr. Veh. J.* **2021**, *12*, 228. [CrossRef]
165. El-Dalahmeh, M.; Al-Greer, M.; El-Dalahmeh, M.; Bashir, I. Capacity Estimation of Lithium-Ion Batteries Based on Adaptive Empirical Wavelet Transform and Long Short-Term Memory Neural Network. *J. Energy Storage* **2023**, *70*, 108046. [CrossRef]
166. Tian, Y.; Wen, J.; Yang, Y.; Shi, Y.; Zeng, J. State-of-Health Prediction of Lithium-Ion Batteries Based on CNN-BiLSTM-AM. *Batteries* **2022**, *8*, 155. [CrossRef]
167. Mei, P.; Karimi, H.R.; Chen, F.; Yang, S.; Huang, C.; Qiu, S. A Learning-Based Vehicle-Cloud Collaboration Approach for Joint Estimation of State-of-Energy and State-of-Health. *Sensors* **2022**, *22*, 9474. [CrossRef]
168. Song, R.; Yang, L.; Chen, L.; Dong, Z. Capacity Estimation Method of Lithium-Ion Batteries Based on Deep Convolution Neural Network. *Int. J. Bio-Inspired Comput.* **2022**, *20*, 119–125. [CrossRef]
169. Wang, J.; Feng, X.; Zhang, X.; Xiang, Y. Improved Modeling of Lithium-Ion Battery Capacity Degradation Using an Individual-State Training Method and Recurrent Softplus Neural Network. *IEEE Access* **2021**, *9*, 7845–7855. [CrossRef]
170. Wen, L.; Bo, N.; Ye, X.; Li, X. A Novel Auto-LSTM-Based State of Health Estimation Method for Lithium-Ion Batteries. *J. Electrochem. Energy Convers. Storage* **2021**, *18*, 030902. [CrossRef]
171. Wei, Y. Prediction of State of Health of Lithium-Ion Battery Using Health Index Informed Attention Model. *Sensors* **2023**, *23*, 2587. [CrossRef] [PubMed]
172. Chen, C.; Wei, J.; Li, Z. Remaining Useful Life Prediction for Lithium-Ion Batteries Based on a Hybrid Deep Learning Model. *Processes* **2023**, *11*, 2333. [CrossRef]
173. Zhu, T.; Wang, W.; Yu, M. A Novel Hybrid Scheme for Remaining Useful Life Prognostic Based on Secondary Decomposition, BiGRU and Error Correction. *Energy* **2023**, *276*, 127565. [CrossRef]
174. Pham, T.; Le, T.; Dang, D.; Bui, H.; Pham, H.; Truong, L.; Nguyen, M.; Vo, H.; Tho, Q.T. ARNS: A Data-Driven Approach for SoH Estimation of Lithium-Ion Battery Using Nested Sequence Models with Considering Relaxation Effect. *IEEE Access* **2022**, *10*, 117067–117083. [CrossRef]
175. Ang, E.Y.M.; Paw, Y.C. Linear Model for Online State of Health Estimation of Lithium-Ion Batteries Using Segmented Discharge Profiles. *IEEE Trans. Transp. Electrif.* **2023**, *9*, 2464–2471. [CrossRef]
176. Hong, S.; Kang, M.; Kim, J.; Baek, J. Sequential Application of Denoising Autoencoder and Long-Short Recurrent Convolutional Network for Noise-Robust Remaining-Useful-Life Prediction Framework of Lithium-Ion Batteries. *Comput. Ind. Eng.* **2023**, *179*, 109231. [CrossRef]
177. Chen, D.; Zheng, X.; Chen, C.; Zhao, W.; Chen, D.; Zheng, X.; Chen, C.; Zhao, W. Remaining Useful Life Prediction of the Lithium-Ion Battery Based on CNN-LSTM Fusion Model and Grey Relational Analysis. *Electron. Res. Arch.* **2023**, *31*, 633–655. [CrossRef]
178. Zhu, C.; Zheng, B.; He, Z.; Gao, M.; Sun, C.; Bao, Z. State of Health Estimation of Lithium-Ion Battery Using Time Convolution Memory Neural Network. *Mob. Inf. Syst.* **2021**, *2021*, 4826409. [CrossRef]
179. Wei, Y.; Wu, D. State of Health and Remaining Useful Life Prediction of Lithium-Ion Batteries with Conditional Graph Convolutional Network. *Expert Syst. Appl.* **2024**, *238*, 122041. [CrossRef]
180. Huang, K.; Yao, K.; Guo, Y.; Lv, Z. State of Health Estimation of Lithium-Ion Batteries Based on Fine-Tuning or Rebuilding Transfer Learning Strategies Combined with New Features Mining. *Energy* **2023**, *282*, 128739. [CrossRef]
181. Zou, B.; Xiong, M.; Wang, H.; Ding, W.; Jiang, P.; Hua, W.; Zhang, Y.; Zhang, L.; Wang, W.; Tan, R. A Deep Learning Approach for State-of-Health Estimation of Lithium-Ion Batteries Based on a Multi-Feature and Attention Mechanism Collaboration. *Batteries* **2023**, *9*, 329. [CrossRef]
182. Liu, H.; Li, Y.; Luo, L.; Zhang, C. A Lithium-Ion Battery Capacity and RUL Prediction Fusion Method Based on Decomposition Strategy and GRU. *Batteries* **2023**, *9*, 323. [CrossRef]

183. Yu, Z.; Liu, N.; Zhang, Y.; Qi, L.; Li, R. Battery SOH Prediction Based on Multi-Dimensional Health Indicators. *Batteries* **2023**, *9*, 80. [CrossRef]
184. Ma, W.; Cai, P.; Sun, F.; Wang, X.; Gong, J. State of Health Estimation for Lithium-Ion Batteries Based on Extreme Learning Machine with Improved Blinex Loss. *Int. J. Electrochem. Sci.* **2022**, *17*, 221170. [CrossRef]
185. Yuan, J.; Qin, Z.; Huang, H.; Gan, X.; Li, S.; Li, B. State of Health Estimation and Remaining Useful Life Prediction for a Lithium-Ion Battery with a Two-Layer Stacking Regressor. *Energies* **2023**, *16*, 2313. [CrossRef]
186. Gao, D.; Liu, X.; Zhu, Z.; Yang, Q. A Hybrid CNN-BiLSTM Approach for Remaining Useful Life Prediction of EVs Lithium-Ion Battery. *Meas. Control* **2023**, *56*, 371–383. [CrossRef]
187. Chen, L.; Xie, S.; Lopes, A.M.; Bao, X. A Vision Transformer-Based Deep Neural Network for State of Health Estimation of Lithium-Ion Batteries. *Int. J. Electr. Power Energy Syst.* **2023**, *152*, 109233. [CrossRef]
188. Han, Y.; Li, C.; Zheng, L.; Lei, G.; Li, L. Remaining Useful Life Prediction of Lithium-Ion Batteries by Using a Denoising Transformer-Based Neural Network. *Energies* **2023**, *16*, 6328. [CrossRef]
189. Wang, M.; Xiang, G.; Cui, L.; Zhang, Q.; Chen, J. Remaining Useful Life Distribution Prediction Framework for Lithium-Ion Battery Fused Prior Knowledge and Monitoring Data. *Meas. Sci. Technol.* **2023**, *34*, 125108. [CrossRef]
190. Marri, I.; Petkovski, E.; Cristaldi, L.; Faifer, M. Comparing Machine Learning Strategies for SoH Estimation of Lithium-Ion Batteries Using a Feature-Based Approach. *Energies* **2023**, *16*, 4423. [CrossRef]
191. Xie, Q.; Liu, R.; Huang, J.; Su, J. Residual Life Prediction of Lithium-Ion Batteries Based on Data Preprocessing and a Priori Knowledge-Assisted CNN-LSTM. *Energy* **2023**, *281*, 128232. [CrossRef]
192. Li, Z.; Li, A.; Bai, F.; Zuo, H.; Zhang, Y. Remaining Useful Life Prediction of Lithium Battery Based on ACNN-Mogrifier LSTM-MMD. *Meas. Sci. Technol.* **2024**, *35*, 016101. [CrossRef]
193. Tarar, M.O.; Naqvi, I.H.; Khalid, Z.; Pecht, M. Accurate Prediction of Remaining Useful Life for Lithium-Ion Battery Using Deep Neural Networks with Memory Features. *Front. Energy Res.* **2023**, *11*, 1059701. [CrossRef]
194. Wu, J.; Liu, Z.; Zhang, Y.; Lei, D.; Zhang, B.; Cao, W. Data-Driven State of Health Estimation for Lithium-Ion Battery Based on Voltage Variation Curves. *J. Energy Storage* **2023**, *73*, 109191. [CrossRef]
195. Wang, Z.; Liu, Y.; Wang, F.; Wang, H.; Su, M. Capacity and Remaining Useful Life Prediction for Lithium-Ion Batteries Based on Sequence Decomposition and a Deep-Learning Network. *J. Energy Storage* **2023**, *72*, 108085. [CrossRef]
196. Chang, Y.-H.; Hsieh, Y.-C.; Chai, Y.-H.; Lin, H.-W. Remaining-Useful-Life Prediction for Li-Ion Batteries. *Energies* **2023**, *16*, 3096. [CrossRef]
197. Wang, J.; Zhu, L.; Dai, H. An Efficient State-of-Health Estimation Method for Lithium-Ion Batteries Based on Feature-Importance Ranking Strategy and PSO-GRNN Algorithm. *J. Energy Storage* **2023**, *72*, 108638. [CrossRef]
198. Nair, P.; Vakharia, V.; Borade, H.; Shah, M.; Wankhede, V. Predicting Li-Ion Battery Remaining Useful Life: An XDFM-Driven Approach with Explainable AI. *Energies* **2023**, *16*, 5725. [CrossRef]
199. Zhang, F.; Shen, Z.; Xu, M.; Xie, Q.; Fu, Q.; Ma, R. Remaining Useful Life Prediction of Lithium-Ion Batteries Based on TCN-DCN Fusion Model Combined with IRRS Filtering. *J. Energy Storage* **2023**, *72*, 108586. [CrossRef]
200. Pan, R.; Liu, T.; Huang, W.; Wang, Y.; Yang, D.; Chen, J. State of Health Estimation for Lithium-Ion Batteries Based on Two-Stage Features Extraction and Gradient Boosting Decision Tree. *Energy* **2023**, *285*, 129460. [CrossRef]
201. Zhang, Y.; Zhang, Y.; Wu, T. Estimation of State of Health Based on Charging Characteristics and Back-Propagation Neural Networks with Improved Atom Search Optimization Algorithm. *Glob. Energy Interconnect.* **2023**, *6*, 228–237. [CrossRef]
202. Jafari, S.; Byun, Y.-C. A CNN-GRU Approach to the Accurate Prediction of Batteries' Remaining Useful Life from Charging Profiles. *Computers* **2023**, *12*, 219. [CrossRef]
203. Wang, Y.; He, Q.; Zhang, D.; Lu, S.; Yuan, C. Improving Li-Ion Battery Health: Predicting Remaining Useful Life Using IWBOA-ELM Algorithm. *J. Energy Storage* **2023**, *72*, 108547. [CrossRef]
204. Wang, F.; Yang, Y.; Huang, T.; Xu, Y. Lifetime Prediction of Electronic Devices Based on the P-Stacking Machine Learning Model. *Microelectron. Reliab.* **2023**, *146*, 115027. [CrossRef]
205. Ansari, S.; Ayob, A.; Lipu, M.S.H.; Hussain, A.; Abdolrasol, M.G.M.; Zainuri, M.A.A.M.; Saad, M.H.M. Optimized Data-Driven Approach for Remaining Useful Life Prediction of Lithium-Ion Batteries Based on Sliding Window and Systematic Sampling. *J. Energy Storage* **2023**, *73*, 109198. [CrossRef]
206. Guo, L.; He, H.; Ren, Y.; Li, R.; Jiang, B.; Gong, J. Prognostics of Lithium-Ion Batteries Health State Based on Adaptive Mode Decomposition and Long Short-Term Memory Neural Network. *Eng. Appl. Artif. Intell.* **2024**, *127*, 107317. [CrossRef]
207. Zhang, Y.; Wang, Y.; Zhang, C.; Qiao, X.; Ge, Y.; Li, X.; Peng, T.; Nazir, M.S. State-of-Health Estimation for Lithium-Ion Battery via an Evolutionary Stacking Ensemble Learning Paradigm of Random Vector Functional Link and Active-State-Tracking Long–Short-Term Memory Neural Network. *Appl. Energy* **2024**, *356*, 122417. [CrossRef]
208. Li, Z.; Bai, F.; Zuo, H.; Zhang, Y. Remaining Useful Life Prediction for Lithium-Ion Batteries Based on Iterative Transfer Learning and Mogrifier LSTM. *Batteries* **2023**, *9*, 448. [CrossRef]

209. Ren, Z.; Du, C.; Zhao, Y. A Novel Method for State of Health Estimation of Lithium-Ion Batteries Based on Deep Learning Neural Network and Transfer Learning. *Batteries* **2023**, *9*, 585. [CrossRef]
210. Zheng, W.; Zhou, X.; Bai, C.; Zhou, D.; Fu, P. Adaptation of Deep Network in Transfer Learning for Estimating State of Health in Electric Vehicles during Operation. *Batteries* **2023**, *9*, 547. [CrossRef]
211. Kuo, P.-H.; Tseng, Y.-R.; Luan, P.-C.; Yau, H.-T. Broad Transfer Learning Network Based Li-Ion Battery Lifetime Prediction Model. *Energy Rep.* **2023**, *10*, 881–893. [CrossRef]
212. Bosello, M.; Falcomer, C.; Rossi, C.; Pau, G. To Charge or to Sell? EV Pack Useful Life Estimation via LSTMs, CNNs, and Autoencoders. *Energies* **2023**, *16*, 2837. [CrossRef]
213. Berghout, T.; Benbouzid, M.; Amirat, Y.; Yao, G. Lithium-Ion Battery State of Health Prediction with a Robust Collaborative Augmented Hidden Layer Feedforward Neural Network Approach. *IEEE Trans. Transp. Electrif.* **2023**, *9*, 4492–4502. [CrossRef]
214. Hong, J.; Chen, Y.; Chai, Q.; Lin, Q.; Wang, W. State-of-Health Estimation of Lithium-Ion Batteries Using a Novel Dual-Stage Attention Mechanism Based Recurrent Neural Network. *J. Energy Storage* **2023**, *72*, 109297. [CrossRef]
215. Wang, S.; Ma, H.; Zhang, Y.; Li, S.; He, W. Remaining Useful Life Prediction Method of Lithium-Ion Batteries Is Based on Variational Modal Decomposition and Deep Learning Integrated Approach. *Energy* **2023**, *282*, 128984. [CrossRef]
216. Zhang, L.; Zhang, J.; Gao, T.; Lyu, L.; Wang, L.; Shi, W.; Jiang, L.; Cai, G. Improved LSTM Based State of Health Estimation Using Random Segments of the Charging Curves for Lithium-Ion Batteries. *J. Energy Storage* **2023**, *74*, 109370. [CrossRef]
217. Guo, F.; Huang, G.; Zhang, W.; Wen, A.; Li, T.; He, H.; Huang, H.; Zhu, S. Lithium Battery State-of-Health Estimation Based on Sample Data Generation and Temporal Convolutional Neural Network. *Energies* **2023**, *16*, 8010. [CrossRef]
218. Liu, Y.; Sun, G.; Liu, X. Remaining Useful Life Prediction of Lithium-Ion Batteries Based on Peak Interval Features and Deep Learning. *J. Energy Storage* **2023**, *73*, 109308. [CrossRef]
219. Jin, Z.; Fang, C.; Wu, J.; Li, J.; Zeng, W.; Zhao, X. Remaining Useful Life Prediction for Lithium-Ion Battery Using a Data-Driven Method. *Int. J. Wirel. Mob. Comput.* **2022**, *23*, 239–249. [CrossRef]
220. Zhao, L.; Song, S.; Wang, P.; Wang, C.; Wang, J.; Guo, M. A MLP-Mixer and Mixture of Expert Model for Remaining Useful Life Prediction of Lithium-Ion Batteries. *Front. Comput. Sci.* **2023**, *18*, 185329. [CrossRef]
221. Wang, X.; Hu, B.; Su, X.; Xu, L.; Zhu, D. State of Health Estimation for Lithium-Ion Batteries Using Random Forest and Gated Recurrent Unit. *J. Energy Storage* **2024**, *76*, 109796. [CrossRef]
222. Chen, L.; Xie, S.; Lopes, A.M.; Li, H.; Bao, X.; Zhang, C.; Li, P. A New SOH Estimation Method for Lithium-Ion Batteries Based on Model-Data-Fusion. *Energy* **2024**, *286*, 129597. [CrossRef]
223. Mazzi, Y.; Ben Sassi, H.; Errahimi, F. Lithium-Ion Battery State of Health Estimation Using a Hybrid Model Based on a Convolutional Neural Network and Bidirectional Gated Recurrent Unit. *Eng. Appl. Artif. Intell.* **2024**, *127*, 107199. [CrossRef]
224. Zhigang, L.; Meng, Z.; Ruohai, D.; Peng, W.; Hui, G.; Hongxi, W. Remaining Useful Life Prediction of Lithium-Ion Batteries Based on KS Agglomeration Function Integrating Multi-Expert Knowledge. *Microelectron. Reliab.* **2023**, *145*, 114985. [CrossRef]
225. Li, C.; Han, X.; Zhang, Q.; Li, M.; Rao, Z.; Liao, W.; Liu, X.; Liu, X.; Li, G. State-of-Health and Remaining-Useful-Life Estimations of Lithium-Ion Battery Based on Temporal Convolutional Network-Long Short-Term Memory. *J. Energy Storage* **2023**, *74*, 109498. [CrossRef]
226. Rincón-Maya, C.; Guevara-Carazas, F.; Hernández-Barajas, F.; Patino-Rodriguez, C.; Usuga-Manco, O. Remaining Useful Life Prediction of Lithium-Ion Battery Using ICC-CNN-LSTM Methodology. *Energies* **2023**, *16*, 7081. [CrossRef]
227. Zhang, C.; Wang, S.; Yu, C.; Wang, Y.; Fernandez, C. A Complete Ensemble Empirical Mode Decomposition with Adaptive Noise Deep Autoregressive Recurrent Neural Network Method for the Whole Life Remaining Useful Life Prediction of Lithium-Ion Batteries. *Ionics* **2023**, *29*, 4337–4349. [CrossRef]
228. Cai, Y.; Li, W.; Zahid, T.; Zheng, C.; Zhang, Q.; Xu, K. Early Prediction of Remaining Useful Life for Lithium-Ion Batteries Based on CEEMDAN-Transformer-DNN Hybrid Model. *Heliyon* **2023**, *9*, e17754. [CrossRef]
229. Feng, J.; Cai, F.; Li, H.; Huang, K.; Yin, H. A Data-Driven Prediction Model for the Remaining Useful Life Prediction of Lithium-Ion Batteries. *Process Saf. Environ. Prot.* **2023**, *180*, 601–615. [CrossRef]
230. Xia, T.; Zhang, X.; Zhu, H.; Zhang, X.; Shen, J. An Accurate Denoising Lithium-Ion Battery Remaining Useful Life Prediction Model Based on CNN and LSTM with Self-Attention. *Ionics* **2023**, *29*, 5315–5328. [CrossRef]
231. Ding, G.; Chen, H. A Novel Lithium-Ion Battery Capacity Prediction Framework Based on SVMD-AO-DELM. *Signal Image Video Process.* **2023**, *17*, 3793–3801. [CrossRef]
232. Xue, J.; Ma, W.; Feng, X.; Guo, P.; Guo, Y.; Hu, X.; Chen, B. Stacking Integrated Learning Model via ELM and GRU with Mixture Correntropy Loss for Robust State of Health Estimation of Lithium-Ion Batteries. *Energy* **2023**, *284*, 129279. [CrossRef]
233. Zheng, X.; Chen, D.; Wang, Y.; Zhuang, L.; Zheng, X.; Chen, D.; Wang, Y.; Zhuang, L. Remaining Useful Life Indirect Prediction of Lithium-Ion Batteries Using CNN-BiGRU Fusion Model and TPE Optimization. *AIMS Energy* **2023**, *11*, 896–917. [CrossRef]
234. Geng, C.; Zhang, T.; Chen, B.; Zhou, Q. Battery State of Health Estimation Using GA-BP Neural Network on Data Feature Mining. *IEICE Electron. Express* **2023**, *20*, 20230370. [CrossRef]

235. Sun, S.; Zhang, H.; Ge, J.; Che, L. State-of-Health Estimation for Lithium-Ion Battery Using Model-Based Feature Optimization and Deep Extreme Learning Machine. *J. Energy Storage* **2023**, *72*, 108732. [CrossRef]
236. Zraibi, B.; Okar, C.; Chaoui, H.; Mansouri, M. Remaining Useful Life Assessment for Lithium-Ion Batteries Using CNN-LSTM-DNN Hybrid Method. *IEEE Trans. Veh. Technol.* **2021**, *70*, 4252–4261. [CrossRef]
237. Zhao, S.; Zhang, C.; Wang, Y. Lithium-Ion Battery Capacity and Remaining Useful Life Prediction Using Board Learning System and Long Short-Term Memory Neural Network. *J. Energy Storage* **2022**, *52*, 104901. [CrossRef]
238. Li, Y.; Sheng, H.; Cheng, Y.; Stroe, D.-I.; Teodorescu, R. State-of-Health Estimation of Lithium-Ion Batteries Based on Semi-Supervised Transfer Component Analysis. *Appl. Energy* **2020**, *277*, 115504. [CrossRef]
239. Guo, Y.; Yang, D.; Zhang, Y.; Wang, L.; Wang, K. Online Estimation of SOH for Lithium-Ion Battery Based on SSA-Elman Neural Network. *Prot. Control Mod. Power Syst.* **2022**, *7*, 40. [CrossRef]
240. Chen, D.; Hong, W.; Zhou, X. Transformer Network for Remaining Useful Life Prediction of Lithium-Ion Batteries. *IEEE Access* **2022**, *10*, 19621–19628. [CrossRef]
241. Nascimento, R.G.; Corbetta, M.; Kulkarni, C.S.; Viana, F.A.C. Hybrid Physics-Informed Neural Networks for Lithium-Ion Battery Modeling and Prognosis. *J. Power Sources* **2021**, *513*, 230526. [CrossRef]
242. Li, Y.; Sheng, H.; Cheng, Y.; Kuang, H. Lithium-Ion Battery State of Health Monitoring Based on Ensemble Learning. In Proceedings of the 2019 IEEE International Instrumentation and Measurement Technology Conference, I2MTC 2019, Auckland, New Zealand, 20–23 May 2019.
243. Li, P.; Zhang, Z.; Grosu, R.; Deng, Z.; Hou, J.; Rong, Y.; Wu, R. An End-to-End Neural Network Framework for State-of-Health Estimation and Remaining Useful Life Prediction of Electric Vehicle Lithium Batteries. *Renew. Sustain. Energy Rev.* **2022**, *156*, 111843. [CrossRef]
244. Gou, B.; Xu, Y.; Feng, X. An Ensemble Learning-Based Data-Driven Method for Online State-of-Health Estimation of Lithium-Ion Batteries. *IEEE Trans. Transp. Electrif.* **2021**, *7*, 422–436. [CrossRef]
245. Wang, S.; Fan, Y.; Jin, S.; Takyi-Aninakwa, P.; Fernandez, C. Improved Anti-Noise Adaptive Long Short-Term Memory Neural Network Modeling for the Robust Remaining Useful Life Prediction of Lithium-Ion Batteries. *Reliab. Eng. Syst. Saf.* **2023**, *230*, 108920. [CrossRef]
246. Catelani, M.; Ciani, L.; Fantacci, R.; Patrizi, G.; Picano, B. Remaining Useful Life Estimation for Prognostics of Lithium-Ion Batteries Based on Recurrent Neural Network. *IEEE Trans. Instrum. Meas.* **2021**, *70*, 1–11. [CrossRef]
247. Khan, N.; Ullah, F.U.M.; Afnan; Ullah, A.; Lee, M.Y.; Baik, S.W. Batteries State of Health Estimation via Efficient Neural Networks with Multiple Channel Charging Profiles. *IEEE Access* **2021**, *9*, 7797–7813. [CrossRef]
248. Sun, H.; Sun, J.; Zhao, K.; Wang, L.; Wang, K. Data-Driven ICA-Bi-LSTM-Combined Lithium Battery SOH Estimation. *Math. Probl. Eng.* **2022**, *2022*, 9645892. [CrossRef]
249. Kim, S.; Choi, Y.Y.; Kim, K.J.; Choi, J.-I. Forecasting State-of-Health of Lithium-Ion Batteries Using Variational Long Short-Term Memory with Transfer Learning. *J. Energy Storage* **2021**, *41*, 102893. [CrossRef]
250. Tang, T.; Yuan, H. A Hybrid Approach Based on Decomposition Algorithm and Neural Network for Remaining Useful Life Prediction of Lithium-Ion Battery. *Reliab. Eng. Syst. Saf.* **2022**, *217*, 108082. [CrossRef]
251. Han, T.; Wang, Z.; Meng, H. End-to-End Capacity Estimation of Lithium-Ion Batteries with an Enhanced Long Short-Term Memory Network Considering Domain Adaptation. *J. Power Sources* **2022**, *520*, 230823. [CrossRef]
252. Ding, P.; Liu, X.; Li, H.; Huang, Z.; Zhang, K.; Shao, L.; Abedinia, O. Useful Life Prediction Based on Wavelet Packet Decomposition and Two-Dimensional Convolutional Neural Network for Lithium-Ion Batteries. *Renew. Sustain. Energy Rev.* **2021**, *148*, 111287. [CrossRef]
253. Zhang, Y.; Wik, T.; Bergström, J.; Pecht, M.; Zou, C. A Machine Learning-Based Framework for Online Prediction of Battery Ageing Trajectory and Lifetime Using Histogram Data. *J. Power Sources* **2022**, *526*, 231110. [CrossRef]
254. Chinomona, B.; Chung, C.; Chang, L.-K.; Su, W.-C.; Tsai, M.-C. Long Short-Term Memory Approach to Estimate Battery Remaining Useful Life Using Partial Data. *IEEE Access* **2020**, *8*, 165419–165431. [CrossRef]
255. Goh, H.H.; Lan, Z.; Zhang, D.; Dai, W.; Kurniawan, T.A.; Goh, K.C. Estimation of the State of Health (SOH) of Batteries Using Discrete Curvature Feature Extraction. *J. Energy Storage* **2022**, *50*, 104646. [CrossRef]
256. Wei, M.; Gu, H.; Ye, M.; Wang, Q.; Xu, X.; Wu, C. Remaining Useful Life Prediction of Lithium-Ion Batteries Based on Monte Carlo Dropout and Gated Recurrent Unit. *Energy Rep.* **2021**, *7*, 2862–2871. [CrossRef]
257. Wang, Z.; Zeng, S.; Guo, J.; Qin, T. Remaining Capacity Estimation of Lithium-Ion Batteries Based on the Constant Voltage Charging Profile. *PLoS ONE* **2018**, *13*, e0200169. [CrossRef]
258. Guo, Y.; Yu, P.; Zhu, C.; Zhao, K.; Wang, L.; Wang, K. A State-of-Health Estimation Method Considering Capacity Recovery of Lithium Batteries. *Int. J. Energy Res.* **2022**, *46*, 23730–23745. [CrossRef]
259. Gu, X.; See, K.W.; Li, P.; Shan, K.; Wang, Y.; Zhao, L.; Lim, K.C.; Zhang, N. A Novel State-of-Health Estimation for the Lithium-Ion Battery Using a Convolutional Neural Network and Transformer Model. *Energy* **2023**, *262*, 125501. [CrossRef]

260. Yang, Z.; Wang, Y.; Kong, C. Remaining Useful Life Prediction of Lithium-Ion Batteries Based on a Mixture of Ensemble Empirical Mode Decomposition and GWO-SVR Model. *IEEE Trans. Instrum. Meas.* **2021**, *70*, 1–11. [CrossRef]
261. Kara, A. A Data-Driven Approach Based on Deep Neural Networks for Lithium-Ion Battery Prognostics. *Neural Comput. Appl.* **2021**, *33*, 13525–13538. [CrossRef]
262. Song, S.; Fei, C.; Xia, H. Lithium-Ion Battery SOH Estimation Based on XGBoost Algorithm with Accuracy Correction. *Energies* **2020**, *13*, 812. [CrossRef]
263. Liu, W.; Xu, Y.; Feng, X. A Hierarchical and Flexible Data-Driven Method for Online State-of-Health Estimation of Li-Ion Battery. *IEEE Trans. Veh. Technol.* **2020**, *69*, 14739–14748. [CrossRef]
264. Wu, J.; Fang, L.; Dong, G.; Lin, M. State of Health Estimation of Lithium-Ion Battery with Improved Radial Basis Function Neural Network. *Energy* **2023**, *262*, 125380. [CrossRef]
265. Cheng, Y.; Song, D.; Wang, Z.; Lu, C.; Zerhouni, N. An Ensemble Prognostic Method for Lithium-Ion Battery Capacity Estimation Based on Time-Varying Weight Allocation. *Appl. Energy* **2020**, *266*, 114817. [CrossRef]
266. Mao, L.; Xu, J.; Chen, J.; Zhao, J.; Wu, Y.; Yao, F. A LSTM-STW and GS-LM Fusion Method for Lithium-Ion Battery RUL Prediction Based on EEMD. *Energies* **2020**, *13*, 2380. [CrossRef]
267. Kohtz, S.; Xu, Y.; Zheng, Z.; Wang, P. Physics-Informed Machine Learning Model for Battery State of Health Prognostics Using Partial Charging Segments. *Mech. Syst. Signal Process.* **2022**, *172*, 109002. [CrossRef]
268. Ardeshiri, R.R.; Liu, M.; Ma, C. Multivariate Stacked Bidirectional Long Short Term Memory for Lithium-Ion Battery Health Management. *Reliab. Eng. Syst. Saf.* **2022**, *224*, 108481. [CrossRef]
269. Gong, D.; Gao, Y.; Kou, Y.; Wang, Y. State of Health Estimation for Lithium-Ion Battery Based on Energy Features. *Energy* **2022**, *257*, 124812. [CrossRef]
270. Wu, J.; Cui, X.; Meng, J.; Peng, J.; Lin, M. Data-Driven Transfer-Stacking-Based State of Health Estimation for Lithium-Ion Batteries. *IEEE Trans. Ind. Electron.* **2024**, *71*, 604–614. [CrossRef]
271. Driscoll, L.; de la Torre, S.; Gomez-Ruiz, J.A. Feature-Based Lithium-Ion Battery State of Health Estimation with Artificial Neural Networks. *J. Energy Storage* **2022**, *50*, 104584. [CrossRef]
272. Qin, P.; Zhao, L.; Liu, Z. State of Health Prediction for Lithium-Ion Battery Using a Gradient Boosting-Based Data-Driven Method. *J. Energy Storage* **2022**, *47*, 103644. [CrossRef]
273. Cao, M.; Zhang, T.; Wang, J.; Liu, Y. A Deep Belief Network Approach to Remaining Capacity Estimation for Lithium-Ion Batteries Based on Charging Process Features. *J. Energy Storage* **2022**, *48*, 103825. [CrossRef]
274. Wei, Y.; Wu, D. Prediction of State of Health and Remaining Useful Life of Lithium-Ion Battery Using Graph Convolutional Network with Dual Attention Mechanisms. *Reliab. Eng. Syst. Saf.* **2023**, *230*, 108947. [CrossRef]
275. Chen, Z.; Chen, L.; Shen, W.; Xu, K. Remaining Useful Life Prediction of Lithium-Ion Battery via a Sequence Decomposition and Deep Learning Integrated Approach. *IEEE Trans. Veh. Technol.* **2022**, *71*, 1466–1479. [CrossRef]
276. Ma, B.; Yang, S.; Zhang, L.; Wang, W.; Chen, S.; Yang, X.; Xie, H.; Yu, H.; Wang, H.; Liu, X. Remaining Useful Life and State of Health Prediction for Lithium Batteries Based on Differential Thermal Voltammetry and a Deep-Learning Model. *J. Power Sources* **2022**, *548*, 232030. [CrossRef]
277. Ruan, H.; Wei, Z.; Shang, W.; Wang, X.; He, H. Artificial Intelligence-Based Health Diagnostic of Lithium-Ion Battery Leveraging Transient Stage of Constant Current and Constant Voltage Charging. *Appl. Energy* **2023**, *336*, 120751. [CrossRef]
278. Tang, A.; Jiang, Y.; Yu, Q.; Zhang, Z. A Hybrid Neural Network Model with Attention Mechanism for State of Health Estimation of Lithium-Ion Batteries. *J. Energy Storage* **2023**, *68*, 107734. [CrossRef]
279. Lin, M.; You, Y.; Wang, W.; Wu, J. Battery Health Prognosis with Gated Recurrent Unit Neural Networks and Hidden Markov Model Considering Uncertainty Quantification. *Reliab. Eng. Syst. Saf.* **2023**, *230*, 108978. [CrossRef]
280. Bockrath, S.; Lorentz, V.; Pruckner, M. State of Health Estimation of Lithium-Ion Batteries with a Temporal Convolutional Neural Network Using Partial Load Profiles. *Appl. Energy* **2023**, *329*, 120307. [CrossRef]
281. Xu, H.; Wu, L.; Xiong, S.; Li, W.; Garg, A.; Gao, L. An Improved CNN-LSTM Model-Based State-of-Health Estimation Approach for Lithium-Ion Batteries. *Energy* **2023**, *276*, 127585. [CrossRef]
282. Liu, Y.; Sun, J.; Shang, Y.; Zhang, X.; Ren, S.; Wang, D. A Novel Remaining Useful Life Prediction Method for Lithium-Ion Battery Based on Long Short-Term Memory Network Optimized by Improved Sparrow Search Algorithm. *J. Energy Storage* **2023**, *61*, 106645. [CrossRef]
283. Bamati, S.; Chaoui, H. Lithium-Ion Batteries Long Horizon Health Prognostic Using Machine Learning. *IEEE Trans. Energy Convers.* **2022**, *37*, 1176–1186. [CrossRef]
284. Cao, M.; Zhang, T.; Yu, B.; Liu, Y. A Method for Interval Prediction of Satellite Battery State of Health Based on Sample Entropy. *IEEE Access* **2019**, *7*, 141549–141561. [CrossRef]
285. Zhang, Z.; Li, L.; Li, X.; Hu, Y.; Huang, K.; Xue, B.; Wang, Y.; Yu, Y. State-of-Health Estimation for the Lithium-Ion Battery Based on Gradient Boosting Decision Tree with Autonomous Selection of Excellent Features. *Int. J. Energy Res.* **2022**, *46*, 1756–1765. [CrossRef]

286. Su, C.; Chen, H.; Wen, Z. Prediction of Remaining Useful Life for Lithium-Ion Battery with Multiple Health Indicators. *Eksploat. i Niezawodn.* **2021**, *23*, 176–183. [CrossRef]
287. Chen, Z.; Xue, Q.; Wu, Y.; Shen, S.; Zhang, Y.; Shen, J. Capacity Prediction and Validation of Lithium-Ion Batteries Based on Long Short-Term Memory Recurrent Neural Network. *IEEE Access* **2020**, *8*, 172783–172798. [CrossRef]
288. He, J.; Tian, Y.; Wu, L. A Hybrid Data-Driven Method for Rapid Prediction of Lithium-Ion Battery Capacity. *Reliab. Eng. Syst. Saf.* **2022**, *226*, 108674. [CrossRef]
289. Lin, C.; Xu, J.; Hou, J.; Liang, Y.; Mei, X. Ensemble Method with Heterogeneous Models for Battery State-of-Health Estimation. *IEEE Trans. Ind. Inform.* **2023**, *19*, 10160–10169. [CrossRef]
290. Jia, J.; Wang, K.; Shi, Y.; Wen, J.; Pang, X.; Zeng, J. A Multi-Scale State of Health Prediction Framework of Lithium-Ion Batteries Considering the Temperature Variation during Battery Discharge. *J. Energy Storage* **2021**, *42*, 103076. [CrossRef]
291. Vakharia, V.; Shah, M.; Nair, P.; Borade, H.; Sahlot, P.; Wankhede, V. Estimation of Lithium-Ion Battery Discharge Capacity by Integrating Optimized Explainable-AI and Stacked LSTM Model. *Batteries* **2023**, *9*, 125. [CrossRef]
292. Li, D.; Yang, L. Remaining Useful Life Prediction of Lithium Battery Based on Sequential CNN–LSTM Method. *J. Electrochem. Energy Convers. Storage* **2021**, *18*, 041005. [CrossRef]
293. Fan, Z.; Zi-xuan, X.; Ming-hu, W. State of Health Estimation for Li-Ion Battery Using Characteristic Voltage Intervals and Genetic Algorithm Optimized Back Propagation Neural Network. *J. Energy Storage* **2023**, *57*, 106277. [CrossRef]
294. Wei, Z.; Han, X.; Li, J. State of Health Assessment for Echelon Utilization Batteries Based on Deep Neural Network Learning with Error Correction. *J. Energy Storage* **2022**, *51*, 104428. [CrossRef]
295. Tang, T.; Yuan, H. An Indirect Remaining Useful Life Prognosis for Li-Ion Batteries Based on Health Indicator and Novel Artificial Neural Network. *J. Energy Storage* **2022**, *52*, 104701. [CrossRef]
296. Chen, X.; Liu, Z.; Sheng, H.; Wu, K.; Mi, J.; Li, Q. Transfer Learning Based Remaining Useful Life Prediction of Lithium-Ion Battery Considering Capacity Regeneration Phenomenon. *J. Energy Storage* **2024**, *76*, 109798. [CrossRef]
297. Bao, Z.; Jiang, J.; Zhu, C.; Gao, M. A New Hybrid Neural Network Method for State-of-Health Estimation of Lithium-Ion Battery. *Energies* **2022**, *15*, 4399. [CrossRef]
298. Wang, Z.; Liu, N.; Chen, C.; Guo, Y. Adaptive Self-Attention LSTM for RUL Prediction of Lithium-Ion Batteries. *Inf. Sci.* **2023**, *635*, 398–413. [CrossRef]
299. Yao, X.-Y.; Chen, G.; Pecht, M.; Chen, B. A Novel Graph-Based Framework for State of Health Prediction of Lithium-Ion Battery. *J. Energy Storage* **2023**, *58*, 106437. [CrossRef]
300. Mao, L.; Hu, H.; Chen, J.; Zhao, J.; Qu, K.; Jiang, L. Online State-of-Health Estimation Method for Lithium-Ion Battery Based on CEEMDAN for Feature Analysis and RBF Neural Network. *IEEE J. Emerg. Sel. Top. Power Electron.* **2023**, *11*, 187–200. [CrossRef]
301. Bi, J.; Lee, J.-C.; Liu, H. Performance Comparison of Long Short-Term Memory and a Temporal Convolutional Network for State of Health Estimation of a Lithium-Ion Battery Using Its Charging Characteristics. *Energies* **2022**, *15*, 2448. [CrossRef]
302. Cui, Y.; Chen, Y. Prognostics of Lithium-Ion Batteries Based on Capacity Regeneration Analysis and Long Short-Term Memory Network. *IEEE Trans. Instrum. Meas.* **2022**, *71*, 1–13. [CrossRef]
303. Chen, Z.; Zhang, S.; Shi, N.; Li, F.; Wang, Y.; Cui, J. Online State-of-Health Estimation of Lithium-Ion Battery Based on Relevance Vector Machine with Dynamic Integration. *Appl. Soft Comput.* **2022**, *129*, 109615. [CrossRef]
304. Zhao, J.; Zhu, Y.; Zhang, B.; Liu, M.; Wang, J.; Liu, C.; Zhang, Y. Method of Predicting SOH and RUL of Lithium-Ion Battery Based on the Combination of LSTM and GPR. *Sustainability* **2022**, *14*, 11865. [CrossRef]
305. Zhang, D.; Li, W.; Han, X.; Lu, B.; Zhang, Q.; Bo, C. Evolving Elman Neural Networks Based State-of-Health Estimation for Satellite Lithium-Ion Batteries. *J. Energy Storage* **2023**, *59*, 106571. [CrossRef]
306. Zhu, M.; Ouyang, Q.; Wan, Y.; Wang, Z. Remaining Useful Life Prediction of Lithium-Ion Batteries: A Hybrid Approach of Grey–Markov Chain Model and Improved Gaussian Process. *IEEE J. Emerg. Sel. Top. Power Electron.* **2023**, *11*, 143–153. [CrossRef]
307. Ang, E.Y.M.; Paw, Y.C. Efficient Linear Predictive Model with Short Term Features for Lithium-Ion Batteries State of Health Estimation. *J. Energy Storage* **2021**, *44*, 103409. [CrossRef]
308. Ouyang, M.; Shen, P. Prediction of Remaining Useful Life of Lithium Batteries Based on WOA-VMD and LSTM. *Energies* **2022**, *15*, 8918. [CrossRef]
309. Zhang, Y.; Wang, Y.; Xia, Y.; Chen, W. A Deep Learning Approach to Estimate the State of Health of Lithium-Ion Batteries under Varied and Incomplete Working Conditions. *J. Energy Storage* **2023**, *58*, 106323. [CrossRef]
310. Ma, B.; Zhang, L.; Yu, H.; Zou, B.; Wang, W.; Zhang, C.; Yang, S.; Liu, X. End-Cloud Collaboration Method Enables Accurate State of Health and Remaining Useful Life Online Estimation in Lithium-Ion Batteries. *J. Energy Chem.* **2023**, *82*, 1–17. [CrossRef]
311. Gao, M.; Bao, Z.; Zhu, C.; Jiang, J.; He, Z.; Dong, Z.; Song, Y. HFCM-LSTM: A Novel Hybrid Framework for State-of-Health Estimation of Lithium-Ion Battery. *Energy Rep.* **2023**, *9*, 2577–2590. [CrossRef]
312. Li, L.; Li, Y.; Mao, R.; Li, L.; Hua, W.; Zhang, J. Remaining Useful Life Prediction for Lithium-Ion Batteries with a Hybrid Model Based on TCN-GRU-DNN and Dual Attention Mechanism. *IEEE Trans. Transp. Electrif.* **2023**, *9*, 4726–4740. [CrossRef]

313. Xu, J.; Liu, B.; Zhang, G.; Zhu, J. State-of-Health Estimation for Lithium-Ion Batteries Based on Partial Charging Segment and Stacking Model Fusion. *Energy Sci. Eng.* **2023**, *11*, 383–397. [CrossRef]
314. Zou, L.; Wen, B.; Wei, Y.; Zhang, Y.; Yang, J.; Zhang, H. Online Prediction of Remaining Useful Life for Li-Ion Batteries Based on Discharge Voltage Data. *Energies* **2022**, *15*, 2237. [CrossRef]
315. Yang, Y. A Machine-Learning Prediction Method of Lithium-Ion Battery Life Based on Charge Process for Different Applications. *Appl. Energy* **2021**, *292*, 116897. [CrossRef]
316. Deng, Z.; Lin, X.; Cai, J.; Hu, X. Battery Health Estimation with Degradation Pattern Recognition and Transfer Learning. *J. Power Sources* **2022**, *525*, 231027. [CrossRef]
317. Zhang, Y.; Peng, Z.; Guan, Y.; Wu, L. Prognostics of Battery Cycle Life in the Early-Cycle Stage Based on Hybrid Model. *Energy* **2021**, *221*, 119901. [CrossRef]
318. Hsu, C.-W.; Xiong, R.; Chen, N.-Y.; Li, J.; Tsou, N.-T. Deep Neural Network Battery Life and Voltage Prediction by Using Data of One Cycle Only. *Appl. Energy* **2022**, *306*, 118134. [CrossRef]
319. Zhang, Q.; Yang, L.; Guo, W.; Qiang, J.; Peng, C.; Li, Q.; Deng, Z. A Deep Learning Method for Lithium-Ion Battery Remaining Useful Life Prediction Based on Sparse Segment Data via Cloud Computing System. *Energy* **2022**, *241*, 122716. [CrossRef]
320. Herring, P.; Balaji Gopal, C.; Aykol, M.; Montoya, J.H.; Anapolsky, A.; Attia, P.M.; Gent, W.; Hummelshøj, J.S.; Hung, L.; Kwon, H.-K.; et al. BEEP: A Python Library for Battery Evaluation and Early Prediction. *SoftwareX* **2020**, *11*, 100506. [CrossRef]
321. Sanz-Gorrachategui, I.; Pastor-Flores, P.; Pajovic, M.; Wang, Y.; Orlik, P.V.; Bernal-Ruiz, C.; Bono-Nuez, A.; Artal-Sevil, J.S. Remaining Useful Life Estimation for LFP Cells in Second-Life Applications. *IEEE Trans. Instrum. Meas.* **2021**, *70*, 1–10. [CrossRef]
322. Ma, G.; Xu, S.; Yang, T.; Du, Z.; Zhu, L.; Ding, H.; Yuan, Y. A Transfer Learning-Based Method for Personalized State of Health Estimation of Lithium-Ion Batteries. *IEEE Trans. Neural Netw. Learn. Syst.* **2024**, *35*, 759–769. [CrossRef]
323. Zhang, Y.; Zhao, M. Cloud-Based in-Situ Battery Life Prediction and Classification Using Machine Learning. *Energy Storage Mater.* **2023**, *57*, 346–359. [CrossRef]
324. Guo, F.; Wu, X.; Liu, L.; Ye, J.; Wang, T.; Fu, L.; Wu, Y. Prediction of Remaining Useful Life and State of Health of Lithium Batteries Based on Time Series Feature and Savitzky-Golay Filter Combined with Gated Recurrent Unit Neural Network. *Energy* **2023**, *270*, 126880. [CrossRef]
325. Che, Y.; Stroe, D.-I.; Hu, X.; Teodorescu, R. Semi-Supervised Self-Learning-Based Lifetime Prediction for Batteries. *IEEE Trans. Ind. Inform.* **2023**, *19*, 6471–6481. [CrossRef]
326. Xu, L.; Deng, Z.; Xie, Y.; Lin, X.; Hu, X. A Novel Hybrid Physics-Based and Data-Driven Approach for Degradation Trajectory Prediction in Li-Ion Batteries. *IEEE Trans. Transp. Electrif.* **2023**, *9*, 2628–2644. [CrossRef]
327. Chen, D.; Zhang, W.; Zhang, C.; Sun, B.; Cong, X.; Wei, S.; Jiang, J. A Novel Deep Learning-Based Life Prediction Method for Lithium-Ion Batteries with Strong Generalization Capability under Multiple Cycle Profiles. *Appl. Energy* **2022**, *327*, 120114. [CrossRef]
328. Fei, Z.; Zhang, Z.; Yang, F.; Tsui, K.-L. A Deep Attention-Assisted and Memory-Augmented Temporal Convolutional Network Based Model for Rapid Lithium-Ion Battery Remaining Useful Life Predictions with Limited Data. *J. Energy Storage* **2023**, *62*, 106903. [CrossRef]
329. Gong, D.; Gao, Y.; Kou, Y.; Wang, Y. Early Prediction of Cycle Life for Lithium-Ion Batteries Based on Evolutionary Computation and Machine Learning. *J. Energy Storage* **2022**, *51*, 104376. [CrossRef]
330. Zhang, S.; Liu, Z.; Su, H. State of Health Estimation for Lithium-Ion Batteries on Few-Shot Learning. *Energy* **2023**, *268*, 126726. [CrossRef]
331. Zhou, K.Q.; Qin, Y.; Yuen, C. Transfer-Learning-Based State-of-Health Estimation for Lithium-Ion Battery with Cycle Synchronization. *IEEE/ASME Trans. Mechatron.* **2023**, *28*, 692–702. [CrossRef]
332. Kim, S.; Jung, H.; Lee, M.; Choi, Y.Y.; Choi, J.-I. Model-Free Reconstruction of Capacity Degradation Trajectory of Lithium-Ion Batteries Using Early Cycle Data. *eTransportation* **2023**, *17*, 100243. [CrossRef]
333. Xu, Q.; Wu, M.; Khoo, E.; Chen, Z.; Li, X. A Hybrid Ensemble Deep Learning Approach for Early Prediction of Battery Remaining Useful Life. *IEEE/CAA J. Autom. Sin.* **2023**, *10*, 177–187. [CrossRef]
334. Celik, B.; Sandt, R.; dos Santos, L.C.P.; Spatschek, R. Prediction of Battery Cycle Life Using Early-Cycle Data, Machine Learning and Data Management. *Batteries* **2022**, *8*, 266. [CrossRef]
335. Chen, Z.; Chen, L.; Ma, Z.; Xu, K.; Zhou, Y.; Shen, W. Joint Modeling for Early Predictions of Li-Ion Battery Cycle Life and Degradation Trajectory. *Energy* **2023**, *277*, 127633. [CrossRef]
336. Ansari, S.; Ayob, A.; Hossain Lipu, M.S.; Hussain, A.; Md Saad, M.H. Jellyfish Optimized Recurrent Neural Network for State of Health Estimation of Lithium-Ion Batteries. *Expert Syst. Appl.* **2024**, *238*, 121904. [CrossRef]
337. Amogne, Z.E.; Wang, F.-K.; Chou, J.-H. Transfer Learning Based on Transferability Measures for State of Health Prediction of Lithium-Ion Batteries. *Batteries* **2023**, *9*, 280. [CrossRef]
338. Kheirkhah-Rad, E.; Parvareh, A.; Moeini-Aghtaie, M.; Dehghanian, P. A Data-Driven State-of-Health Estimation Model for Lithium-Ion Batteries Using Referenced-Based Charging Time. *IEEE Trans. Power Deliv.* **2023**, *38*, 3406–3416. [CrossRef]

339. Chou, J.-H.; Wang, F.-K.; Lo, S.-C. A Novel Fine-Tuning Model Based on Transfer Learning for Future Capacity Prediction of Lithium-Ion Batteries. *Batteries* **2023**, *9*, 325. [CrossRef]
340. Gao, J.; Yang, D.; Wang, S.; Li, Z.; Wang, L.; Wang, K. State of Health Estimation of Lithium-Ion Batteries Based on Mixers-Bidirectional Temporal Convolutional Neural Network. *J. Energy Storage* **2023**, *73*, 109248. [CrossRef]
341. Zhao, G.; Kang, Y.; Huang, P.; Duan, B.; Zhang, C. Battery Health Prognostic Using Efficient and Robust Aging Trajectory Matching with Ensemble Deep Transfer Learning. *Energy* **2023**, *282*, 128228. [CrossRef]
342. Lu, Y.; Zhou, S.; Zhou, X.; Yang, S.; Liu, M.; Liu, X.; Ling, H.; Lian, Y. A Novel Method of Prediction for Capacity and Remaining Useful Life of Lithium-Ion Battery Based on Multi-Time Scale Weibull Accelerated Failure Time Regression. *J. Energy Storage* **2023**, *68*, 107589. [CrossRef]
343. Pepe, S.; Ciucci, F. Long-Range Battery State-of-Health and End-of-Life Prediction with Neural Networks and Feature Engineering. *Appl. Energy* **2023**, *350*, 121761. [CrossRef]
344. Fei, Z.; Zhang, Z.; Yang, F.; Tsui, K.-L. Deep Learning Powered Rapid Lifetime Classification of Lithium-Ion Batteries. *eTransportation* **2023**, *18*, 100286. [CrossRef]
345. Wang, C.; Chen, Y.; Luan, W.; Li, S.; Yao, Y.; Chen, H. Interpretable Deep Learning for Accelerated Fading Recognition of Lithium-Ion Batteries. *eTransportation* **2023**, *18*, 100281. [CrossRef]
346. Najera-Flores, D.A.; Hu, Z.; Chadha, M.; Todd, M.D. A Physics-Constrained Bayesian Neural Network for Battery Remaining Useful Life Prediction. *Appl. Math. Model.* **2023**, *122*, 42–59. [CrossRef]
347. Schauser, N.S.; Lininger, C.N.; Leland, E.S.; Sholklapper, T.Z. An Open Access Tool for Exploring Machine Learning Model Choice for Battery Life Cycle Prediction. *Front. Energy Res.* **2022**, *10*, 1058999. [CrossRef]
348. Lu, Z.; Fei, Z.; Wang, B.; Yang, F. A Feature Fusion-Based Convolutional Neural Network for Battery State-of-Health Estimation with Mining of Partial Voltage Curve. *Energy* **2024**, *288*, 129690. [CrossRef]
349. Luo, C.; Zhang, Z.; Zhu, S.; Li, Y. State-of-Health Prediction of Lithium-Ion Batteries Based on Diffusion Model with Transfer Learning. *Energies* **2023**, *16*, 3815. [CrossRef]
350. Chen, X.; Chen, Z.; Zhang, M.; Wang, Z.; Liu, M.; Fu, M.; Wang, P. A Remaining Useful Life Estimation Method Based on Long Short-Term Memory and Federated Learning for Electric Vehicles in Smart Cities. *PeerJ Comput. Sci.* **2023**, *9*, e1652. [CrossRef]
351. Shin, J.; Kim, Y.; Lee, J.M. Feature Construction for On-Board Early Prediction of Electric Vehicle Battery Cycle Life. *Korean J. Chem. Eng.* **2023**, *40*, 1850–1862. [CrossRef]
352. Guo, Y.; Wang, Y.; Ding, P.; Huang, K. Future Degradation Trajectory Prediction of Lithium-Ion Battery Based on a Three-Step Similarity Evaluation Criterion for Battery Selection and Transfer Learning. *J. Energy Storage* **2023**, *72*, 108763. [CrossRef]
353. Chen, D.; Zhang, W.; Zhang, C.; Sun, B.; Zhang, L.; Cong, X. Data-Driven Rapid Lifetime Prediction Method for Lithium-Ion Batteries under Diverse Fast Charging Protocols. *J. Energy Storage* **2023**, *74*, 109285. [CrossRef]
354. Qin, H.; Fan, X.; Fan, Y.; Wang, R.; Shang, Q.; Zhang, D. A Transferable Prediction Approach for the Remaining Useful Life of Lithium-Ion Batteries Based on Small Samples. *Appl. Sci.* **2023**, *13*, 8498. [CrossRef]
355. Chou, J.-H.; Wang, F.-K.; Lo, S.-C. Predicting Future Capacity of Lithium-Ion Batteries Using Transfer Learning Method. *J. Energy Storage* **2023**, *71*, 108120. [CrossRef]
356. Liu, Y.; Fan, G.; Zhou, B.; Chen, S.; Sun, Z.; Wang, Y.; Zhang, X. Rapid and Flexible Battery Capacity Estimation Using Random Short-Time Charging Segments Based on Residual Convolutional Networks. *Appl. Energy* **2023**, *351*, 121925. [CrossRef]
357. Ma, G.; Yang, X.; Xu, S.; Cheng, C.; He, X. ERMN: An Enhanced Meta-Learning Approach for State of Health Estimation of Lithium-Ion Batteries. *J. Energy Storage* **2023**, *72*, 108628. [CrossRef]
358. Lin, Y.-H.; Guan, L.-X.; Chang, L.; Zio, E. A Semisupervised Deep Hybrid Multitask Model for RUL Prediction. *IEEE Trans. Instrum. Meas.* **2023**, *72*, 1–11. [CrossRef]
359. Li, F.; Min, Y.; Zhang, Y.; Zhang, Y.; Zuo, H.; Bai, F. State-of-Health Estimation Method for Fast-Charging Lithium-Ion Batteries Based on Stacking Ensemble Sparse Gaussian Process Regression. *Reliab. Eng. Syst. Saf.* **2024**, *242*, 109787. [CrossRef]
360. Yu, Y.; Hu, C.; Si, X.; Zheng, J.; Zhang, J. Averaged Bi-LSTM Networks for RUL Prognostics with Non-Life-Cycle Labeled Dataset. *Neurocomputing* **2020**, *402*, 134–147. [CrossRef]
361. Liu, Y.; Zhao, G.; Peng, X. Deep Learning Prognostics for Lithium-Ion Battery Based on Ensembled Long Short-Term Memory Networks. *IEEE Access* **2019**, *7*, 155130–155142. [CrossRef]
362. Chen, X.; Liu, Z. A Long Short-Term Memory Neural Network Based Wiener Process Model for Remaining Useful Life Prediction. *Reliab. Eng. Syst. Saf.* **2022**, *226*, 108651. [CrossRef]
363. Guo, Y.; Huang, K.; Yu, X.; Wang, Y. State-of-Health Estimation for Lithium-Ion Batteries Based on Historical Dependency of Charging Data and Ensemble SVR. *Electrochim. Acta* **2022**, *428*, 140940. [CrossRef]
364. Hu, W.; Zhao, S. Remaining Useful Life Prediction of Lithium-Ion Batteries Based on Wavelet Denoising and Transformer Neural Network. *Front. Energy Res.* **2022**, *10*, 969168. [CrossRef]
365. Pan, H.; Chen, C.; Gu, M. A Method for Predicting the Remaining Useful Life of Lithium Batteries Considering Capacity Regeneration and Random Fluctuations. *Energies* **2022**, *15*, 2498. [CrossRef]

366. Zhu, Z.; Yang, Q.; Liu, X.; Gao, D. Attention-Based CNN-BiLSTM for SOH and RUL Estimation of Lithium-Ion Batteries. *J. Algorithm. Comput. Technol.* **2022**, *16*, 174830262211305. [CrossRef]
367. Hemdani, J.; Degaa, L.; Soltani, M.; Rizoug, N.; Telmoudi, A.J.; Chaari, A. Battery Lifetime Prediction via Neural Networks with Discharge Capacity and State of Health. *Energies* **2022**, *15*, 8558. [CrossRef]
368. Zhou, Y.; Wang, S.; Xie, Y.; Shen, X.; Fernandez, C. Remaining Useful Life Prediction and State of Health Diagnosis for Lithium-Ion Batteries Based on Improved Grey Wolf Optimization Algorithm-Deep Extreme Learning Machine Algorithm. *Energy* **2023**, *285*, 128761. [CrossRef]
369. Lin, C.; Xu, J.; Jiang, D.; Hou, J.; Liang, Y.; Zhang, X.; Li, E.; Mei, X. A Comparative Study of Data-Driven Battery Capacity Estimation Based on Partial Charging Curves. *J. Energy Chem.* **2024**, *88*, 409–420. [CrossRef]
370. Ruan, H.; Chen, J.; Ai, W.; Wu, B. Generalised Diagnostic Framework for Rapid Battery Degradation Quantification with Deep Learning. *Energy AI* **2022**, *9*, 100158. [CrossRef]
371. Zhao, H.; Chen, Z.; Shu, X.; Shen, J.; Lei, Z.; Zhang, Y. State of Health Estimation for Lithium-Ion Batteries Based on Hybrid Attention and Deep Learning. *Reliab. Eng. Syst. Saf.* **2023**, *232*, 109066. [CrossRef]
372. Fan, G.; Zhang, X. Battery Capacity Estimation Using 10-Second Relaxation Voltage and a Convolutional Neural Network. *Appl. Energy* **2023**, *330*, 120308. [CrossRef]
373. Gong, Q.; Wang, P.; Cheng, Z. A Data-Driven Model Framework Based on Deep Learning for Estimating the States of Lithium-Ion Batteries. *J. Electrochem. Soc.* **2022**, *169*, 030532. [CrossRef]
374. Xu, X.; Tang, S.; Han, X.; Lu, L.; Wu, Y.; Yu, C.; Sun, X.; Xie, J.; Feng, X.; Ouyang, M. Fast Capacity Prediction of Lithium-Ion Batteries Using Aging Mechanism-Informed Bidirectional Long Short-Term Memory Network. *Reliab. Eng. Syst. Saf.* **2023**, *234*, 109185. [CrossRef]
375. Lin, M.; Yan, C.; Wang, W.; Dong, G.; Meng, J.; Wu, J. A Data-Driven Approach for Estimating State-of-Health of Lithium-Ion Batteries Considering Internal Resistance. *Energy* **2023**, *277*, 127675. [CrossRef]
376. Liu, B.; Xu, J.; Xia, W. State-of-Health Estimation for Lithium-Ion Battery Based on an Attention-Based CNN-GRU Model with Reconstructed Feature Series. *Int. J. Energy Res.* **2023**, *2023*, 8569161. [CrossRef]
377. Wang, Y.; Kou, P.; Fan, J.; Zhou, N. A Novel Capacity Estimation Method for Li-Ion Battery Cell by Applying Ensemble Learning to Extremely Sparse Significant Points. *IEEE Access* **2022**, *10*, 96427–96441. [CrossRef]
378. Chen, S.; Zhang, H.; Zeng, L.; Fan, Y.; Chang, L.; Zhang, Y. Secondary Structural Ensemble Learning Cluster for Estimating the State of Health of Lithium-Ion Batteries. *ACS Omega* **2022**, *7*, 17406–17415. [CrossRef] [PubMed]
379. Zhang, X.; Fan, J.; Zou, Y.; Sun, W. Realizing Accurate Battery Capacity Estimation Using 4 Min 1C Discharging Data. *Energy* **2023**, *282*, 128744. [CrossRef]
380. Yang, N.; Yu, T.; Luo, Q.; Wang, K. Fast and Accurate Health Assessment of Lithium-Ion Batteries Based on Typical Voltage Segments. *Front. Energy Res.* **2022**, *10*, 925947. [CrossRef]
381. Lim, L.D.; Tan, A.F.J.; Tomacruz, J.G.T.; Castro, M.T.; Remolona, M.F.M.; Ocon, J.D. Cyclic Degradation Prediction of Lithium-Ion Batteries Using Data-Driven Machine Learning. *Chem. Eng. Trans.* **2022**, *94*, 787–792. [CrossRef]
382. Wang, W.; Yang, G.; Li, M.; Yan, Z.; Zhang, L.; Yu, H.; Yang, K.; Jiang, P.; Hua, W.; Zhang, Y.; et al. State-of-Health Estimation for Lithium-Ion Batteries Based on Bi-LSTM-AM and LLE Feature Extraction. *Front. Energy Res.* **2023**, *11*, 1205165. [CrossRef]
383. Li, W.; Li, Y.; Garg, A.; Gao, L. Enhancing Real-Time Degradation Prediction of Lithium-Ion Battery: A Digital Twin Framework with CNN-LSTM-Attention Model. *Energy* **2024**, *286*, 129681. [CrossRef]
384. Lu, J.; Xiong, R.; Tian, J.; Wang, C.; Hsu, C.-W.; Tsou, N.-T.; Sun, F.; Li, J. Battery Degradation Prediction against Uncertain Future Conditions with Recurrent Neural Network Enabled Deep Learning. *Energy Storage Mater.* **2022**, *50*, 139–151. [CrossRef]
385. Ma, G.; Xu, S.; Jiang, B.; Cheng, C.; Yang, X.; Shen, Y.; Yang, T.; Huang, Y.; Ding, H.; Yuan, Y. Real-Time Personalized Health Status Prediction of Lithium-Ion Batteries Using Deep Transfer Learning. *Energy Environ. Sci.* **2022**, *15*, 4083–4094. [CrossRef]
386. Wang, J.; Zhang, F.; Zhang, J.; Liu, W.; Zhou, K. A Flexible RUL Prediction Method Based on Poly-Cell LSTM with Applications to Lithium Battery Data. *Reliab. Eng. Syst. Saf.* **2023**, *231*, 108976. [CrossRef]
387. Xia, J.; Shi, Q.; Li, H.; Zhou, M.; Wang, W.; Wang, K.; Jiang, K. Historical Data-Independent Remaining Useful Life Prediction Method Based on Dual-Input Deep Learning Neural Network. *J. Energy Storage* **2023**, *72*, 108427. [CrossRef]
388. Jiang, Y.; Song, W. Predicting the Cycle Life of Lithium-Ion Batteries Using Data-Driven Machine Learning Based on Discharge Voltage Curves. *Batteries* **2023**, *9*, 413. [CrossRef]
389. Zhang, S.; Zhu, H.; Wu, J.; Chen, Z. Voltage Relaxation-Based State-of-Health Estimation of Lithium-Ion Batteries Using Convolutional Neural Networks and Transfer Learning. *J. Energy Storage* **2023**, *73*, 108579. [CrossRef]
390. Wang, Y.; Zhu, J.; Cao, L.; Gopaluni, B.; Cao, Y. Long Short-Term Memory Network with Transfer Learning for Lithium-Ion Battery Capacity Fade and Cycle Life Prediction. *Appl. Energy* **2023**, *350*, 121660. [CrossRef]
391. Chen, S.-Z.; Liang, Z.; Yuan, H.; Yang, L.; Xu, F.; Fan, Y. A Novel State of Health Estimation Method for Lithium-Ion Batteries Based on Constant-Voltage Charging Partial Data and Convolutional Neural Network. *Energy* **2023**, *283*, 129103. [CrossRef]

392. Chen, S.-Z.; Liang, Z.; Yuan, H.; Yang, L.; Xu, F.; Zhang, Y. Li-Ion Battery State-of-Health Estimation Based on the Combination of Statistical and Geometric Features of the Constant-Voltage Charging Stage. *J. Energy Storage* **2023**, *72*, 108647. [CrossRef]
393. Fan, Y.; Li, Y.; Zhao, J.; Wang, L.; Yan, C.; Wu, X.; Zhang, P.; Wang, J.; Gao, G.; Wei, L. Online State-of-Health Estimation for Fast-Charging Lithium-Ion Batteries Based on a Transformer–Long Short-Term Memory Neural Network. *Batteries* **2023**, *9*, 539. [CrossRef]
394. Jafari, S.; Byun, Y.-C. Optimizing Battery RUL Prediction of Lithium-Ion Batteries Based on Harris Hawk Optimization Approach Using Random Forest and LightGBM. *IEEE Access* **2023**, *11*, 87034–87046. [CrossRef]
395. Granado, L.; Ben-Marzouk, M.; Solano Saenz, E.; Boukal, Y.; Jugé, S. Machine Learning Predictions of Lithium-Ion Battery State-of-Health for eVTOL Applications. *J. Power Sources* **2022**, *548*, 232051. [CrossRef]
396. Pozzato, G.; Allam, A.; Onori, S. Lithium-Ion Battery Aging Dataset Based on Electric Vehicle Real-Driving Profiles. *Data Br.* **2022**, *41*, 107995. [CrossRef]
397. Zhang, Y.; Tang, Q.; Zhang, Y.; Wang, J.; Stimming, U.; Lee, A.A. Identifying Degradation Patterns of Lithium Ion Batteries from Impedance Spectroscopy Using Machine Learning. *Nat. Commun.* **2020**, *11*, 1706. [CrossRef] [PubMed]
398. Fernando, A.; Kuipers, M.; Angenendt, G.; Kairies, K.-P.; Dubarry, M. Benchmark Dataset for the Study of the Relaxation of Commercial NMC-811 and LFP Cells. *Cell Rep. Phys. Sci.* **2024**, *5*, 101754. [CrossRef]
399. Khaleghi, S.; Firouz, Y.; Berecibar, M.; Van Mierlo, J.; Bossche, P. Van Den Ensemble Gradient Boosted Tree for SoH Estimation Based on Diagnostic Features. *Energies* **2020**, *13*, 1262. [CrossRef]
400. Jafari, S.; Shahbazi, Z.; Byun, Y.-C. Lithium-Ion Battery Health Prediction on Hybrid Vehicles Using Machine Learning Approach. *Energies* **2022**, *15*, 4753. [CrossRef]
401. Xu, S.; Zha, F.-L.; Huang, B.-W.; Yu, B.; Huang, H.-B.; Zhou, T.; Mao, W.-Q.; Wu, J.-J.; Wei, J.-Q.; Gong, S.-K.; et al. Research on the State of Health Estimation of Lithium-Ion Batteries for Energy Storage Based on XGB-AKF Method. *Front. Energy Res.* **2023**, *10*, 999676. [CrossRef]
402. Jiao, Z.; Wang, H.; Xing, J.; Yang, Q.; Yang, M.; Zhou, Y.; Zhao, J. LightGBM-Based Framework for Lithium-Ion Battery Remaining Useful Life Prediction Under Driving Conditions. *IEEE Trans. Ind. Inform.* **2023**, *19*, 11353–11362. [CrossRef]
403. Liu, H.; Xiao, Q.; Jin, Y.; Mu, Y.; Meng, J.; Zhang, T.; Jia, H.; Teodorescu, R. Improved LightGBM-Based Framework for Electric Vehicle Lithium-Ion Battery Remaining Useful Life Prediction Using Multi Health Indicators. *Symmetry* **2022**, *14*, 1584. [CrossRef]
404. Zhang, Z.; Wang, S.; Lin, N.; Wang, Z.; Liu, P. State of Health Estimation of Lithium-Ion Batteries in Electric Vehicles Based on Regional Capacity and LGBM. *Sustainability* **2023**, *15*, 2052. [CrossRef]
405. Dong, J.; Yu, Z.; Zhang, X.; Luo, J.; Zou, Q.; Feng, C.; Ma, X. Data-Driven Predictive Prognostic Model for Power Batteries Based on Machine Learning. *Process Saf. Environ. Prot.* **2023**, *172*, 894–907. [CrossRef]
406. Li, R.; Hong, J.; Zhang, H.; Chen, X. Data-Driven Battery State of Health Estimation Based on Interval Capacity for Real-World Electric Vehicles. *Energy* **2022**, *257*, 124771. [CrossRef]
407. Mawonou, K.S.R.; Eddahech, A.; Dumur, D.; Beauvois, D.; Godoy, E. State-of-Health Estimators Coupled to a Random Forest Approach for Lithium-Ion Battery Aging Factor Ranking. *J. Power Sources* **2021**, *484*, 229154. [CrossRef]
408. Géron, A. *Hands-On Machine Learning with Scikit-Learn, Keras, and TensorFlow*; O'Reilly Media, Inc.: Sebastopol, CA, USA, 2022; ISBN 1-09-812246-1.
409. Wang, J.; Zhang, S.; Li, C.; Wu, L.; Wang, Y. A Data-Driven Method with Mode Decomposition Mechanism for Remaining Useful Life Prediction of Lithium-Ion Batteries. *IEEE Trans. Power Electron.* **2022**, *37*, 13684–13695. [CrossRef]
410. Luo, L.; Zhang, C.; Tian, Y.; Liu, H. State-of-Health Estimate for the Lithium-Ion Battery Based on Constant Voltage Current Entropy and Charging Duration. *World Electr. Veh. J.* **2022**, *13*, 148. [CrossRef]
411. Su, L.; Wu, M.; Li, Z.; Zhang, J. Cycle Life Prediction of Lithium-Ion Batteries Based on Data-Driven Methods. *eTransportation* **2021**, *10*, 100137. [CrossRef]
412. Ibraheem, R.; Strange, C.; dos Reis, G. Capacity and Internal Resistance of Lithium-Ion Batteries: Full Degradation Curve Prediction from Voltage Response at Constant Current at Discharge. *J. Power Sources* **2023**, *556*, 232477. [CrossRef]
413. Liu, K.; Tang, X.; Teodorescu, R.; Gao, F.; Meng, J. Future Ageing Trajectory Prediction for Lithium-Ion Battery Considering the Knee Point Effect. *IEEE Trans. Energy Convers.* **2022**, *37*, 1282–1291. [CrossRef]
414. Buchanan, S.; Crawford, C. Probabilistic Lithium-Ion Battery State-of-Health Prediction Using Convolutional Neural Networks and Gaussian Process Regression. *J. Energy Storage* **2024**, *76*, 109799. [CrossRef]
415. Zhou, D.; Yin, H.; Fu, P.; Song, X.; Lu, W.; Yuan, L.; Fu, Z. Prognostics for State of Health of Lithium-Ion Batteries Based on Gaussian Process Regression. *Math. Probl. Eng.* **2018**, *2018*, 8358025. [CrossRef]
416. Chen, Z.; Xue, Q.; Xiao, R.; Liu, Y.; Shen, J. State of Health Estimation for Lithium-Ion Batteries Based on Fusion of Autoregressive Moving Average Model and Elman Neural Network. *IEEE Access* **2019**, *7*, 102662–102678. [CrossRef]
417. Schofer, K.; Laufer, F.; Stadler, J.; Hahn, S.; Gaiselmann, G.; Latz, A.; Birke, K.P. Machine Learning-Based Lifetime Prediction of Lithium-Ion Cells. *Adv. Sci.* **2022**, *9*, 2200630. [CrossRef]

418. Mitchell, L.; Subramanian, V. *Deep Learning with Pytorch 1. x Implement Deep Learning Techniques and Neural Network Architecture Variants Using Python*, 2nd ed.; Packt Publishing, Limited: Birmingham, UK, 2019; ISBN 978-1-83855-300-5.
419. Muller, A.C.; Guido, S. *Introduction to Machine Learning with Python*; O'Reilly: Sebastopol, CA, USA, 2017.
420. Goodfellow, I.; Bengio, Y.; Courville, A. *Deep Learning*; MIT Press: Cambridge, MA, USA, 2016; ISBN 0-262-33737-1.
421. Schmidhuber, J. Deep Learning in Neural Networks: An Overview. *Neural Netw.* **2015**, *61*, 85–117. [CrossRef] [PubMed]
422. Wu, Y.; Xue, Q.; Shen, J.; Lei, Z.; Chen, Z.; Liu, Y. State of Health Estimation for Lithium-Ion Batteries Based on Healthy Features and Long Short-Term Memory. *IEEE Access* **2020**, *8*, 28533–28547. [CrossRef]
423. Gong, Y.; Zhang, X.; Gao, D.; Li, H.; Yan, L.; Peng, J.; Huang, Z. State-of-Health Estimation of Lithium-Ion Batteries Based on Improved Long Short-Term Memory Algorithm. *J. Energy Storage* **2022**, *53*, 105046. [CrossRef]
424. Tsai, C.-F.; Chen, M.-L. Credit Rating by Hybrid Machine Learning Techniques. *Appl. Soft Comput.* **2010**, *10*, 374–380. [CrossRef]
425. Liu, K.; Kang, L.; Xie, D. Online State of Health Estimation of Lithium-Ion Batteries Based on Charging Process and Long Short-Term Memory Recurrent Neural Network. *Batteries* **2023**, *9*, 94. [CrossRef]
426. Chen, X.-D.; Yang, H.-Y.; Wun, J.-S.; Wang, C.-H.; Li, L.-L. Life Prediction of Lithium-Ion Battery Based on a Hybrid Model. *Energy Explor. Exploit.* **2020**, *38*, 1854–1878. [CrossRef]
427. Jafari, S.; Byun, Y.-C.; Ko, S. A Novel Approach for Predicting Remaining Useful Life and Capacity Fade in Lithium-Ion Batteries Using Hybrid Machine Learning. *IEEE Access* **2023**, *11*, 131950–131963. [CrossRef]
428. Lee, J.; Sun, H.; Liu, Y.; Li, X. A Machine Learning Framework for Remaining Useful Lifetime Prediction of Li-Ion Batteries Using Diverse Neural Networks. *Energy AI* **2024**, *15*, 100319. [CrossRef]
429. Weiss, K.; Khoshgoftaar, T.M.; Wang, D. A Survey of Transfer Learning. *J. Big Data* **2016**, *3*, 9. [CrossRef]
430. Zhuang, F.; Qi, Z.; Duan, K.; Xi, D.; Zhu, Y.; Zhu, H.; Xiong, H.; He, Q. A Comprehensive Survey on Transfer Learning. *Proc. IEEE* **2021**, *109*, 43–76. [CrossRef]
431. Torrey, L.; Shavlik, J. *Handbook of Research on Machine Learning Applications and Trends: Algorithms, Methods, and Techniques*; IGI Publishing: Hershey, PA, USA, 2010.
432. Shu, X.; Shen, J.; Li, G.; Zhang, Y.; Chen, Z.; Liu, Y. A Flexible State-of-Health Prediction Scheme for Lithium-Ion Battery Packs with Long Short-Term Memory Network and Transfer Learning. *IEEE Trans. Transp. Electrif.* **2021**, *7*, 2238–2248. [CrossRef]
433. Ma, J.; Shang, P.; Zou, X.; Ma, N.; Ding, Y.; Sun, J.; Cheng, Y.; Tao, L.; Lu, C.; Su, Y.; et al. A Hybrid Transfer Learning Scheme for Remaining Useful Life Prediction and Cycle Life Test Optimization of Different Formulation Li-Ion Power Batteries. *Appl. Energy* **2021**, *282*, 116167. [CrossRef]
434. Torres, N.N.S.; Ledesma, J.J.G.; Cavallari, M.R.; Ando Junior, O.H. Amazon Kit: Proposal for an Innovative Energy Generation and Storage Solution for Sustainable Development of Isolated Communities. *Sustainability* **2024**, *16*, 6280. [CrossRef]
435. Torres, N.N.S.; Diaz, V.N.S.; Ando Junior, O.H.; Ledesma, J.J.G. Analysis of the Technical Feasibility of Using Artificial Intelligence for Smoothing Active Power in a Photovoltaic System Connected to the Power System. *Braz. Arch. Biol. Technol.* **2021**, *64*, e21210196. [CrossRef]
436. Diaz, V.S.; Cantane, D.A.; Santos, A.Q.O.; Ando Junior, O.H. Comparative Analysis of Degradation Assessment of Battery Energy Storage Systems in PV Smoothing Application. *Energies* **2021**, *14*, 3600. [CrossRef]
437. Ando Junior, O.H.; Bretas, A.S.; Leborgne, R.C. Methodology for Calculation and Management for Indicators of Power Quality Energy. *IEEE Lat. Am. Trans.* **2015**, *13*, 2217–2224. [CrossRef]
438. Sylvestrin, G.R.; Scherer, H.F.; Ando Junior, O.H. Hardware and Software Development of an Open Source Battery Management System. *IEEE Lat. Am. Trans.* **2021**, *19*, 1153–1163. [CrossRef]
439. Gimenes, T.K.; da Silva, M.P.C.; Giménez Ledesma, J.J.; Ando, O.H. Impact of distributed energy resources on power quality: Brazilian scenario analysis. *Electr. Power Syst. Res.* **2022**, *211*, 108249. [CrossRef]

A.2: Publicação 2

Fase: em revisão.

EXTRAÇÃO ABRANGENTE DE ATRIBUTOS PARA O PROGNÓSTICO DA SAÚDE DE BATERIAS: IDENTIFICAÇÃO DE INDICADORES PREDITIVOS DO ESTADO DE SAÚDE

Giovane Ronei Sylvestrin[1-2], Joylan Nunes Maciel[1-2] and Oswaldo Hideo Ando Junior[2-3]

[1]Federal University of Latin American Integration (UNILA), Foz do Iguaçu 85867-000, Brazil.
giovane.sylvestrin@gmail.com (G.R.S.), joylan.maciel@unila.edu.br (J.N.M.)
[2]Research Group on Energy & Energy Sustainability (GPEnSE), Pernambuco 54518-430, PE, Brazil.
[3]Federal University of Paraiba (UFPB), Paraiba, Brazil, 56036-000,
oswaldo.junior@cear.ufpb.br (O.H.A.J.)

Abstract
Accurate estimation of battery state of health (SOH) is crucial for ensuring the safety, reliability, and operational efficiency of energy storage systems in electric vehicles, consumer electronics, and grid applications. Traditional approaches often rely on a limited set of handcrafted features derived from electrochemical analyses, such as incremental capacity, differential voltage, and constant-current/constant-voltage (CC-CV) phases, which restrict their predictive power and generalizability. This study introduces a comprehensive machine learning pipeline for large-scale feature engineering and SOH modeling using only standard sensor data: current, voltage, temperature, and time. Using a public dataset, we generate over 40,000 features across seven domain-informed groups that capture both charge and discharge dynamics. Feature relevance is assessed through univariate analyses (Spearman correlation, Predictive Power Score, and single-feature models) and multivariate modeling within a unified selection pipeline. Prediction targets include remaining useful life (RUL) and future discharge capacity at 10, 50, 100, and 250 cycles ahead. In total, we develop 40 final LightGBM (Light Gradient Boosting Machine) models, spanning the complete feature space and individual feature groups. Model optimization employs a hybrid selection strategy combining SHAP (SHapley Additive exPlanations)-based importance ranking, forward feature selection, and recovery techniques using BorutaShap and minimum redundancy maximum relevance (MRMR). Across all models, 773 unique features are retained, forming a compact yet highly informative subset. The best RUL models achieve a mean absolute percentage error of approximately 10%, while capacity-forecasting errors remain below 1% across all prediction horizons. Notably, unconventional sliding-window features consistently rank among the most informative predictors, often surpassing traditional indicators. These findings demonstrate that broad and systematic feature exploration, integrated with robust univariate–multivariate selection and interpretable modeling, substantially improves SOH prediction accuracy and generalizability. The proposed framework is scalable and adaptable for data-driven SOH estimation, offering a strong basis for advancing battery diagnostics and prognostics.

Keywords: State of Health (SOH), Remaining Useful Life (RUL), Lithium-Ion Batteries, Machine Learning, Feature Extraction, Feature Selection.

Highlights:

- Introduces a **reproducible framework extracting >40,000 features** from battery signals and derivative analyses.
- Proposes a **systematic pipeline for feature selection** that integrates univariate screening, group-wise multivariate evaluation.
- **Applies the pipeline to 40 models for SOH targets** (RUL, future capacity at $N \in \{10, 50, 100, 250\}$), achieving MAPE ≈10% (RUL) and <1% (capacity).

- **Identifies 773 finalist features as benchmarks**, demonstrating scalability for BMS, diagnostics, lifetime prediction, and second-life applications.
- Shows **sliding-window features compose ~88% of selected subsets**, highlighting predictive strength and model interpretability.

List of Abbreviations

- BMS – battery management system
- CC – constant current
- CV – constant voltage
- CVCT – constant-voltage charge time
- DV – differential voltage
- ECM – equivalent circuit model
- EIS – electrochemical impedance spectroscopy
- EOL – end-of-life
- EV – electric vehicle
- I – current
- IC – incremental capacity
- LAM - loss of active material
- LLI - loss of lithium inventory
- MAE – mean absolute error
- MAPE – mean absolute percentage error
- MRMR – minimum redundancy maximum relevance
- OOS – out of sample
- PBW – peak bandwidth
- PPS – power predictive score
- R – resistance
- RMSE – root mean squared error
- RUL – remaining useful life
- SHAP – shapley additive explanations
- SEI – solid electrolyte interphase
- SOC – state of charge
- SOH – state of health
- T – temperature
- V – voltage

1. Introduction

Lithium-ion batteries have emerged as the dominant energy storage solution across a wide range of applications, including electric vehicles (EVs), stationary energy systems, and portable electronics, driven by their high energy density, durability, and steadily decreasing costs. According to the International Energy Agency (IEA), battery demand for EVs exceeded 750 GWh in 2023, marking a 40% increase compared to 2022 [1]. The global stock of EVs surpassed 45 million in 2023 and is projected to reach 250 million by 2030 and over 525 million by 2035, with a compound annual growth rate of approximately 23% [1]. This expansion heightens the need for reliable battery health assessment to ensure safety, performance, and cost-effectiveness over the full lifecycle.

Like all electrochemical systems, lithium-ion cells degrade with use and time, exhibiting capacity fade and resistance growth driven by operating and environmental conditions (e.g., C-rate, depth of discharge, temperature, duty cycle) [2]. Accurate estimation of State of Health (SOH) is therefore essential for safe operation, predictive maintenance, warranty management, and second-life deployment [3][4]. Several indicators have been proposed in the literature to quantify battery health and forecast future performance. Among them, SOH remains the most widely adopted, typically defined as the ratio of the current usable capacity

to the rated capacity at the beginning of life [5]. In addition to SOH, other prognostic metrics include the Remaining Useful Life (RUL), the estimated number of cycles or time until the battery reaches its end-of-life threshold, and capacity trajectory models, which characterize the degradation path over time [6]. The ability to predict these indicators based on partial or early-cycle data is particularly valuable for real-time monitoring, intelligent battery management systems (BMS), and second-use decision-making [4,7].

Approaches to health estimation span physics-based models, with electrochemical and equivalent-circuit formulations, and data-driven models that learn directly from sensor signals (voltage, current, temperature, time) [5,6]. In both paradigms, the informativeness of features (health indicators) is a primary determinant of predictive accuracy and generalization [8]. Consequently, systematic feature design and selection remain central challenges in battery diagnostics and prognostics [5,8].

Prior data-driven studies have typically relied on a limited set of handcrafted features derived from charge-discharge profiles, often restricted to simple statistical descriptors or specific cycle segments and prior knowledge dominion [9–14]. A second influential line of research has focused on features extracted from the capacity-voltage curve Q(V) and its differentials, Incremental Capacity (IC, dQ/dV) and Differential Voltage (DV, dV/dQ), which reveal electrochemical signatures by transforming voltage plateaus into peaks and valleys. These analyses have proven useful for aging-mechanism identification as well as SOH and RUL estimation across diverse chemistries and formats [6,15–18].

Despite these advances, three gaps persist. First, most studies remain constrained to a relatively small set of handcrafted features, typically a few dozen, and often restrict their scope to either the charging or discharging phase. Moreover, there is a noticeable lack of systematic frameworks that explore more comprehensive feature sets, including temporal descriptors such as lag features and sliding windows. Second, candidate features are frequently screened with a single heuristic (e.g., correlation or a model's importance), risking the premature removal of features that are weak individually but complementary jointly. Third, there is limited use of scalable, reproducible pipelines capable of handling thousands of candidates features while explicitly evaluating interactions and redundancy in a multivariate setting, and few works compare feature-group utility across multiple target definitions.

To address these limitations, we propose a scalable pipeline for large-scale feature engineering and predictive modeling of battery health using only standard sensor data (current, voltage, temperature, time). We systematically generate more than 40,000 features across seven domain-informed groups: General Charge, General Discharge, CCCV-based Charge, dQ/dV-based Charge, dQ/dV-based Discharge, dV/dQ-based Charge, and dV/dQ-based Discharge. These features include basic statistics, entropy and frequency-domain measures, and temporally aware constructs - lags, sliding windows from 1 to 100 cycles, and cycle-shifted differences. We evaluate two classes of targets: RUL and future discharge capacity at horizons $N \in \{10,50,100,250\}$ cycles ahead. This set spans short to long-term forecasting while preserving sufficient sample volume for model training (longer horizons would censor a larger fraction of the dataset and materially reduce training data). In total, 40 models were trained and interpreted using SHAP (SHapley Additive exPlanations) to identify the most influential features.

Feature relevance is assessed from complementary ways. We perform univariate analyses with Spearman correlation, Predictive Power Score (PPS), and single-feature models, followed by multivariate modeling within a unified, reproducible selection pipeline. The multivariate stage leverages SHAP-based importance, forward selection, and dual "recovery" filters using BorutaShap and minimum redundancy maximum relevance (MRMR) to retain features that are either individually strong or synergistic in combination.

Therefore, the main contributions of this study are:

- A reproducible, large-scale feature engineering protocol, with more than 40,000 features, that unifies signal and derivative-based indicators with temporal descriptors;
- A unified univariate-multivariate selection pipeline that is scalable to thousands of features and explicitly evaluates interactions and redundancy;

- A systematic comparison of seven feature groups across RUL and capacity-at-horizon targets;
- A compact, high-value feature subset derived from charge and discharge processes, robust across multiple target definitions, with consistently predictive power.

The remainder of the paper is organized as follows: Section 2 reviews related works on data-driven SOH estimation, emphasizing the features that were extracted and analyzed; Section 3 introduces the materials and methods, including the dataset, target definitions, feature engineering process, and the proposed pipeline for feature evaluation and selection; Section 4 discusses results, highlighting key univariate and multivariate features and overall model performance; and Section 5 concludes with final remarks and directions for future research.

2. Related Works

Battery health estimation has been investigated through multiple methodological perspectives that can be broadly grouped into direct measurement methods, model-based approaches, and data-driven methods. Direct measurement techniques, such as Coulomb counting and electrochemical impedance spectroscopy (EIS), are capable of providing accurate health indicators but typically require specific test conditions and long execution times, which limit their applicability in online and real use cases [19,20].

Model-based approaches in equivalent circuit models (ECMs) approximate electrochemical processes using electrical analogies based on resistors and capacitors [21]. By monitoring parameters such as ohmic resistance, polarization resistance, and capacitance, these models provide valuable insights into degradation [22–24]. Their parameters are often estimated through adaptive filters, including Kalman filter variants [25,26]. While ECMs improve computational tractability compared to full electrochemical models, they still face limitations in robustness and adaptability, as parameter identification often requires EIS or controlled experiments that are impractical in embedded applications [27–29]. Electrochemical and physics-informed models, such as P2D or electro-thermal formulations, capture degradation mechanisms like lithium plating, active material loss, and solid electrolyte interphase (SEI) growth [30–32]. These models enable fundamental insights into battery aging, but solving the associated partial differential equations involves hundreds of uncertain parameters, making them computationally prohibitive and difficult to generalize under noisy, real-world conditions [32].

In contrast, data-driven methods, particularly those based on machine learning, have gained prominence in recent years as mechanism-agnostic alternatives [33]. They map SOH and related targets directly from features derived from measurable signals (voltage, current, temperature, time, etc.), offering reduced computational complexity and greater scalability [5,34]. Such approaches leverage statistical learning to handle uncertainty, exploit high-dimensional feature spaces, and model degradation without explicit reliance on physics-based assumptions [35,36]. The rapid growth of data-driven research has also been propelled by the increasing availability of public datasets, which enable the development, benchmarking, and fair comparison of methods. A comprehensive survey of open-access datasets for battery health estimation is presented in [37], consolidating the key resources that are now widely used for experimental validation and reproducibility.

Several studies focused on the development of machine learning pipelines for battery SOH prediction that rely on raw signals such as voltage, current, temperature, and time. One of the most common approaches involves extracting features directly from these signals without further transformation. For instance, [9] uses the constant current (CC) and constant voltage (CV) phases of the charging process to extract 30 domain-based features. The most relevant features are then selected using a random forest-based recursive feature elimination with cross-validation. Similarly, [10] extracts energy-related features from the CC and CV segments, as well as energy in equal discharge voltage intervals, using them to predict SOH through Gaussian process regression. In [11], the authors propose 26 health indicators

derived from voltage, current, temperature, and time measurements during CC and CV charging steps, such as the area under the current curve during CC and the maximum slope of the current curve during CV. These features are subsequently structured as a graph for modeling. In [12], five charging-related features, including initial charge voltage, CC-CV charge capacity, and final voltage/current values, are used for capacity prediction with a k-nearest neighbor's model.

In [13] 44 features are extracted from both charging and discharging phases. These include statistical descriptors (minimum, maximum, range, skewness, kurtosis, 5th and 6th moment) of voltage, current, and temperature, along with the duration of each process. Feature selection is performed using Spearman correlation with the target variable and redundancy elimination, followed by random forest-based importance filtering. Likewise, [14] collects 300 seconds of data from various points of the charging process and extracts 10 statistical features from voltage signals, such as mean, variance, skewness, and kurtosis.

Despite the simplicity of using raw data statistics, studies have demonstrated that transforming these signals into derived curves can yield more predictive power. The Q(V) curve obtained during charge and discharge cycles, carries information about the electrochemical behavior of lithium-ion batteries [38]. Derivative analyses of this curve, such as IC and DV, have gained prominence for non-invasive battery diagnostics and SOH estimation [39]. The IC curve, defined as dQ/dV versus voltage, transforms flat voltage plateaus into well-defined peaks and valleys, which correspond to specific phase transitions and electrochemical reactions [5,40]. The temporal evolution of these features reflects degradation mechanisms such as loss of active material and structural reorganization of electrodes [40]. In contrast, the DV curve, defined as dV/dQ versus capacity, provides complementary insight by highlighting transitions along the capacity axis. However, since capacity is itself a degradation-sensitive quantity, IC analysis is generally considered more robust for long-term SOH tracking, with voltage serving as a more stable reference [5].

In [15], 20 features are extracted from Q(V) curves in both charge and discharge cycles to enable early prediction of RUL. These features include statistics computed over differences between Q(V) curves from early and late cycles (e.g., mean difference between cycles 2 and 100). Similarly, [16] estimates RUL using statistical descriptors (minimum, maximum, mean, variance, skewness) derived from Q(V) curves, in addition to domain-specific features such as those proposed by [6], which rely on the distance between Q(V) curves across cycles. In [41], 43 features are extracted, including 11 derived from IC/DV analysis, alongside others based on voltage, current, and temperature. Feature selection combines Pearson correlation filtering and wrapper-based techniques. In [38], a total of 72 features are extracted from the first 250 cycles of raw battery data. These include statistical measures, features from original voltage-capacity/time curves, and processed curves (Q(V), dQ/dV, dV/dQ). Additional studies [6,37,39–47] further support the effectiveness of IC/DV analysis in enhancing SOH and RUL estimation accuracy.

A comparative overview of representative studies is summarized in Table 1, which outlines the number of features, data requirements, and feature types employed. The review reveals four recurring patterns: (i) a narrow feature space, typically restricted to a few dozen handcrafted variables, even when combining raw measurements and derivative-based descriptors; (ii) the absence of systematic methodologies for large-scale feature extraction, with most studies relying on incremental reuse of domain knowledge from prior works; (iii) a limited exploitation of temporal dependencies, as most approaches rely on the last available cycle, while historical information, when used, is usually restricted to simple early-cycle statistics. This overlooks more systematic strategies, such as sliding-window or lag-based descriptors, which could better capture long-term patterns and support prediction throughout the battery's lifecycle; and (iv) feature selection methods that remain predominantly univariate (e.g., correlation), overlooking multivariate relationships and redundancy handling.

These findings reinforce the three main gaps identified in introduction: a restricted feature space, oversimplified feature selection, and the lack of scalable, reproducible pipelines. The performance of data-driven models is strongly dependent on the quality of feature engineering, which remains an open challenge in the field [48].

In contrast, the framework proposed in this work directly addresses these limitations by (i) systematically expanding the feature pool to encompass raw, derivative, and temporal descriptors, (ii) integrating both univariate and multivariate feature selection strategies to preserve complementary predictors, and (iii) providing a scalable pipeline that unifies feature extraction, selection, interpretability, and benchmarking across multiple SOH-based targets, including RUL and future capacity.

Table 1 – Comparative overview of feature extraction conditions for SOH-based prediction studies.

Ref.	#Features	Cycle Segment	Historical Data Requirement and Observations	Feature Types
State of health estimation for lithium-ion battery based on energy features [10]	3	Charge	Last cycle	CC-CV
Machine learning pipeline for battery state-of-health estimation [9]	30	Charge	Last cycle and 1-cycle lag features Cumulative charge capacity and energy as historical inputs	CC-CV
A Hybrid Ensemble Deep Learning Approach for Early Prediction of Battery Remaining Useful Life [16]	25	Discharge	Early 100 cycles for RUL prediction Features derived from cycle interactions: 100-2, 100-10, 100-91) Charging time of first 5 cycles used as features	Q(V)
Prediction of remaining useful life for lithium-ion battery with multiple health indicators [49]	4	Discharge	Last cycle	V, T, R, time
A Method for Interval Prediction of Satellite Battery State of Health Based on Sample Entropy [50]	2	Discharge	Last cycle	V
Battery Health Prediction Using Fusion-Based Feature Selection and Machine Learning [41]	43	Charge and discharge	Last cycle	dQ/dV, dV/dQ, V, T, time
An indirect remaining useful life prognosis for Li-ion batteries based on health indicator and novel artificial neural network [51]	10	Charge and discharge	Last cycle	time, V, I, T
Lifespan prediction of lithium-ion batteries based on various extracted features and gradient boosting regression tree model [38]	72	Discharge	Early 250 cycles for cycle life prediction Features derived from cycle interactions: 30-100, 30-150, 30-200, 30-250	Q(V)
Accurate and Efficient SOH Estimation for Retired Batteries [4]	12	Charge	Last cycle	V, time
Early prediction of cycle life for lithium-ion batteries based on evolutionary computation and machine learning [15]	20	Charge and discharge	Early 100 cycles as input for cycle life prediction Interaction features among cycles 100, 50, and 2	Q(V), R
A novel graph-based framework for state of health prediction of lithium-ion battery [11]	26	Charge	Last cycle	CC-CV
An open access tool for exploring machine learning model choice for battery life cycle prediction [52]	13	Discharge	Early 100 cycles as input for cycle life prediction Interaction features among cycles 100 and 2	Q(V)
Data-driven method based on particle swarm optimization and k-nearest neighbor regression for estimating capacity of lithium-ion battery [12]	5	Charge	Last cycle	CC-CV
Time Series Feature extraction for Lithium-Ion batteries State-Of-Health prediction [53]	48	Charge and discharge	Last cycle	V, I, T
Machine learning for predicting battery capacity for electric vehicles [8]	39	Discharge	Last cycle	dQ/dV, dV/dQ
Lithium-Ion Battery State of Health Monitoring Based on Ensemble Learning [54]	6	Discharge	Last cycle	dQ/dV, V, time
A machine learning-based framework for online prediction of battery ageing trajectory and lifetime using histogram data [13]	44	Charge and discharge	Last cycle	V, I, T, time

Ref.	#Features	Cycle Segment	Historical Data Requirement and Observations	Feature Types
Deep neural network battery life and voltage prediction by using data of one cycle only [55]	12	Charge and discharge	Last cycle	V, I, T, time
State-of-health rapid estimation for lithium-ion battery based on an interpretable stacking ensemble model with short-term voltage profiles [14]	10	Charge	Last cycle	V
Remaining Useful Life Estimation for LFP Cells in Second-Life Applications [56]	6	Discharge	Last cycle	dQ/dV(V), R

3. Materials and Methods

The following sections present the methodology for feature extraction and evaluation, as well as the proposed modeling pipeline, which includes both univariate and multivariate feature selection. The public dataset used for validation, along with the modeling conditions, is also described.

3.1 Dataset and Target Definition

This study uses the publicly available MIT Battery Dataset, introduced by [6], which contains comprehensive cycling data for commercial lithium iron phosphate ($LiFePO_4$/graphite - APR18650M1A) cells. A total of 124 cells were cycled under controlled laboratory conditions until reaching 80% of their nominal capacity, a standard end-of-life (EOL) criterion. Each cell has a nominal capacity of 1.1 Ah and a nominal voltage of 3.3 V, and was operated at a constant ambient temperature of 30 °C.

Charging followed a multi-step CC-CV protocol, with one of 72 possible fast-charging profiles per cell. These profiles, in the format $C_1(Q_1)$-C_2, specify two constant-current rates (C_1 and C_2) and the state-of-charge (SOC) threshold Q_1(%) at which the current changes. After reaching 80% SOC, charging continued at 1C using the CC-CV method with a cutoff voltage of 3.6 V and a current cutoff at C/50. Discharge conditions were identical across all cycles, performed at a fixed 4C rate. Cell lifetimes varied widely, ranging from 150 to 2,300 cycles.

For each cycle, voltage, current, temperature, internal resistance, and time were recorded. To emulate the constraints of a practical BMS, only voltage, current, temperature, and time were used for feature extraction and analysis. Discharge capacity per cycle was computed from current and time data, potentially differing slightly from values logged by the cycler. Figure 1 shows the distribution of cycle lifetimes and representative degradation trajectories.

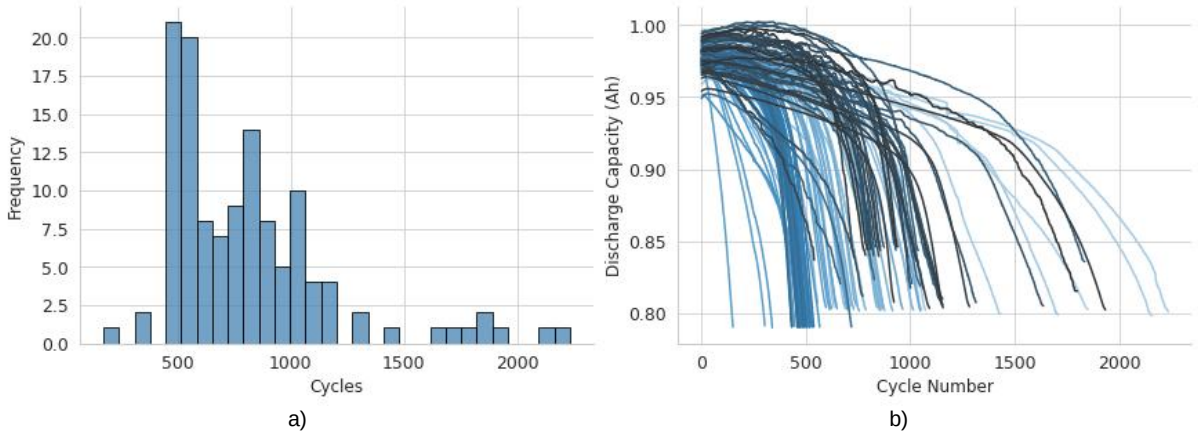

Figure 1 - MIT dataset: a) Total cycles per cell; b) Discharge capacity trajectory per cell.

The predictive targets consist of key health indicators used to characterize the battery's future degradation. Two categories of predictive targets were defined, following prior studies [5,37,57]:

- **RUL**: the number of cycles until the EOL threshold (80% of initial capacity), a widely adopted metric in SOH prognostics [58,59].
- **Multi-horizon discharge capacity forecasting**: capacity at N cycles ahead, denoted *Q_discharge_next_N_cycles*, where N ∈ {10, 50, 100, 250}. These horizons balance the need to capture both short-term and long-term degradation trends [13,60] while preserving sufficient data volume for modeling.

RUL estimation is critical for early failure prediction, preventive maintenance, and decision-making regarding battery replacement or repurposing [51,61]. In the context of second-life battery deployment, such as in stationary energy storage systems, accurate RUL prediction enables effective screening of retired cells to determine their residual value and suitability for continued use [62,63]. Multi-horizon capacity forecasting offers finer insight into the degradation trajectory, enabling adaptive BMS strategies such as dynamic charging, load balancing, and thermal management [64,65], as well as integration into digital twin frameworks for real-time simulation and prognostics, including electric vehicles, grid-scale energy storage systems, and aerospace platforms [66,67].

Since the analysis of features involves the development and evaluation of predictive models, the dataset was split at the cell level into training (88 cells), test (20 cells), and out-of-sample (OOS, 16 cells) sets, stratified by total cycle count to preserve degradation-trajectory distributions. The training and test sets were used for model fitting, hyperparameter tuning, and internal validation, while the OOS set was held out entirely for final performance evaluation. Each cycle was treated as an independent sample, increasing the number of training instances and enabling cycle-wise predictions. Figure 2 illustrates the RUL distribution across subsets and an example degradation-trajectory prediction for cell b3c33 (OOS) at cycle 600 (generated by one of the models discussed in later sections).

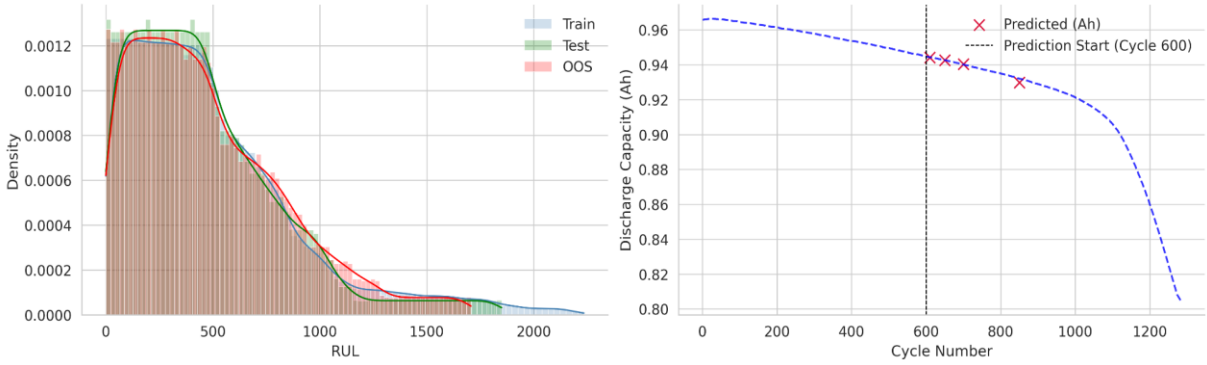

a) b)

Figure 2 - Analyzed targets: a) RUL subsets distribution; b) example of capacity prediction using horizons of 10, 50, 100 and 250 cycles ahead.

3.2 Feature Engineering

Accurate SOH prediction using machine learning models critically depends on a feature extraction process capable of capturing both the operational dynamics of the cell and the electrochemical degradation mechanisms underlying capacity fade and resistance growth [5,68]. For lithium-ion batteries, degradation can be primarily categorized into three main modes: loss of lithium inventory (LLI), loss of active material (LAM), and increase in internal cell resistance [68].

LLI arises from irreversible side reactions that consume lithium ions, making them unavailable for intercalation during subsequent cycles. Such reactions include SEI formation on the graphite anode, electrolyte decomposition, and lithium plating [42]. LAM is associated with the structural and chemical deterioration of electrode materials, while internal resistance growth often results from the development of parasitic surface phases and the loss of electronic contact within porous electrode structures, impeding both ionic and electronic transport [5].

Given the complexity and interplay of these degradation mechanisms, we developed a feature engineering pipeline designed to extract multi-faceted indicators of battery health from both raw operational measurements and voltage-capacity derived analyses. This approach is based on the hypothesis that degradation signatures manifest differently across charge and discharge phases, and in both direct measurements and transformed representations of battery behavior. Accordingly, features were extracted from two complementary domains:

- **Signal-based measurements**: voltage, current, temperature, and elapsed time;
- **Differential analyses of capacity-voltage curves**: IC and DV curves, i.e., dQ/dV(V) and dV/dQ(Q). IC reflect voltage behavior (a direct health indicator), DV curves represent capacity evolution (a secondary indicator that becomes less reliable as cells age [69,70].

In total, seven distinct feature sets were generated:

- From raw data: General Charge, General Discharge, and CCCV-based Charge;
- From voltage-capacity derivative curves: dQ/dV-based Charge, dQ/dV-based Discharge, dV/dQ-based Charge, and dV/dQ-based Discharge.

Feature definitions were informed by a systematic literature review [26], ensuring both established and unconventional descriptors were included. The strategy was deliberately broad to stress-test which aggregation operations, statistical descriptors, time-window strategies, and curve-based metrics are most informative for degradation modeling.

By relying on tabular descriptors derived from standard BMS-accessible signals rather than directly modeling raw time-series, the pipeline enhances model interpretability. This enables clear attribution of predictive power to individual features or feature groups, which is essential for practical diagnostics. Moreover, separating features by operational stage (charge vs. discharge) allows the framework to remain applicable even in data-constrained settings — such as on-board EV BMS, where only partial cycle information (e.g., charging data) is recorded.

The feature extraction approaches were selected based on a literature review [37], ensuring both established and unconventional descriptors were included. The strategy was deliberately broad to stress-test which aggregation operations, statistical descriptors, time-window strategies, and curve-based metrics are most informative for degradation modeling. By relying on tabular descriptors derived from standard BMS-accessible signals rather than directly modeling raw time-series, the pipeline enhances model interpretability. This enables clear attribution of predictive power to individual features or feature groups, which is essential for practical diagnostics. Moreover, separating features by operational stage (charge vs. discharge) allows the framework to remain applicable even in data-constrained settings, such as on-board EV BMS, which often record data primarily during controlled charging events. This ensures that relevant features exclusive to charge or discharge can still be extracted and used effectively.

Within each of the defined feature groups, the extracted variables are organized into four main categories:

- **Primary features**: extracted from data within the cycle itself, and typically consist of basic statistical descriptors (e.g., mean, standard deviation, kurtosis).
- **Lag features**: derived from the temporal evolution of primary features across preceding cycles, including differences, ratios, and trend-based metrics.
- **Sliding window features**: rolling-window aggregations of primary features over *N* previous cycles, capturing local temporal dynamics.
- **Cycle-shifted difference features**: statistical descriptors applied to pointwise differences between interpolated curves (Q(V), dQ/dV(V), dV/dQ(Q)) from two different cycles, capturing morphological curve changes over time.

A total of 42,614 features were extracted across the seven developed feature groups, as shown in Table 2, combining both signal-based and derivative-based approaches rooted in voltage-capacity curves and their differential representations. The complete features descriptions are presented in the following section.

Table 2 - Volumetrics of features extracted in each feature group.

Group	Domain	Total features
General charge features	Signal-based measurements	7,840
General discharge features	Signal-based measurements	7,840
CCCV-based charge features	Signal-based measurements	6,400
dV/dQ-based charge features	Differential analyses	3,058
dV/dQ-based discharge features	Differential analyses	3,049
dQ/dV-based charge features	Differential analyses	7,689
dQ/dV-based discharge features	Differential analyses	6,738

3.2.1 Signal-based features

The General Charge and General Discharge feature groups comprise a comprehensive set of variables extracted from voltage, current, temperature, and time signals during the respective phases of lithium-ion battery operation. These features include:

- Statistical descriptors (e.g., mean, standard deviation, skewness, kurtosis, entropy).
- Electrochemical indicators such as internal resistance, accumulated charge, and cumulative energy throughput.
- Model-based parameters obtained via curve-fitting of current–voltage (I-V) relationships.
- Temporal dynamics captured through lagged values and rolling-window aggregations across cycles.

These features are generated through mathematical manipulation of the raw signals, grounded in principles of pattern recognition and information theory [9]. Such transformations enable the detection of degradation-sensitive patterns embedded in the time-series sensor data. Prior studies have shown that variations in voltage and current profiles, as well as their derived statistical characteristics, are strongly correlated with electrochemical aging mechanisms, including LLI, LAM, and the growth of the SEI [6,65]. Furthermore, operational temperature profiles provide insights into parasitic side reactions and thermal degradation pathways that accelerate capacity fade [71].

A third signal-based feature group, CCCV Charge, is derived from the widely adopted constant-current/constant-voltage charging protocol. This charging strategy consists of two electrochemically distinct phases:

- Constant Current (CC): During the late stage of this phase, lithium plating may occur before complete lithiation of the graphite anode, particularly under high charging currents [72,73]. This phenomenon, driven by electrode polarization, can depress the anode potential below 0 V, favoring metallic lithium deposition. The duration of the CC phase, therefore, serves as a degradation-sensitive indicator, with progressive reductions linked to increased polarization resistance [73].
- Constant Voltage (CV): This phase primarily reflects the relaxation of residual polarization and the completion of lithium intercalation [9]. As the battery ages, the constant-voltage charge time (CVCT) typically increases due to higher internal resistance, reduced charge-transfer kinetics, and greater polarization [72,74].

The combined temporal evolution of CC and CV durations thus provides complementary insight into aging-related changes in resistance growth, charge transfer efficiency, and lithium plating propensity [74]. Figure 3 illustrates a representative charge-discharge cycle from the analyzed dataset, highlighting voltage and current profiles over time. The General Charge and

General Discharge groups extract features directly from the raw signals, while the CCCV Charge group specifically targets the two subphases of the charging process.

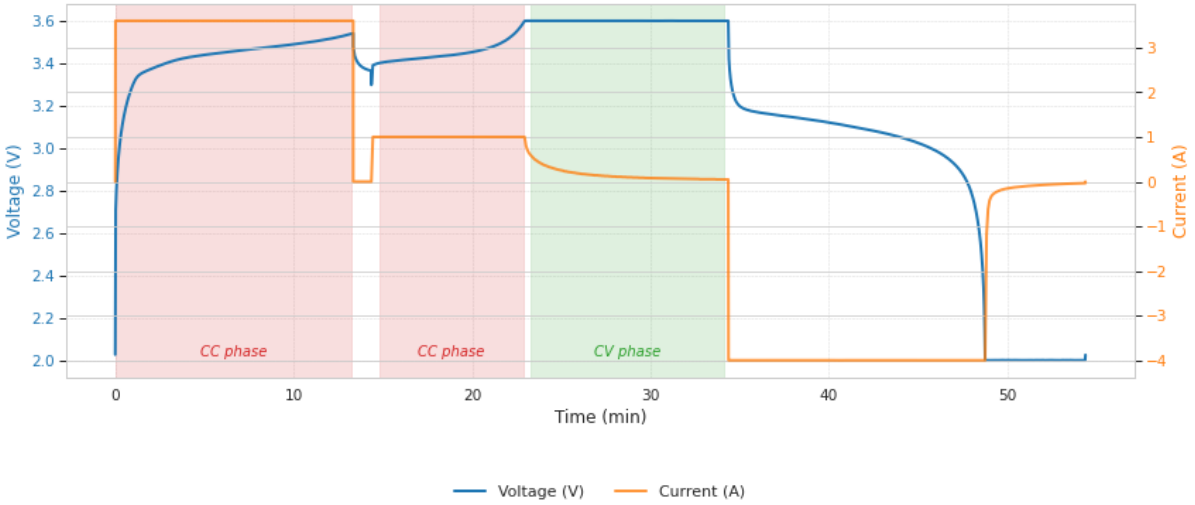

Figure 3 - Complete charge (CC-CV) and discharge cycle considering voltage and current measurements over time.

Table 3 summarizes the number of features extracted for each group, considering the three main feature categories defined in this work: (i) primary features, (ii) temporal lag features, and (iii) sliding-window features. A total of 7,840 features were generated for both the General Charge and General Discharge groups, and 6,400 features for the CCCV Charge group.

Table 3 - Description of signal-based extracted features.

Group	Features Type	Total Features	Input	Description
General Charge/Discharge	Primary	49 (per group)	*I (Current)*	Statistical descriptors of current: mean, standard deviation, percentiles (2nd, 25th, 50th, 75th, 98th), minimum, skewness, kurtosis, and sample entropy.
			V (Voltage)	Statistical descriptors of voltage: mean, standard deviation, percentiles (2nd, 25th, 50th, 75th, 98th), maximum, skewness, kurtosis, sample entropy, and voltage stabilization time.
			T (Temperature)	Statistical descriptors of temperature: mean, standard deviation, percentiles (2nd, 25th, 50th, 75th, 98th), skewness, kurtosis, and sample entropy.
			Time	Total duration of the charge or discharge phase.
			Q (Capacity)	Maximum accumulated charge and ratio with nominal capacity.
			E (Energy)	Maximum accumulated energy.
			R = V/I (Internal resistance)	Statistical descriptors of estimated resistance: mean, standard deviation, percentiles (2nd, 25th, 50th, 75th, 98th), skewness, kurtosis, and sample entropy.

Group	Features Type	Total Features	Input	Description
			I × V (Power relation)	Spearman correlation, slope, and intercept from linear regression between current and voltage signals.
CCCV-based Charge	Primary	40	V, I, time	Energy ratio (CC/CV) and energy difference (CC–CV); initial voltage in CC phase; duration of CC and CV phases; time ratio (CC/CV); mean voltage during CC and mean current during CV; statistical descriptors of estimated resistance (V/I) in CC and CV (min, max, mean, median, percentiles 2nd, 25th, 75th, 98th); slope of voltage vs. time in the CC phase and slope of current vs. time in the CV phase; sample entropy and Shannon entropy in both CC and CV phases; skewness and kurtosis in CC and CV; Frechet and Hausdorff distances of the signal trajectories in CC and CV phases.
General Charge/Discharge	Lag	1.911 (per group)	Primary features	Derived from primary features computed over previous cycles (lags of 1, 2, 5, 10, 20, 30, 40, 50, 60, 70, 80, 90, and 100 cycles). These features include the lagged values themselves, as well as the differences and ratios between the current values and their lagged counterparts.
CCCV-based Charge	Lag	1.560	Primary features	
General Charge/Discharge	Sliding window	5.880 (per group)	Primary features	Computed using sliding windows of 5, 10, 25, 50, 75, and 100 previous cycles. For each window, statistical metrics (mean, standard deviation, range, and slope) are calculated over the primary features. Additionally, differences and ratios are computed between the current values and the aggregated values within each window. Ratios between statistics across different window sizes for the same feature (e.g., mean over 10 vs. 25 cycles) are also included, allowing the model to capture multi-scale temporal patterns and recent shifts in battery behavior.
CCCV-based Charge	Sliding window	4.800	Primary features	

3.2.2 Derivative-based Features

Derivative analyses such as IC/DV are attractive for online applications, as they require only voltage and capacity measurements, making them suitable for practical implementation in BMS [39,45]. Nevertheless, both approaches are inherently sensitive to sampling resolution and measurement noise, requiring appropriate signal processing to extract reliable indicators. These properties make IC and DV curves foundational tools for developing data-driven, derivative-based features tailored to SOH estimation and RUL prediction.

In this work, derivative-based features were generated from both Q(V) and its differential representations, organized into four groups: dQ/dV-based Charge, dQ/dV-based Discharge, dV/dQ-based Charge, and dV/dQ-based Discharge. The extraction procedure followed two stages. First, Q(V) curves were reconstructed by interpolating raw experimental data into 1000 equally spaced voltage points using the SciPy interp1d function. For charging, only the constant-current portion was considered, since the CV phase yields trivial flat segments. To mitigate noise while preserving curve morphology, the Savitzky–Golay filter was applied. Second, derivatives (dQ/dV(V) and dV/dQ(Q)) were computed and further smoothed with the same filtering technique.

With the processed curves in hand, we extracted the four categories of features: (i) primary, (ii) lag-based, (iii) sliding window, and (iv) cycle-shifted difference features. Cycle-shifted difference features captures subtle temporal changes in the electrochemical behavior of the cell and enhances the feature set's sensitivity to aging patterns. Figure 4 illustrates these degradation trends. In panel (a), the capacity–voltage curves progressively shift downward as the number of cycles increases, reflecting the gradual loss of capacity. In panel (b), the differential capacity curves (−dQ/dV) show a decreasing peak amplitude with cycling, providing a complementary indicator of ageing.

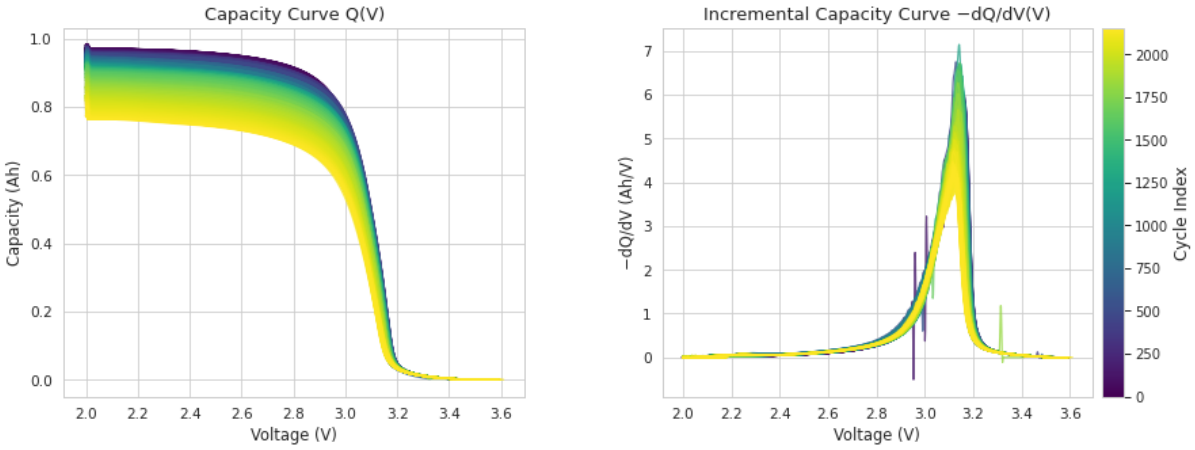

a) b)

Figure 4 - Evolution Q(V) and IC curves: a) Capacity-voltage curves across cycling; b) Incremental Capacity curves (−dQ/dV) versus voltage, with decreasing peak amplitude throughout the cycles.

Table 4 summarizes the total number and description of features extracted within each defined group. In total, the following number of features were extracted: 7,689 for dQ/dV-based Charge, 6,738 for dQ/dV-based Discharge, 3,058 for dV/dQ-based Charge, and 3,049 for dV/dQ-based Discharge. This large and diverse feature pool ensures that both voltage-domain and capacity-domain degradation signatures are comprehensively captured for subsequent modeling.

Table 4 - Description of derivative-based extracted features.

Group	Features Type	SIze	Input	Description
dQ/dV-based Charge	Primary	19	Q(V)	Minimum, maximum, mean, median, 2nd and 98th percentiles (p02, p98), 25th and 75th percentiles (p25, p75), skewness, kurtosis, variance, fundamental frequency, dominant frequency, peak bandwidth (PBW), voltage at maximum Q(V), sample entropy, Shannon entropy, area under the Q(V) curve, slope coefficient of the Q(V) curve
dQ/dV-based Discharge	Primary	19	Q(V)	

Group	Features Type	SIze	Input	Description
dQ/dV-based Charge	Primary	28	dQ/dV(V)	Minimum, mean, median, 2nd, 25th, 75th, and 98th percentiles (p02, p25, p75, p98), variance, standard deviation, skewness, kurtosis, sample entropy, voltage at maximum dQ/dV, area under the dQ/dV(V) curve, area before the peak value, area after the peak value, sample entropy before and after the peak, fundamental frequency, dominant frequency, peak bandwidth (PBW), number of peaks in the dQ/dV(V) curve, amplitude of the highest peak, voltage at the highest peak, area around the main peak, integral of peak areas, total area of peak region, and mean voltage spacing between peaks.
dQ/dV-based Discharge	Primary	21	dQ/dV(V)	Minimum, mean, median, 2nd, 25th, 75th, and 98th percentiles (p02, p25, p75, p98), variance, standard deviation, skewness, kurtosis, sample entropy, voltage at minimum dQ/dV, area under the dQ/dV(V) curve, area before the minimum value, area after the minimum value, sample entropy before and after the minimum, fundamental frequency, dominant frequency, and peak bandwidth (PBW).
dV/dQ-based Charge	Primary	17	dV/dQ(Q)	Minimum, mean, median, 2nd, 25th, 75th, and 98th percentiles (p2, p25, p75, p98), variance, standard deviation, skewness, kurtosis, sample entropy, associated capacity at the global minimum (Q at min dV/dQ), area under the curve, fundamental frequency (Fourier), dominant frequency (maximum magnitude), and power bandwidth (PBW).
dV/dQ-based Discharge	Primary	18	dV/dQ(Q)	Minimum, mean, median, 2nd, 25th, 75th, and 98th percentiles (p2, p25, p75, p98), variance, standard deviation, skewness, kurtosis, sample entropy, capacities at the two local minima (Q at local minima of dV/dQ), capacity at the second most pronounced minimum (Q at secondary minimum of dV/dQ), area under the curve, fundamental frequency (Fourier), dominant frequency (maximum magnitude), and power bandwidth (PBW).
dV/dQ-based Charge	cycle-shifted difference	169	Q(V)	For each point on the curve, differences were computed relative to the same points in previous cycles (lags of 1, 2, 5, 10, 20, …, 100 cycles). From these temporal difference profiles, the following statistical features were extracted: variance, minimum, mean, median, 2nd, 25th, 75th, and 98th percentiles (p2, p25, p75, p98), skewness, kurtosis, entropy, linear regression slope (angular coefficient), and intercept (linear coefficient)
dQ/dV-based Discharge	cycle-shifted difference	169	Q(V)	
dQ/dV-based Charge	cycle-shifted difference	169	dQ/dV(V)	
dQ/dV-based Discharge	cycle-shifted difference	169	dQ/dV(V)	
dV/dQ-based Charge	cycle-shifted difference	169	dV/dQ(Q)	
dV/dQ-based Discharge	cycle-shifted difference	169	dV/dQ(Q)	

Group	Features Type	SIze	Input	Description
dQ/dV-based Charge	Lag	1.833	Primary features	Derived from primary features computed over previous cycles (lags of 1, 2, 5, 10, 20, 30, 40, 50, 60, 70, 80, 90, and 100 cycles). These features include the lagged values themselves, as well as the differences and ratios between the current values and their lagged counterparts.
dQ/dV-based Discharge	Lag	1.560	Primary features	
dV/dQ-based Charge	Lag	663	Primary features	
dV/dQ-based Discharge	Lag	702	Primary features	
dQ/dV-based Charge	Sliding window	5.640	Primary features	Computed using sliding windows of 5, 10, 25, 50, 75, and 100 previous cycles. For each window, statistical metrics (mean, standard deviation, range, and slope) are calculated over the primary features. Additionally, differences and ratios are computed between the current values and the aggregated values within each window. Ratios between statistics across different window sizes for the same feature (e.g., mean over 10 vs. 25 cycles) are also included, allowing the model to capture multi-scale temporal patterns and recent shifts in battery behavior.
dQ/dV-based Discharge	Sliding window	4.800	Primary features	
dV/dQ-based Charge	Sliding window	2.040	Primary features	
dV/dQ-based Discharge	Sliding window	2.160	Primary features	

3.3 Feature Evaluation and Selection

While univariate analyses provide useful insights into the individual predictive strength of variables, they often overlook complex interactions and dependencies among features. In real-world systems like lithium-ion battery degradation, where electrochemical and physical processes are deeply interrelated, analyzing features in isolation may lead to incomplete or misleading conclusions. This limitation underscores the necessity of evaluating features within a multivariate framework, where joint effects, redundancies, and nonlinear interactions can be systematically accounted for.

We combine complementary univariate and multivariate analyses in a unified pipeline to (i) screen ~42,000 features candidates efficiently, (ii) preserve interactions that univariate filters would miss, and (iii) deliver compact, high-utility subsets for SOH prediction. Throughout, we consider two modeling regimes: “All Groups” (all seven feature groups enabled) and “Group Models” (pipeline applied separately to each group). All selection and tuning steps use the training/test partitions, the OOS set is held out for final validation only (Section 3.1).

To provide a clear overview of the methodology, Figure 5 summarizes the proposed feature extraction and selection pipeline. The process begins with multiple groups of input features, which are first assessed in the "Pre-selection Features” block. At this stage, features are evaluated using two complementary strategies: (i) univariate assessment through Spearman correlation, PPS, and single-feature models, and (ii) multivariate evaluation within each feature group using machine learning models. The outcome of this step is a pre-selected subset of features, representing a significant dimensionality reduction compared to the original set. In the final stage, “Multivariate Features Evaluation and Selection”, advanced strategies are applied to further refine the feature set. These include model-based optimization combined with selection algorithms such as Forward Selection, BorutaShap, and MRMR, together with SHAP-based interpretability analysis and a feature recovery methodology. This sequential design ensures a balance between dimensionality reduction, predictive performance, and explainability.

For clarity, the next subsections expand on the main components of the pipeline. Section 3.3.1 introduces the input feature groups, Section 3.3.2 covers the pre-selection approaches, and Section 3.3.3 focuses on the final multivariate evaluation and selection stage.

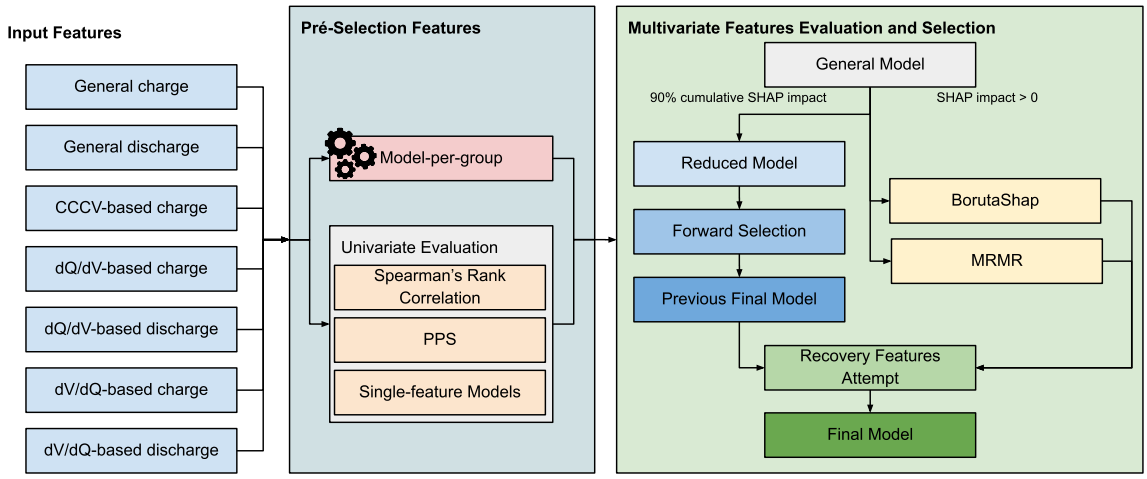

Figure 5 - Proposed feature extraction and selection pipeline.

3.3.1 Univariate Feature Evaluation

A widely adopted approach for preliminary feature assessment is the univariate analysis, in which each feature is individually evaluated in relation to the target variable. The goal of this step is to verify whether a given feature exhibits any predictive power, that is, whether it can explain, even partially, the behavior of the target variable. Three complementary univariate evaluation strategies were employed:

- **Spearman's Rank Correlation**: Spearman's correlation is a nonparametric measure of the strength and direction of a monotonic relationship between two variables. Unlike Pearson's correlation, it does not assume linearity and is more robust to outliers and non-normal distributions, conditions often observed in battery datasets due to the presence of degradation events or abrupt changes in performance [75]. Correlation strength was interpreted as follows: very weak ($|\rho| < 0.1$), weak ($0.1 \leq |\rho| < 0.3$), moderate ($0.3 \leq |\rho| < 0.5$), strong ($0.5 \leq |\rho| < 0.7$), very strong ($0.7 \leq |\rho| < 0.9$) and near-Perfect ($|\rho| \geq 0.9$) [75]. Correlations approaching 1.0 were considered near-perfect. While informative, this method is limited in its capacity to capture non-monotonic and nonlinear relationships.
- **Predictive Power Score (PPS)**: To overcome the limitations of classical correlation measures, we also employed the PPS [76], a model-based, asymmetric metric designed to capture any predictive relationship, linear or nonlinear, monotonic or not. Unlike correlation coefficients, PPS returns values in the range [0,1], where 0 indicates no predictive power and 1 indicates perfect predictive power. Its asymmetry makes it particularly suited for machine learning applications, as it explicitly evaluates the capacity of a feature to predict a target, rather than their mutual association. This is especially relevant in the context of battery health modeling, where degradation mechanisms are typically nonlinear and exhibit lag effects, hysteresis, and state-dependent transitions. PPS strength was interpreted as follows: weak ($0.01 \leq PPS < 0.2$), moderate ($0.2 \leq PPS < 0.4$), strong ($0.4 \leq PPS < 0.6$), very strong ($0.6 \leq PPS < 0.8$) and near-perfect ($PPS \geq 0.8$).
- **Single-feature models**: Beyond statistical and model-based scores, we further evaluated the predictive potential of each feature through univariate modeling. For this, a LightGBM regression model was trained using each feature individually as the sole predictor of the target variable. A default set of hyperparameters was applied across all univariate models to ensure fair comparison and focus solely on the relative predictive capacity of each feature, independent of tuning effects. The models were

evaluated using root mean squared error (RMSE), providing a direct metric of how well each feature could predict the target. As a baseline for filtering, we included a randomly generated feature with no informative content. Features performing below this random baseline were considered uninformative and were discarded from subsequent modeling stages. This additional step provided a safeguard against the inclusion of noisy or spurious features.

For downstream breadth, we retain the union of the top-300 features by absolute Spearman, top-300 by PPS, and top-300 by single-feature performance. This selection volume was based on the analysis of the distribution of each univariate indicator, mainly retaining features with a moderate level of predictive power. The level of intersection between each pre-selected group by indicator varied between 20% and 45%.

3.3.2 Multivariate Feature Evaluation (per-group pre-selection)

Because univariate filters cannot recover cross-feature synergy, we conduct a lightweight multivariate pass within each feature group to identify group-level contributors:

- **Relevance Filtering**: Features that performed worse than a random variable in the univariate single-feature model evaluation is discarded. This is a conservative filter, and typically only a small proportion of features are removed at this step.
- **Initial Group Model**: For each group, a LightGBM model is trained using a fast hyperparameter optimization process, with a fast Optuna search (early pruning enabled. All features that passed the relevance filter are used as inputs.
- **SHAP-Based Filtering (90% rule)**: SHAP are computed to assess the contribution of each feature. We select features that collectively account for 90% of the total SHAP impact, sorted by importance. This step performs a more rigorous filtering, discarding features with negligible contribution to the model's predictive power.
- **Reduced Group Model**: A second, more refined LightGBM model is trained using only the SHAP-selected features. This model uses a more extensive hyperparameter search to improve performance.
- **Second SHAP pass (85% rule)**: Retain features contributing to 85% cumulative SHAP in the reduced model. These constitute the group-level multivariate pre-selection.

Finally, we merge all group-level pre-selected features with the univariate pre-selected features. Depending on the target, this pre-selected pool ranges from 666 to 1,172 features.

3.3.3 Global Feature-Selection Pipeline (final model building)

The merged pre-selected pool enters a global, model-aware selection procedure, as the input to the “Multivariate Features Evaluation and Selection” block in Figure 5. This stage involves an extensive process of feature selection and model tuning, carried out according to the following steps:

1. **General Model**: An initial model is trained using all pre-selected features, employing hyperparameter optimization via Optuna to establish a baseline performance and identify preliminary feature interactions.
2. **SHAP Value Analysis**: Feature importance is assessed using the mean absolute SHAP values. Features contributing to 90% of the cumulative SHAP impact are retained. Additionally, features with SHAP values greater than zero, regardless of their position in the cumulative ranking, are marked as candidates for recovery set.
3. **Reduced Model**: A refined model is trained using only the features retained through the 90% cumulative SHAP filter. Hyperparameters are re-optimized for this reduced feature space.
4. **Forward Feature Selection**: A forward selection procedure is performed using the hyperparameters and SHAP-ranked features from the reduced model. The model is initially trained with the single most important feature. Then, features are added one-by-one following their SHAP ranking, and each addition is retained only if it improves the performance metric. The process continues iteratively, updating the reference metric at each step. The progression of the forward selection process is visualized in the example Figure S.1 (Supplementary Material), where more than 100 candidate

features are displayed along the x-axis, and the adopted error metric is reported on the y-axis. At each iteration, features that contribute to reducing the best error achieved so far are marked in green ("Feature Add True"), whereas rejected features are shown in red ("Feature Add False"). After an initial stage, the method tends to stabilize, leading to a reduced number of newly added features; however, in some cases, individual features may still interact with the previously selected group and yield further improvements in model performance.

5. **Previous Final Model**: A model is trained using the final subset of features obtained through forward selection. This model acts as the baseline for the recovery step.
6. **Recovery Features Set Selection**: Features from the SHAP analysis step with positive importance values (but not included in the forward-selected model) undergo an additional round of univariate evaluation using two complementary techniques: BorutaSHAP and MRMR. Features that are confirmed important by either method are flagged for potential reintegration.
    a. **BorutaSHAP**: This wrapper method leverages SHAP values and shadow features to iteratively assess feature importance [77]. Features labeled as "confirmed" are selected for reinsertion. This method has the advantage of being model-aware while controlling for randomness and overfitting.
    b. **MRMR**: A filter method that selects features with high relevance to the target variable while minimizing redundancy among them [78]. Given that MRMR requires the number of features k to be specified, we set $k = 150$ to ensure a broad recovery evaluation.
7. **Recovery Feature Attempt**: Each candidate from the recovery set is individually added to the forward-selected feature set. A model is retrained, and the candidate is retained only if its inclusion improves the performance metric. This evaluation is repeated sequentially for all recovery features. The evolution of this recovery process is illustrated in Figure S.2, where the x-axis represents each iteration in which recovery features were evaluated and the y-axis corresponds to the error metric. In this example, nearly 300 features were assessed, and 9 were retained, as their inclusion consistently improved the model's performance relative to the current feature set.
8. **Final Model**: A final model is trained using the complete set of selected features (including those recovered in the previous step). Hyperparameters are re-optimized using Optuna, with up to 1,000 boosting rounds and an early stopping criterion of 300 rounds to prevent overfitting.

This rigorous pipeline yields a robust model, ensuring that both interactions among features and potential importance overlooked in earlier stages are thoroughly explored. The same procedure is applied individually to each feature group model, maintaining the pre-selection and multivariate evaluation strategy across all groups.

The core learning algorithm employed throughout this process is the LightGBM model, chosen due to its gradient boosting framework based on decision trees, which offers a favorable balance between predictive power and computational efficiency [79]. LGBM is particularly well-suited for structured tabular data due to its robustness to outliers, ability to handle missing values, and capacity to model non-linear interactions and correlated features without requiring explicit feature engineering. Its leaf-wise tree growth strategy also contributes to its efficiency in capturing complex relationships in large datasets [79].

For hyperparameter optimization, we employ Optuna, a flexible and high-performance framework designed for efficient hyperparameter search. Optuna supports both Bayesian optimization and pruning strategies, enabling faster convergence and more effective exploration of the parameter space [80]. Its integration with LGBM and support for parallel execution further enhance scalability and adaptability to different experimental configurations.

All filtering/selection uses the training/test folds defined in Section 3.1. The OOS set is never touched until final reporting. Early stopping and Optuna pruning curb overfitting; forward selection operates with fixed hyperparameters to avoid selection-tuning feedback.

4. Results and Discussion

A substantial proportion of features exhibited at least a moderate Spearman correlation ($|\rho| \geq 0.3$) with the targets, with ~25% of extracted features per target surpassing this threshold. Detailed distributions were as follows:

- **RUL**: Weak (13,146), Moderate (5,664), Strong (3,152), Very Strong (2,451), Near-Perfect (151).
- **Q_discharge_next_10_cycles**: Weak (13,399), Moderate (5,946), Strong (2,801), Very Strong (1,104), Near-Perfect (144).
- **Q_discharge_next_50_cycles**: Weak (12,716), Moderate (5,713), Strong (2,536), Very Strong (1,290), Near-Perfect (129).
- **Q_discharge_next_100_cycles**: Weak (12,610), Moderate (5,181), Strong (1,948), Very Strong (1,336), Near-Perfect (88).
- **Q_discharge_next_250_cycles**: Weak (11,983), Moderate (3,379), Strong (1,155), Very Strong (779), Near-Perfect (4).

As detailed in Supplementary Material Table S.1, discharge-related groups, particularly derived from dQ/dV-based Discharge, consistently showed the highest proportions of strongly correlated features. In contrast, CCCV-based Charge features displayed lower volumes of strong correlations, though still included predictors of potential relevance.

When applying PPS with a moderate threshold (≥0.2), about ~5% of features per target exhibited non-linear predictive power, with the following distribution:

- **RUL**: Weak (4,486), Moderate (1,868), Strong (586), Very Strong (169), Near-Perfect (0).
- **Q_discharge_next_10_cycles**: Weak (4,909), Moderate (2,227), Strong (1,139), Very Strong (186), Near-Perfect (46).
- **Q_discharge_next_50_cycles**: Weak (4,376), Moderate (2,022), Strong (1,192), Very Strong (204), Near-Perfect (8).
- **Q_discharge_next_100_cycles**: Weak (3,624), Moderate (1,770), Strong (983), Very Strong (184), Near-Perfect (0).
- **Q_discharge_next_250_cycles**: Weak (2,618), Moderate (1,307), Strong (347), Very Strong (372), Near-Perfect (4).

This smaller subset reflects both PPS's ability to capture non-linear relationships and its more selective nature. As shown in Table S.2, PPS highlighted similar trends with Spearman correlation analysis: dQ/dV-based Discharge features as dominant contributors, complemented by a smaller but valuable subset from CCCV-based Charge.

To further assess the univariate potential of the extracted features, Figure 6 synthesizes the three evaluation methods, segmented into secondary feature groups according to their origin for RUL target analysis. Additional summaries for the capacity-forecasting targets are provided in the Supplementary Material (Figures S.3-S.6). Signal-based features are divided into the primary groups General Charge/Discharge and CCCV-based Charge, while derivative features are further categorized as dV/dQ-based Charge, dV/dQ-based Discharge, dQ/dV-based Charge, dQ/dV-based Discharge, Q(V)-based Charge, and Q(V)-based Discharge. The boxplots illustrate not only the interquartile range (25th–75th percentiles) but also more extreme percentiles, enabling a more comprehensive view of feature distributions.

In terms of absolute Spearman correlation, for the RUL target, the strongest distributions are observed in capacity-derivative features extracted from the charging process, particularly those in the dQ/dV-based Charge group. The Q(V)-based Charge group also exhibits high concentrations of correlation, outperforming its discharge-based counterpart. A similar pattern is observed for the 10-cycle-ahead capacity target. At 50 cycles ahead, the trend persists, although Q(V)-based features display comparable distributions across both charge and discharge processes. For the 100-cycle-ahead target, derivative discharge features gain prominence, with dV/dQ-based Discharge emerging as the most relevant subgroup. At 250 cycles ahead, the distributions across secondary groups become more balanced, with a slight advantage for dQ/dV-based Charge. Across all capacity-related targets, General Discharge

features consistently include some of the most highly correlated variables, albeit concentrated in the extreme upper tail of the distribution.

When model-based univariate indicators are considered, the PPS metric for the RUL target emphasizes derivative features, especially dQ/dV-based Charge and Q(V)-based Discharge. Conversely, the single-feature model approach yields lower error distributions for Q(V)-based Discharge and dQ/dV-based Discharge. For the 10 and 50-cycle-ahead capacity targets, PPS and single-feature model results broadly align with the RUL pattern. At 100 cycles ahead, PPS continues to highlight the same derivative groups, but the single-feature approach shifts emphasis toward CCCV-based Charge and Q(V)-based Discharge. For 250 cycles ahead, PPS results become more evenly distributed across groups, with CCCV-based Charge, General Discharge, and dV/dQ-based Discharge showing relative prominence, while the single-feature models maintain a stronger focus on CCCV-based Charge and Q(V)-based Discharge.

The absence of a consistent ranking across univariate methods underscores the importance of combining multiple filtering criteria when selecting features, thereby balancing different predictive signals. Notably, while CCCV-based Charge features have limited prominence in correlation-based rankings, the single-feature approach suggests that they hold meaningful predictive potential for capacity forecasting. Finally, item “b” of Figure 6 and the corresponding items in Supplementary Figures S.3-S.6 illustrate the concentration of high-predictive-power features within specific types of extracted variables. Across all univariate approaches, the highest predictive potential is observed in primary features, statistical descriptors computed within the same cycle, followed by similar performance levels for sliding-window and lag-based features.

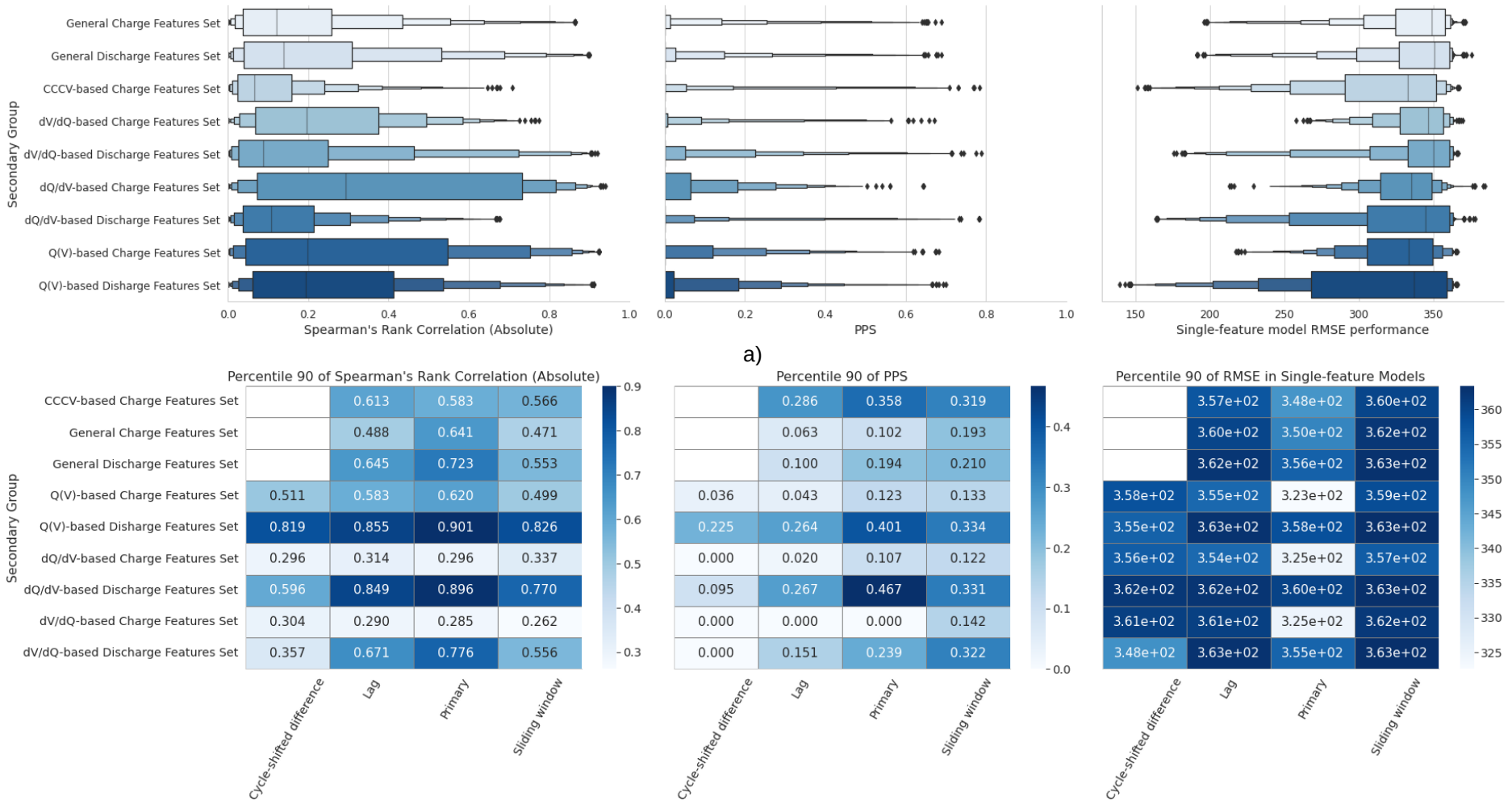

Figure 6 - Summary of the univariate analysis by RUL target group: a) Distribution across feature sets of Spearman correlation, PPS, and RMSE single-feature models; b) Relationship between feature set and feature type at the 90th percentile of Spearman correlation, PPS, and RMSE single-feature models.

To identify the features with the highest overall univariate potential, the three evaluation approaches were integrated into a single combined score, computed as the simple average of their normalized values. For a fair comparison, each indicator was first transformed using scikit-learn's QuantileTransformer, scaling values to the [0,1] range, where scores closer to 1 indicate better feature performance. Table 5 reports the median combined score for each secondary group. Across almost all target variables, features extracted from Q(V) curves, both charge and discharge, consistently ranked among the highest. Closely following these were the CCCV-based features, which were marginally superior for most capacity-related targets. When analyzed by feature type in Table 6, results were consistent with the cross-matrix plots in Figure 6b and Supplementary Figures S.3b-S.6b: primary features clearly outperformed the others, followed by lag-based and cycle-shifted difference features. Conversely, sliding-window features showed the lowest median combined scores.

Table 5 – Median combined univariate score across secondary feature groups.

Secondary Group	RUL	Q_discharge_next_10_cycles	Q_discharge_next_50_cycles	Q_discharge_next_100_cycles	Q_discharge_next_250_cycles
CCCV-based Charge Features Set	0,393	0,421	0,377	0,386	0,416
General Charge Features Set	0,297	0,324	0,343	0,334	0,339
General Discharge Features Set	0,295	0,287	0,304	0,320	0,320
Q(V)-based Charge Features Set	0,390	0,385	0,383	0,368	0,335
Q(V)-based Disharge Features Set	0,412	0,367	0,373	0,387	0,394
dQ/dV-based Charge Features Set	0,345	0,369	0,346	0,334	0,307
dQ/dV-based Discharge Features Set	0,347	0,311	0,320	0,321	0,347
dV/dQ-based Charge Features Set	0,289	0,246	0,250	0,248	0,243
dV/dQ-based Discharge Features Set	0,264	0,194	0,200	0,217	0,249

Table 6 - Median combined univariate score across type feature.

Type	RUL	Q_discharge_next_10_cycles	Q_discharge_next_50_cycles	Q_discharge_next_100_cycles	Q_discharge_next_250_cycles
Cycle-shifted difference	0,372	0,352	0,348	0,348	0,352
Lag	0,354	0,359	0,358	0,357	0,356
Primary	0,459	0,445	0,466	0,478	0,489
Sliding window	0,322	0,316	0,315	0,317	0,322

Supplementary Material tables S.3-S.12 list the top 15 features for charge and discharge processes for each target variable. In the charging process, 10 features appeared in the top 15 for all targets, including the feature "window_range_last_100_cycles_sampen_cc_charge", representing the range (max-min) of sample entropy for voltage during the CC stage of charging, computed over the last 100 cycles, which was selected for RUL as well as for discharge capacity at 50, 100, and 150 cycles ahead. For the discharging process, 8 features were recurrent across targets, all associated with at least two future capacity variables. The substantial variability in selected features across targets suggests that the univariate predictive capacity is not concentrated in a single type of descriptor. Instead, different battery health indicators appear to capture complementary aspects of the degradation process, reinforcing the importance of employing diverse feature extraction and selection strategies.

The multivariate feature analysis follows the selection pipeline outlined in Figure 5 (Section 3.3) Two modeling strategies were adopted:

- **All Groups**: the pipeline is applied using all feature groups jointly, enabling the development of finalist models with the entire feature space.
- **Group Models**: the pipeline is applied separately to each feature group, yielding finalist models that rely exclusively on features from the respective group.

When all extracted feature groups are enabled, a total of 135 unique features are selected for finalist model development. The final features for each target variable are listed in Supplementary Material tables S.13-S.51. Among these, only 12 features appear in more than one model. The feature "dif_between_discharge_max_energy_and_window_std_last_50_cycles_discharge_max_energy", the difference between the maximum discharge energy in the current cycle and the standard deviation of maximum discharge energy over the last 50 cycles, appears most frequently, being included in 3 of the 5 models (capacity at 50, 100, and 250 cycles ahead). Another recurrent feature is "window_range_last_75_cycles_charge_kurt_resistance", the range (max-min) of kurtosis of instantaneous resistance during charging over the last 75 cycles, which appears in both the RUL model and the 100-cycle-ahead capacity model.

This low overlap of features across finalist models, even though four of the targets are capacity-related, suggests that battery degradation prediction tends to vary according to the specific health indicator being modeled. Short-horizon capacity indicators are often explained by different features than those relevant for long-horizon forecasts (e.g., capacity at 250 cycles ahead). Likewise, RUL may not share the same explanatory basis as future capacity variables.

Table 7 presents the distribution of finalist features by group for each target variable. For RUL prediction, there is a relatively balanced representation across all feature groups, with notable contributions from General, CCCV, and dQ/dV-based Discharge features. For short-horizon capacity prediction, finalist models rely almost exclusively on General Discharge features, indicating that short-term degradation is largely captured by direct analysis of discharge voltage-current curves. In the 50-cycle-ahead capacity model, General Discharge remains dominant, but nearly half of the selected features come from four additional groups, including charging-related features, a pattern also observed in the 100 and 250-cycle-ahead capacity models.

Table 7 – Distribution of the number of finalist features by Groups.

Group	RUL	Q_discharge_next_10_cycles	Q_discharge_next_50_cycles	Q_discharge_next_100_cycles	Q_discharge_next_250_cycles
General Charge Features Set	8	0	1	4	5
General Discharge Features Set	6	8	11	16	14
CCCV-based Charge Features Set	8	0	5	11	8
dQ/dV-based Charge Features Set	3	1	0	4	1
dQ/dV-based Discharge Features Set	9	0	3	5	7
dV/dQ-based Charge Features Set	4	0	0	0	1
dV/dQ-based Discharge Features Set	0	0	3	2	0

Breaking down the 148 finalist features by secondary groups shows that general discharge dominates, contributing 55 features (37.2%), followed by CC-CV-based charge features with 32 (21.6%) and general charge with 18 (12.2%). Q(V)-based discharge accounts for 16 features (10.8%), while derivative-based groups contribute smaller shares: dQ/dV-based discharge with 10 (6.8%), dV/dQ-based charge with 6 (4.1%), Q(V)-based charge and dQ/dV-based charge with 4 each (2.7%), and dV/dQ-based discharge with 3 (2.0%). Derivative-based features account for approximately 29% of the selected variables in the All Groups models, a

markedly different pattern from the univariate analysis, where these features appeared more dominant. When considering the type of features, there is a clear predominance of sliding window variables, representing roughly 88% of all finalists in each model, followed by lag features (~10%). Primary and cycle-shifted difference features appear only twice each, specifically in the models forecasting capacity 50 and 100 cycles ahead. This contrast with the univariate results, where primary features showed stronger individual performance, highlights that in a multivariate setting, the interplay and complementarity among features often outweigh the standalone predictive potential of any single variable.

When comparing the features selected in the final models with the top-ranked variables from the univariate combined-score analysis (Tables A.3-A.12), only 18 features overlapped. The highest degree of overlap occurred in the model forecasting capacity 10 cycles ahead, where 4 out of 9 selected features were also among the top univariate performers. This highlights the critical role of multivariate feature selection, as variables with high individual correlation or predictive power do not necessarily translate into optimal predictors within a robust multivariate framework. Interactions among variables can be decisive in model performance, with seemingly weaker univariate features contributing meaningful segmentation or interaction effects when combined with others.

Under the Group Models approach, a total of 724 features were employed across 35 finalist models after applying the proposed pipeline, comprising 700 unique variables. The distribution of unique features per group was as follows:

- General Charge Features Set: 129 features, 27 appearing in more than one model.
- General Discharge Features Set: 92 features, 14 reused across models.
- dV/dQ-based Charge Features Set: 62 features, 18 reused.
- dV/dQ-based Discharge Features Set: 80 features, 29 reused.
- dQ/dV-based Charge Features Set: 129 features, 19 reused.
- dQ/dV-based Discharge Features Set: 129 features, 21 reused.
- CCCV-based Charge Features Set: 103 features, 16 reused.

As with the All Groups approach, feature overlap between models was low, reinforcing the notion that predicting different target variables tends to leverage distinct patterns extracted from battery operating data. Similar to the All Groups results, sliding window features dominated, representing ~83% of all finalist variables, followed by lag features (13%), and primary and cycle-shifted difference variables (2% each). Within the sliding window category, both in All Groups and Group Models, a wide range of history lengths was observed in the finalist features, from 5 cycles to the upper bound of 100 cycles. This flexibility suggests that reducing the historical window length could yield models of comparable performance, potentially enabling more practical and time-efficient laboratory testing protocols for battery characterization.

A summary of the performance for the 40 models developed using the proposed pipeline is presented in Table 8. Metrics include RMSE (Root Mean Squared Error), MAE (Mean Absolute Error), and MAPE (Mean Absolute Percentage Error) on both the Test and OOS datasets (Section 3.1). For all capacity-related targets, the All Groups approach achieved the best performance, with all extracted features participating in the selection process. For RUL prediction, All Groups also outperformed in terms of RMSE, although marginally lower MAE and MAPE values were observed in certain group-specific models.

Performance levels were comparable to those reported in the literature, as discussed in [37]. While direct benchmarking is limited by differences in modeling and validation setups, the MAE achieved with our pipeline showed a ~50% improvement over [38], which also employed a tree-boosting algorithm but relied on 18 derivative features from incremental capacity analysis over up to 250 cycles (in contrast to our limit of 100 cycles). This gain can be attributed to the intensive feature extraction and selection process, which is particularly impactful for tree-based models on tabular data.

In scenarios with restricted data availability, such as applications where only charging or discharging processes can be monitored, models from the CCCV-based group performed comparably to the All Groups approach across all targets. For RUL prediction using discharge data, the dQ/dV-based model slightly outperformed the General Discharge model. However,

for capacity targets, General Discharge features provided superior results. Overall, the findings indicate that, within a boosting framework, combining features from diverse origins yields the best results. Even under constrained data conditions, the proposed pipeline enables rigorous feature evaluation to produce models approaching the performance of fully informed models, thereby offering robust predictive capability despite incomplete behavioral information.

Table 8 – Performance of finalist models.

Model	Target	Final features	RMSE		MAE		MAPE	
			Test	OOS	Test	OOS	Test	OOS
All Groups	RUL	38	63,483	94,303	29,956	34,187	9,941	10,772
General Charge		29	124,425	124,075	27,895	34,794	10,593	13,990
General Discharge		11	87,595	103,129	28,943	21,974	10,926	8,037
dV/dQ-based Charge		12	117,704	149,335	45,058	54,630	16,100	18,172
dV/dQ-based Discharge		29	69,416	104,087	28,011	28,219	9,901	10,139
dQ/dV-based Charge		33	100,717	136,421	45,098	47,675	15,395	16,421
dQ/dV-based Discharge		46	68,550	102,219	27,319	31,578	9,472	11,010
CCCV-based Charge		24	75,984	110,022	26,434	32,811	9,829	12,232
All Groups	Q_discharge_next_10_cycles	9	1,26E-03	1,48E-03	4,10E-04	4,23E-04	4,39E-02	4,50E-02
General Charge		40	4,68E-03	4,97E-03	1,24E-03	1,44E-03	1,33E-01	1,53E-01
General Discharge		12	1,27E-03	1,24E-03	4,18E-04	4,15E-04	4,46E-02	4,40E-02
dV/dQ-based Charge		17	1,28E-02	1,66E-02	4,86E-03	7,69E-03	5,25E-01	8,15E-01
dV/dQ-based Discharge		24	6,87E-03	6,47E-03	3,81E-03	4,13E-03	4,08E-01	4,38E-01
dQ/dV-based Charge		30	9,83E-03	1,28E-02	3,58E-03	6,21E-03	3,83E-01	6,61E-01
dQ/dV-based Discharge		30	5,19E-03	6,95E-03	2,36E-03	3,77E-03	2,54E-01	4,02E-01
CCCV-based Charge		24	4,22E-03	7,55E-03	1,67E-03	1,72E-03	1,78E-01	1,81E-01
All Groups	Q_discharge_next_50_cycles	23	4,28E-03	4,07E-03	1,15E-03	1,03E-03	1,23E-01	1,08E-01
General Charge		36	5,69E-03	6,34E-03	1,74E-03	1,84E-03	1,85E-01	1,94E-01
General Discharge		31	4,12E-03	3,89E-03	1,52E-03	1,39E-03	1,61E-01	1,46E-01
dV/dQ-based Charge		27	1,52E-02	1,68E-02	5,26E-03	8,43E-03	5,64E-01	8,95E-01
dV/dQ-based Discharge		31	7,84E-03	7,16E-03	3,90E-03	4,44E-03	4,16E-01	4,76E-01

Model	Target	Final features	RMSE		MAE		MAPE	
			Test	OOS	Test	OOS	Test	OOS
dQ/dV-based Charge		33	1,21E-02	1,29E-02	4,83E-03	6,02E-03	5,17E-01	6,42E-01
dQ/dV-based Discharge		21	6,59E-03	6,89E-03	3,10E-03	3,58E-03	3,32E-01	3,84E-01
CCCV-based Charge		21	5,54E-03	7,44E-03	2,17E-03	1,93E-03	2,31E-01	2,03E-01
All Groups	Q_discharge_next_100 _cycles	42	6,78E-03	7,38E-03	2,12E-03	1,97E-03	2,26E-01	2,08E-01
General Charge		28	1,04E-02	1,09E-02	2,67E-03	2,26E-03	2,83E-01	2,38E-01
General Discharge		30	7,65E-03	7,24E-03	2,35E-03	2,23E-03	2,50E-01	2,34E-01
dV/dQ-based Charge		27	1,76E-02	1,77E-02	6,96E-03	8,00E-03	7,42E-01	8,56E-01
dV/dQ-based Discharge		22	1,17E-02	1,04E-02	4,10E-03	4,80E-03	4,39E-01	5,13E-01
dQ/dV-based Charge		30	1,36E-02	1,43E-02	4,73E-03	5,86E-03	5,05E-01	6,26E-01
dQ/dV-based Discharge		32	1,11E-02	1,06E-02	3,97E-03	4,82E-03	4,22E-01	5,15E-01
CCCV-based Charge		28	7,63E-03	9,62E-03	2,99E-03	2,57E-03	3,18E-01	2,71E-01
All Groups	Q_discharge_next_250 _cycles	36	1,54E-02	1,34E-02	4,12E-03	3,42E-03	4,39E-01	3,61E-01
General Charge		32	2,69E-02	1,71E-02	5,53E-03	4,58E-03	5,94E-01	4,83E-01
General Discharge		23	1,69E-02	1,63E-02	4,78E-03	4,42E-03	5,13E-01	4,68E-01
dV/dQ-based Charge		10	2,60E-02	2,22E-02	9,38E-03	8,98E-03	1,00E+00	9,66E-01
dV/dQ-based Discharge		16	1,85E-02	1,78E-02	7,76E-03	8,48E-03	8,35E-01	9,08E-01
dQ/dV-based Charge		30	2,11E-02	2,08E-02	7,71E-03	8,40E-03	8,41E-01	9,05E-01
dQ/dV-based Discharge		31	1,76E-02	1,53E-02	6,51E-03	6,71E-03	7,00E-01	7,26E-01
CCCV-based Charge		28	1,85E-02	1,48E-02	4,02E-03	4,35E-03	4,32E-01	4,62E-01

The interpretability of the developed models was assessed using SHAP dependence plots and by analyzing the segmentation patterns of the finalist features across value intervals. Figure 7 presents the SHAP impact values for the top 10 features of the All Groups model in the RUL prediction task. Distinct segment patterns can be observed across all displayed features, allowing the identification of specific value ranges that positively or negatively influence the predicted remaining cycles relative to the model's median behavior. Since the underlying algorithm is tree-based, not every variation in a feature produces an effect; rather, certain value ranges exert consistent influence. For example, when the mean skewness of voltage during the CC charging phase over the last 50 cycles exceeds 1, the model tends to predict a higher RUL.

Figure 8 further examines the same features by dividing them into five intervals containing approximately equal proportions of samples. For each interval, the mean RUL is computed, revealing trends of increase or decrease in the predicted remaining cycles as the feature value changes. Well-structured features tend to display a clear monotonic ordering, or exhibit strong segmentation behavior in specific ranges. For instance, the mean kurtosis of charging current over the last 100 cycles shows a distinct pattern: for more negative values (less than -1.8), the average sample corresponds to approximately 800 remaining cycles, substantially higher than in other ranges.

Such individual feature analyses contribute to validating the relationships captured by the model. Visual inspection enables the identification of patterns that can aid in understanding the battery degradation process, as well as providing a means to “translate” possible interactions considered by the machine learning algorithm in its predictions. The complete set of segment analyses for the main features of each developed model is provided in the Supplementary Material (Figures S.7-S.14).

The comprehensive analysis demonstrates the critical role of combining univariate and multivariate approaches for effective feature selection in lithium-ion battery degradation modeling. Univariate methods identified a substantial volume of potentially relevant features, particularly highlighting the strong predictive power of Q(V)-based and dQ/dV-based derivative feature groups, as well as the CCCV-based charge group. However, the multivariate pipeline refined these findings by emphasizing the dominance of sliding window features, which accounted for approximately 88% of the final selected variables, revealing the added value of capturing temporal dependencies and interactions that univariate analyses cannot detect.

The multivariate “All Groups” modeling approach, which integrates all feature groups, consistently outperformed group-specific models across most target variables, especially for capacity prediction horizons. This reinforces the advantage of leveraging diverse feature origins to capture complex degradation patterns. Despite the relative scarcity of feature overlap among final models, reflecting distinct degradation signatures across different prediction horizons and targets, the pipeline’s ability to adaptively select features for each scenario highlights its robustness and flexibility.

Performance metrics indicate that the proposed pipeline achieves results comparable or superior to existing literature benchmarks, with significant gains attributed to rigorous feature extraction and selection strategies. Importantly, the pipeline remains effective even under data constraints, such as limiting inputs to charge- or discharge-derived features, demonstrating practical applicability in varied experimental settings.

Interpretability analyses using SHAP values further enhance the model’s utility by providing clear, physically interpretable relationships between key features and battery health indicators. This transparency not only aids scientific understanding but also supports trust and adoption in real-world battery management systems. Overall, the results validate the proposed multistage feature selection and modeling pipeline as a powerful framework for accurate, interpretable, and adaptable battery degradation prediction, underscoring the importance of integrating diverse feature types and rigorous selection methods in high-dimensional datasets.

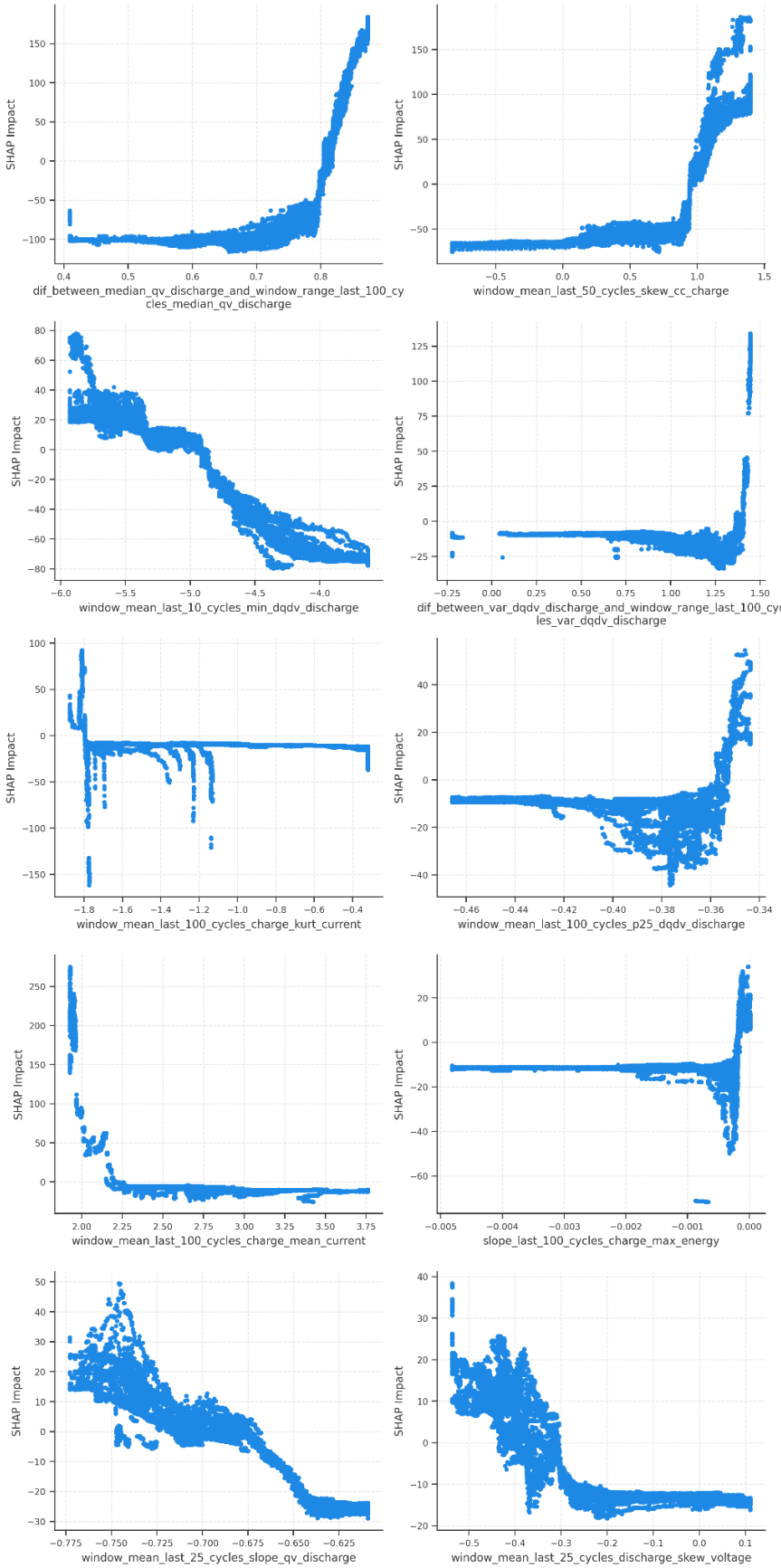

Figure 7 – SHAP dependence plots for the top 10 features of the All Groups model in RUL target.

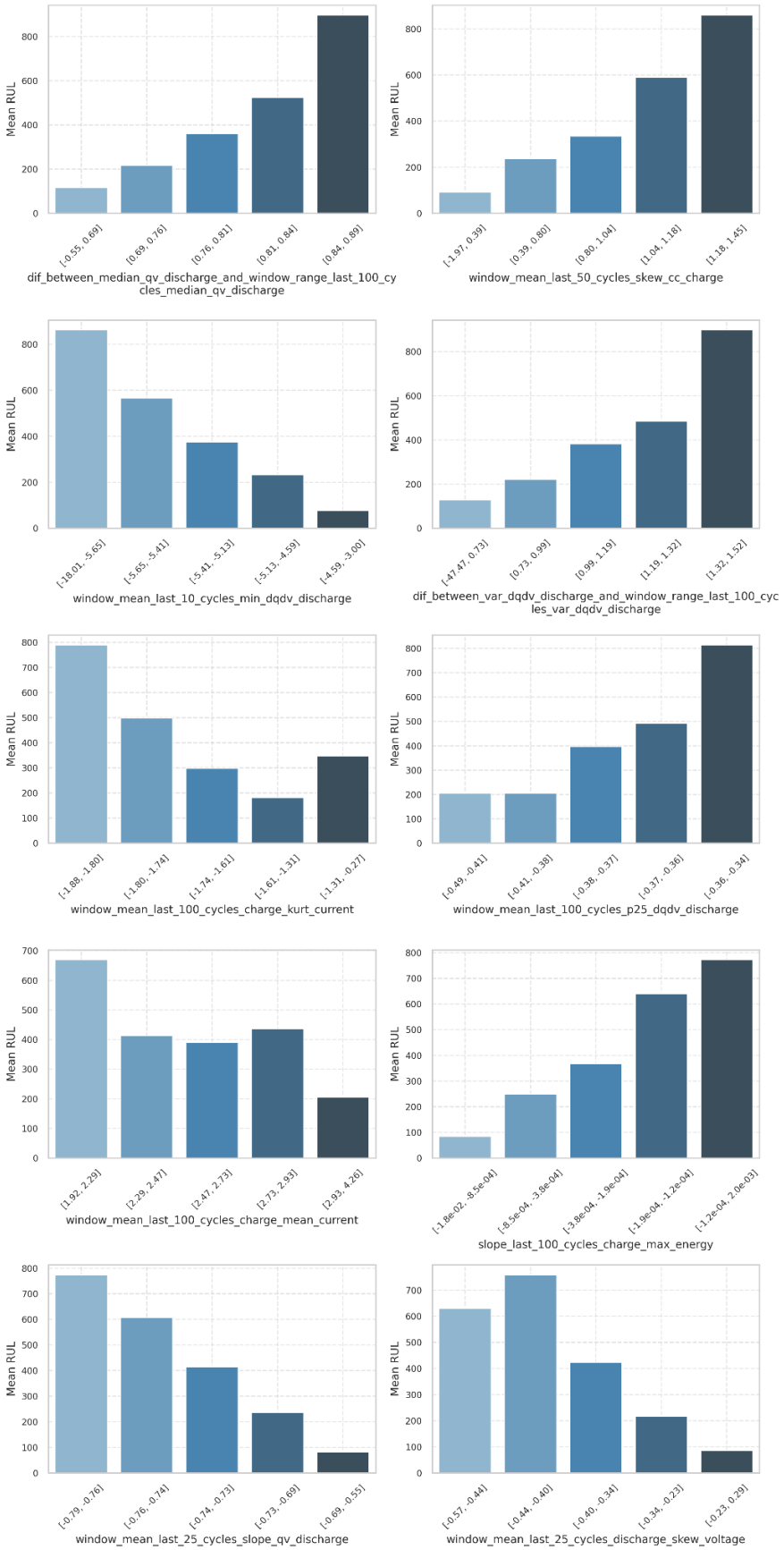

Figure 8 – Segmentation analysis for the top 10 features of the All Groups model in RUL target.

5. Conclusions

This work advances the field of battery health prediction by introducing the first large-scale, systematic framework for feature extraction and selection in SOH-based estimation. Unlike prior studies constrained to a few dozen handcrafted descriptors, our pipeline explores more than 40,000 features, unifying existing approaches with novel groups derived from both raw signals and derivative analyses. A key contribution is the systematic incorporation of sliding-window features, rarely considered in the literature, which capture degradation trajectories without requiring long historical horizons. Even under a last-cycle setting, the framework generates over 250 primary descriptors, well above any comparable work, demonstrating that valuable predictive information has been consistently overlooked.

The feature design was grounded on both raw charge and discharge signals (voltage, current, and temperature) and derivative analyses of capacity-voltage curves, such as incremental capacity and differential voltage. Seven feature groups were developed (General Charge, General Discharge, CCCV-based Charge, dQ/dV-based Charge, dQ/dV-based Discharge, dV/dQ-based Discharge, and dV/dQ-based Charge) combining statistical descriptors of the current cycle with lag-based transformations, cycle-shifted differences, and an extensive sliding-window framework. To our knowledge, no previous study in the field has explored feature extraction at such dimensionality while maintaining a standardized aggregation structure suitable for a broad range of battery datasets.

The proposed pipeline integrates univariate and multivariate selection strategies, including correlation, PPS, single-feature models, SHAP-based ranking, forward selection, BorutaShap, and MRMR. This hybrid strategy enables the identification of features whose predictive value emerges not only from individual associations with the target but also from interactions among predictors. Applied to multiple targets, RUL and future discharge capacity at horizons of 10, 50, 100, and 250 cycles, the pipeline consistently reduced the feature space to compact, high-impact subsets. Using LightGBM as the modeling backbone, the “All Groups” approach achieved the best overall performance, with MAPE ≈ 10% for RUL and <1% for future capacity, confirming the advantage of integrating diverse feature sources to capture complex degradation behaviors. Compared to related study relying on tree-boosting with limited derivative features, the proposed framework reduced error rates by nearly 50%, reinforcing predictive robustness and generalization through the larger feature pool and systematic feature selection. Group-specific models also demonstrated strong predictive potential, highlighting the framework’s adaptability under restricted data availability.

Analysis of the final selected features revealed a strong predominance of sliding-window descriptors (≈88%) and limited overlap across target-specific models. This suggests that degradation mechanisms vary across prediction horizons, with short and long-term capacity forecasts relying on distinct feature signatures. SHAP-based interpretability confirmed that the selected predictors not only enhance prediction accuracy but also reflect physically meaningful patterns aligned with battery degradation processes. Unlike prior studies, this work systematically demonstrated the predictive relevance of sliding-window features and their interaction with current-cycle descriptors, establishing them as valuable assets for SOH modeling regardless of the chosen target. Across the 40 models developed, a total of 773 finalist features were identified and are provided as a resource for advancing feature-based modeling in battery health prediction. This large-scale benchmark highlights the underexplored potential of high-dimensional feature engineering in battery SOH prediction, particularly for non-neural network approaches that operate on tabular sensor data.

Beyond predictive performance, the modular and dataset-agnostic design ensures practical applicability. The feature extraction process remains viable even with restrictions charge/discharge cycles, and the selection pipeline can be adapted to different algorithms and deployment environments. This flexibility makes the framework directly relevant to real-world scenarios, including online implementation in BMSs to EVs or stationary systems, laboratory diagnostics without historical records, second-life assessments, and predictive maintenance strategies. In doing so, it highlights the untapped potential of feature engineering in SOH

prediction, setting a new benchmark for scalable, generalizable, and interpretable modeling in battery health research.

Future work will explore reducing historical windows for earlier prediction, evaluating deep learning models on high-impact feature subsets and raw signals, and investigating ensemble and classification strategies to estimate health-stage probabilities. By combining large-scale feature extraction, systematic selection, and interpretability, this study delivers a scalable and transferable methodology that advances the state of the art in SOH and RUL data-driven prediction.

References

[1] International Energy Agency, Global EV Outlook 2024 Moving towards increased affordability, 2024. https://www.iea.org/reports/global-ev-outlook-2024.

[2] G.L. Plett, Battery management systems, Volume II: Equivalent-circuit methods, Artech House, 2015.

[3] L. Lu, X. Han, J. Li, J. Hua, M. Ouyang, A review on the key issues for lithium-ion battery management in electric vehicles, J Power Sources 226 (2013) 272–288. https://doi.org/10.1016/j.jpowsour.2012.10.060.

[4] J.-H. Teng, R.-J. Chen, P.-T. Lee, C.-W. Hsu, Accurate and Efficient SOH Estimation for Retired Batteries, Energies (Basel) 16 (2023) 1240. https://doi.org/10.3390/en16031240.

[5] Y. Li, K. Liu, A.M. Foley, A. Zülke, M. Berecibar, E. Nanini-Maury, J. Van Mierlo, H.E. Hoster, Data-driven health estimation and lifetime prediction of lithium-ion batteries: A review, Renewable and Sustainable Energy Reviews 113 (2019) 109254. https://doi.org/10.1016/j.rser.2019.109254.

[6] K.A. Severson, P.M. Attia, N. Jin, N. Perkins, B. Jiang, Z. Yang, M.H. Chen, M. Aykol, P.K. Herring, D. Fraggedakis, M.Z. Bazant, S.J. Harris, W.C. Chueh, R.D. Braatz, Data-driven prediction of battery cycle life before capacity degradation, Nat Energy 4 (2019) 383–391. https://doi.org/10.1038/s41560-019-0356-8.

[7] X. Hu, C. Zou, C. Zhang, Y. Li, Technological Developments in Batteries: A Survey of Principal Roles, Types, and Management Needs, IEEE Power and Energy Magazine 15 (2017) 20–31. https://doi.org/10.1109/MPE.2017.2708812.

[8] J. Zhao, H. Ling, J. Liu, J. Wang, A.F. Burke, Y. Lian, Machine learning for predicting battery capacity for electric vehicles, ETransportation 15 (2023) 100214. https://doi.org/10.1016/j.etran.2022.100214.

[9] D. Roman, S. Saxena, V. Robu, M. Pecht, D. Flynn, Machine learning pipeline for battery state-of-health estimation, Nat Mach Intell 3 (2021) 447–456. https://doi.org/10.1038/s42256-021-00312-3.

[10] D. Gong, Y. Gao, Y. Kou, Y. Wang, State of health estimation for lithium-ion battery based on energy features, Energy 257 (2022) 124812. https://doi.org/10.1016/j.energy.2022.124812.

[11] X.-Y. Yao, G. Chen, M. Pecht, B. Chen, A novel graph-based framework for state of health prediction of lithium-ion battery, J Energy Storage 58 (2023) 106437. https://doi.org/10.1016/j.est.2022.106437.

[12] C. Hu, G. Jain, P. Zhang, C. Schmidt, P. Gomadam, T. Gorka, Data-driven method based on particle swarm optimization and k-nearest neighbor regression for estimating capacity of lithium-ion battery, Appl Energy 129 (2014) 49–55. https://doi.org/https://doi.org/10.1016/j.apenergy.2014.04.077.

[13] Y. Zhang, T. Wik, J. Bergström, M. Pecht, C. Zou, A machine learning-based framework for online prediction of battery ageing trajectory and lifetime using histogram data, J Power Sources 526 (2022) 231110. https://doi.org/10.1016/j.jpowsour.2022.231110.

[14] G. Li, B. Li, C. Li, S. Wang, State-of-health rapid estimation for lithium-ion battery based on an interpretable stacking ensemble model with short-term voltage profiles, Energy 263 (2023) 126064. https://doi.org/10.1016/j.energy.2022.126064.

[15] D. Gong, Y. Gao, Y. Kou, Y. Wang, Early prediction of cycle life for lithium-ion batteries based on evolutionary computation and machine learning, J Energy Storage 51 (2022) 104376. https://doi.org/10.1016/j.est.2022.104376.
[16] Q. Xu, M. Wu, E. Khoo, Z. Chen, X. Li, A Hybrid Ensemble Deep Learning Approach for Early Prediction of Battery Remaining Useful Life, IEEE/CAA Journal of Automatica Sinica 10 (2023) 177–187. https://doi.org/10.1109/JAS.2023.123024.
[17] I. Bloom, A.N. Jansen, D.P. Abraham, J. Knuth, S.A. Jones, V.S. Battaglia, G.L. Henriksen, Differential voltage analyses of high-power, lithium-ion cells: 1. Technique and application, J Power Sources 139 (2005) 295–303. https://doi.org/https://doi.org/10.1016/j.jpowsour.2004.07.021.
[18] M. Dubarry, C. Truchot, B.Y. Liaw, Synthesize battery degradation modes via a diagnostic and prognostic model, J Power Sources 219 (2012) 204–216. https://doi.org/https://doi.org/10.1016/j.jpowsour.2012.07.016.
[19] X. Shu, G. Li, Y. Zhang, J. Shen, Z. Chen, Y. Liu, Online diagnosis of state of health for lithium-ion batteries based on short-term charging profiles, J Power Sources 471 (2020). https://doi.org/10.1016/j.jpowsour.2020.228478.
[20] B. Gou, Y. Xu, X. Feng, An Ensemble Learning-Based Data-Driven Method for Online State-of-Health Estimation of Lithium-Ion Batteries, IEEE Transactions on Transportation Electrification 7 (2021) 422–436. https://doi.org/10.1109/TTE.2020.3029295.
[21] G.L. Plett, Battery management systems, Volume II: Equivalent-circuit methods, Artech House, 2015.
[22] K.F. Qian, X.T. Liu, Hybrid optimization strategy for lithium-ion battery's State of Charge/Health using joint of dual Kalman filter and Modified Sine-cosine Algorithm, J Energy Storage 44 (2021) 103319. https://doi.org/10.1016/J.EST.2021.103319.
[23] M.K. Tran, M. Mathew, S. Janhunen, S. Panchal, K. Raahemifar, R. Fraser, M. Fowler, A comprehensive equivalent circuit model for lithium-ion batteries, incorporating the effects of state of health, state of charge, and temperature on model parameters, J Energy Storage 43 (2021) 103252. https://doi.org/10.1016/J.EST.2021.103252.
[24] R. Xiong, J. Tian, H. Mu, C. Wang, A systematic model-based degradation behavior recognition and health monitoring method for lithium-ion batteries, Appl Energy 207 (2017) 372–383. https://doi.org/10.1016/J.APENERGY.2017.05.124.
[25] G.L. Plett, Extended Kalman filtering for battery management systems of LiPB-based HEV battery packs, J Power Sources 134 (2004) 262–276. https://doi.org/10.1016/j.jpowsour.2004.02.032.
[26] X. Li, Z. Huang, J. Tian, Y. Tian, State-of-charge estimation tolerant of battery aging based on a physics-based model and an adaptive cubature Kalman filter, Energy 220 (2021) 119767. https://doi.org/10.1016/J.ENERGY.2021.119767.
[27] M. Daigle, C. Kulkarni, Electrochemistry-based Battery Modeling for Prognostics, 2013.
[28] A. Farmann, D.U. Sauer, Comparative study of reduced order equivalent circuit models for on-board state-of-available-power prediction of lithium-ion batteries in electric vehicles, Appl Energy 225 (2018) 1102–1122. https://doi.org/10.1016/J.APENERGY.2018.05.066.
[29] Y. Zheng, Z. Shi, D. Guo, H. Dai, X. Han, A simplification of the time-domain equivalent circuit model for lithium-ion batteries based on low-frequency electrochemical impedance spectra, J Power Sources 489 (2021) 229505. https://doi.org/10.1016/J.JPOWSOUR.2021.229505.
[30] Y. Tian, C. Lin, H. Li, J. Du, R. Xiong, Detecting undesired lithium plating on anodes for lithium-ion batteries – A review on the in-situ methods, Appl Energy 300 (2021) 117386. https://doi.org/10.1016/J.APENERGY.2021.117386.
[31] J. Li, R.G. Landers, J. Park, A comprehensive single-particle-degradation model for battery state-of-health prediction, J Power Sources 456 (2020) 227950. https://doi.org/10.1016/J.JPOWSOUR.2020.227950.

[32] W. Liu, P. Liu, D. Mitlin, Review of Emerging Concepts in SEI Analysis and Artificial SEI Membranes for Lithium, Sodium, and Potassium Metal Battery Anodes, Adv Energy Mater 10 (2020) 2002297. https://doi.org/10.1002/AENM.202002297.

[33] M.-F. Ge, Y. Liu, X. Jiang, J. Liu, A review on state of health estimations and remaining useful life prognostics of lithium-ion batteries, Measurement 174 (2021) 109057. https://doi.org/10.1016/j.measurement.2021.109057.

[34] K. Das, R. Kumar, Electric vehicle battery capacity degradation and health estimation using machine-learning techniques: a review, Clean Energy 7 (2023) 1268–1281. https://doi.org/10.1093/ce/zkad054.

[35] W. He, Z. Li, T. Liu, Z. Liu, X. Guo, J. Du, X. Li, P. Sun, W. Ming, Research progress and application of deep learning in remaining useful life, state of health and battery thermal management of lithium batteries, J Energy Storage 70 (2023) 107868. https://doi.org/https://doi.org/10.1016/j.est.2023.107868.

[36] A. Samanta, S. Williamson, Machine Learning-based Remaining Useful Life Prediction Techniques for Lithium-ion Battery Management Systems: A Comprehensive Review, IEEJ Journal of Industry Applications 12 (2023) 22004793. https://doi.org/10.1541/ieejjia.22004793.

[37] G.R. Sylvestrin, J.N. Maciel, M.L.M. Amorim, J.P. Carmo, J.A. Afonso, S.F. Lopes, O.H. Ando Junior, State of the Art in Electric Batteries' State-of-Health (SoH) Estimation with Machine Learning: A Review, Energies (Basel) 18 (2025). https://doi.org/10.3390/en18030746.

[38] F. Yang, D. Wang, F. Xu, Z. Huang, K.-L. Tsui, Lifespan prediction of lithium-ion batteries based on various extracted features and gradient boosting regression tree model, J Power Sources 476 (2020) 228654. https://doi.org/10.1016/j.jpowsour.2020.228654.

[39] C. Weng, Y. Cui, J. Sun, H. Peng, On-board state of health monitoring of lithium-ion batteries using incremental capacity analysis with support vector regression, J Power Sources 235 (2013) 36–44. https://doi.org/https://doi.org/10.1016/j.jpowsour.2013.02.012.

[40] I. Bloom, A.N. Jansen, D.P. Abraham, J. Knuth, S.A. Jones, V.S. Battaglia, G.L. Henriksen, Differential voltage analyses of high-power, lithium-ion cells: 1. Technique and application, J Power Sources 139 (2005) 295–303. https://doi.org/https://doi.org/10.1016/j.jpowsour.2004.07.021.

[41] X. Hu, Y. Che, X. Lin, S. Onori, Battery Health Prediction Using Fusion-Based Feature Selection and Machine Learning, IEEE Transactions on Transportation Electrification 7 (2021) 382–398. https://doi.org/10.1109/TTE.2020.3017090.

[42] A. Barré, B. Deguilhem, S. Grolleau, M. Gérard, F. Suard, D. Riu, A review on lithium-ion battery ageing mechanisms and estimations for automotive applications, J Power Sources 241 (2013) 680–689. https://doi.org/10.1016/j.jpowsour.2013.05.040 Review.

[43] Z. Wang, J. Ma, L. Zhang, State-of-Health Estimation for Lithium-Ion Batteries Based on the Multi-Island Genetic Algorithm and the Gaussian Process Regression, IEEE Access 5 (2017) 21286–21295. https://doi.org/10.1109/ACCESS.2017.2759094.

[44] X. Li, Z. Wang, L. Zhang, C. Zou, David.D. Dorrell, State-of-health estimation for Li-ion batteries by combing the incremental capacity analysis method with grey relational analysis, J Power Sources 410–411 (2019) 106–114. https://doi.org/https://doi.org/10.1016/j.jpowsour.2018.10.069.

[45] Y. Li, M. Abdel-Monem, R. Gopalakrishnan, M. Berecibar, E. Nanini-Maury, N. Omar, P. van den Bossche, J. Van Mierlo, A quick on-line state of health estimation method for Li-ion battery with incremental capacity curves processed by Gaussian filter, J Power Sources 373 (2018) 40–53. https://doi.org/https://doi.org/10.1016/j.jpowsour.2017.10.092.

[46] I. Bloom, L.K. Walker, J.K. Basco, D.P. Abraham, J.P. Christophersen, C.D. Ho, Differential voltage analyses of high-power lithium-ion cells. 4. Cells containing NMC, J Power Sources 195 (2010) 877–882. https://doi.org/https://doi.org/10.1016/j.jpowsour.2009.08.019.

[47] M. Berecibar, M. Garmendia, I. Gandiaga, J. Crego, I. Villarreal, State of health estimation algorithm of LiFePO4 battery packs based on differential voltage curves for battery management system application, Energy 103 (2016) 784–796. https://doi.org/https://doi.org/10.1016/j.energy.2016.02.163.

[48] X. Shu, J. Shen, G. Li, Y. Zhang, Z. Chen, Y. Liu, A Flexible State-of-Health Prediction Scheme for Lithium-Ion Battery Packs With Long Short-Term Memory Network and Transfer Learning, IEEE Transactions on Transportation Electrification 7 (2021) 2238–2248. https://doi.org/10.1109/TTE.2021.3074638.

[49] C. Su, H. Chen, Z. Wen, Prediction of remaining useful life for lithium-ion battery with multiple health indicators, Eksploatacja i Niezawodność 23 (2021) 176–183.

[50] M. Cao, T. Zhang, B. Yu, Y. Liu, A Method for Interval Prediction of Satellite Battery State of Health Based on Sample Entropy, IEEE Access 7 (2019) 141549–141561. https://doi.org/10.1109/ACCESS.2019.2939593.

[51] T. Tang, H. Yuan, An indirect remaining useful life prognosis for Li-ion batteries based on health indicator and novel artificial neural network, J Energy Storage 52 (2022) 104701. https://doi.org/https://doi.org/10.1016/j.est.2022.104701.

[52] N.S. Schauser, C.N. Lininger, E.S. Leland, T.Z. Sholklapper, An open access tool for exploring machine learning model choice for battery life cycle prediction, Front Energy Res 10 (2022) 1058999. https://doi.org/10.3389/fenrg.2022.1058999.

[53] I. Jorge, T. Mesbahi, A. Samet, R. Boné, Time Series Feature extraction for Lithium-Ion batteries State-Of-Health prediction, J Energy Storage 59 (2023) 106436. https://doi.org/10.1016/j.est.2022.106436.

[54] Y. Li, H. Sheng, Y. Cheng, H. Kuang, Lithium-ion battery state of health monitoring based on ensemble learning, in: 2019 IEEE International Instrumentation and Measurement Technology Conference, I2MTC 2019, School of Automation Engineering, University of Electronic Science and Technology of China, Chengdu, China, 2019. https://doi.org/10.1109/I2MTC.2019.8826824.

[55] C.-W. Hsu, R. Xiong, N.-Y. Chen, J. Li, N.-T. Tsou, Deep neural network battery life and voltage prediction by using data of one cycle only, Appl Energy 306 (2022) 118134. https://doi.org/10.1016/j.apenergy.2021.118134.

[56] I. Sanz-Gorrachategui, P. Pastor-Flores, M. Pajovic, Y. Wang, P. V Orlik, C. Bernal-Ruiz, A. Bono-Nuez, J.S. Artal-Sevil, Remaining Useful Life Estimation for LFP Cells in Second-Life Applications, IEEE Trans Instrum Meas 70 (2021) 1–10. https://doi.org/10.1109/TIM.2021.3055791.

[57] C. Vidal, P. Malysz, P. Kollmeyer, A. Emadi, Machine Learning Applied to Electrified Vehicle Battery State of Charge and State of Health Estimation: State-of-the-Art, IEEE Access 8 (2020) 52796–52814. https://doi.org/10.1109/ACCESS.2020.2980961.

[58] J. Yang, M. Beatty, D. Strickland, M. Abedi-Varnosfaderani, J. Warren, Second-Life Battery Capacity Estimation and Method Comparison, Energies (Basel) 16 (2023). https://doi.org/10.3390/en16073244.

[59] T. Tang, H. Yuan, An indirect remaining useful life prognosis for Li-ion batteries based on health indicator and novel artificial neural network, J Energy Storage 52 (2022) 104701. https://doi.org/https://doi.org/10.1016/j.est.2022.104701.

[60] M. Johnen, S. Pitzen, U. Kamps, M. Kateri, D.U. Sauer, Modeling long-term capacity degradation of lithium-ion batteries, (n.d.).

[61] J. Yang, M. Beatty, D. Strickland, M. Abedi-Varnosfaderani, J. Warren, Second-Life Battery Capacity Estimation and Method Comparison, Energies (Basel) 16 (2023). https://doi.org/10.3390/en16073244.

[62] X. Gu, H. Bai, X. Cui, J. Zhu, W. Zhuang, Z. Li, X. Hu, Z. Song, Challenges and opportunities for second-life batteries: Key technologies and economy, Renewable and Sustainable Energy Reviews 192 (2024) 114191. https://doi.org/10.1016/J.RSER.2023.114191.

[63] C. Heymans, S.B. Walker, S.B. Young, M. Fowler, Economic analysis of second use electric vehicle batteries for residential energy storage and load-levelling, Energy Policy 71 (2014) 22–30. https://doi.org/10.1016/J.ENPOL.2014.04.016.

[64] M. Berecibar, I. Gandiaga, I. Villarreal, N. Omar, J. Van Mierlo, P. Van Den Bossche, Critical review of state of health estimation methods of Li-ion batteries for real applications, Renewable and Sustainable Energy Reviews 56 (2016) 572–587. https://doi.org/10.1016/J.RSER.2015.11.042.

[65] R.R. Richardson, M.A. Osborne, D.A. Howey, Battery health prediction under generalized conditions using a Gaussian process transition model, J Energy Storage 23 (2019) 320–328. https://doi.org/10.1016/J.EST.2019.03.022.

[66] M. Schimpe, M. Naumann, N. Truong, H.C. Hesse, S. Santhanagopalan, A. Saxon, A. Jossen, Energy efficiency evaluation of a stationary lithium-ion battery container storage system via electro-thermal modeling and detailed component analysis, Appl Energy 210 (2018) 211–229. https://doi.org/10.1016/J.APENERGY.2017.10.129.

[67] F. Naseri, S. Gil, C. Barbu, E. Cetkin, G. Yarimca, A.C. Jensen, P.G. Larsen, C. Gomes, Digital twin of electric vehicle battery systems: Comprehensive review of the use cases, requirements, and platforms, Renewable and Sustainable Energy Reviews 179 (2023) 113280. https://doi.org/10.1016/J.RSER.2023.113280.

[68] H. Wenzl, I. Baring-Gould, R. Kaiser, B.Y. Liaw, P. Lundsager, J. Manwell, A. Ruddell, V. Svoboda, Life prediction of batteries for selecting the technically most suitable and cost effective battery, J Power Sources 144 (2005) 373–384. https://doi.org/10.1016/J.JPOWSOUR.2004.11.045.

[69] A.J. Smith, J.C. Burns, X. Zhao, D. Xiong, J.R. Dahn, A High Precision Coulometry Study of the SEI Growth in Li/Graphite Cells, J Electrochem Soc 158 (2011) A447. https://doi.org/10.1149/1.3557892/XML.

[70] X.G. Yang, Y. Leng, G. Zhang, S. Ge, C.Y. Wang, Modeling of lithium plating induced aging of lithium-ion batteries: Transition from linear to nonlinear aging, J Power Sources 360 (2017) 28–40. https://doi.org/10.1016/J.JPOWSOUR.2017.05.110.

[71] C.R. Birkl, M.R. Roberts, E. McTurk, P.G. Bruce, D.A. Howey, Degradation diagnostics for lithium ion cells, J Power Sources 341 (2017) 373–386. https://doi.org/10.1016/J.JPOWSOUR.2016.12.011.

[72] S.S. Zhang, K. Xu, T.R. Jow, Study of the charging process of a LiCoO2-based Li-ion battery, J Power Sources 160 (2006) 1349–1354. https://doi.org/10.1016/J.JPOWSOUR.2006.02.087.

[73] J. Zhou, P.H.L. Notten, Studies on the degradation of Li-ion batteries by the use of microreference electrodes, J Power Sources 177 (2008) 553–560. https://doi.org/10.1016/J.JPOWSOUR.2007.11.032.

[74] N. Williard, W. He, M. Osterman, M. Pecht, Comparative Analysis of Features for Determining State of Health in Lithium-Ion Batteries, Int J Progn Health Manag 4 (2013). https://doi.org/10.36001/IJPHM.2013.V4I1.1437.

[75] J. Cohen, Statistical Power Analysis for the Behavioral Sciences, Statistical Power Analysis for the Behavioral Sciences (2013). https://doi.org/10.4324/9780203771587.

[76] GitHub - 8080labs/ppscore: Predictive Power Score (PPS) in Python, (n.d.). https://github.com/8080labs/ppscore (accessed August 14, 2025).

[77] M.B. Kursa, W.R. Rudnicki, Feature Selection with the Boruta Package, J Stat Softw 36 (2010) 1–13. https://doi.org/10.18637/jss.v036.i11.

[78] H. Peng, F. Long, C. Ding, Feature selection based on mutual information criteria of max-dependency, max-relevance, and min-redundancy, IEEE Trans Pattern Anal Mach Intell 27 (2005) 1226–1238. https://doi.org/10.1109/TPAMI.2005.159.

[79] G. Ke, Q. Meng, T. Finley, T. Wang, W. Chen, W. Ma, Q. Ye, T.-Y. Liu, LightGBM: A Highly Efficient Gradient Boosting Decision Tree, in: I. Guyon, U. Von Luxburg, S. Bengio, H. Wallach, R. Fergus, S. Vishwanathan, R. Garnett (Eds.), Adv Neural Inf Process Syst, Curran Associates, Inc., 2017. https://proceedings.neurips.cc/paper_files/paper/2017/file/6449f44a102fde848669bdd9eb6b76fa-Paper.pdf.

[80] T. Akiba, S. Sano, T. Yanase, T. Ohta, M. Koyama, Optuna: A Next-generation Hyperparameter Optimization Framework, in: Proceedings of the 25th ACM SIGKDD International Conference on Knowledge Discovery & Data Mining, Association for

Computing Machinery, New York, NY, USA, 2019: pp. 2623–2631. https://doi.org/10.1145/3292500.3330701.

A.3: Publicação 3

Fase: em revisão.

ESTIMATIVA DA VIDA ÚTIL REMANESCENTE COM HISTÓRICO CURTO EM BATERIAS LI-ION: ARQUITETURAS MULTIRRAMOS CNN-LSTM/GRU E ENSEMBLE POR STACKING

Giovane Ronei Sylvestrin[1-2], Joylan Nunes Maciel[1-2] and Oswaldo Hideo Ando Junior[2-3]

[1]Federal University of Latin American Integration (UNILA), Foz do Iguaçu 85867-000, Brazil.
giovane.sylvestrin@gmail.com (G.R.S.), joylan.maciel@unila.edu.br (J.N.M.)
[2]Research Group on Energy & Energy Sustainability (GPEnSE), Pernambuco 54518-430, PE, Brazil.
[3]Federal University of Paraiba (UFPB), Paraiba, Brazil, 56036-000,
oswaldo.junior@cear.ufpb.br (O.H.A.J.)

Abstract
Reliable estimation of state of health and remaining useful life (RUL) is essential for safe operation, cost reduction, and enabling second-life applications of lithium-ion batteries. We investigate short-history RUL prediction using only six cycles (the current plus five previous) from the MIT Battery Dataset. We combine two information domains: (i) raw voltage, current, and temperature signals segmented by the constant-current/constant-voltage (CC/CV) charging regime; and (ii) features derived from incremental capacity (IC) and differential voltage (DV) analysis. From these, we extract 5,578 features for a base model Light Gradient Boosting Machine (LightGBM) model. In parallel, we implement 12 multibranch deep learning (DL) architectures, convolutional neural networks (CNNs) with one- and two-dimensional convolutions (1D/2D) paired with long short-term memory (LSTM) or gated recurrent unit (GRU) layers, using fusion by concatenation or attention directly on the sequences. A stacking meta model that fuses boosting and DL delivers the best test performance, with a mean absolute percentage error (MAPE) of 6%. The LightGBM base model attains 9% MAPE despite the short history, which is comparable to studies using 100-250 cycles. Practically, the results show that short-history data, coupled with joint integration across feature domains, supports operational decision-making, enabling second-life triage and predictive maintenance, while reducing characterization test time.

Keywords: state of health (SOH), remaining useful life (RUL), lithium-ion batteries, machine learning (ML), deep learning (DL), stacking.

List of Abbreviations

- ATT – Cross-branch attention (TransformerEncoder)
- B – Batch size
- BN – Batch Normalization
- BMS – Battery Management System
- BranchDropout – Dropout that disables entire branches per training example
- Branches (C_in) – Number of branches and input channels per branch (C_in)
- CC – Constant Current
- CCCT – Constant-Current Charge Time
- CNN1D / CNN2D – One- / two-dimensional Convolutional Neural Network
- Conv1D / Conv2D – 1D / 2D convolutional layers
- CV – Constant Voltage
- DV – Differential Voltage
- dims – Feature dimensionality (number of variables)
- ECM – Equivalent Circuit Model
- EIS – Electrochemical Impedance Spectroscopy
- EOL – End of Life

- EV – Electric Vehicle
- GRU / BiGRU – Gated Recurrent Unit (unidirectional) / bidirectional
- H – Number of stacked temporal slices (lags)
- I – Current
- IC – Incremental Capacity
- input / hidden / layers – RNN input size / hidden-state size / number of layers
- k – Convolution kernel size
- LAM – Loss of Active Material
- LLI – Loss of Lithium Inventory
- LN – Layer Normalization
- Log-Normal – Distribution used in the probabilistic head
- lr – Learning rate
- LSTM / BiLSTM – Long Short-Term Memory (unidirectional) / bidirectional
- MAE – Mean Absolute Error
- MAPE – Mean Absolute Percentage Error
- MaxPool(·) – Max pooling (parentheses indicate kernel/stride)
- MLP – Multilayer Perceptron (linear layers + ReLU + dropout)
- R – Electrical resistance (internal resistance)
- ReLU – Rectified Linear Unit
- Residual (attn) – Residual connection on the attention path (stabilization)
- RMSE – Root Mean Squared Error
- RUL – Remaining Useful Life
- SEI – Solid Electrolyte Interphase
- SHAP – SHapley Additive exPlanations
- SOC – State of Charge
- SOH – State of Health
- T – Temperature
- TransformerEncoder (d, L, FF) – Transformer encoder with model dimension d, L layers, and feed-forward width FF
- V – Voltage
- W / W_out – Sequence width (window) / width after the CNN
- μ / log σ – Parameters of the log-normal (log-mean and log-standard deviation)
- $\oplus$ – Concatenation along the channel/feature axis

1. Introduction

Lithium-ion batteries establish themselves as the dominant storage technology for electric vehicles (EVs) and stationary systems, propelled by sustained gains in cost and performance [1]. In parallel, circular-economy imperatives, reuse and recycling, intensify the need for reliable health diagnostics and prognostics to operate safely, reduce costs, and enable second-life deployment at scale [2]. Battery health is commonly characterized by three indicators: state of health (SOH), which quantifies the current capacity relative to beginning-of-life; end of life (EOL), often defined as capacity below 80% or a doubling of internal resistance [2,3]; and remaining useful life (RUL), which estimates the number of cycles/time to EOL and is critical for predictive maintenance, asset management in battery management systems (BMSs), and triage of batches for stationary second-life applications [3,4].

Approaches to health estimation span direct measurements (e.g., coulomb counting, electrochemical impedance spectroscopy (EIS)), physics-based models (equivalent-circuit models with Kalman-type filters; electrochemical/P2D models), and data-driven methods that map SOH/RUL from measurable signals—voltage (V), current (I), temperature (T), and time—and derived variables [2,5–12]. In practice, direct measurements and physics-based models may require controlled testing and/or costly parameterization that hinder wide [9–11]. Data-driven methods gain traction for their scalability and adaptability to varied usage regimes; however, much of the literature still assumes long operating histories (~100 cycles) and/or

relatively narrow feature sets, with limited joint use of raw V/I/T signals and diagnostic derivatives such as incremental capacity (dQ/dV) and differential voltage (dV/dQ).

Despite recent advances, many studies constrain the feature space, often to a few dozen variables guided by prior knowledge [13–18], and treat information sources in isolation: (i) raw sensor signals (V/I/T) or (ii) derivative analyses (dV/dQ(Q), dQ/dV(V)), rarely integrated within a single pipeline. Combining both sources can provide strong mechanisms to identify SOH across chemistries [19–21]. In deep learning (DL), sequential inputs frequently limit themselves to preprocessed V/I/T, with little simultaneous use of derivatives and constant-current/constant-voltage (CC/CV) segmentation. Moreover, many studies assume long histories for real-world application (~100 cycles) or depend on beginning-of-life data, increasing testing burden and complicating large-scale triage.

We therefore identify the following gaps in the current literature: (G1) reliance on long histories and/or beginning-of-life data, which raises testing costs and restricts early-stage deployment and triage; (G2) underutilization, in combination, of raw signals (V/I/T/time), charge-process segmentation (CC/CV), and derivative variables (dQ/dV, dV/dQ), which are still often explored in separate pipelines; (G3) lack of multibranch/multichannel architectures aligned with electrochemical protocols (charge, discharge, CC, CV) that embed physics-informed biases with a short history; (G4) limited exploration of stacking between DL and tabular boosting; and (G5) lack of systematic, scalable pipelines for feature extraction and selection.

In this context, this paper develops and evaluates a short-history RUL pipeline that integrates: (i) hybrid multibranch DL architectures, CNN (1D/2D) with long short-term memory (LSTM)/gated recurrent unit (GRU), fed by charge/discharge curves (V/I/T), Q(V), and their derivatives; (ii) a Light Gradient Boosting Machine (LightGBM) model trained from 5,578 features extracted from raw and derivative signals using an intensive, systematic extraction/selection process; and (iii) two stacking strategies to fuse DL and LightGBM. To balance performance with deployability, particularly for second-life triage and accelerated characterization, we constrain the window to only six cycles (current cycle plus five lags). For implementation and analysis, we use the public dataset introduced in [19], comprising 124 lithium-ion cells.

Accordingly, the principal contributions of this work are as follows:

- Short-history RUL: We use only six cycles (current and five lags), reducing testing time/cost while maintaining performance.
- Cross-domain feature integration: We build a unified pipeline combining raw signals (V/I/T), Q(V), dQ/dV(V), dV/dQ(Q), and CC/CV segmentation, addressing G2.
- Multibranch/multichannel DL (12 variants): CNN1D/2D with LSTM/GRU, including bidirectional variants and fusion by concatenation and attention, addressing G3.
- Boosting base model with interpretability: We implement a LightGBM model from an extensive feature set (5,578) with a systematic, robust selection pipeline, enhancing interpretability of finalist variables, addressing G5.
- Two stacking strategies: (i) meta-LightGBM over predictions (LightGBM + DL) and (ii) tabular LightGBM features combined with DL predictions, addressing G4 and G1.

The results show that this combination enables short-history RUL with consistent gains over individual models and signals practical applicability for rapid second-life triage and battery characterization. The remainder of the paper is organized as follows. Section 2 reviews the main concepts, algorithms, and approaches used herein. Section 3 presents materials and methods, including the dataset, data segmentation for modeling and validation, the feature-extraction pipeline, and DL architectures. Section 4 reports results and discussion, comparing the performance of the 15 implemented models. Section 5 concludes the paper and outlines directions for future research.

2. Theoretical Background

This section provides a concise review of core concepts underpinning the study. We first outline degradation mechanisms in lithium-ion batteries and show how sensor measurements yield features across complementary domains that support SOH prediction. We then briefly review related work and the fundamentals of boosting models, neural network architectures, and model stacking.

2.1 Degradation mechanisms and feature domains

Degradation in lithium-ion batteries is commonly grouped into three principal modes: loss of lithium inventory (LLI), loss of active material (LAM), and growth of internal resistance [22]. LLI arises from irreversible side reactions that consume cyclable lithium, such as formation/thickening of the solid electrolyte interphase (SEI) on graphite anodes, electrolyte decomposition, and lithium plating [23]. LAM is associated with structural and chemical damage to electrode materials. Resistance growth emerges from parasitic surface phases and loss of electronic contact within the porous matrix, impairing both ionic and electronic transport [2].

These degradation signatures are observed through analysis of basic battery measurements. Variations in voltage and current profiles, and their derived statistics, correlate with mechanisms such as LLI, LAM, and SEI growth [19,24], while temperature profiles reveal parasitic reactions and thermal pathways that accelerate capacity fade [25]. Under CC/CV charging, two electrochemically distinct phases offer useful indicators: in CC, especially near the end of the step and under high currents, polarization can drive the anode potential below 0 V and promote lithium plating; progressive reductions in CC duration are sensitive to rising resistance/polarization [26,27]. In CV, polarization relaxes and lithium intercalation completes; the constant-voltage charge time (CVCT) tends to increase with higher internal resistance and slower charge-transfer kinetics [13,26,28]. The joint evolution of CC and CV durations thus provides complementary information on resistive growth, charge-transfer efficiency, and propensity for metallic-lithium deposition [28].

From a feature-engineering perspective, two domains are particularly informative and complementary:

- Signal-based domain: indicators extracted directly from V(t), I(t), T(t), and charge/discharge capacity, preserving chronology and operating regimes (including CC/CV). Characteristic times (e.g., CC and CV durations), gradients, asymmetry measures, and relations across segments are sensitive to polarization, resistance, and intercalation efficiency.
- Differential-analysis domain (IC/DV): incremental capacity dQ/dV vs. V (IC) and differential voltage dV/dQ vs. Q (DV) accentuate peaks/plateaus associated with phase and transport processes. Peak shifts indicate changes in stoichiometric windows/LLI; reductions in peak height/area reflect LAM; and peak broadening denotes increased overpotential/resistance. Because they depend only on voltage and capacity, IC/DV are attractive for embedded use in BMS; however, their sensitivity to noise and sampling resolution demands appropriate signal processing to yield reliable indicators [29,30].

In summary, raw signals capture temporal dynamics and polarization effects, whereas IC/DV enhance sensitivity to electrochemical markers. Combining these domains yields a set of physically informed features for SOH/RUL estimation.

2.2 Related work

Data-driven approaches to battery health prognostics span from linear models to deep architectures. A classic implementation is presented in [19], which performs early RUL prediction via linear regression using just over a dozen variables from the first 100 cycles (Q(V), V, T). Recent surveys [31] show the predominance of deep networks, accounting for roughly 60% of impactful studies in the area, with recurrent use of LSTM/GRU and hybrid

combinations with CNNs to capture local patterns in the curves alongside temporal dependencies [32,33].

Examples include LSTM applied to discharge-capacity series to model long-range dependencies [34]; BiLSTM with transfer learning for capacity prediction in [35]; GRU for online capacity estimation in [36]; and RUL prognostics in [37] using 100 cycles of history and indicators from T, V, and internal resistance. In hybrid designs, [38] combines CNN-LSTM with V/I/T inputs from charge and discharge (14-cycle history) for RUL; [39] adopts CNN1D-BiGRU with V/I/T and 30-100 cycles of history. Additional relevant hybrid works appear in [40–47].

Deep models can be costly and typically require substantial datasets to avoid overfitting [48]. Consequently, many studies also explore tree ensembles (bagging/boosting) and model stacking that blends simpler neural networks, linear models, and tree-based learners [31], at the expense of more intensive feature engineering [2]. Boosting with LightGBM and XGBoost for SOH/RUL prognostics is reported in [49–52], while stacking with multiple boosting and linear algorithms appears in [18], offering an alternative to the data and training costs of deep models.

Within this landscape, studies based on the MIT Battery Dataset enable comparisons under conditions similar to those in this work. In [53], DNNs with ResNet and attention estimate RUL directly from V/I/T using either a single-cycle history or a 100-cycle variant, dispensing with feature engineering. Boosting methods are applied to early life prediction from the first 100 cycles: [54] uses GBRT (Gradient Boosting Regression Trees), retaining ~20 variables from an initial set of 72 charge/discharge features based on V, I, T, and IC-derived analysis; [20] employs XGBoost and reinforces the effectiveness of gradient-boosted trees. By contrast, dilated CNNs in [55] predict RUL directly from V/I/T using only 4 cycles of history, achieving mean absolute percentage errors of ~10.6%, surpassing feature-based approaches that require 100 cycles (~14.6-15.7%). A hybrid approach in [56] integrates the domain features of [19] with per-cycle local statistics (V/I/T, Q(V)) in a CNN1D–LSTM architecture for RUL over the first 100 cycles; [57] relies solely on charge curves and V/I/T signals with a CNN3D–CNN2D design using 5 initial and 15 recent cycles. In [58], deep transfer learning for RUL prediction based on partial charge curves is assessed with a CNN–LSTM: the model is pre-trained offline and, online, only the recurrent module is adapted using 30 recent cycles, indicating that short windows (dozens of cycles) can suffice. In a second-life context, [59] explores two strategies: (i) direct estimation of RUL/capacity from charge/discharge attributes and (ii) indirect estimation via capacity prediction followed by conversion to RUL. The authors extract classical attributes (normalized capacity and internal resistance) and introduce peak-capacitance variables along with TIEDVD (Time Interval of Equal Discharging Voltage Difference). The pipeline couples a classifier to separate short- and long-RUL cases with an MLP regressor, using 10 cycles of history.

To complement recent advances and address the mapped gaps, we adopt a reproducible, large-scale feature-engineering pipeline with substantially greater volumetry than is typical, jointly integrating multiple feature domains and evaluating them with boosting in a short-history setting. In parallel, we investigate multibranch/multichannel DL that explicitly fuses those domains with an architecture not previously assessed in the literature. Finally, we combine both fronts via stacking to test gains in RUL prognostics. To the best of our review, the joint combination of (i) massive, multi-stage feature extraction/selection, (ii) explicit cross-domain integration with a short history, and (iii) a tabular-deep ensemble has not been reported together on the MIT Battery Dataset, reinforcing both the originality and the practical applicability of the proposed approach.

2.3 Boosting-based models

Gradient-boosting algorithms build additive models by fitting successive decision trees that iteratively minimize a differentiable loss in the direction of the negative gradient (functional gradient descent), with regularization mechanisms such as shrinkage and subsampling [52,60]. This formulation, introduced in [61], establishes the modern basis of gradient-boosted decision trees (GBDTs) widely used for high-dimensional tabular data with nonlinear relationships.

LightGBM (LGBM) is an efficient GBDT implementation grounded on three technical pillars: (i) histogram-based learning, which discretizes continuous values into bins to reduce computation and memory; (ii) leaf-wise (best-first) growth, which expands the leaf with the largest loss reduction (constrained by *max_depth*); and (iii) optimizations such as GOSS (Gradient-based One-Side Sampling), which prioritizes samples with large gradients, and EFB (Exclusive Feature Bundling), which bundles mutually exclusive features to lower the effective dimensionality with minimal information loss [62,63]. Together, these choices accelerate training and scale to large datasets while maintaining competitive performance [62]. LGBM also provides native handling of missing values (learned optimal split direction for NaNs), sparse-data support, parallelization, and a variety of objectives/metrics for regression (including quantile, Poisson, Tweedie), which makes it versatile for SOH/RUL problems with heterogeneous feature sets [64].

In this study, we use LGBM on tabular features to: (i) capture nonlinearities and higher-order interactions without physics-based modeling; (ii) accommodate collinearity and disparate scales; (iii) offer multiple bias-variance controls (*num_leaves*, *min_data_in_leaf*, bagging, and feature subsampling) alongside importance measures that aid interpretation and selection; and (iv) integrate naturally with neural predictions in stacking schemes, acting as a meta model over features and/or base model outputs.

2.4 Deep-learning architectures

Deep learning is a representation-learning paradigm in which multiple layers of nonlinear transformations compose to produce increasingly abstract, hierarchical representations of the data [65]. These models learn features directly from data, reducing reliance on manual feature engineering and enabling end-to-end prediction [65,66]. In battery prognostics, DL effectively extracts temporal and relational patterns from raw V/I/T traces, often outperforming purely feature-based approaches and, in some cases, supporting predictive uncertainty quantification [67].

2.4.1 Convolutional Neural Networks (CNNs)

CNNs model locally structured data via local connectivity and weight sharing, yielding translation equivariance and far greater parameter efficiency than MLPs [65]. Conceptually, a CNN replaces dense matrix multiplications with convolutions in at least one layer, imposing a locality prior well suited to signals and time series [65,68]. Typical building blocks include: (i) convolution, where filters scan a 1D signal or a 2D map to extract local patterns, optionally with dilation to enlarge the receptive field without increasing parameters [68]; (ii) nonlinearity, e.g., ReLU, to capture nonlinear relations [68]; (iii) normalization, to stabilize and accelerate training by mitigating internal covariate shift [65]; (iv) pooling, to reduce dimensionality and aggregate local context; and dropout, as stochastic regularization to curb overfitting, especially in the final dense layers [65].

2D CNNs apply filters over two spatial axes, classically image height/width [68], but, for battery data, time versus another structured dimension. Two-dimensional arrangements arise by stacking historical cycles (time × lag) or by aggregating channels/regimes over a common time axis, enabling 2D filters to capture simultaneous local covariations across time and across lags/channels [57]. This supports joint modeling of spatiotemporal patterns.

1D CNNs convolve along the temporal axis while treating variables as channels [69]. They are effective for time series, offering low computational cost and a strong locality bias; with dilation and/or wider kernels they can rival RNNs for medium-range dependencies [65]. On short histories, 1D CNNs often deliver fewer parameters and a favorable signal-to-complexity ratio, while naturally accommodating multi-channel inputs and providing dimensionality reduction before dense heads.

In many systems, CNNs act as encoders, producing latent representations that feed predictive heads (dense layers) or sequential modules (LSTM/GRU) in hybrid architectures [70]. For batteries, CNN1D can encode temporal V/I/T curves, whereas CNN2D can integrate time × lag or time × regime (charge/discharge; CC/CV; IC/DV) to capture inter-cycle and cross-source structure.

2.4.2 Recurrent networks: LSTM/GRU

RNNs model temporal dependencies by propagating a hidden state along the sequence, but “vanilla” RNNs suffer from vanishing/exploding gradients over long horizons, motivating gated architectures that regulate information flow [65,71].

Long Short-Term Memory (LSTM) introduces a cell memory and three gates (input, forget, output). The forget gate controls retention of past state, mitigating gradient decay via an approximately constant error carousel; input/output gates regulate write/read of useful content [71]. LSTMs capture medium/long-range patterns with improved stability, at the cost of more parameters and training time [71,72].

Gated Recurrent Unit (GRU) simplifies LSTM by merging gates and removing a separate cell state, using update and reset gates that combine memory with the hidden state [65]. GRUs typically train faster and use fewer parameters while offering performance comparable to LSTMs. Both architectures admit bidirectional variants (BiLSTM/BiGRU), which process the sequence in forward and backward directions [65].

In regression tasks where a sequence maps to a scalar (e.g., estimating SOH/RUL from signal windows), LSTM/GRU serve as temporal encoders, condensing the sequence into a latent representation that feeds dense layers [33]. In hybrid designs, CNN1D/2D extract local behaviors, while the recurrent module captures longer-range dependencies and temporal ordering, combining robust local patterning (CNN) with broader temporal context (LSTM/GRU).

2.5 Model stacking

Model stacking is an ensemble strategy that combines predictions from multiple base learners (level-0) using a meta-learner (level-1) that learns to weight and correct the constituent models’ biases, with the aim of achieving better generalization than any single model [73]. The core idea is to exploit complementary inductive biases, reducing error via bias–variance trade-offs and improving robustness under moderate distribution shift [73].

Level-0 models are diverse algorithms trained independently on the same target. Diversity, in architectures, input features, and loss functions, is the main driver of gains. The level-1 meta-learner ingests the base models’ predictions and, optionally, uncertainty estimates/quantiles and simple meta-features, and learns a combination rule [73,74]. In practice, simple and well-regularized meta-learners are common, or tree-based models when nonlinear interactions among predictions are expected [74].

One training scheme for stacking is blending [74]. A fixed hold-out subset is reserved to train the meta-learner; base models are trained on a disjoint split, fully isolated from the meta set. A third split is kept for final evaluation (test). Base models are optimized and trained on their own data and then generate predictions on the hold-out set, which is used to fit and tune the meta-learner. This procedure is straightforward and eliminates leakage risk [74].

Stacking can yield a more robust final model due to: (i) complementarity, weakly correlated errors allow the ensemble to aggregate signal; (ii) implicit regularization, the meta-learner can down-weight underperforming specialists in specific regions and emphasize the most suitable ones; and (iii) flexibility, it seamlessly integrates neural networks, tree ensembles, and linear models, each exploiting its strengths [75,76]. The approach, however, incurs additional costs in data partitioning and complexity, requiring extra pipelines and optimization/training procedures [73].

3. Materials and Methods

This section details the methodology used in this study. We describe the dataset, the distribution of the target variable (RUL) under the modeling split, and the end-to-end pipeline for model development, including large-scale feature engineering, training of the LightGBM base model, deep-learning models, and stacking.

3.1 Dataset, target (RUL), and data partitioning

We use the dataset introduced in [19], comprising cycling data from 124 commercial $LiFePO_4$/graphite cells (APR18650M1A) tested in the laboratory until reaching 80% of nominal capacity. Cells have nominal 1.1 Ah and 3.3 V and operate at 30 °C. Charging follows a CC/CV protocol with 72 fast-charge profiles per cell, in the form $C_1(Q_1)$-C_2: the current is switched at state of charge SOC Q_1, then continued at 1C in CCCV to 3.6 V with a cutoff at C/50. Discharge uses a fixed 4C rate for all cycles. Total cycle life spans ~150 to ~2300 cycles across cells. For each cycle, V, I, T, time, and internal resistance are recorded; to emulate BMS constraints, we use V/I/T/time as the basis for feature extraction and derive discharge capacity Q by integrating current over time.

The target variable, RUL, is defined as the number of remaining cycles from cycle n to EOL (capacity ≤ 80% of the initial capacity). We compute RUL cycle-by-cycle for all pre-EOL cycles. We focus on RUL in cycles (not in elapsed time), aligned with triage and second-life applications.

For model development and evaluation, we adopt a cell-wise split, i.e., each cell appears in exactly one subset, avoiding leakage between cycles of the same cell. Additionally, we stratify by total cycle life to preserve the distribution of degradation trajectories, yielding three mutually exclusive sets:

- Base-train (88 cells): used to train and tune base models with cross-validation grouped by cell.
- Meta-train (20 cells): used to train and tune the stacking meta model. Inputs to the meta model are predictions obtained by applying the base models, trained on base-train, onto meta-train (a blending-style scheme).
- Test (16 cells): held out from all modeling; used once for the final evaluation and clean comparison of all base and ensemble models.

We treat each cycle as one sample, which increases the number of instances and enables per-cycle predictions. Figure 1 presents: (a) the distribution of total cycles; (b) capacity-fade curves per cell over cycles; and (c) the RUL distribution under the stratified partition.

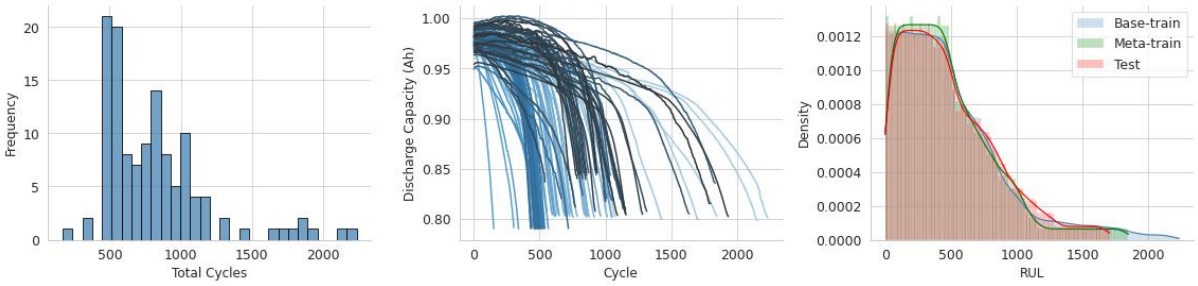

a) b) c)

Figure 1: Dataset overview: (a) distribution of total cycle life; (b) per-cell capacity-fade trajectories; (c) RUL distribution by split.

3.2 Modeling pipeline

Figure 2 outlines the end-to-end workflow, which follows three main streams:

- Input extraction: we extract inputs (raw V/I/T/time/R/Q and IC/DV derivatives) using the feature-engineering pipeline proposed in [77] for the LightGBM base model, and we extract the multichannel sequences (curves) that feed the DL architectures. Both tabular features and sequences include the current cycle (lag 0) and the previous five cycles (lags 1-5).
- Base model training: we train the base learners (LightGBM and 12 DL variants) on the base-train split. The finalist features of the LightGBM base model and the per-model RUL predictions augment both the meta-train and test sets.
- Meta model training and evaluation: we fit the stacking meta-learner on meta-train using base predictions, and then evaluate on the held-out test set, comparing all base and ensemble models.

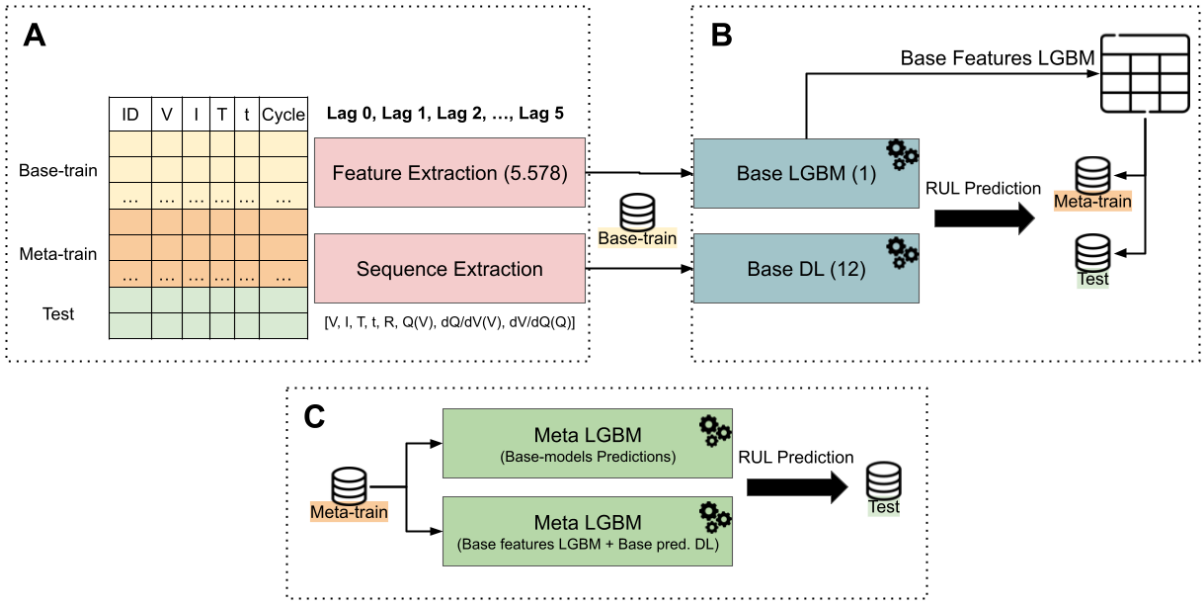

Figure 2: Overview of the modeling workflow.

Each model is trained with 5-fold cross-validation grouped by cell. In every fold, cells used for fitting are disjoint from those in validation. Hyperparameters are optimized with Optuna, which couples Bayesian search with early pruning to accelerate convergence and exploration [78].

We use two complementary domains, signal-based (raw curves) and derivative-based (IC/DV), organized into seven input groups:

- General Charge: raw V(t), I(t), T(t), charge-time trace, and derived R and Q over time.
- General Discharge: raw V(t), I(t), T(t), discharge-time trace, and derived R and Q over time.
- CCCV-based Charge: raw V(t), I(t), T(t) segmented into CC and CV phases, with derived R and Q over time.
- dQ/dV-based Charge: dQ/dV(V) during CC charging.
- dV/dQ-based Charge: dV/dQ(Q) during CC charging.
- dQ/dV-based Discharge: dQ/dV(V) during discharge.
- dV/dQ-based Discharge: dV/dQ(Q) during discharge.

These groups feed (i) the tabular model via extraction of 5,578 features, and (ii) the DL models via multichannel sequences.

We develop 15 models in total: 13 base learners and 2 stacking ensembles. For the LightGBM base model, 5,578 features are extracted and selected as in [77]. DL base models follow a multibranch/multichannel design with six branches: (i) charge raw signals (6 channels); (ii) discharge raw signals (6 channels); (iii) charge CC raw signals (5 channels); (iv) charge CV raw signals (5 channels); (v) charge derivatives IC/DV (3 channels); (vi) discharge derivatives IC/DV (3 channels). Within each branch we vary CNN2D or CNN1D encoders, followed by LSTM/GRU (including bidirectional variants), and fuse branches by concatenation or attention before a fully connected (FC) head. The 12 DL variants evaluated are presented in Table 1.

Table 1: DL architecture variants.

Encoder	**Recurrent unit**	**Fusion**	***Head***
CNN2D	LSTM	Concatenation	FC
CNN2D	BiLSTM	Concatenation	FC
CNN2D	LSTM	Attention	FC
CNN1D	LSTM	Concatenation	FC
CNN1D	BiLSTM	Concatenation	FC

CNN1D	LSTM	Attention	FC
CNN2D	GRU	Concatenation	FC
CNN2D	BiGRU	Concatenation	FC
CNN2D	GRU	Attention	FC
CNN1D	GRU	Concatenation	FC
CNN1D	BiGRU	Concatenation	FC
CNN1D	GRU	Attention	FC

For the stacking models, two approaches were considered:

- Stacking-Predictions. The meta-learner (LightGBM) is trained on meta-train using base model predictions as inputs. The subset of base predictions included is selected via Optuna jointly with meta model hyperparameters. During selection, each candidate prediction is represented in a 13-length indicator vector; optimization sets a prediction's flag to 1 (kept) or 0 (dropped).
- Stacking-Features+Predictions. The meta-learner (LightGBM) receives the finalist tabular features (excluding the LightGBM base model own target features) plus the DL predictions selected in (i). Fitting occurs on meta-train; final evaluation is on test.

All preprocessing and modeling steps (normalization, feature extraction/selection, and hyperparameter tuning) are fit within-fold using only that fold's training data. Predictions supplied to the meta-learner are generated by models not trained on those samples (a blending scheme with disjoint sets). The test split remains fully isolated until final evaluation. We optimize hyperparameters with RMSE as the objective. For model assessment we employ the metric set in Table 2, combining common choices (MAE, RMSE) with robust, median-based measures and percentage errors. To normalize scale differences across tests, especially when comparing studies with different data/splits, we also report NMAE, which normalizes MAE by the evaluated set's IQR.

Table 2: Metrics used for performance evaluation.

Metric	Unit	Range	Description
MAE	cycles	≥ 0	Mean absolute error.
RMSE	cycles	≥ 0	Root mean squared error.
MAPE	%	≥ 0	Mean absolute percentage error.
MedAE	cycles	≥ 0	Median absolute error.
RMedSE	cycles	≥ 0	Root median squared error.
MedAPE	%	≥ 0	Median absolute percentage error.
sMAPE	%	0–200%	Symmetric percentage error (*mean(2*|ŷ−y| / (|y|+|ŷ|)*).
WAPE	%	0–100%	Weighted absolute percentage error (Σ|ŷ−y| / Σ|y|).
NMAE (MAE/IQR)	-	≥ 0	MAE normalized by the IQR of the ground truth.
R^2	-	(−∞, 1]	Coefficient of determination (explained variance)..

3.3 LightGBM base model

Following the pipeline in [77], we extract and select a broad set of features to capture degradation signatures across two complementary domains under a short history of six cycles (current cycle and five lags). The working hypothesis is that distinct mechanisms (LLI, LAM, resistive growth) imprint different patterns across charge/discharge phases and across direct measurements versus derivative representations.

The variable domains considered are: (i) a signal-based domain (V, I, T, and time); and (ii) a derivative-based domain (IC and DV curves). From these domains, we construct seven feature groups for the current cycle and five lags: General charge, General discharge, CCCV-based charge (signal-based), dV/dQ-based charge (DV), dV/dQ-based discharge (DV),

dQ/dV-based charge (IC), dQ/dV-based discharge (IC). We extract 5,578 features prior to selection, distributed as follows in Table 3. Within each group, features fall into four categories:

- Primary (intra-cycle): within-cycle statistics and shapes (means, standard deviations, percentiles, slopes, plateaus, CC/CV durations, etc.).
- Lag (inter-cycle): deltas/ratios and trends between t and {t-1, t-2, …, t-5}.
- Sliding windows: rolling aggregations over the previous
- N cycles (local dynamics).
- inter-cycle differences: pointwise descriptors of differences between interpolated curves Q(V), dQ/dV(V), and dV/dQ(Q) from two cycles, capturing shifts across recent cycles.

Table 3: Feature counts by group.

Group	Domain	Total features
General charge features	Signal-based measurements	980
General discharge features	Signal-based measurements	980
CCCV-based charge features	Signal-based measurements	800
dV/dQ-based charge features	Differential analyses	424
dV/dQ-based discharge features	Differential analyses	444
dQ/dV-based charge features	Differential analyses	1,024
dQ/dV-based discharge features	Differential analyses	926

Feature selection was implemented on the base-train split and proceeds in two stages:

- Pre-selection: a stage to retain a reduced, yet still broad, set of variables.
  - Univariate: Spearman correlation, PPS (predictive power score), and 1-variable LGBM models to retain variables with strong univariate association to RUL.
  - Group-wise multivariate: rapid LGBM screening within each group to keep promising subsets.
- Final multivariate selection: a combination of model-driven optimization and algorithmic selectors such as Forward Selection, BorutaShap, and MRMR. First, all pre-selected variables enter a global model; we retain those accounting for 90% cumulative SHAP impact. This subset undergoes forward selection to form a provisional model. In parallel, the original pre-selected pool is processed by BorutaShap and MRMR to create a rescue set. Each rescue candidate is tested against the provisional model; if it yields a measurable gain, we re-optimize and refit to obtain the finalist model.

Using Optuna, we tune the LGBM hyperparameters over the following space: learning_rate, n_estimators; model capacity via *num_leaves*, *max_depth*; regularization via *min_child_samples*, *min_child_weight*, and *min_split_gain*; subsampling via *colsample_bytree*, subsample; objective ∈ {regression (L2), *regression_l1* (L1)}; and *boosting_type* fixed to gbdt. The same optimization approach is applied to the stacking LGBM meta-learner.

3.4 DL-based base models

We implement 12 base models with neural architectures following the layout in Figure 3.

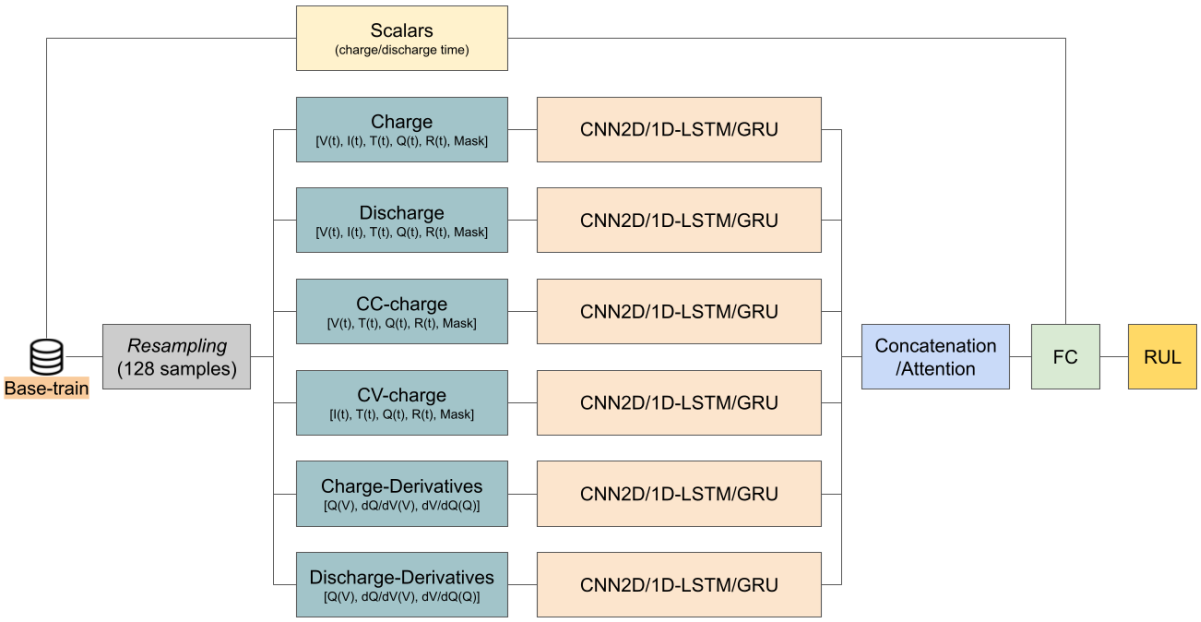

Figure 3: DL base model implementation.

Each input sequence is resampled to 128 evenly spaced points to standardize length, required by the neural implementations. For time-related sequences, the maximum sequence length is set to the 99th percentile of the corresponding process duration measured on the meta-train split; we apply the same rule consistently to all other splits using the meta-train statistics. In addition, we extract 24 scalar variables describing charge/discharge durations in the last cycle and its lags (lag 0 to lag 5), including CC/CV times. These scalars are fused directly in the prediction head via a fully connected MLP.

Sequences are routed to six branches: Charge, Discharge, CC-charge, CV-charge, Charge-Derivatives (IC/DV), and Discharge-Derivatives (IC/DV). Channel definitions (per branch) are specified in Figure 3. For Charge/Discharge/Charge-CC/Charge-CV, a mask channel (0/1) indicates whether a given attribute is present at each time step. For derivative branches, curves are generated within the minimum and maximum voltage values; the mask concept was not employed.

Each branch adopts either a CNN2D or CNN1D encoder followed by LSTM/GRU (with bidirectional variants). For CNN2D, the branch input is a tensor (B, C, H, W) with batch size B, channels C, number of lags H, and sequence length W=128. For CNN1D, we keep the same (B, C, H, W) layout but apply a lag mixer before 1D convolutions: we reshape (B, C, H, W) → (B, C·H, W) and apply a grouped 1×1 Conv1d (kernel=1, groups=C) that, for each channel, learns a linear combination of its H lags shared across time. Figure 4 presents an overview of the 2D and 1D representations used.

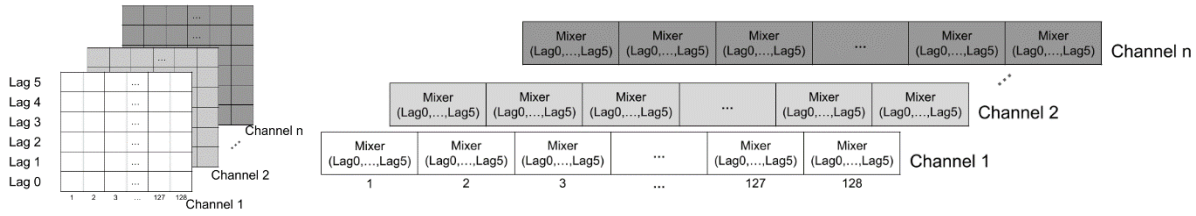

a) b)

Figure 4: CNN representations: (a) CNN2D; (b) CNN1D.

CNN stacks (2D/1D) consist of convolution → BatchNorm → ReLU → pooling, preserving the lag dimension and downsampling only along sequence length. After the recurrent module (LSTM/GRU), each branch's final vector passes through Dropout and LayerNorm to yield a fixed-size embedding.

Fusion proceeds either by concatenation, concatenating the six embeddings and fusing them with the 24 scalars via dense layers, or by attention: the six embeddings are stacked into $Z \in R^{6\times d}$; BranchDropout randomly zeroes branch embeddings during training to reduce co-adaptation and improve robustness to noisy/missing channels; a type embedding encodes branch identity; and a TransformerEncoder processes Z. The aggregated [CLS] token feeds the regression head. To stabilize early training, we add a residual pull toward the mean, and we concatenate three summaries (attention output, mean, and max) before concatenating with the scalars. The prediction head is probabilistic: a fully connected MLP outputs for a log-normal distribution, trained with negative log-likelihood. For point estimates we report the median, and we also extract quantiles (e.g., p10–p90) to form uncertainty intervals without auxiliary models. Hyperparameters are optimized with Optuna over the:

- CNN channel counts (depth/width: number of blocks and filters per block).
- LSTM/GRU hidden size.
- Number of stacked LSTM/GRU layers.
- "Internal" dropout between recurrent layers.
- "External" dropout on branch embeddings and the MLP.
- MLP width and number of hidden layers before the outputs.

The same architectural template is applied to all branches within a given trial. We first optimize the base CNN2D/1D-LSTM/GRU with concatenation, then replicate best configurations for bidirectional and attention variants. All inputs are standardized with *StandardScaler* before network training to maintain comparable magnitudes across channels.

3.5 Development environment

We develop models in a conda environment with Python 3.10. Hardware: Intel® Core™ i7-13650HX (13th gen, 2.60 GHz), 16 GB RAM, and NVIDIA GeForce RTX 3050 Laptop GPU with 6 GB of dedicated memory. Graphics driver 32.0.15.7261 (2025-02-25) with CUDA 11.8 acceleration. Neural architectures are implemented in PyTorch. Key package versions: *pandas 2.3.2, scikit-learn 1.7.1, pytorch 2.5.1, lightgbm 3.3.2, scipy 1.15.3, pyarrow 21.0.0, h5py 3.14.0, zarr 2.18.3, optuna 4.5.0*.

4. Results and Discussion

Applying the feature extraction and selection pipeline to the LightGBM base model yields 41 finalist features, listed in Table 4 together with their primary group, secondary source group, and feature type. With the exception of the dQ/dV-based charge group, all six remaining groups contribute representatives to the finalist set, underscoring the high diversity of source signatures that can be exploited from the data. The dQ/dV-based discharge, General charge, CCCV-based charge, and General discharge groups each account for approximately 20-25% of the finalist variables. Moreover, short-history sliding-window features make up ~90% of the finalist feature types, indicating that even a short cycle history still provides rich measures of statistical dispersion capable of stratifying/predicting RUL.

Table 4: Finalist features of the LGBM base model.

Feature	Group	Secondary Group	Type	SHAP Impact
window_mean_last_5_cycles_skew_cc_charge	CCCV-based Charge Feature Set	CCCV-based Charge Feature Set	Sliding window	105.506
window_mean_last_5_cycles_std_dqdv_discharge	dQ/dV-based Discharge Feature Set	dQ/dV-based Discharge Feature Set	Sliding window	95.940
window_mean_last_5_cycles_charge_std_current	General Charge Feature Set	General Charge Feature Set	Sliding window	38.507
window_mean_last_5_cycles_charge_kurt_current	General Charge Feature Set	General Charge Feature Set	Sliding window	38.262
median_qv_discharge	dQ/dV-based Discharge Feature Set	Q(V) discharge	Primary	33.127
window_mean_last_5_cycles_discharge_correlation_voltage_current	General Discharge Feature Set	General Discharge Feature Set	Sliding window	13.707

dif_between_p98_dvdq_discharge_and_window_range_last_5_cycles_p98_dvdq_discharge	dV/dQ-based Discharge Feature Set	dV/dQ-based Discharge Feature Set	Sliding window	13.358
window_mean_last_5_cycles_discharge_p50_voltage	General Discharge Feature Set	General Discharge Feature Set	Sliding window	8.995
window_mean_last_5_cycles_charge_p98_current	General Charge Feature Set	General Charge Feature Set	Sliding window	8.628
window_mean_last_5_cycles_discharge_skew_voltage	General Discharge Feature Set	General Discharge Feature Set	Sliding window	8.350
window_mean_last_5_cycles_charge_mean_current	General Charge Feature Set	General Charge Feature Set	Sliding window	7.815
window_mean_last_5_cycles_discharge_p50_resistance	General Discharge Feature Set	General Discharge Feature Set	Sliding window	7.560
dif_between_discharge_p50_voltage_and_window_range_last_5_cycles_discharge_p50_voltage	General Discharge Feature Set	General Discharge Feature Set	Sliding window	7.537
charge_sum_time_1_cycle_behind	General Charge Feature Set	General Charge Feature Set	Lag	6.785
window_mean_last_5_cycles_slope_cccv_ccct_charge	CCCV-based Charge Feature Set	CCCV-based Charge Feature Set	Sliding window	6.565
window_mean_last_5_cycles_p25_dqdv_discharge	dQ/dV-based Discharge Feature Set	dQ/dV-based Discharge Feature Set	Sliding window	6.411
window_mean_last_5_cycles_charge_kurt_temperature	General Charge Feature Set	General Charge Feature Set	Sliding window	6.263
dif_between_slope_qv_discharge_and_window_range_last_5_cycles_slope_qv_discharge	dQ/dV-based Discharge Feature Set	Q(V) discharge	Sliding window	6.160
dif_between_median_qv_discharge_and_window_std_last_5_cycles_median_qv_discharge	dQ/dV-based Discharge Feature Set	Q(V) discharge	Sliding window	6.010
window_mean_last_5_cycles_median_dqdv_discharge	dQ/dV-based Discharge Feature Set	dQ/dV-based Discharge Feature Set	Sliding window	5.901
window_mean_last_5_cycles_p98_dvdq_discharge	dV/dQ-based Discharge Feature Set	dV/dQ-based Discharge Feature Set	Sliding window	5.714
window_mean_last_5_cycles_shannonen_cv_charge	CCCV-based Charge Feature Set	CCCV-based Charge Feature Set	Sliding window	5.702
window_mean_last_5_cycles_median_qv_discharge	dQ/dV-based Discharge Feature Set	Q(V) discharge	Sliding window	4.941
window_mean_last_5_cycles_dif_energy_cc_cv_charge	CCCV-based Charge Feature Set	CCCV-based Charge Feature Set	Sliding window	4.885
window_mean_last_5_cycles_min_dqdv_discharge	dQ/dV-based Discharge Feature Set	dQ/dV-based Discharge Feature Set	Sliding window	4.756
window_mean_last_5_cycles_p75_resistence_cc_charge	CCCV-based Charge Feature Set	CCCV-based Charge Feature Set	Sliding window	4.560
dif_between_charge_sum_time_and_window_range_last_5_cycles_charge_sum_time	General Charge Feature Set	General Charge Feature Set	Sliding window	4.545
median_qv_discharge_5_cycle_behind	dQ/dV-based Discharge Feature Set	Q(V) discharge	Lag	4.530
window_mean_last_5_cycles_dqdv_pbw	dQ/dV-based Discharge Feature Set	dQ/dV-based Discharge Feature Set	Sliding window	4.188
window_mean_last_5_cycles_charge_min_current	General Charge Feature Set	General Charge Feature Set	Sliding window	4.156
window_mean_last_5_cycles_p75_resistence_cv_charge	CCCV-based Charge Feature Set	CCCV-based Charge Feature Set	Sliding window	4.118
window_mean_last_5_cycles_p98_dvdq_discharge	dV/dQ-based Charge Feature Set	dV/dQ-based Charge Feature Set	Sliding window	3.782
window_mean_last_5_cycles_discharge_p25_temperature	General Discharge Feature Set	General Discharge Feature Set	Sliding window	3.405
window_mean_last_5_cycles_discharge_kurt_voltage	General Discharge Feature Set	General Discharge Feature Set	Sliding window	3.361
window_mean_last_5_cycles_shannonen_cc_charge	CCCV-based Charge Feature Set	CCCV-based Charge Feature Set	Sliding window	3.013
window_mean_last_5_cycles_discharge_p98_current	General Discharge Feature Set	General Discharge Feature Set	Sliding window	2.769
window_mean_last_5_cycles_skew_dvdq_discharge	dV/dQ-based Charge Feature Set	dV/dQ-based Charge Feature Set	Sliding window	2.647
window_mean_last_5_cycles_charge_p75_current	General Charge Feature Set	General Charge Feature Set	Sliding window	2.553
window_mean_last_5_cycles_p98_resistence_cv_charge	CCCV-based Charge Feature Set	CCCV-based Charge Feature Set	Sliding window	2.247
window_mean_last_5_cycles_charge_beta_current_voltage	General Charge Feature Set	General Charge Feature Set	Sliding window	2.115
kurt_cc_charge_5_cycle_behind	CCCV-based Charge Feature Set	CCCV-based Charge Feature Set	Lag	1.722

Regarding interpretability of the LGBM base model, the SHAP dependence plots in Figure 5 reveal nonlinear effects with thresholds and saturation ranges across the 12 most influential variables. Practically: (i) recent charge/discharge stability, low variability, and a more “regular” shape over the last five cycles are associated with positive SHAP (higher predicted RUL), while extreme dispersion/tails are penalized; (ii) turning points emerge that flip the sign or accelerate the magnitude of the effect; and (iii) some predictors exhibit plateaus where additional increments deliver only marginal gains. These patterns indicate operational regimes (bands) in which small variations induce large changes in prediction, useful for feature engineering and for guiding operating policies and the interpretation of sensor signals.

Most variables are statistics of variability and shape (std, skew, kurtosis, p50/p98), i.e., the model treats recent stability as impacting health. The strongest predictor indicates that the mean skew of voltage measurements in the constant-current segment of charge over the last five cycles plus the current cycle shows a turning point around ~1.0-1.1: below this range, the effect is negative; above it, the impact rises sharply—higher charge-phase skew pushes RUL upward.

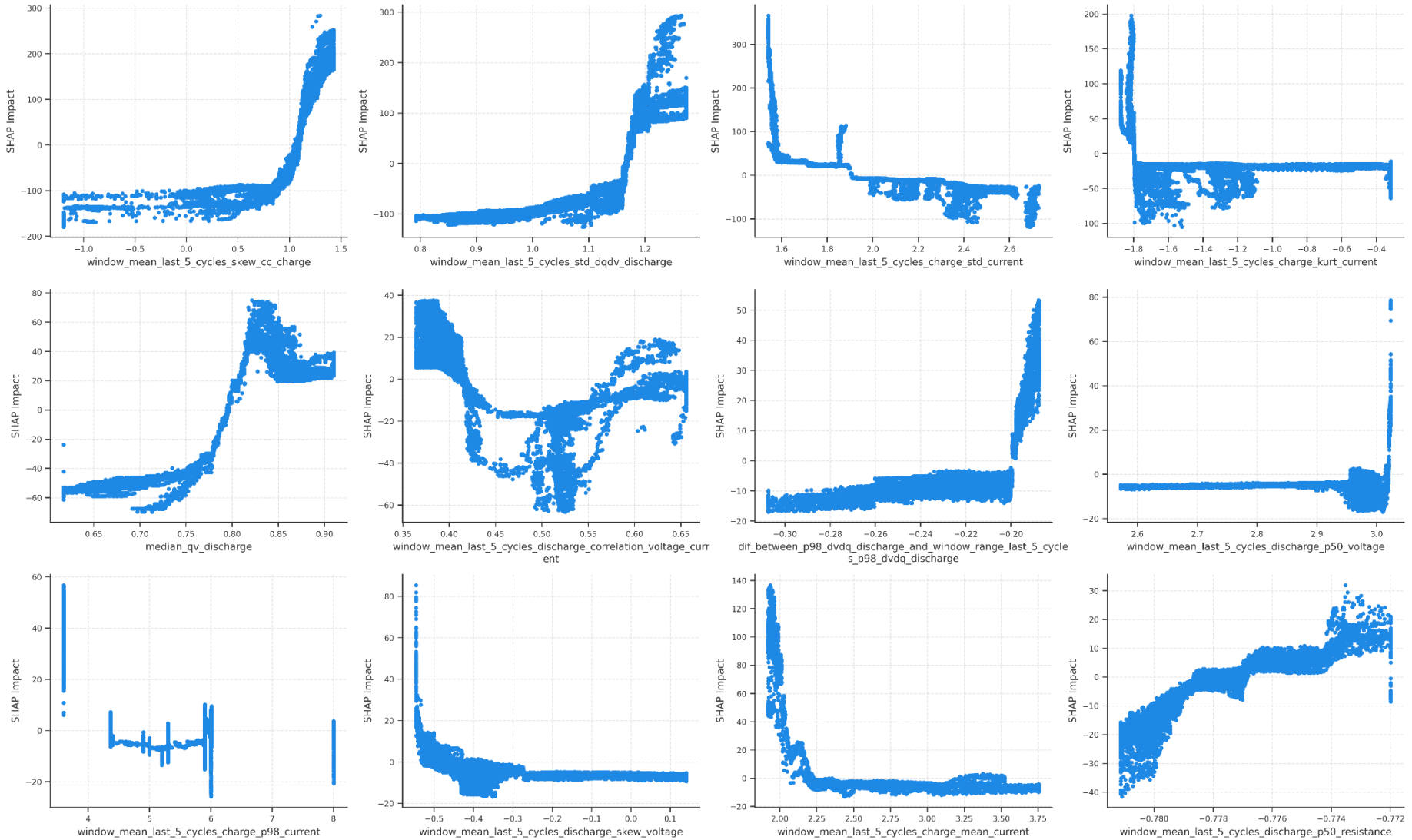

Figure 5: SHAP interpretability with dependence plots for the 12 most important features of the LGBM base model.

The hyperparameters of the finalist LGBM base model are reported in Table 5.

Table 5: LGBM base model hyperparameters.

Hyperparameter	**Value**
learning_rate	*0.01586625520600975*
n_estimators	800
num_leaves	16
max_depth	6
min_child_samples	130
min_child_weight	*0.000434591683109998*
boosting_type	*"gbdt"*
objective	*"regression"*
colsample_bytree	*0.9877872308787795*
subsample	*0.5483764076770935*
min_split_gain	*0.02140715154614596*
random_state	601

For the 12 base models with DL architectures, Table 6 summarizes the final implemented details for the LSTM variants and Table 7 for the GRU variants. The 2D configurations with deeper CNN backbones ([64, 128, (256)]) expand the RNN input vector (e.g., up to ~1,536), increasing representational capacity at higher computational cost; in contrast, 1D CNNs combined with a LagMixer compress the problem (input ≈ 64), improving memory and latency efficiency. Replacing LSTM with GRU preserves overall behavior while simplifying the recurrent state and, at parity of hidden size, yields slightly leaner models. Enabling bidirectionality doubles the per-branch output (64→128), enhancing context capture. In the fusion stage, concatenation maximizes capacity (vectors of length 384/768) but grows linearly with the number of branches, whereas attention produces a compact summary vector (attn ⊕ mean ⊕ max).

Table 6: Summary of base models DL architectures with LSTM.

Item	CNN2D-LSTM	CNN2D-BiLSTM	CNN2D-LSTM-ATT	CNN1D-LSTM	CNN1D-BiLSTM	CNN1D-LSTM-ATT
Branches (C_in)	6 branches: 2×(6), 2×(5), 2×(3)	6 branches: 2×(6), 2×(5), 2×(3)	6 branches: 2×(6), 2×(5), 2×(3)	6 branches: 2×(6), 2×(5), 2×(3)	6 branches: 2×(6), 2×(5), 2×(3)	6 branches: 2×(6), 2×(5), 2×(3)
Lags / Window	(H=6) lag0–lag5, (W=128)	(H=6) lag0–lag5, (W=128)	(H=6) lag0–lag5, (W=128)	(H=6), (W=128)	(H=6), (W=128)	(H=6), (W=128)
CNN per branch	2D: [64,128]; each block = Conv2D 3×3 + BN + ReLU + MaxPool(1×2)	2D: [64,128]; each block = Conv2D 3×3 + BN + ReLU + MaxPool(1×2)	2D: [64,128]; each block = Conv2D 3×3 + BN + ReLU + MaxPool(1×2)	1D: [32,64,128]; each block = Conv1D k=5 + BN + ReLU + MaxPool(2)	1D: [32,64,128]; each block = Conv1D k=5 + BN + ReLU + MaxPool(2)	1D: [32,64,128]; each block = Conv1D k=5 + BN + ReLU + MaxPool(2)
After CNN	(B,128,6,32)	(B,128,6,32)	(B,128,6,32)	(B,128,W_out=16)	(B,128,W_out=16)	(B,128,W_out=16)
LSTM per branch	input=768, hidden=64, layers=1, bidir=No	input=768, hidden=64, layers=1, bidir=Yes	input=768, hidden=64, layers=1, bidir=No	input=128, hidden=128, layers=1, bidir=No	input=128, hidden=128, layers=1, bidir=Yes	input=128, hidden=128, layers=1, bidir=No
Per-branch output	64 dims (Dropout p=0,3801 + LN(64))	128 dims (Dropout p=0,3801 + LN(128))	64 dims (Dropout p=0,3801 + LN(64))	128 dims (Dropout p=0,1786 + LN(128))	256 dims (Dropout p=0,1786 + LN(256))	128 dims (Dropout p=0,1786 + LN(128))
Fusion	Concatenation	Concatenation	Attention (TransformerEncoder d=64, 1 layer) + BranchDropout + residual	Concatenation	Concatenation	Attention (TransformerEncoder d=128, 1 layer) + BranchDropout + residual
Fused vector	6×64 = 384	6×128 = 768	attn ⊕ mean ⊕ max → 3×64 = 192	6×128 = 768	6×256 = 1536	attn ⊕ mean ⊕ max → 3×128 = 384
Added scalars	+24 → 408	+24 → 792	+24 → 216	+24 → 792	+24 → 1560	+24 → 408
Head (MLP)	408→128→64 (ReLU + Dropout p=0,3801)	792→128→64 (ReLU + Dropout p=0,3801)	216→128→64 (ReLU + Dropout p=0,3801)	792→256→128 (ReLU + Dropout p=0,1786)	1560→256→128 (ReLU + Dropout p=0,1786)	408→256→128 (ReLU + Dropout p=0,1786)
Outputs	(μ:64→1), (logσ:64→1) – Log-Normal	(μ:64→1), (logσ:64→1) – Log-Normal	(μ:64→1), (logσ:64→1) – Log-Normal	(μ:128→1), (logσ:128→1) – Log-Normal	(μ:128→1), (logσ:128→1) – Log-Normal	(μ:128→1), (logσ:128→1) – Log-Normal
Params ~	~1.8 M	~3.1 M	~1.85 M	~1.34 M	~2.33 M	~1.5 M

Table 7: Summary of base model DL architectures with GRU.

Item	CNN2D-GRU	CNN2D-BiGRU	CNN2D-GRU-ATT	CNN1D-GRU	CNN1D-BiGRU	CNN1D-GRU-ATT
Branches (C_in)	6 branches: 2×(6), 2×(5), 2×(3)	6 branches: 2×(6), 2×(5), 2×(3)	6 branches: 2×(6), 2×(5), 2×(3)	6 branches: 2×(6), 2×(5), 2×(3)	6 branches: 2×(6), 2×(5), 2×(3)	6 branches: 2×(6), 2×(5), 2×(3)
Lags / Window	(H=6) lag0–lag5, (W=128)	(H=6) lag0–lag5, (W=128)	(H=6) lag0–lag5, (W=128)	(H=6), (W=128)	(H=6), (W=128)	(H=6), (W=128)
CNN per branch	2D: [64,128,256]; each block = Conv2D 3×3 + BN + ReLU + MaxPool(1×2)	2D: [64,128,256]; each block = Conv2D 3×3 + BN + ReLU + MaxPool(1×2)	2D: [64,128,256]; each block = Conv2D 3×3 + BN + ReLU + MaxPool(1×2)	1D: [32,64]; each block = Conv1D k=5 + BN + ReLU + MaxPool(2)	1D: [32,64]; each block = Conv1D k=5 + BN + ReLU + MaxPool(2)	1D: [32,64]; each block = Conv1D k=5 + BN + ReLU + MaxPool(2)
After CNN	(B,256,6,16)	(B,256,6,16)	(B,256,6,16)	(B,64, W_out=32)	(B,64, W_out=32)	(B,64, W_out=32)
LSTM per branch	input=1536, hidden=64, layers=1, bidir=No	input=1536, hidden=64, layers=1, bidir=Yes	input=1536, hidden=64, layers=1, bidir=No	input=64, hidden=64, layers=2, bidir=No	input=64, hidden=64, layers=2, bidir=Yes	input=64, hidden=64, layers=2, bidir=No
Per-branch output	64 dims (Dropout p=0,1941 + LN(64))	128 dims (Dropout p=0,1941 + LN(128))	64 dims (Dropout p=0,1941 + LN(64))	64 dims (Dropout p=0,2434 + LN(64))	128 dims (Dropout p=0,2434 + LN(128))	64 dims (Dropout p=0,2434 + LN(64))
Fusion	Concatenation	Concatenation	Attention (TransformerEncoder d=64, 1 layer, FF=1024) + BranchDropout + residual	Concatenation	Concatenation	Attention (TransformerEncoder d=64, 2 layers, FF=512) + BranchDropout + residual
Fused vector	6×64 = 384	6×128 = 768	attn ⊕ mean ⊕ max → 3×64 = 192	6×64 = 384	6×128 = 768	attn ⊕ mean ⊕ max → 3×64 = 192
Added scalars	+24 → 408	+24 → 792	+24 → 216	+24 → 408	+24 → 792	+24 → 216
Head (MLP)	408→512→256 (ReLU + Dropout p=0,1941)	792→512→256 (ReLU + Dropout p=0,1941)	216→512→256 (ReLU + Dropout p=0,1941)	408→256→128 (ReLU + Dropout p=0,2434)	792→256→128 (ReLU + Dropout p=0,2434)	216→256→128 (ReLU + Dropout p=0,2434)
Outputs	(μ:256→1), (logσ:256→1) – Log-Normal	(μ:256→1), (logσ:256→1) – Log-Normal	(μ:256→1), (logσ:256→1) – Log-Normal	(μ:128→1), (logσ:128→1) – Log-Normal	(μ:128→1), (logσ:128→1) – Log-Normal	(μ:128→1), (logσ:128→1) – Log-Normal
Params ~	~2.4 M	~3.3 M	~2.1 M	~0.85 M	~1.5 M	~1.1 M

Performance results for the base models (trained with cross-validation on the base-train split) and the stacking models (trained with cross-validation on the meta-train split) are reported in Table 8 for performance on the meta-train set (which can be regarded as one of the test views for the base models) and in Table 9 for performance on the held-out test set. Two stacking configurations were evaluated: Stacking I, in which Optuna-driven variable selection chose the predictions from CNN1D-LSTM, CNN1D-BiLSTM, CNN1D-BiGRU, and LGBM as inputs; and Stacking II, in which the LGBM base model was replaced by its 41 finalist features. In general, the selected based predictions yield stronger median-based metrics, and the LGBM component tends to alter prediction patterns within certain ranges due to its tree-boosting behavior.

Across all models evaluated on the test split, Stacking I achieved most of the best metrics, reducing RMSE by roughly 10 cycles relative to the best base model (CNN1D-BiLSTM). Stacking II also improved upon CNN1D-BiLSTM, particularly on MedAPE, MedAE, and RMedSE. Among the DL architectures, LSTM variants tended to outperform GRU, and CNN1D outperformed CNN2D on this dataset. Attention-based variants did not yield gains and trailed their concatenation counterparts.

Table 8: Performance metrics for base models on the meta-train set.

Model	MAE (cycles)	RMSE (cycles)	MAPE (%)	MedAE (cycles)	RMedSE (cycles)	MedAPE (%)	sMAPE (%)	WAPE (%)	NMAE	R2
CNN1D-LSTM	32.036	55.029	6.534	18.167	18.167	5.541	6.499	6.625	0.069	0.977
CNN1D-LSTM-ATT	35.212	48.746	7.975	26.697	26.697	7.239	7.792	7.204	0.075	0.982
CNN1D-BiLSTM	37.820	59.612	8.583	24.091	24.091	6.781	8.529	7.802	0.080	0.973
CNN1D-BiGRU	44.113	79.044	8.674	22.569	22.569	7.126	8.491	9.130	0.097	0.951
CNN2D-GRU-ATT	36.199	48.747	9.040	27.623	27.623	7.879	8.902	7.392	0.077	0.982
LGBM	39.518	58.137	9.150	24.792	24.792	7.743	9.023	8.050	0.085	0.974
CNN1D-GRU-ATT	44.165	67.091	9.447	26.094	26.094	7.861	9.576	9.071	0.094	0.965
CNN2D-LSTM	38.306	52.857	9.818	26.839	26.839	7.639	9.511	7.810	0.082	0.978
CNN2D-BiLSTM	45.355	65.300	10.207	31.521	31.521	8.818	10.213	9.238	0.098	0.967
CNN2D-LSTM-ATT	47.707	70.455	10.321	29.782	29.782	8.441	10.497	9.770	0.102	0.962
CNN1D-GRU	52.342	82.787	10.650	29.469	29.469	9.315	10.991	10.753	0.112	0.947
CNN2D-GRU	34.076	45.706	10.757	27.927	27.927	7.406	10.059	6.894	0.075	0.984
CNN2D-BiGRU	40.687	56.163	11.154	29.683	29.683	8.389	10.510	8.245	0.089	0.975

Table 9: Performance metrics on the test set.

Model	MAE (cycles)	RMSE (cycles)	MAPE (%)	MedAE (cycles)	RMedSE (cycles)	MedAPE (%)	sMAPE (%)	WAPE (%)	NMAE	R2
STACKING I	26.081	40.639	6.006	14.912	14.912	4.923	6.076	5.822	0.059	0.980
STACKING II	29.658	53.063	6.388	15.080	15.080	4.731	6.408	6.543	0.069	0.965
CNN1D-BiLSTM	29.520	50.026	6.624	15.929	15.929	5.183	6.794	6.519	0.069	0.970
CNN1D-LSTM	35.527	57.450	7.672	19.672	19.672	6.507	7.822	8.180	0.085	0.957
CNN2D-GRU-ATT	40.277	63.578	8.542	21.358	21.358	7.214	8.427	8.941	0.092	0.952
CNN1D-LSTM-ATT	40.517	64.925	8.610	19.261	19.261	7.158	8.477	9.042	0.094	0.949
LGBM	40.087	63.417	9.419	21.561	21.561	6.897	9.196	8.975	0.094	0.952
CNN1D-BiGRU	43.361	73.582	9.423	21.454	21.454	7.121	9.445	9.886	0.102	0.935
CNN2D-BiGRU	39.219	64.227	10.109	21.962	21.962	7.578	9.696	8.649	0.091	0.950
CNN1D-GRU	41.845	64.019	10.369	25.766	25.766	8.199	10.737	9.437	0.098	0.951
CNN2D-LSTM	43.934	73.309	10.380	24.083	24.083	8.118	10.320	9.833	0.101	0.934
CNN2D-GRU	41.991	64.855	10.704	25.436	25.436	7.824	10.142	9.257	0.098	0.949
CNN2D-LSTM-ATT	43.472	68.086	10.971	26.768	26.768	7.860	10.894	9.706	0.102	0.945
CNN1D-GRU-ATT	53.514	83.730	12.358	26.097	26.097	9.220	12.187	12.028	0.121	0.918
CNN2D-BiLSTM	57.432	87.186	13.057	28.875	28.875	12.066	13.277	12.731	0.133	0.909

For the best-performing model (Stacking I), Figure 6 analyzes predictions across bands of true RUL. In all RUL ranges, the model's median prediction closely matches the true median, with larger deviations for samples whose current RUL is on the order of 1,000, where there is a tendency to underpredict. This corresponds to the right tail of the RUL distribution and is relatively infrequent in this dataset. A similar pattern was reported by [53], with marked error increases for cells exceeding 750 total life cycles.

The same analysis by SOH bands is shown in Figure 7. In this case, the empirical and predicted RUL distributions by SOH band are visibly closer; the deviation observed earlier concentrates at the extreme right of the 0.99-1.00 SOH band, reinforcing that this behavior is atypical.

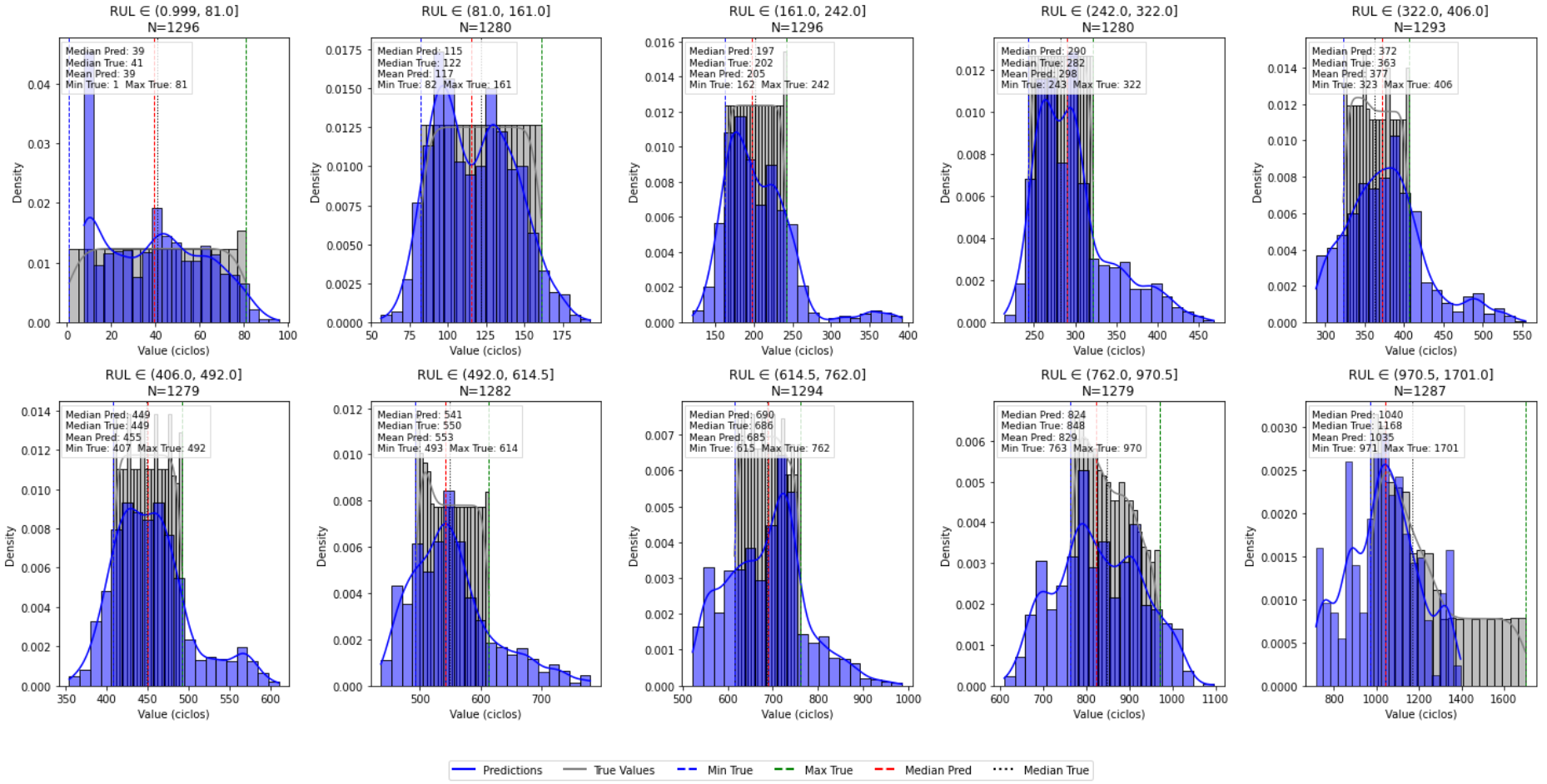

Figure 6: Comparative analysis of Stacking I predictions versus true RUL by bands.

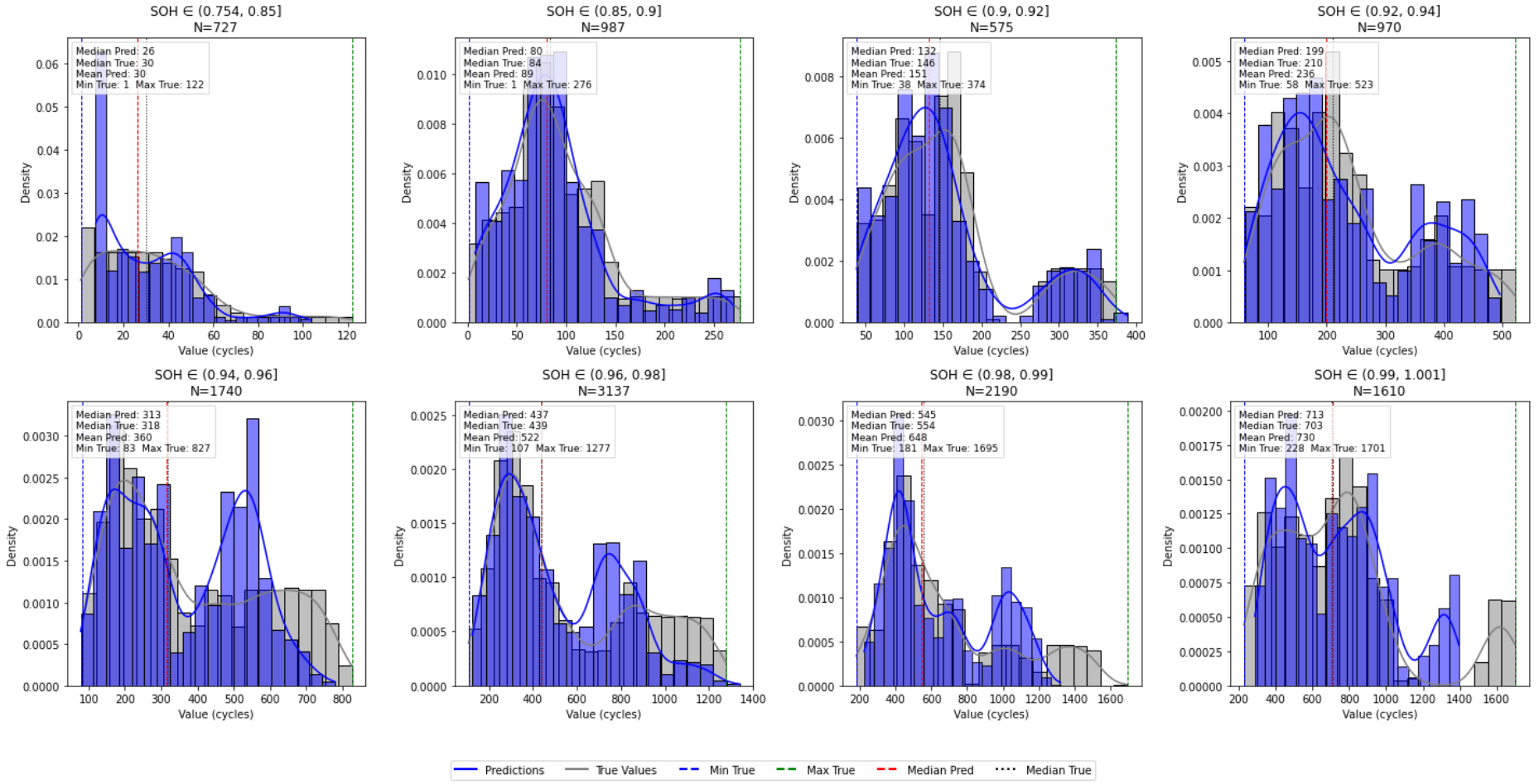

Figure 7: Comparative analysis of Stacking I predictions versus true SOH by bands.

The behavior of prediction-error metrics across RUL and SOH bands is reflected in Table 10 and Table 11. The stratified analysis of Stacking I reveals a “U-shaped” error profile over RUL: at very low RUL (near end of life), absolute error is small (MAE ~5 cycles), but percentage metrics inflate (MAPE = 31%, sMAPE ~21%, WAPE ~12%) due to the small denominator; in intermediate bands (~600-970 cycles), relative errors are lowest (sMAPE/WAPE ~5%) with moderate MAE (~34-48 cycles); and at the upper extreme of RUL (~970-1700 cycles), both absolute (MAE ~81 cycles) and relative errors (sMAPE ~7,9%) increase, suggesting greater uncertainty in an early-life regime. Stratification by SOH corroborates this pattern: in degraded SOH (0,754–0,85), MAE remains low (~5 cycles), but MAPE/sMAPE/WAPE spike (~49%/31%/19%) for the same percentage effect; the best relative regime occurs at high SOH (0,99–1,00), with sMAPE/WAPE ~3,8% and minimum NMAE (~0,075), while intermediate bands (0,94-0,98) concentrate larger absolute errors (MAE ~29–41). Together, these results indicate that the model is most stable in the operational core (medium/high RUL and high SOH), whereas end-of-life decisions warrant attention to absolute metrics (MAE/MedAE).

Table 10: Stacking I performance by true RUL band.

True RUL interval	MAE (cycles)	RMSE (cycles)	MAPE (%)	MedAE (cycles)	RMedSE (cycles)	MedAPE (%)	sMAPE (%)	WAPE (%)	NMAE
(-0.001, 81.0]	4.996	6.467	31.259	4.415	4.415	11.497	21.427	12.186	0.125
(81.0, 161.0]	7.070	8.921	5.815	5.795	5.795	5.050	5.976	5.819	0.179
(161.0, 242.0]	13.478	16.272	6.629	12.276	12.276	6.071	6.705	6.672	0.337
(242.0, 322.0]	22.589	33.462	7.852	15.065	15.065	5.359	7.451	7.996	0.572
(322.0, 406.0]	25.654	32.176	7.110	22.542	22.542	6.330	7.008	7.038	0.618
(406.0, 492.0]	25.322	31.719	5.658	21.546	21.546	4.785	5.626	5.638	0.603
(492.0, 614.5]	30.225	38.786	5.508	24.372	24.372	4.475	5.516	5.495	0.472
(614.5, 762.0]	34.026	49.284	4.931	18.207	18.207	2.587	4.955	4.942	0.463
(762.0, 970.5]	48.382	63.045	5.638	36.321	36.321	4.163	5.651	5.686	0.504
(970.5, 1701.0]	81.489	101.282	7.463	71.511	71.511	6.485	7.850	7.488	0.645

Table 11: Stacking I performance by true SOH band.

True SOH interval	MAE (cycles)	RMSE (cycles)	MAPE (%)	MedAE (cycles)	RMedSE (cycles)	MedAPE (%)	sMAPE (%)	WAPE (%)	NMAE
(0.754, 0.85]	5.24116	7.03660	49.28105	4.43774	4.43775	18.25394	30.93180	19.13430	0.19412
(0.85, 0.9]	5.10179	6.39576	10.31707	4.30540	4.30540	6.40553	9.60710	6.82210	0.12004
(0.9, 0.92]	7.54464	9.55671	6.30048	6.19664	6.19672	5.62636	6.52720	6.01670	0.11563
(0.92, 0.94]	14.68884	22.74623	7.07818	10.47362	10.47401	5.49044	7.01080	7.24970	0.12663
(0.94, 0.96]	29.27252	41.83840	7.67356	17.98951	17.98957	6.76468	7.66710	8.43480	0.10568
(0.96, 0.98]	41.00810	60.25015	7.44422	26.05806	26.05806	6.70596	7.53590	7.93270	0.09593
(0.98, 0.99]	34.48851	45.70735	6.18323	26.21656	26.21656	5.01659	6.06010	6.02040	0.12406
(0.99, 1.001]	25.47547	36.80833	3.91699	17.13058	17.13058	2.82186	3.81470	3.82640	0.07520

Table 12 provides a comparative performance analysis against studies that also leveraged the MIT dataset. This comparison is indicative and empirical, since each study adopts different splits and horizons, altering the test-set RUL distribution and directly affecting metrics (especially at low RUL). Within this context, the LGBM base model achieved MAPE ~9%, very close to the percentage errors reported by [20] (early prediction) and [54], which, however, relied on 100 and 250 cycles, respectively. This underscores the strong pattern-extraction capability of the tabular variables produced by the pipeline. Regarding Stacking I, the stacking approach is promising, outperforming most surveyed works in percentage error, except for the CNN3D-CNN2D study, which used early-life information and a larger historical window.

Considering this empirical comparison, the present study differs and contributes on four fronts: (i) short history (5 past cycles plus current), showing that MAPE ~9% is attainable with the LGBM base model; (ii) a broad, well-defined, and systematic tabular pipeline for feature extraction and selection; (iii) multibranch DL with 12 variants (CNN1D/2D-LSTM/GRU) using

not only raw current, voltage, and temperature, but also sequences from IC and DV analyses; and (iv) stacking that fuses DL embeddings with boosting, surpassing most publications while generally requiring less data. The RUL/SOH-stratified evaluation further reveals a “U-shaped” error pattern, providing interpretability for prediction uncertainties.

Table 12: Performance comparison with related RUL prediction and early-prediction studies on the MIT dataset.

Ref.	Algorithm	RMSE	MAPE	Notes
[59]	MLP	90	-	Used 113 of 124 cells; 10-cycle history
[58]	CNN+RNN	240	9.8	30-cycle history
[57]	CNN3D-CNN2D	-	3.55	Uses first 5 cycles, then 15 historical cycles
[56]	CNN-LSTM		11.31	Early prediction with 100 initial cycles
[55]	CNN	76	10.6	4-cycle history
[20]	XGBoost	91.13	7.92	Early prediction with 100 initial cycles
[54]	GBT	84.9	7.5	250-cycle history
[53]	DNN	65 (1) 40 (2)		Uses last cycle (1) or 100 cycles (2); considers RUL < 750 cycles.
-	**Proposed (*Stacking* I)**	**40.60**	**6.01**	**Uses 6-cycle history -**

5. Conclusions

This study showed that RUL can be estimated with a short history (current cycle and 5 lags) by combining feature engineering, DL architectures, and stacking-based meta-learning. The tabular pipeline for the LGBM model started from 5,578 variables (V/I/T/time signals, CC/CV segmentation, and IC/DV derivatives) and, via multivariate selection, converged to 41 finalists spanning 6 of the 7 extracted groups. Roughly 90% of the final set comprises sliding-window statistics, suggesting that dispersion and shape measures over the last six cycles capture useful degradation signatures. SHAP analysis evidenced nonlinearities and saturation regimes; for example, voltage skew in the CC charge regime exhibited a turning point (~1.0-1.1): below this range, the contribution to RUL is negative; above it, the effect rises sharply.

Across 12 DL base models, CNN1D consistently outperformed CNN2D on the test set, consistent with short history and a better signal/complexity ratio in 1D. LSTM tended to outperform GRU, and branch concatenation prevailed over attention mechanisms. The best base model was CNN1D-BiLSTM, with MedAE 15.93 cycles and RMSE 50.03 cycles, while stand-alone LGBM achieved MedAE 21.56 cycles and RMSE 63.42 cycles. Ensembles delivered the strongest final results on the test set: Stacking I (LGBM meta over selected predictions from CNN1D-LSTM, CNN1D-BiLSTM, CNN1D-BiGRU, and LGBM) reached MedAE 14.91 cycles and RMSE 40.64 cycles, surpassing the best base model (−6.4% in MedAE, −18.8% in RMSE) and LGBM (-31% and -35.9%). Stacking II (LGBM finalist variables + DL predictions) maintained competitive medians (MedAE 15.08 cycles and MedAPE 4.73%) with RMSE 53.06 cycles, indicating solid central performance but greater tail sensitivity. Stratification of Stacking I by RUL bands revealed a U-shaped error profile: near EoL, percentage metrics inflate; in intermediate bands (~600-970 cycles) relative errors are lowest; and for cells with high total cycle counts and high RUL (~970-1700) both absolute and relative errors increase. Stratification by SOH corroborated these conclusions.

Empirically, the stacking model’s results align with the best performances reported in studies that used the same dataset, underscoring the promise of this ensemble for RUL prediction. Notably, the LGBM base model here achieved MAPE ~9%, close to other works that also used tree-boosting yet relied on histories in the hundreds of cycles, indicating strong discriminative power of the tabular variables even with only six cycles.

Practically, we demonstrate that six cycles of history suffice to obtain low central errors and consistent gains via model fusion, particularly attractive for battery triage and second-use repurposing, as well as predictive maintenance under test-time constraints. Key limitations include: (i) domain generalization, with results tied to a specific cell chemistry

($LiFePO_4$/graphite) under controlled conditions; and (ii) heteroscedasticity/tail behavior associated with higher uncertainty at high RUL and near EoL.

As future directions, we propose: (i) exploring domain transfer (self-supervised pretraining and light fine-tuning) to improve generalization across chemistries and usage profiles in other datasets, especially low-volume ones; (ii) developing RUL models tailored to second life, conditioned on prior usage histories of repurposed cells; and (iii) addressing the data gap by creating a public dataset of second-use cells under stationary profiles up to a new EoL threshold. In sum, this work establishes a practical, reproducible route to short-history RUL prediction by combining complementary sources (signals, CC/CV, IC/DV) and diverse inductive biases (boosting and DL), and positions stacking as competitive in this regime.

References

[1] International Energy Agency, Global EV Outlook 2024 Moving towards increased affordability, 2024. https://www.iea.org/reports/global-ev-outlook-2024.

[2] Y. Li, K. Liu, A.M. Foley, A. Zülke, M. Berecibar, E. Nanini-Maury, J. Van Mierlo, H.E. Hoster, Data-driven health estimation and lifetime prediction of lithium-ion batteries: A review, Renewable and Sustainable Energy Reviews 113 (2019) 109254. https://doi.org/10.1016/j.rser.2019.109254.

[3] M.S.H. Lipu, M.A. Hannan, A. Hussain, M.M. Hoque, P.J. Ker, M.H.M. Saad, A. Ayob, A review of state of health and remaining useful life estimation methods for lithium-ion battery in electric vehicles: Challenges and recommendations, J Clean Prod 205 (2018) 115–133. https://doi.org/10.1016/J.JCLEPRO.2018.09.065.

[4] J.-H. Teng, R.-J. Chen, P.-T. Lee, C.-W. Hsu, Accurate and Efficient SOH Estimation for Retired Batteries, Energies (Basel) 16 (2023) 1240. https://doi.org/10.3390/en16031240.

[5] X. Shu, G. Li, Y. Zhang, J. Shen, Z. Chen, Y. Liu, Online diagnosis of state of health for lithium-ion batteries based on short-term charging profiles, J Power Sources 471 (2020). https://doi.org/10.1016/j.jpowsour.2020.228478.

[6] B. Gou, Y. Xu, X. Feng, An Ensemble Learning-Based Data-Driven Method for Online State-of-Health Estimation of Lithium-Ion Batteries, IEEE Transactions on Transportation Electrification 7 (2021) 422–436. https://doi.org/10.1109/TTE.2020.3029295.

[7] G.L. Plett, Extended Kalman filtering for battery management systems of LiPB-based HEV battery packs, J Power Sources 134 (2004) 262–276. https://doi.org/10.1016/j.jpowsour.2004.02.032.

[8] X. Li, Z. Huang, J. Tian, Y. Tian, State-of-charge estimation tolerant of battery aging based on a physics-based model and an adaptive cubature Kalman filter, Energy 220 (2021) 119767. https://doi.org/10.1016/J.ENERGY.2021.119767.

[9] Y. Tian, C. Lin, H. Li, J. Du, R. Xiong, Detecting undesired lithium plating on anodes for lithium-ion batteries – A review on the in-situ methods, Appl Energy 300 (2021) 117386. https://doi.org/10.1016/J.APENERGY.2021.117386.

[10] J. Li, R.G. Landers, J. Park, A comprehensive single-particle-degradation model for battery state-of-health prediction, J Power Sources 456 (2020) 227950. https://doi.org/10.1016/J.JPOWSOUR.2020.227950.

[11] W. Liu, P. Liu, D. Mitlin, Review of Emerging Concepts in SEI Analysis and Artificial SEI Membranes for Lithium, Sodium, and Potassium Metal Battery Anodes, Adv Energy Mater 10 (2020) 2002297. https://doi.org/10.1002/AENM.202002297.

[12] K. Das, R. Kumar, Electric vehicle battery capacity degradation and health estimation using machine-learning techniques: a review, Clean Energy 7 (2023) 1268–1281. https://doi.org/10.1093/ce/zkad054.

[13] D. Roman, S. Saxena, V. Robu, M. Pecht, D. Flynn, Machine learning pipeline for battery state-of-health estimation, Nat Mach Intell 3 (2021) 447–456. https://doi.org/10.1038/s42256-021-00312-3.

[14] D. Gong, Y. Gao, Y. Kou, Y. Wang, State of health estimation for lithium-ion battery based on energy features, Energy 257 (2022) 124812. https://doi.org/10.1016/j.energy.2022.124812.

[15] X.-Y. Yao, G. Chen, M. Pecht, B. Chen, A novel graph-based framework for state of health prediction of lithium-ion battery, J Energy Storage 58 (2023) 106437. https://doi.org/10.1016/j.est.2022.106437.

[16] C. Hu, G. Jain, P. Zhang, C. Schmidt, P. Gomadam, T. Gorka, Data-driven method based on particle swarm optimization and k-nearest neighbor regression for estimating capacity of lithium-ion battery, Appl Energy 129 (2014) 49–55. https://doi.org/https://doi.org/10.1016/j.apenergy.2014.04.077.

[17] Y. Zhang, T. Wik, J. Bergström, M. Pecht, C. Zou, A machine learning-based framework for online prediction of battery ageing trajectory and lifetime using histogram data, J Power Sources 526 (2022) 231110. https://doi.org/10.1016/j.jpowsour.2022.231110.

[18] G. Li, B. Li, C. Li, S. Wang, State-of-health rapid estimation for lithium-ion battery based on an interpretable stacking ensemble model with short-term voltage profiles, Energy 263 (2023) 126064. https://doi.org/10.1016/j.energy.2022.126064.

[19] K.A. Severson, P.M. Attia, N. Jin, N. Perkins, B. Jiang, Z. Yang, M.H. Chen, M. Aykol, P.K. Herring, D. Fraggedakis, M.Z. Bazant, S.J. Harris, W.C. Chueh, R.D. Braatz, Data-driven prediction of battery cycle life before capacity degradation, Nat Energy 4 (2019) 383–391. https://doi.org/10.1038/s41560-019-0356-8.

[20] D. Gong, Y. Gao, Y. Kou, Y. Wang, Early prediction of cycle life for lithium-ion batteries based on evolutionary computation and machine learning, J Energy Storage 51 (2022) 104376. https://doi.org/10.1016/j.est.2022.104376.

[21] I. Bloom, A.N. Jansen, D.P. Abraham, J. Knuth, S.A. Jones, V.S. Battaglia, G.L. Henriksen, Differential voltage analyses of high-power, lithium-ion cells: 1. Technique and application, J Power Sources 139 (2005) 295–303. https://doi.org/https://doi.org/10.1016/j.jpowsour.2004.07.021.

[22] H. Wenzl, I. Baring-Gould, R. Kaiser, B.Y. Liaw, P. Lundsager, J. Manwell, A. Ruddell, V. Svoboda, Life prediction of batteries for selecting the technically most suitable and cost effective battery, J Power Sources 144 (2005) 373–384. https://doi.org/10.1016/J.JPOWSOUR.2004.11.045.

[23] A. Barré, B. Deguilhem, S. Grolleau, M. Gérard, F. Suard, D. Riu, A review on lithium-ion battery ageing mechanisms and estimations for automotive applications, J Power Sources 241 (2013) 680–689. https://doi.org/10.1016/j.jpowsour.2013.05.040 Review.

[24] R.R. Richardson, M.A. Osborne, D.A. Howey, Battery health prediction under generalized conditions using a Gaussian process transition model, J Energy Storage 23 (2019) 320–328. https://doi.org/10.1016/J.EST.2019.03.022.

[25] C.R. Birkl, M.R. Roberts, E. McTurk, P.G. Bruce, D.A. Howey, Degradation diagnostics for lithium ion cells, J Power Sources 341 (2017) 373–386. https://doi.org/10.1016/J.JPOWSOUR.2016.12.011.

[26] S.S. Zhang, K. Xu, T.R. Jow, Study of the charging process of a LiCoO2-based Li-ion battery, J Power Sources 160 (2006) 1349–1354. https://doi.org/10.1016/J.JPOWSOUR.2006.02.087.

[27] J. Zhou, P.H.L. Notten, Studies on the degradation of Li-ion batteries by the use of microreference electrodes, J Power Sources 177 (2008) 553–560. https://doi.org/10.1016/J.JPOWSOUR.2007.11.032.

[28] N. Williard, W. He, M. Osterman, M. Pecht, Comparative Analysis of Features for Determining State of Health in Lithium-Ion Batteries, Int J Progn Health Manag 4 (2013). https://doi.org/10.36001/IJPHM.2013.V4I1.1437.

[29] Y. Li, M. Abdel-Monem, R. Gopalakrishnan, M. Berecibar, E. Nanini-Maury, N. Omar, P. van den Bossche, J. Van Mierlo, A quick on-line state of health estimation method for Li-ion battery with incremental capacity curves processed by Gaussian filter, J Power Sources 373 (2018) 40–53. https://doi.org/https://doi.org/10.1016/j.jpowsour.2017.10.092.

[30] C. Weng, Y. Cui, J. Sun, H. Peng, On-board state of health monitoring of lithium-ion batteries using incremental capacity analysis with support vector regression, J Power Sources 235 (2013) 36–44. https://doi.org/https://doi.org/10.1016/j.jpowsour.2013.02.012.

[31] G.R. Sylvestrin, J.N. Maciel, M.L.M. Amorim, J.P. Carmo, J.A. Afonso, S.F. Lopes, O.H. Ando Junior, State of the Art in Electric Batteries' State-of-Health (SoH) Estimation with Machine Learning: A Review, Energies (Basel) 18 (2025). https://doi.org/10.3390/en18030746.

[32] F.M. Zhao, D.X. Gao, Y.M. Cheng, Q. Yang, Application of state of health estimation and remaining useful life prediction for lithium-ion batteries based on AT-CNN-BiLSTM, Sci Rep 14 (2024) 1–15. https://doi.org/10.1038/S41598-024-80421-2;SUBJMETA.

[33] K. Luo, X. Chen, H. Zheng, Z. Shi, A review of deep learning approach to predicting the state of health and state of charge of lithium-ion batteries, Journal of Energy Chemistry 74 (2022) 159–173. https://doi.org/10.1016/j.jechem.2022.06.049.

[34] Y. Zhang, R. Xiong, H. He, M.G. Pecht, Long Short-Term Memory Recurrent Neural Network for Remaining Useful Life Prediction of Lithium-Ion Batteries, IEEE Trans Veh Technol 67 (2018) 5695–5705. https://doi.org/10.1109/TVT.2018.2805189.

[35] S. Kim, Y.Y. Choi, K.J. Kim, J.-I. Choi, Forecasting state-of-health of lithium-ion batteries using variational long short-term memory with transfer learning, J Energy Storage 41 (2021) 102893. https://doi.org/https://doi.org/10.1016/j.est.2021.102893.

[36] Y. Che, Z. Deng, X. Lin, L. Hu, X. Hu, Predictive Battery Health Management With Transfer Learning and Online Model Correction, IEEE Trans Veh Technol 70 (2021) 1269–1277. https://doi.org/10.1109/TVT.2021.3055811.

[37] M. Wei, H. Gu, M. Ye, Q. Wang, X. Xu, C. Wu, Remaining useful life prediction of lithium-ion batteries based on Monte Carlo Dropout and gated recurrent unit, Energy Reports 7 (2021) 2862–2871. https://doi.org/10.1016/J.EGYR.2021.05.019.

[38] L. Ren, J. Dong, X. Wang, Z. Meng, L. Zhao, M.J. Deen, A Data-Driven Auto-CNN-LSTM Prediction Model for Lithium-Ion Battery Remaining Useful Life, IEEE Trans Industr Inform 17 (2021) 3478–3487. https://doi.org/10.1109/TII.2020.3008223.

[39] Y. Mazzi, H. Ben Sassi, F. Errahimi, Lithium-ion battery state of health estimation using a hybrid model based on a convolutional neural network and bidirectional gated recurrent unit, Eng Appl Artif Intell 127 (2024) 107199. https://doi.org/https://doi.org/10.1016/j.engappai.2023.107199.

[40] K. Kaur, A. Garg, X. Cui, S. Singh, B.K. Panigrahi, Deep learning networks for capacity estimation for monitoring SOH of Li-ion batteries for electric vehicles, Int J Energy Res 45 (2021) 3113–3128. https://doi.org/10.1002/ER.6005.

[41] A. Kara, A data-driven approach based on deep neural networks for lithium-ion battery prognostics, Neural Comput Appl 33 (2021) 13525–13538. https://doi.org/10.1007/s00521-021-05976-x.

[42] A. Tang, Y. Jiang, Q. Yu, Z. Zhang, A hybrid neural network model with attention mechanism for state of health estimation of lithium-ion batteries, J Energy Storage 68 (2023) 107734. https://doi.org/https://doi.org/10.1016/j.est.2023.107734.

[43] X. Yao, K. Su, H. Zhang, S. Zhang, H. Zhang, J. Zhang, Remaining useful life prediction for lithium-ion batteries in highway electromechanical equipment based on feature-encoded LSTM-CNN network, Energy 323 (2025) 135719. https://doi.org/10.1016/J.ENERGY.2025.135719.

[44] W. Li, Y. Li, A. Garg, L. Gao, Enhancing real-time degradation prediction of lithium-ion battery: A digital twin framework with CNN-LSTM-attention model, Energy 286 (2024) 129681. https://doi.org/https://doi.org/10.1016/j.energy.2023.129681.

[45] Y. Fan, F. Xiao, C. Li, G. Yang, X. Tang, A novel deep learning framework for state of health estimation of lithium-ion battery, J Energy Storage 32 (2020). https://doi.org/10.1016/j.est.2020.101741.

[46] B. Liu, J. Xu, W. Xia, State-of-Health Estimation for Lithium-Ion Battery Based on an Attention-Based CNN-GRU Model with Reconstructed Feature Series, Int J Energy Res 2023 (2023) 8569161. https://doi.org/10.1155/2023/8569161.

[47] S. Jafari, Y.-C. Byun, A CNN-GRU Approach to the Accurate Prediction of Batteries' Remaining Useful Life from Charging Profiles, Computers 12 (2023). https://doi.org/10.3390/computers12110219.
[48] S. Wang, S. Jin, D. Bai, Y. Fan, H. Shi, C. Fernandez, A critical review of improved deep learning methods for the remaining useful life prediction of lithium-ion batteries, Energy Reports 7 (2021) 5562–5574. https://doi.org/10.1016/j.egyr.2021.08.182.
[49] S. Song, C. Fei, H. Xia, Lithium-Ion Battery SOH Estimation Based on XGBoost Algorithm with Accuracy Correction, Energies (Basel) 13 (2020) 812. https://doi.org/10.3390/en13040812.
[50] S. Jafari, Z. Shahbazi, Y.-C. Byun, Lithium-Ion Battery Health Prediction on Hybrid Vehicles Using Machine Learning Approach, Energies (Basel) 15 (2022) 4753. https://doi.org/10.3390/en15134753.
[51] S. Xu, F.L. Zha, B.W. Huang, B. Yu, H.B. Huang, T. Zhou, W.Q. Mao, J.J. Wu, J.Q. Wei, S.K. Gong, T. Wan, X.Y. Duan, S.F. Xiong, Research on the state of health estimation of lithium-ion batteries for energy storage based on XGB-AKF method, Front Energy Res 10 (2023) 999676. https://doi.org/10.3389/FENRG.2022.999676/BIBTEX.
[52] Z. Jiao, H. Wang, J. Xing, Q. Yang, M. Yang, Y. Zhou, J. Zhao, LightGBM-Based Framework for Lithium-Ion Battery Remaining Useful Life Prediction Under Driving Conditions, IEEE Trans Industr Inform 19 (2023) 11353–11362. https://doi.org/10.1109/TII.2023.3246124.
[53] C.-W. Hsu, R. Xiong, N.-Y. Chen, J. Li, N.-T. Tsou, Deep neural network battery life and voltage prediction by using data of one cycle only, Appl Energy 306 (2022) 118134. https://doi.org/10.1016/j.apenergy.2021.118134.
[54] F. Yang, D. Wang, F. Xu, Z. Huang, K.-L. Tsui, Lifespan prediction of lithium-ion batteries based on various extracted features and gradient boosting regression tree model, J Power Sources 476 (2020) 228654. https://doi.org/10.1016/j.jpowsour.2020.228654.
[55] J. Hong, D. Lee, E.-R. Jeong, Y. Yi, Towards the swift prediction of the remaining useful life of lithium-ion batteries with end-to-end deep learning, Appl Energy 278 (2020) 115646. https://doi.org/10.1016/j.apenergy.2020.115646.
[56] Q. Xu, M. Wu, E. Khoo, Z. Chen, X. Li, A Hybrid Ensemble Deep Learning Approach for Early Prediction of Battery Remaining Useful Life, IEEE/CAA Journal of Automatica Sinica 10 (2023) 177–187. https://doi.org/10.1109/JAS.2023.123024.
[57] Y. Yang, A machine-learning prediction method of lithium-ion battery life based on charge process for different applications, Appl Energy 292 (2021) 116897. https://doi.org/10.1016/j.apenergy.2021.116897.
[58] G. Ma, S. Xu, B. Jiang, C. Cheng, X. Yang, Y. Shen, T. Yang, Y. Huang, H. Ding, Y. Yuan, Real-time personalized health status prediction of lithium-ion batteries using deep transfer learning, Energy Environ Sci 15 (2022) 4083–4094. https://doi.org/10.1039/D2EE01676A.
[59] I. Sanz-Gorrachategui, P. Pastor-Flores, M. Pajovic, Y. Wang, P. V Orlik, C. Bernal-Ruiz, A. Bono-Nuez, J.S. Artal-Sevil, Remaining Useful Life Estimation for LFP Cells in Second-Life Applications, IEEE Trans Instrum Meas 70 (2021) 1–10. https://doi.org/10.1109/TIM.2021.3055791.
[60] Parameters — LightGBM 4.6.0.99 documentation, (n.d.). https://lightgbm.readthedocs.io/en/latest/Parameters.html (accessed September 25, 2025).
[61] J.H. Friedman, Greedy function approximation: A gradient boosting machine., The Annals of Statistics 29 (2001) 1189–1232. https://doi.org/10.1214/aos/1013203451.
[62] G. Ke, Q. Meng, T. Finley, T. Wang, W. Chen, W. Ma, Q. Ye, T.-Y. Liu, LightGBM: A Highly Efficient Gradient Boosting Decision Tree, in: I. Guyon, U. Von Luxburg, S. Bengio, H. Wallach, R. Fergus, S. Vishwanathan, R. Garnett (Eds.), Adv Neural Inf Process Syst, Curran Associates, Inc., 2017. https://proceedings.neurips.cc/paper_files/paper/2017/file/6449f44a102fde848669bdd9eb6b76fa-Paper.pdf.

[63] Features — LightGBM 4.6.0.99 documentation, (n.d.). https://lightgbm.readthedocs.io/en/latest/Features.html (accessed September 25, 2025).
[64] Advanced Topics — LightGBM 4.6.0.99 documentation, (n.d.). https://lightgbm.readthedocs.io/en/latest/Advanced-Topics.html (accessed September 25, 2025).
[65] Ian Goodfellow, Aaron Courville, Yoshua Bengio, Deep Learning, (2016) 1–23. http://www.deeplearningbook.org (accessed September 26, 2025).
[66] C. Zhu, M. Gao, Z. He, H. Wu, C. Sun, Z. Zhang, Z. Bao, State of health prediction for li-ion batteries with end-to-end deep learning, J Energy Storage 65 (2023) 107218. https://doi.org/https://doi.org/10.1016/j.est.2023.107218.
[67] B. Zraibi, M. Mansouri, S.E. Loukili, Comparing deep learning methods to predict the remaining useful life of lithium-ion batteries, Mater Today Proc 62 (2022) 6298–6304. https://doi.org/10.1016/j.matpr.2022.04.082.
[68] S. Kiranyaz, T. Ince, O. Abdeljaber, O. Avci, M. Gabbouj, 1-D Convolutional Neural Networks for Signal Processing Applications, ICASSP, IEEE International Conference on Acoustics, Speech and Signal Processing - Proceedings 2019-May (2019) 8360–8364. https://doi.org/10.1109/ICASSP.2019.8682194.
[69] S. Bai, J.Z. Kolter, V. Koltun, An Empirical Evaluation of Generic Convolutional and Recurrent Networks for Sequence Modeling, (2018). https://arxiv.org/pdf/1803.01271 (accessed September 26, 2025).
[70] J. Schmidhuber, Deep learning in neural networks: An overview, Neural Networks 61 (2015) 85–117. https://doi.org/10.1016/j.neunet.2014.09.003.
[71] S. Hochreiter, J. Schmidhuber, Long Short-Term Memory, Neural Comput 9 (1997) 1735–1780. https://doi.org/10.1162/NECO.1997.9.8.1735.
[72] M. Bosello, C. Falcomer, C. Rossi, G. Pau, To Charge or to Sell? EV Pack Useful Life Estimation via LSTMs, CNNs, and Autoencoders, Energies (Basel) 16 (2023) 2837. https://doi.org/10.3390/en16062837.
[73] D.H. Wolpert, Stacked generalization, Neural Networks 5 (1992) 241–259. https://doi.org/10.1016/S0893-6080(05)80023-1.
[74] Z.H. Zhou, Ensemble methods: Foundations and algorithms, Ensemble Methods: Foundations and Algorithms (2012) 1–218. https://doi.org/10.1201/B12207/ENSEMBLE-METHODS-ZHI-HUA-ZHOU/RIGHTS-AND-PERMISSIONS.
[75] F. Wang, Y. Yang, T. Huang, Y. Xu, Lifetime prediction of electronic devices based on the P-stacking machine learning model, Microelectronics Reliability 146 (2023) 115027. https://doi.org/https://doi.org/10.1016/j.microrel.2023.115027.
[76] J. Wu, X. Cui, J. Meng, J. Peng, M. Lin, Data-Driven Transfer-Stacking-Based State of Health Estimation for Lithium-Ion Batteries, IEEE Transactions on Industrial Electronics 71 (2024) 604–614. https://doi.org/10.1109/TIE.2023.3247735.
[77] Giovane Ronei Sylvestrin; Joylan Nunes Maciel; Oswaldo Hideo Ando Junior, Comprehensive Feature Extraction for Battery Health Prognostics: Identifying Predictive Indicators of State of Health, J Power Sources (2025).
[78] T. Akiba, S. Sano, T. Yanase, T. Ohta, M. Koyama, Optuna: A Next-generation Hyperparameter Optimization Framework, in: Proceedings of the 25th ACM SIGKDD International Conference on Knowledge Discovery & Data Mining, Association for Computing Machinery, New York, NY, USA, 2019: pp. 2623–2631. https://doi.org/10.1145/3292500.3330701.